Cochlear Implants: bridging the gap between computational model and clinic

Kalkman, R.K.

Cochlear Implants

Bridging the gap between computational model and clinic

Randy Kalkman

Cochlear Implants

Bridging the gap between computational model and clinic

Randy Kevin Kalkman

ISBN 978-94-90858-77-3

Printed by *Mostert & Van Onderen!* in Leiden, The Netherlands

Cochlear Implants

Bridging the gap between computational model and clinic

Proefschrift

ter verkrijging van
de graad van doctor aan de Universiteit Leiden,
op gezag van rector magnificus prof.dr.ir. H. Bijl,
volgens besluit van het college voor promoties
te verdedigen op donderdag 20 april 2023
klokke 11.15 uur

door

Randy Kevin Kalkman

geboren te Vlaardingen
in 1978

Promotor: Prof. dr. ir. J.H.M. Fijns

Copromotor: Dr. ir. J.J. Briaire

Leden promotiecommissie:

Prof. dr. P.P.G. van Benthem	
Dr. ir. M.J. van Gendt	
Prof. dr. W. Nogueira	Hannover Medical School
Prof. dr. T. Hanekom	University of Pretoria

Aan mijn ouders, Jan en Trudy

Table of contents

Chapter 1

General introduction

Cochlear Implants

Cochlear Implants (CIs) are medical devices that have been widely used in the past decades to restore hearing for people with certain types of substantial hearing loss. Their basic working principle is to evoke sound perception by directly stimulating the auditory nerve in the cochlea with electrical pulses, bypassing the need to transfer sound through the outer and middle ear to the inner ear mechanically. They are currently the most successful hearing prosthetic for individuals who, for whatever reason, cannot meaningfully understand or even detect (amplified) sound, but whose auditory nerves are still present and healthy enough to convey signals to the brain.

There are several different manufacturers of CIs, each producing multiple different CI models, but all CIs presently available follow the same general design. Figure 1.1 illustrates an overview of the basic setup of a CI in a patient. The implant itself is completely subdermal, with no components or wires going through the skin and the device does not contain an internal battery, so the CI is dependent on external hardware for both signal and power transmission. The external devices consist of a microphone and speech processor, which capture and convert sound into a digital signal that is transmitted to the CI through a pair of sending/receiving coils (one external, the other subdermal), using magnetic induction at radio frequencies. The external coil is usually located in a so-called headpiece, which is connected to the speech processor by wire and is held in place over the location of the subdermal coil using a pair of ferromagnets placed in the coils' centres, though in some designs, the head piece and speech processor are integrated into a single unit.

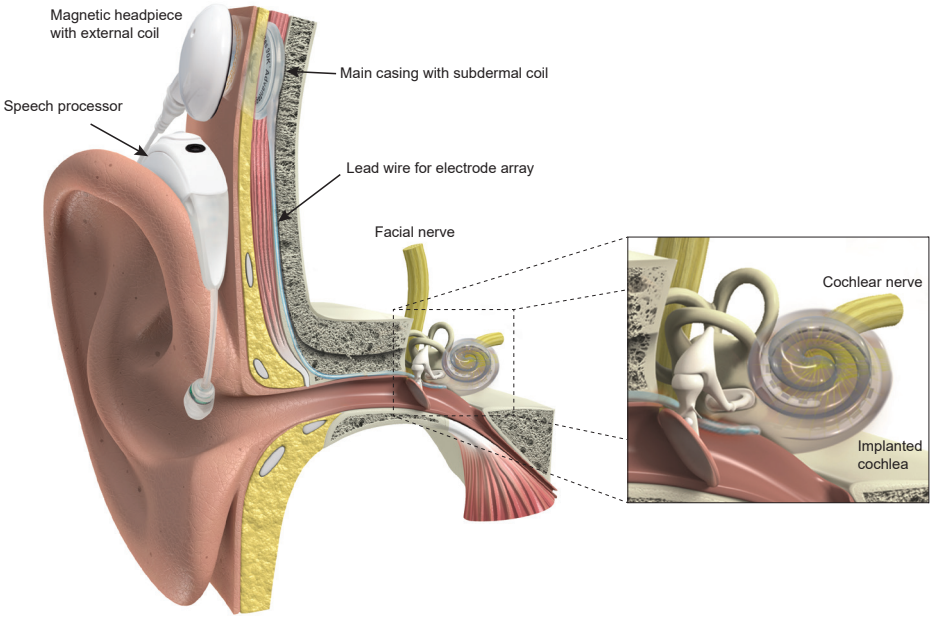

Figure 1.1. *Overview of a cochlear implant and its external components (image courtesy of Advanced Bionics). The inset on the right shows a blow-up of the cochlea implanted with the electrode array.*

The subdermal coil is part of the main casing of the CI, which is embedded in the skull of the patient in a surgically drilled-out bed. The casing also contains the electronic components necessary to process the received signal and activate the intracochlear electrode array, which is connected to the casing by a lead wire that runs through a drilled-out tunnel through the temporal bone that surrounds the cochlea. The electrode array is essentially a thin silicone tube with a number of exposed platinum electrode contacts spaced out along its length, which is inserted into the cochlea through the round window or via a cochleostomy.

The cochlea is, in simple terms, a snail shell-like structure inside the skull, a spiralling tunnel that is divided into three main compartments: the scala tympani, the scala media and the scala vestibuli (figure 1.2). The scala tympani is separated from the other two scalae by the osseous spiral lamina and basilar membrane/organ of Corti, while the scala media and scala vestibuli are separated by Reissner's membrane. In normal acoustic hearing, sound transferred to the cochlea through the outer and middle ear causes the basilar membrane to oscillate, which generates movement of the stereocilia of the outer and inner hair cells in the organ of Corti. The hair cells of these stereocilia respond to this mechanical motion by inducing an electrical signal in the auditory nerve fibres that carry this signal from the organ of Corti, through the osseous spiral lamina into the cochlear modiolus, where all the nerve fibres in the cochlea bundle up and proceed towards the brain.

The basilar membrane's oscillating behaviour is frequency dependent and as such it can be considered a kind of mechanical Fourier transformer. High frequency sound will cause the basilar membrane to resonate mainly at the base of the cochlea and lowering the frequency of the sound will move the area of maximum resonance towards the apex. Since there are auditory neurons spread out along the entire length of the basilar membrane/organ of Corti, this means that each auditory neuron normally only responds to a sound frequency (or frequency range) that corresponds to its position along the length of the basilar membrane. This principle is referred to as the tonotopic organisation of the auditory neurons and it is an important way for the auditory system to convey pitch information to the brain.

CIs take advantage of this tonotopic organisation due to the fact that their electrode arrays have multiple electrode contacts spaced out along the length of the electrode array. When inserted as intended into the scala tympani, each electrode contact will be located at a different depth in the cochlea and will electrically stimulate a different subpopulation of auditory neurons, which will typically be the nerve fibres that are closest to the electrode contact in question. Due to the tonotopic organisation, each electrode contact is therefore expected to invoke a different pitch percept, corresponding to how deeply it is located in the cochlea.

In clinical application, the CI's electrode contacts usually only inject current into the cochlea in so-called monopolar mode. This stimulation mode is so named because only one contact on the electrode array is activated, while the return electrode is located

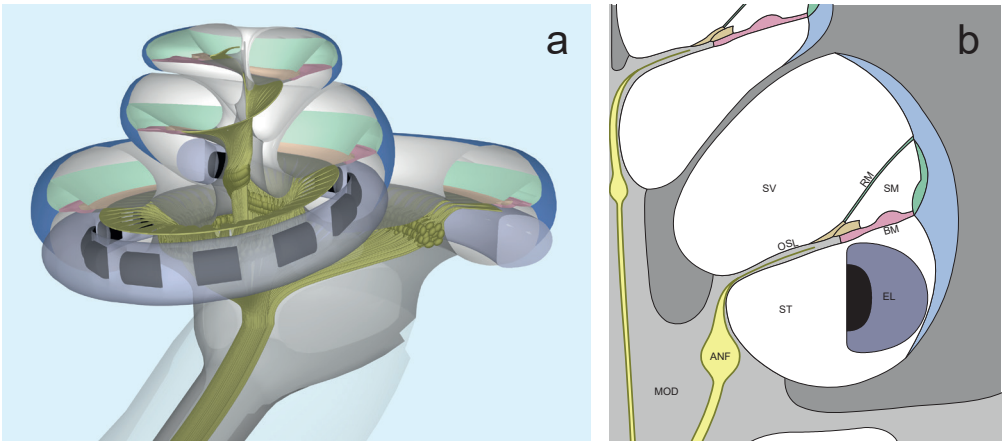

Figure 1.2. *Schematic overview of select structures inside the (human) cochlea. Panel a shows a partial cross-section of a cochlea from the computational model central to this thesis. Panel b shows a line drawing of the cross-section at the beginning of the second turn of the cochlea. The main compartments denoted are the scala vestibuli (SV), scala media (SM) and scala tympani (ST), the latter of which contains the electrode array (EL). These compartments are separated by the osseous spiral lamina (OSL), basilar membrane (BM) and Reissner's membrane (RM). Also depicted are the auditory nerve fibres (ANF), which run though the osseous spiral lamina and the cochlear modiolus (MOD).*

relatively far away from the cochlea (either on the CI's casing itself or through a separate electrode with its own lead wire, placed outside the skull underneath the temporalis muscle), meaning that the electrical field inside the cochlea is by approximation equal to that of a hypothetical monopole.

The stimulus applied to the electrode typically consists of symmetric biphasic pulses, illustrated in figure 1.3a. These pulses are charge-balanced, meaning the same amount of electrical charge passes through the electrode contact during the cathodic phase as during the anodic phase. This is a requirement for safe electrical stimulation of the auditory nerves; failure to charge-balance the pulses could lead to a charge build-up inside the cochlea, which could produce ototoxic reactions and damage the auditory neurons. The duration of the pulse is generally set to a fixed value, while the amplitudes of the pulses are used to increase the intensity of the stimulus (i.e., the loudness perceived by the patient), which is determined dynamically by the external speech processor when it codes sound into electrode array stimuli using a preconfigured speech coding strategy.

In modern speech coding strategies, output is split over a number of separate 'channels', each assigned to a different auditory frequency range, analogous to the natural tonotopic organisation of the cochlea described above. Generally, each channel corresponds to an individual contact along the electrode array, stimulating in monopolar mode, though channels can also be defined as multipolar configurations instead. The output stimuli are arranged so that no two channels are ever stimulated simultaneously, as demonstrated in

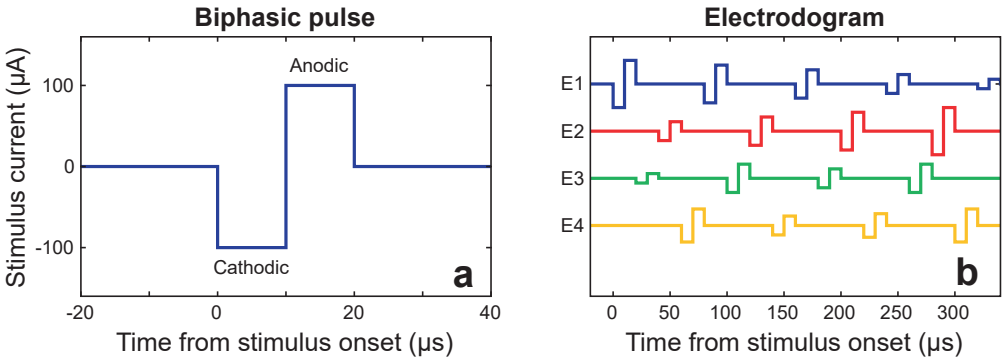

Figure 1.3. *Illustration of biphasic pulses typically used in cochlear implant stimulation. Panel a shows a single, cathodic-first symmetric biphasic pulse with a phase width of 10 μs and an amplitude of 100 μV, plotted over time. Panel b shows a mock stimulation sequence for some hypothetical stimulus on an electrode array with four electrodes/channels (E1-E4). The order of stimulation for the electrodes is staggered; none of them are ever stimulated simultaneously.*

figure 1.3b. This is done to prevent electrical interaction between the individual channels/electrodes, as stimulating multiple intracochlear contacts haphazardly will cause perceptual problems for the patient, due to the electrical fields generated by each active contact unpredictably adding to or subtracting from each other at the level of the auditory nerves.

Though CIs are remarkably successful medical devices, they are not without their limitations. For instance, CI-induced hearing is not comparable to natural hearing; the human cochlea has roughly 30,000 auditory nerve fibres which normally relay signals to the brain more or less independently from each other, while CIs are not able to stimulate these fibres with any finesse or precision. Modern CIs have only 12 to 24 electrode contacts and each contact stimulates a relatively large and wide subpopulation of neurons simultaneously with each stimulus. Though this is sufficient to restore speech understanding in most patients, the quality of the 'sound' leaves something to be desired and CIs are notoriously bad at conveying pitch information accurately. Furthermore, complications can pop up, such as unintended co-stimulation of non-auditory nerve fibres, chiefly in the facial nerve, which runs close to the cochlea, stimulation of which can trigger painful muscle spasms in one side of the patient's face. Therefore, despite the CI's success, there is an ongoing need for further research on how to improve and optimise its design and performance.

Computational modelling

Though the above summary of how CIs function applies to all modern clinically available devices in broad strokes, there are many details in which commercial implants and clinical practices differ. Each manufacturer has made different design decisions and each of them offers multiple devices intended for different clinical circumstances. This means that there is a variety of different CIs available, with different electrode array designs (e.g.,

differing in length, thickness, number of electrode contacts, target placement within the scala tympani) and hardware capabilities (e.g., available stimulus parameters, telemetry options, the ability to stimulate multiple contacts simultaneously in a controlled manner). In addition, the external and internal hardware of modern CIs are versatile enough to allow for more experimental speech coding and stimulation strategies than the ones used in standard clinical settings.

All of this means there is a great need for research into the precise functioning and optimisation of CI-enabled hearing. This is difficult, since the human cochlea itself is small, only roughly 1 cm in maximum diameter, with all of the relevant anatomical structures much smaller than that (for example an individual auditory nerve fibre is only a few micrometres thick) and the whole structure is completely embedded in bone, making it very difficult to interact with it in an ethically responsible way. Experiments with human subjects are therefore mainly limited to psychophysical testing and objective measures obtained through the CI's telemetry capabilities. Animal testing opens up more options, but it has the drawback that there are many anatomical and (neuro)physiological differences between animals and humans, which complicates comparison of animal data to human data and still requires experimentation on the small, difficult to access, inner ear.

However, the underlying physics of electrical neural stimulation can be well understood in terms of classical electromagnetism. The cochlear system is too complex to meaningfully describe CI functioning analytically, but it is an ideal candidate for computational modelling. The electrical fields induced by the CI can be simulated using a volume conduction model that solves the relevant Maxwell equations for a geometrical approximation of the human cochlea and an implanted electrode array. These calculated fields can subsequently be used to simulate responses of auditory nerve fibres, modelled as active electrical networks that react to the CI's stimuli.

The work of this thesis was to develop and use such a computational model to offer insight into the working mechanisms of CI stimulation and to enable virtual experiments that would be unfeasible or outright impossible in real life. The model that was used for this thesis was not built from scratch but was an updated and expanded version of the one developed at Leiden University Medical Centre by Johan H.M. Frijns and Jeroen J. Briaire. In essence, this thesis forms a continuation of their PhD work.

The general goals of each of the modelling studies presented in this thesis were

(I) To improve the accuracy of the Leiden computational CI-model to gain a better understanding of CI-induced hearing.

(II) Where possible, validate the model using available data from electrophysiological or psychophysical experiments.

(III) To use the model to offer predictions that may help to improve the function or design of CIs in the future.

Overview of this thesis

Chapter 2 gives a historical overview of computational modelling of cochlear implants, including the work that directly preceded this thesis (as well as the work presented in chapters 3 through 6).

Chapter 3 describes how the Leiden computational CI model was used to study place-pitch percepts resulting from CI stimuli. For this purpose, the model was updated to include more realistically curved auditory nerve fibre trajectories, based on histological data.

Chapter 4 concerns the modelling of facial nerve stimulation and otosclerosis. A representation of the facial nerve was added to the model, after which the effects of otosclerosis were simulated by reducing the electrical conductivity of temporal bone so that the implications for the stimulation thresholds of the auditory and facial nerves could be examined.

Chapter 5 presents a model analysis of so-called dual electrode stimulation strategies, which involve stimulating two electrode contacts, either simultaneously or in quick succession, in order to create intermediate place-pitch percepts.

Chapter 6 details a study of different current focussing strategies in the model. Current focussing strategies use simultaneous opposite polarity stimulation on multiple electrode contacts in an attempt to restrict spread of neural excitation. For this study, nerve fibre trajectories in the model were updated to include the spatial distribution of cell bodies of the auditory neurons in the cochlear modiolus.

Chapter 7 examines the effect of stimulus polarity in the model and tests the hypothesis that polarity sensitivity to CI stimuli may be used as an indicator of auditory neural health. For this study, the nerve fibre model was updated to one based on available human neurophysiological data.

Finally, chapter 8 presents a general discussion of the work of this thesis and directions for future research.

Chapter 2

Stimulation strategies and electrode design in computational models of the electrically stimulated cochlea: an overview of existing literature

Randy K. Kalkman
Jeroen J. Briaire
and Johan H.M. Frijns

Network: Computation in Neural Systems 2016 (27:2-3), 107–134

Abstract

Since the 1970s, computational modelling has been used to investigate the fundamental mechanisms of cochlear implant stimulation. Lumped parameter models and analytical models have been used to simulate cochlear potentials, as well as three-dimensional volume conduction models based on the Finite Difference, Finite Element and Boundary Element methods. Additionally, in order to simulate neural responses, several of these cochlear models have been combined with nerve models, which were either simple activation functions or active nerve fibre models of the cochlear auditory neurons. This review paper will present an overview of the ways in which these computational models have been employed to study different stimulation strategies and electrode designs. Research into stimulation strategies has concentrated mainly on multipolar stimulation as a means of achieving current focussing and current steering, while modelling work on electrode design has been chiefly concerned with finding the optimal position and insertion depth of the electrode array. Finally, the present and future of computational modelling of the electrically stimulated cochlea is discussed.

1 Introduction

Cochlear implants stimulate the auditory nerve electrically, thereby providing an audible sound percept to the hearing impaired implant user. Since both the electrical fields generated by the implant as well as the dynamic responses of the auditory neurons can be described in terms of electromagnetic physics, the functioning of cochlear implants is an ideal subject for computational modelling. Indeed, the earliest computational model relevant to the study of the electrically stimulated cochlea dates back to the 1970s, when Strelioff (1973) used a so-called lumped parameter model to describe electrical properties of cochlear structures (figure 2.1). Computational models from the early years of cochlear implant research used this type of lumped parameter approach to describe electrical stimulation of the cochlea (Black and Clark, 1980; Black et al., 1983; Suesserman and Spelman, 1993; Rodenhiser and Spelman, 1995; Spelman et al., 1995; Jolly et al., 1996; Kral et al., 1998), in addition to employing analytical functions (O'Leary et al., 1985; Spelman et al., 1995; Jolly et al., 1996). These lumped parameter and analytical models were not yet coupled to computational models of the auditory nerve, so they were restricted to examining the electric potentials and current distributions inside the cochlea.

Meanwhile, in the field of neural science, computational models of electrically stimulated nerve fibres were being developed, starting with the pioneering work of Frankenhæuser and Huxley (1964) on the myelinated nerve fibre of toads. Subsequent researchers developed the principle of neurons modelled as electrical networks (McNeal, 1976; Reilly et al., 1985; Rattay, 1987), leading to the first electrical cable model of the mammalian auditory neuron (Colombo and Parkins, 1987).

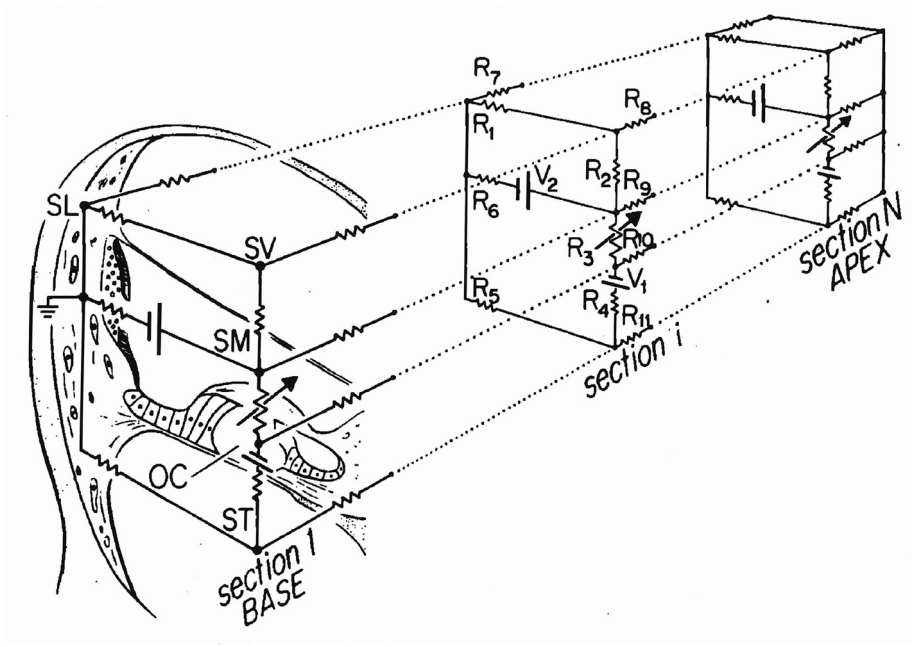

Figure 2.1. *Illustration of the lumped parameter model from Strelioff (1973).*

Although earlier studies had already used three-dimensional volume conduction models to investigate electric potentials in the cochlea (Girzon, 1987; Sapozhnikov, 1990), Finley et al. were the first to publish simulations of a three-dimensional volume conduction model combined with a (preliminary) cable model of the auditory nerve (Finley et al., 1990). They used the Finite Element Method (FEM) to calculate the electric potential distribution in their unrolled human cochlear geometry and then coupled the results to their version of an auditory nerve fibre model, which was based on the neural modelling works referenced above. From there on, several research groups have used volume conduction models to simulate electric potentials in increasingly sophisticated geometries of implanted cochleae. First as unrolled cochleae (figure 2.2), then with rotationally symmetric geometries (figure 2.3), and finally as increasingly realistic spiralling structures (figure 2.4) (Finley et al., 1990; Frijns et al., 1995; Briaire and Frijns, 2000; Frijns et al., 2001; Hanekom, 2001; Rattay et al., 2001a; Choi et al., 2004; 2005; Choi et al., 2006; Tognola et al., 2007; Whiten, 2007; Nogueira et al., 2014; Pau et al., 2014; Kalkman et al., 2015; Malherbe et al., 2016; Wong et al., 2016). Despite this tendency to move to more detailed cochlear geometries, simpler mathematical models of unrolled cochleae have retained their usefulness and are still employed in specific situations (Litvak et al., 2007; Bonham and Litvak, 2008; Goldwyn et al., 2010).

Additionally, electrical models of the auditory nerve have been further refined by incorporating data from electrophysiological single fibre experiments on mammalian neurons and morphological details of the human auditory nerve (Frijns et al., 1995; Rattay et al., 2001b; Briaire and Frijns, 2005; Dekker et al., 2014). However, not all of the developed cochlear models have incorporated active neural models; instead, some studies employ the so-called activation function to estimate neural responses (Finley et al., 1990; Litvak et al., 2007; Bonham and Litvak, 2008; Choi and Hsu, 2009; Goldwyn

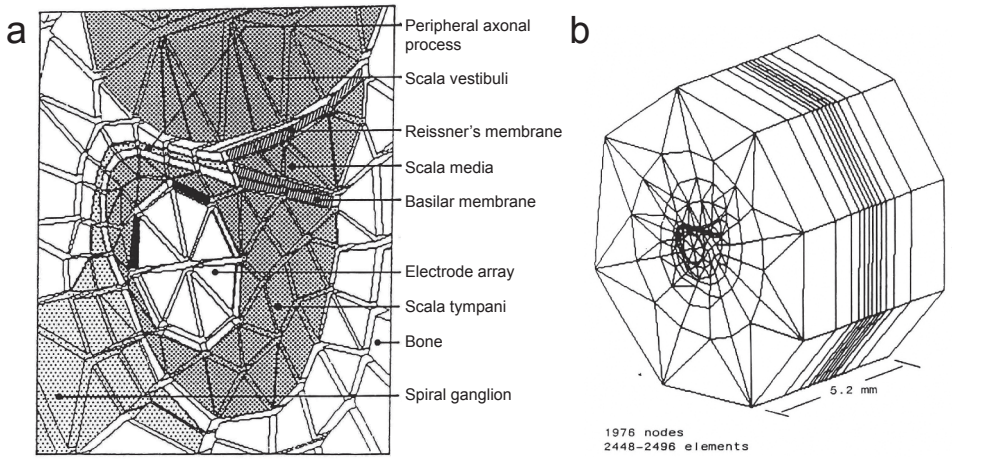

Figure 2.2. *Illustration of the unrolled human cochlea geometry used by Finley et al. (1990). Figure a shows a close-up view of how the cross section of the cochlea and electrode is segmented; Figure b shows the full geometry.*

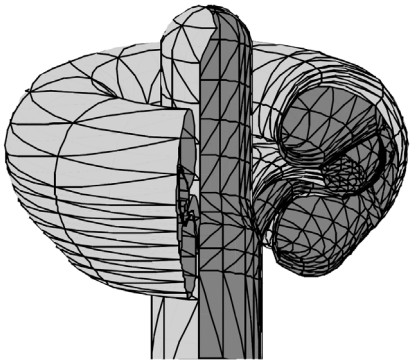

Figure 2.3. *Rotationally symmetric geometry of the guinea pig cochlea from Frijns et al. (1995,1996).*

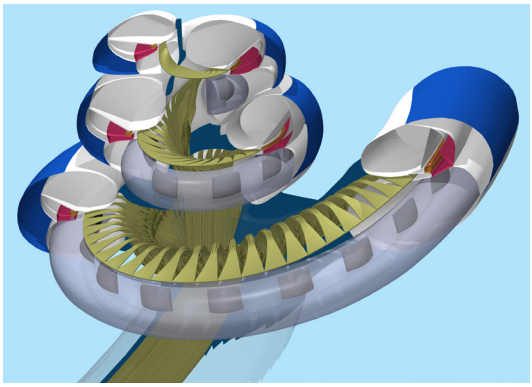

Figure 2.4. *Spiralling tapered geometry of the implanted human cochlea from Kalkman et al. (2015).*

et al., 2010; Wong et al., 2016). This activation function is equal to the second spatial derivative of the electric potential along the nerve fibres (Rattay, 1986). Although relatively simple to implement, the activation function only gives an indication of neural thresholds, and cannot be used to model more complex aspects of neural stimulation. For instance, simulating neural responses to pulse trains requires either active nerve fibre models or stochastic nerve models, the latter of which have mainly been implemented as models of single nodes or fibres (Bruce et al., 1999a; Bruce et al., 1999b; Rubinstein et al., 1999; Imennov and Rubinstein, 2009; Woo et al., 2010). Furthermore, active nerve models also enable the simulation and validation of electrically evoked compound action potentials (eCAPs) (Briaire and Frijns, 2005; 2006; Whiten, 2007; Smit et al., 2009; Westen et al., 2011; Choi and Wang, 2014).

Computational models are well suited to provide insight into the underlying mechanisms of cochlear stimulation. Furthermore, they can be used to simulate various types of experiments that are impractical or impossible to perform in cochlear implant patients or animal models. For example, new types of electrode arrays can be tested and experimental stimulation paradigms can be evaluated iteratively, without the need for human or animal test subjects, or any of the practical requirements for performing *in vivo* tests. The aim of the present paper is to review the modelling studies that have been performed over the years to gain insight into stimulation strategies and electrode designs.

2 Multipolar stimulation

Multipolar stimulation has been a major theme throughout cochlear implant modelling research. In the years before the now commonly used Continuously Interleaved Sampling (CIS) strategy (Wilson et al., 1991), there was much interest in multipolar stimulation as a way of reducing the extensive electrical interaction inherent in simultaneous monopolar

stimulation, which was hampering cochlear implant performance at the time. However, even though the majority of modern clinical stimulation strategies avoid simultaneous activation of cochlear implant electrode contacts, multipolar stimulation has continued to be of interest in the research field, particularly as a means of producing more localised regions of neural excitation in order to increase spatial selectivity (current focussing).

In this section we will be reviewing modelling studies which have investigated various forms of multipolar stimulation. As will be shown, the most commonly investigated multipolar configurations have been bipolar and tripolar stimulation. In bipolar stimulation, two intracochlear electrode contacts are stimulated in opposite polarity, which causes no net current to leave or enter the cochlea (figure 2.5a). In tripolar stimulation, three intracochlear contacts are stimulated, one of which is considered the centre contact and the other two flanking/inhibiting contacts that stimulate at a polarity opposite to that of the centre contact (figure 2.5b). The current amplitudes injected on the flanking contacts are half that of the centre contact, so that, as in bipolar stimulation, the net current in the cochlea is zero.

Other multipolar configurations have simulated as well, one of which is called the partial tripole (figure 2.5c). Partial tripolar stimulation is, as the name implies, essentially a mitigated version of tripolar stimulation, where the current amplitude of the flanking

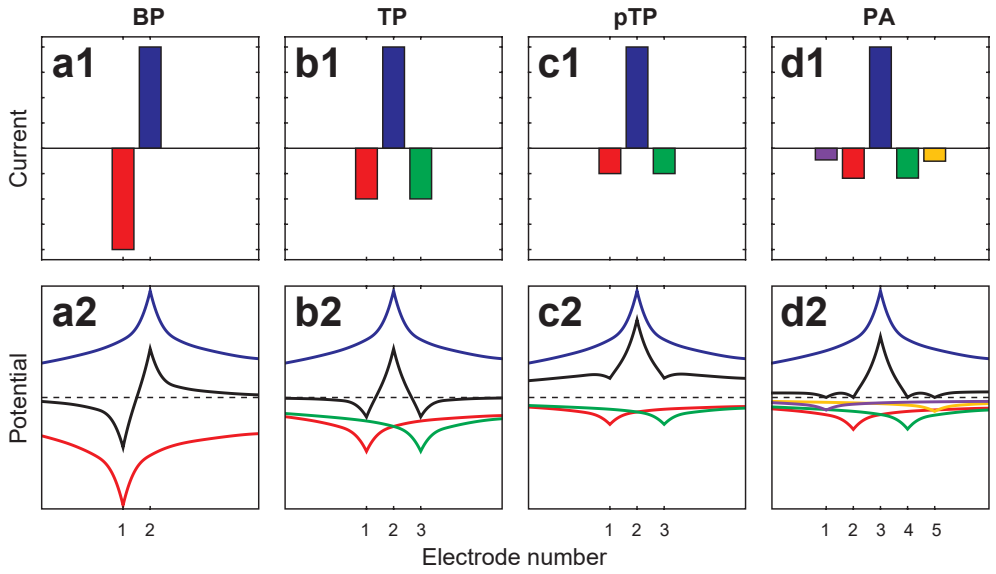

Figure 2.5. *Schematic illustration of different multipolar strategies: bipolar stimulation (a1&a2), tripolar stimulation (b1&b2), partial tripolar stimulation with σ = 0.5 (c1&c2), and phased array stimulation for an electrode array with five contacts (d1&d2). The top figures (a1–d1) show the stimulus current amplitudes used for each multipolar strategy, and bottom figures (a2–d2) show the resulting electrical potentials along the electrode array for each individual contact (blue, red, green, purple, and orange curves), as well as their combined potential (black curve).*

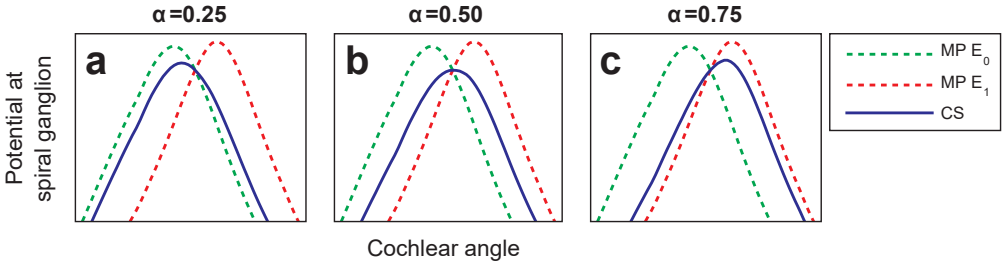

Figure 2.6. *Schematic illustration of the current steering strategy. The curves show the electrical potential along the spiral ganglion generated by two electrode contacts, labelled E0 and E1, stimulated individually in monopolar mode (green and red dotted curves), and stimulated together as a current steered electrode pair for different values of α (blue curves). Figure a, b, and c show the potentials at α = 0.25, α = 0.5, and α = 0.75, respectively. Since the monopolar curve for E0 (green) is essentially the current steered potential for α = 0 and the curve of E1 (red) is that of α = 1, it is clear that the current steered curve (blue) gradually shifts from the monopolar field of E0 to that of E1 as the value of α increases. Note that although the peak of current steered potential is lower for intermediate values of α, this does not necessarily imply that the neural threshold is also lower.*

contacts is multiplied by a fraction, usually denoted as σ. This means that the net current injected into the cochlea is not zero, but that part of the current, equal to (1- σ) times the amplitude of the centre contact, leaves or enters the cochlea to or from the return electrode. Note that by this definition σ=1 results in a normal tripole, while σ=0 simply amounts to monopolar stimulation.

Another, relatively new, multipolar configuration is referred to as phased array stimulation (figure 2.5d), which was proposed in a study by Van den Honert and Kelsall (Van den Honert and Kelsall, 2007), though its concept traces back to the work of Van Compernolle (1985). In phased array stimulation, all contacts of the array are stimulated in such a way that the electrode potentials are zero everywhere except at one specific contact, which we will designate the centre contact (though it need not be located in the centre of the array). The currents required to achieve this are computed using an impedance matrix, determined by recording electrode potentials for each stimulating contact of the array.

The aforementioned multipolar configurations are all used as a means of current focussing; however, other applications for multipolar stimulation exist. In this section we will also encounter the so called current steering paradigm (figure 2.6), also referred to as simultaneous dual electrode stimulation. In current steering, two electrode contacts are stimulated at equal polarity, with the current amplitudes of both controlled by a parameter that is usually denoted as α. The current amplitude on one of the contacts is then equal to a base value multiplied by α, while the amplitude of the other contact is equal to a base value multiplied by (1- α). This means that increasing the value of α from 0 to 1 will gradually shift the potential field from one electrode to the other, with the intent of creating 'virtual channels' that lie in between the two stimulating contacts.

2.1 Multipoles in simple mathematical models

The earlier lumped parameter modelling studies examined electric potentials from monopolar and bipolar stimulation in the cochlea and compared them to electrophysiological experiments in cats (Black and Clark, 1980; Black et al., 1983; O'Leary et al., 1985). They came to the conclusion that bipolar stimuli produced sharper, more localised potentials than monopolar ones did. Furthermore, Black and Clark observed that the spread of current through the cochlear scalae could be quite different than the current spread in other parts of the cochlea, such as the organ of Corti (Black and Clark, 1980), which underlined the usefulness of modelling as a way of estimating electrical field distributions in cochlear locations that are difficult or impossible to access clinically or electrophysiologically.

Spelman et al. performed several modelling studies which explored the possibilities of multipolar stimulation. In the first, Suesserman and Spelman examined potentials at the organ of Corti induced by parallel stimulation of bipolar and (partial) tripolar configurations in a lumped parameter model of the first turn of the guinea pig cochlea, with the goal of determining independent channels that could safely be stimulated simultaneously (Suesserman and Spelman, 1993). Their results showed that bipolar stimuli produced localised potential peaks at the organ of Corti, and suggested that tripolar configurations would be capable of generating peaks that were even sharper than those of bipolar stimuli.

Since it was apparent that multichannel cochlear implants were able to shape potential fields by parallel stimulation of channels, Rodenhiser and Spelman investigated the possibility of creating focussed electrical fields calculated from impedance data of individual cochlear implant electrode contacts (Rodenhiser and Spelman, 1995). Based on the work of Van Compernolle (1985), they used their lumped parameter model to calculate potentials induced along the organ of Corti by each electrode contact and used them to define an impedance matrix. This impedance matrix was then used to find the optimal combination of driving currents necessary to generate potentials that were similar to a desired potential curve, by employing the least-squares method. The results indicated that current focussing using impedance data was a promising technique, but the authors noted that the smaller potential peaks induced by focused stimuli might make them too electrically inefficient or even unsafe to use in clinical practice.

In their third modelling study, Spelman et al. (1995) combined insights from their lumped parameter model with an analytical model of the neural activation function and electrophysiological measurements performed in monkeys and guinea pigs. The study used monopolar and bipolar stimuli, in addition to what they referred to as 'quadrupolar' stimulation, which is nowadays known as tripolar stimulation (Spelman et al. reasoned that it can be seen as two dipoles, with one of the polarities from both dipoles physically overlapping each other). They found that, when comparing tripolar to monopolar stimulation, the model did not agree very well with psychophysical thresholds measured in monkeys. They hypothesized that this disagreement was due to separate areas of excitation caused by the two inhibiting flanking electrodes of the tripolar configuration. This hypothesis was further elaborated on by Clopton and Spelman in an accompanying neural modelling study

(Clopton and Spelman, 1995). Results from guinea pig measurements from Spelman et al. (1995) also supported the idea that current steering and current focussing were feasible with cochlear implants, although with certain constraints.

The final modelling study from Spelman et al. investigated tripolar stimulation once more (which was again referred to as quadrupolar stimulation), for which they used both an analytical model of point sources located in an infinite homogeneous isotropic medium as well as their lumped parameter model (Jolly et al., 1996). Their results reiterated the idea that tripolar stimulation has reduced current spread and electrical channel interaction, making parallel stimulation feasible and possibly improving pitch and electrode pair discrimination. However, their results again suggested the possible presence of 'side-lobes': secondary areas of excitation near the flanking contacts.

In 2007, Litvak et al. published a joint modelling and psychophysical study on loudness growth with partial tripolar stimulation (Litvak et al., 2007). Their model had a straightforward approach similar to the analytical part of Jolly et al.'s model, describing point sources located in an infinite homogeneous medium at a parametric distance from neuronal elements. They calculated neural activation functions for partial tripolar stimulation, while varying the parameter σ, the electrode-neuron distance, and changing the spacing between the centre contact and flanking contacts. Their psychophysical experiments consisted of loudness balancing of partial tripolar stimuli in seven subjects for different values of σ and flanking electrode spacing. They found that for increasing values of σ more current was needed to achieve comfortable loudness, to the point where in some subjects the compliance limits of the implant were reached. This effect was generally greater when there was more electrical interaction between the stimulating contacts, such as for larger electrode-neuron distances or smaller electrode spacing. However, they also found that in some cases the increase in required current diminished at higher values of σ, which their modelling results suggested was due to the occurrence of side lobes. They concluded that (partial) tripolar stimulation reduced spatial selectivity and that choosing an optimal value of σ could help avoid possible side-lobe excitation and keep stimulation within compliance limits.

The next year, Bonham and Litvak presented another study, which not only looked at dipoles and (partial) tripoles, but also at current steering (Bonham and Litvak, 2008). The study contained data from modelling, electrophysiology and psychophysics, in addition to reviewing earlier studies. They used a FEM model with a simple geometry of a conductive tube representing the scala tympani which contained several spherical electrodes, and which was located in an infinite homogeneous medium. Neural activation functions were determined along rudimentary neural trajectories located outside the tube, orthogonal to its axis. Concerning (partial) tripoles, Bonham and Litvak's observations were in agreement with Litvak et al.'s findings; however, the novelty of the study was in its findings on current steering. Modelling results showed that it was possible to steer the electric potential and the region of neural excitation, which was confirmed by electrophysiological data in the inferior colliculus. Bonham and Litvak concluded that a combination of current focussing and steering might improve cochlear implant perception.

Goldwyn et al. used a similar geometrical set-up for their modelling study on partial tripolar stimulation, however, instead of using the FEM, they derived an analytical solution of the electric potential distribution generated by point sources in an infinite tube, and used it to determine activation functions (Goldwyn et al., 2010). Goldwyn et al. looked at partial tripoles at different electrode positions and included localised degeneration in their neural distribution. Results were in general agreement with previous studies, and they additionally showed that (partial) tripoles were sensitive to dead neural regions, as spatially restricted excitation region of a tripole could conceivably overlap with an area of neural degeneration. This led Goldwyn et al. to speculate that (partial) tripolar stimulation could be used be used clinically to locate possible neural dead regions in cochlear implant patients.

2.2 Multipoles in volume conduction models of the cochlea

Finley et al. investigated four bipolar configurations in their three-dimensional volume conduction model of the unrolled human cochlea (Finley et al., 1990). First they examined a 'pure radial' bipolar set-up, where two stimulating plate contacts were located at the same insertion depth, in other words in the same mid-modiolar cross-section. Secondly they used a 'pure longitudinal' set-up, where the two contacts were separated along the length of the scala tympani. Their third configuration was the 'offset radial' set-up, which was a combination of radial and longitudinal spacing of the two contacts. Their fourth configuration was bipolar stimulation of two banded contacts spaced longitudinally. In the banded configuration, the electrode array was located along the lateral wall; in the other three configurations the array was located along the modiolar wall. Their results suggested that a pure radial set-up was the most capable of localised neural stimulation, but they noted that their results were strongly dependent on the presence of the neural peripheral processes. The main conclusion from Finley et al. was that, while the basic principles involved in electrical stimulation of the auditory nerve were simple, combining electrical field generation with neural activation could cause complex results. Electrical fields depended heavily on electrode configuration and the neural responsiveness depended on the morphological and electrophysiological details of the nerve fibres. Nonetheless they expressed confidence that an understanding of the mechanisms behind cochlear implant functioning would lead to better electrode designs and stimulation strategies.

In 1995, Frijns et al. investigated longitudinal bipolar stimulation in a rotationally symmetric representation of the guinea pig cochlea (Frijns et al., 1995). Their model used the Boundary Element Method (BEM) to compute electric potentials generated by bipolar current sources; these potentials were then used as input for a deterministic active nerve fibre model of the auditory neurons of the guinea pig, which was a generalised version of the Schwarz-Eikhof-Frijns (SEF) model, called gSEF. Excitation patterns showed two distinct areas of excitation near the current sources, and that this excitation was largely occurring at the neural peripheral processes, especially at lower stimulus levels. Furthermore, the rotational nature of the model had introduced so-called ectopic or cross-turn stimulation into the model; at high current levels, fibres belonging to cochlear turns that did not

contain current sources were being stimulated, due to the relatively close spacing of the neural axons in the cochlear modiolus.

Frijns et al. expanded on the study by examining radial dipoles as well as longitudinal dipoles in the same cochlear geometry (Frijns et al., 1996), showing that radial dipoles excite neurons at lower thresholds than longitudinal dipoles. They also concluded that, unlike longitudinal dipoles, radial dipoles do not generate separated regions of excitation near the current sources. However, experiments with different pulse shapes revealed that the use of monophasic pulses could reduce one of the two regions of excitation in longitudinal bipolar stimulation, due to the fact that neural excitation thresholds for anodic pulses were generally higher than for cathodic pulses; this increased spatial selectivity and could potentially double the number of non-overlapping stimulation sites. Since monophasic pulses are considered unsafe for long term *in vivo* stimulation, Frijns et al. suggested mimicking monophasic stimulation by using charge-balanced asymmetric biphasic pulses (nowadays referred to as pseudo-monophasic pulses), which was shown to produce equivalent results in the model. It should be noted, however, that in Frijns et al.'s model the neurons were more sensitive to cathodic pulses than to anodic pulses, while later experiments in human subjects have shown the opposite effect (Macherey et al., 2008; Macherey et al., 2010); this discrepancy in the computational model has not yet been fully explained.

A subsequent paper updated their guinea pig cochlea to a tapered spiralling geometry (Briaire and Frijns, 2000) and found comparable results, including the presence of ectopic stimulation. The tapered spiralling geometry allowed the cochlear scalae to act as a transmission line along the entire length of the cochlea, and resulted in asymmetric potential distributions. The study also looked more closely at the near-field potentials of current sources in the scala tympani and found that while scalar potentials roughly followed an exponential decay in the far field (as was widely assumed in preceding lumped parameter models), cochlear potentials near the current source contained an additional spherical component. The cochlear geometry of Frijns et al. would be further updated to human anatomy and a geometrical representation of an electrode array a year later (Frijns et al., 2001).

Around the same time, Hanekom published a model of the implanted human cochlea (Hanekom, 2001). Hanekom's model contained a spiralling (but not tapered) FEM geometry of the first one and a half turn of the human cochlea, complete with electrode arrays modelled in either lateral or medial position, and was coupled with a neural model which was based on the gSEF model of Frijns et al. (1995; 1996). The electrode configurations modelled by Hanekom were reminiscent to those of Finley et al. (1990); longitudinal bipolar stimulation, radial stimulation, offset radial stimulation and pseudo-monopolar stimulation (i.e., monopolar stimulation with a distant, but intracochlear, reference contact) were simulated, at different electrode spacings and using plate contacts as well as banded contacts. As in the studies above, ectopic stimulation and asymmetric potential distributions were observed, and results showed that longitudinal dipoles generated two areas of excitation, while radial dipoles did not. Additionally, threshold levels for bipolar

stimulation were higher than those of pseudo-monopolar stimulation, and increased as the spacing between the two stimulating contacts decreased.

Also in that year, Rattay et al. presented another cochlear implant model containing a tapered spiralling FEM geometry of the implanted human cochlea (Rattay et al., 2001a). Neural simulations were performed using a deterministic nerve fibre model presented in a companion study (Rattay et al., 2001b). The study examined monopolar, bipolar and tripolar stimulation; their results were consistent with the idea that bipolar and tripolar stimulation has higher thresholds, but narrower spread of excitation. They also concluded that the spatial trajectories of auditory nerve fibres are of importance when modelling electrically induced neural excitation in the cochlea, as strongly curved parts of the neurons were found to be easier to excite.

More insights would follow from the PhD thesis of Whiten, which presented comprehensive modelling work of the implanted cochlea (Whiten, 2007). Unlike the geometries of previous volume conduction models, which were created by interpolating single histological slices, Whiten's geometry was based on high resolution imaging and three-dimensional segmentation of the temporal bones of two implanted patients. Electrical field distributions were calculated using the Finite Difference Method (FDM), and were used in conjunction with a deterministic gSEF-based nerve fibre model. Whiten also had access to a wealth of objective and psychophysical data obtained from the two temporal bone subjects, which were used to validate the model. The study suggested that the electrical resistivity value of the temporal bone surrounding the human cochlea was about ten times higher than the value used in previous models, which was derived from electrophysiological measurements in guinea pigs (Suesserman, 1992). Later modelling studies would also re-evaluate the electrical resistivity of temporal bone based on clinical intracochlear potential recordings, and arrived at the same conclusion, with comparable resistivity values (Kalkman et al., 2014; Malherbe et al., 2015). Because of the tenfold increase in temporal bone resistivity, Whiten found much wider spread of excitation for monopolar and bipolar stimulation than previous modelling studies, due to the increased electrical insulation of the cochlear scalae. Whiten also presented data for partial tripolar stimulation (referred to as 'hybrid-quadrupolar'), and observed that it was successful at focussing the electrical current density, but that side lobes would emerge at (nearly) full tripolar stimulation.

A 2011 modelling study by Frijns et al. investigated phased array stimulation in a human cochlear geometry (Frijns et al., 2011), which showed neural excitation patterns that were considerably more narrow than monopolar stimulation patterns, albeit at higher threshold levels. The results also suggested that phased array channels could maintain their spatial selectivity during parallel stimulation, and that it was less prone to producing side lobes than tripolar stimulation. The study concluded that phased array stimulation, while requiring more electrical power than monopolar stimulation, was more energy efficient than tripolar stimulation and was therefore less likely to exceed compliance limits.

A subsequent modelling study from the same group examined various current focusing strategies in an updated version of their model (Kalkman et al., 2015). The model had

previously been updated to include four different human cochlear geometries, two of which were based on µCT imaging, as well as using more realistic nerve fibre trajectories and modified tissue conductivities, which were derived from patient-specific modelling of intracochlear potentials (Kalkman et al., 2014). The 2015 study on current focussing strategies added a realistic spatial distribution of the auditory neurons' cell bodies, which meant that they were not linearly aligned, as they had been in all previously published modelling studies, but were spread out in the spiral ganglion, essentially filling up Rosenthal's canal in the modiolus. Spatial selectivity of stimuli was expressed in terms of excitation density: the percentage of neurons excited at a specific length along the spiral ganglion (figure 2.7). This showed that current focussing strategies, such as (partial) tripolar stimulation and phased arrays, are capable of penetrating the spiral ganglion more

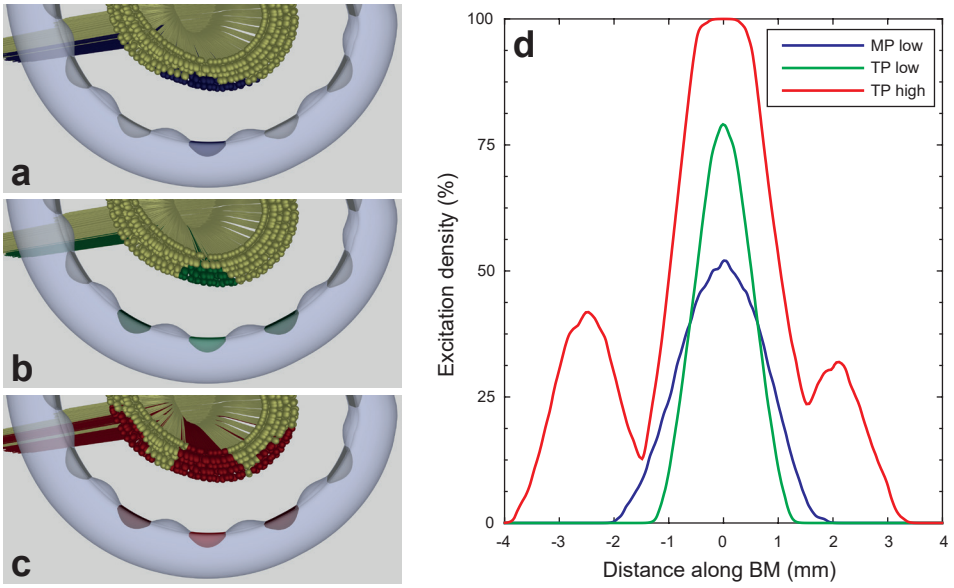

Figure 2.7. *Illustration of excitation patterns and excitation density plots from Kalkman et al. (2015). Figures a–c show neural excitation patterns in auditory neurons with degenerated peripheral processes for three different situations: (a) monopolar stimulation at low amplitude, (b) tripolar stimulation at low amplitude, exciting the same number of neurons as the monopolar stimulus above, and (c) tripolar stimulation at high amplitude. Blue, green, and red fibres in Figures a, b, and c indicate excited neurons. In Figure d, the corresponding excitation density curves are plotted, which show the percentage of neurons that are being excited along the cochlea. The blue curve corresponds to the monopolar excitation pattern shown in Figure a, the green curve to the low amplitude tripolar excitation pattern shown in Figure b, and the red curve corresponds to the excitation pattern generated by high-amplitude tripolar stimulation shown in Figure c. Comparing Figures a and b and their curves in Figure d, it is clear that tripolar stimulation excites neurons in a more spatially restricted pattern than monopolar stimulation does with the same number of excited neurons. In Figure c and the red curve in Figure d, the excitation pattern produced by a high-amplitude tripolar stimulus reveals the presence of side lobes on either side of the main excitation region, close to the flanking contacts.*

deeply than monopolar stimulation, when exciting the same number of auditory neurons (figure 2.7a,b,d). Previous modelling studies had also shown current focussing strategies exciting a larger number of neurons at a location close to the stimulating contacts, but had expressed it in terms of stochastic response of linearly aligned neurons (Litvak et al., 2007; Goldwyn et al., 2010), while Kalkman et al. presented it as a purely spatial effect, using deterministic nerve fibres. Additionally, as in the modelling studies before it, the side lobe effect for tripolar stimulation was demonstrated (figure 2.7c and d) and it was again shown, in both modelling results as well as (preliminary) psychophysical loudness growth curves, that current focussing strategies require more power to achieve sufficient loudness levels than monopolar stimulation. Furthermore, the study reiterated the idea that, for current focussing to be effective, a sufficient level of electrical channel interaction was needed at the site of neural stimulation.

Aside from current focussing, there have also been several modelling studies that have investigated the subject of current steering. Choi and Hsu presented a study that examined current steered potential fields and activation functions in a half-turn rotational FEM geometry of the human cochlea (Choi and Hsu, 2009). The results of the study showed gradually shifting activation function curves when varying the value of the current steering parameter α.

In the same year, Frijns et al. published a modelling study on current steering, which they referred to as dual electrode stimulation (Frijns et al., 2009b). The study looked at excitation patterns generated by current steered stimuli, using both simultaneous stimulation of the current steering electrode pair, as well as rapid sequential stimulation of the contacts. The study identified two current steering modalities; the first consisted of a single region of neural excitation that shifted gradually from one electrode contact to another, which could be considered the intended goal of current steering. In the second modality, there were two areas of excitation, one of which would diminish as the other expanded while increasing or decreasing α. The first modality mainly occurred for high stimulus levels, using simultaneous stimulation of electrode contacts with a large degree of electrical interaction, for example, closely spaced or lateral wall contacts. The second modality often occurred at low stimulus levels, for sequential stimulation and in cases where the peripheral processes were the main sites of excitation. Furthermore the study showed that for sequentially stimulated current steering loudness correction was needed at intermediate values of α, whereas simultaneous current steering required almost no correction of injected current to maintain constant loudness across the total range of α.

A later study used the same model in conjunction with psychophysical testing in twelve implanted subjects, involving loudness balancing for current steered stimuli near threshold level, rather than at maximum comfortable loudness (MCL) level (Snel-Bongers et al., 2013). Psychophysical loudness correction factors were plotted against α, which were triangular in shape for most subjects, comparable to correction factors determined at MCL for sequentially stimulated current steering in earlier experiments (Frijns et al., 2009b); in other words, for α=0.5 more current was needed to achieve threshold than for other values of α. For some subjects however, the loudness balancing curve showed a dip

around α=0.5; modelling results indicated that this was consistent with the dual excitation region modality described in Frijns et al. (2009b). Modelling results also suggested that the occurrence of the dip could be related to the degree of degeneration of the peripheral neural processes, especially the unmyelinated terminal, which is suspected of being the primary site of neural degeneration after, for example, noise trauma (Kujawa and Liberman, 2009; Lin et al., 2011).

3 Electrode design

Design of the electrode array itself has been another important subject of modelling research, with the main points of interest being determining the optimal distance from the modiolar wall and insertion depth of the electrode array. By their nature, the early lumped parameter model were not suitable for investigating the effects of array design, so it was not until the advent of three-dimensional volume conduction modelling that electrode design aspects could be tested in computational models.

The first three-dimensional modelling study that looked at the effect of electrode position was that of Finley et al. (1990). They had placed the banded electrodes in their study along the lateral wall of the cochlear geometry, while their array with plate electrode contacts was in a perimodiolar position. Though this meant that the results conflated the effects of electrode size, shape and location, they did observe that the laterally placed banded contacts produced more broadly spreading electrical fields and lower activation function amplitudes than the medially placed array, which suggested higher neural thresholds and larger spread of excitation.

In the rotationally symmetric cochlea models of Frijns et al., point sources were placed inside the scala tympani in lateral, midscalar and medial position, as well as underneath the osseous spiral lamina (Frijns et al., 1995; Frijns et al., 1996), similar to cat experiments performed by Shepherd et al. (1993). Consistent with the physiological cat data, neural excitation thresholds decreased as the current sources were placed close to the modiolus; the lowest thresholds were found for the current source underneath the osseous spiral lamina, provided the neural peripheral process was present. A later study investigated the effect of lateral and medial placement of an electrode array in spiralling geometries of the guinea pig and human cochlea (Frijns et al., 2001). Instead of using ideal point current sources, a geometrical representation of the Clarion HiFocus electrode array both with and without a positioner was used. Monopolar stimulation in the basal turn of the human cochlear geometry showed lower thresholds for medial arrays, with higher spatial selectivity. However, after the basal turn this reduction of threshold was considerably smaller, while at the same time the model predicted that apical contacts close to the modiolus were more likely to produce ectopic stimulation than those located along the lateral wall. This led Frijns et al. to conclude that a perimodiolar placement of the array was beneficial in the basal turn, but that it should be avoided in more apical parts of the cochlea. Furthermore, it was observed that the positioner was able to electrically insulate apical regions of the cochlea from current injected in the basal turn.

In the same paper, comparison of the results from the human geometry to those from the guinea pig geometry revealed that differences in anatomical features between the two cochleae, specifically the size and shape of the basal turn, had notable effects on the neural excitation patterns. In particular, ectopic stimulation was affected, having a higher chance of occurring in the basal turn of the guinea pig cochlea than in that of the human cochlea. These differences underlined the importance of using species-specific cochlear geometries in models, and urged caution in interpreting data from animal studies when applying them to human situations.

Hanekom's 2001 study found similar results in their spiralling geometry, and concluded that medial placement of the array was preferable to lateral placement, due to lower thresholds, better spatial selectivity and a smaller reliance on the presence of the neural peripheral processes (Hanekom, 2001). In a subsequent study, Hanekom also investigated the effect of adding encapsulation tissue around the electrode array, modelled as a 50 μm layer of fibrous tissue, which surrounded the electrode array either directly, or with a 50 μm layer of perilymph in between the array and its encapsulation (Hanekom, 2005). Results showed that without a layer of perilymph, the encapsulation tissue caused lower thresholds, and a reduction in spread of excitation, while with the layer of perilymph the effects on threshold and spread of excitation were small and inconsistent. Furthermore, Hanekom found that changes in threshold due to encapsulation were stronger for medial arrays than for lateral ones.

Briaire and Frijns followed with a study on neural degeneration in the human cochlea, where neural excitation for lateral and medial electrodes was simulated for intact neurons and for neurons with completely degenerated peripheral processes (Briaire and Frijns, 2006). The study reiterated the results of Frijns et al. (2001), and the idea that lateral arrays are more likely to excite neurons at their peripheral processes, which makes thresholds and spatial selectivity of lateral contacts more sensitive to neural degeneration than those of perimodiolar electrodes.

Though the modelling work of Whiten (2007) also predicted lower thresholds and increased spatial selectivity for medial electrodes, the effect was much smaller than it was for previous modelling studies. Whiten attributed this difference to using a higher temporal bone resistivity, which caused more current to flow in longitudinal direction along the scala tympani compared to other models. In most modelling studies that followed, however, the electrode's distance from the modiolar wall or neural elements remained an important parameter that affected modelling outcomes. In particular, the results of the subsequent studies on multipolar stimulation, described in sections 2.1 and 2.2, generally agreed that increasing the electrode-neuron distance caused more electrical interaction to occur at the excitable elements, which was considered beneficial for current focussing and steering purposes (Litvak et al., 2007; Choi and Hsu, 2009; Frijns et al., 2009b; Goldwyn et al., 2010; Frijns et al., 2011; Kalkman et al., 2015).

In a series of five papers published in 2009, Cohen presented a stochastic model of electrical stimulation in a population of single node fibres (Cohen, 2009a; b; c; d; e). In the second paper of the series, Cohen simulated electrical potentials in a rotationally

symmetric FEM model of a single turn of the human cochlea, containing either a Nucleus straight array or a Nucleus contour array (Cohen, 2009b). Results showed that, at the neural elements, the contour array produced electrical potential distributions that were higher and sharper than those of the more laterally located straight array. Despite its relatively simple representation of both the cochlea and the nerve fibres, Cohen's model was able to describe data from eCAP masking experiments and loudness growth functions of individual patients quite well.

Another 2009 modelling study investigated the effect of otosclerosis on facial nerve stimulation by cochlear implants, using Frijns et al.'s computational model (Frijns et al., 2009a). Thresholds were determined for auditory nerve and facial nerve stimulation, for lateral and medial electrodes, with either plate contacts, half-banded contacts or full-banded contacts. To model the effects of otosclerosis, the conductivity of the temporal bone surrounding the cochlea was varied. Results of the study reinforced the intuitively obvious clinical observations that lateral wall electrodes are more likely to stimulate the facial nerve than medially placed electrodes, and that full banded contacts are more likely to produce facial nerve stimulation than plate contacts or half-banded contacts that faced the modiolus. Furthermore, lowering the conductivity of temporal bone in the model increased the likelihood of facial nerve stimulation; the novel insight, however, was that this was not so much due to the lowering of facial nerve thresholds (as was commonly thought) as it was due to the raising of auditory MCL levels.

More recently, the updated Frijns et al. model was used to predict pitch percepts in cochlear implant induced hearing (Kalkman et al., 2014; Van der Marel et al., 2016). Instead of using radial nerve fibre trajectories, as in earlier studies, the nerve fibres in this study were given realistically curved trajectories which took the length difference between the organ of Corti and the spiral ganglion into account, based on histological data (Stakhovskaya et al., 2007). Pitch percepts were predicted based on neural excitation patterns in four different cochlear geometries, induced by lateral and medial electrode contacts of up to 805° insertion depth; nerve fibres were modelled both with and without peripheral processes. The study found that simulated pitch percepts in the first cochlear turn were more or less the same for lateral and medial contacts, and followed the pitch predicted by direct application of the Greenwood function to the electrodes' positions in the cochlea. Furthermore, Kalkman et al. found that beyond the first cochlear turn, medial electrodes tended to produce lower pitch percepts than lateral ones when the peripheral processes were intact. Intuitively this made sense, considering the closer proximity of the medial electrode to the spiral ganglion. However, predicted pitch of the medial electrodes generally did not reach values expected from direct spiral ganglion stimulation as long as the peripheral processes were present. Without peripheral processes, lateral and medial pitch percepts were very similar, and more closely followed the pitch expected from direct spiral ganglion stimulation. Electrode contacts located deeper than approximately 540° from the round window (which was near the end of the spiral ganglion in the model) produced unpredictable pitch percepts that were spectrally broad and showed considerable overlap with their neighbouring contacts, which called their usefulness into question.

A 2010 psychophysical study by Carlyon et al. used an earlier iteration of the same computational model to compare data from pitch matching experiments to model predictions, and found that they were in good agreement (Carlyon et al., 2010). However, the test subjects' electrodes that were used in the pitch matching experiments were all located in the first cochlear turn, so modelling results in apical regions of the cochlea could not be validated.

Finally, while the above studies have all examined the influence of electrode design on cochlear electrical fields and neural excitation, cochlear implant modelling studies that investigate the fundamental processes occurring at the electrode contacts themselves are surprisingly rare. Additionally, all of the previously described volume conduction models employ the quasi-static approximation of assuming that the electrode array and all of the cochlear structures are purely resistive. In reality, there is an electrochemical interface impedance at the boundary between stimulating contacts and the scalar perilymph, which has a capacitive component (Vanpoucke et al., 2004). Lai and Choi proposed a method to implement this interface impedance into FEM models of the implanted cochlea (Lai and Choi, 2007). In a spiralling geometry of an implanted human cochlea, they modelled the interface as a thin 50 μm layer on the surface of the electrode contacts, which had a complex permittivity value. The study used geometrical representations of half-banded, full-banded and flat plate contacts, and showed that the interfacial layer produced the same potentials as their equivalent electrical circuits. Plots of the neural activation functions suggested that the electrochemical interface impedance could have an influence on neural excitation, though the nature and extent of this influence was not clear.

To assess the current density distribution on platinum electrodes used for electrical stimulation of neurons, Rubinstein et al. (1987) developed a model of disc-shaped electrode contacts, both surface mounted and recessed into the electrode carrier. The model numerically solved Laplace's equation for the quasi-static electrical fields using a Green's function approach, and found that the current density across the electrode contact was not uniform, with the current density increasing as one gets closer to the edge. The model also showed that recessing the electrode would make the current density distribution more uniform, which was deemed advantageous, since non-uniform current distribution could locally exceed electrochemical safety limits near the edge of the electrode.

Recently, Sue et al. have presented modelling work on the effects of electrochemical processes and electrode recession on current distributions across half-banded platinum contacts embedded in an electrode carrier, located in a perilymph-filled cylindrical geometry representing the cochlear scalae (Sue et al., 2013; Sue et al., 2015). Their results showed that faradaic current density was dependent on time, and that, in accordance with Rubinstein et al. (1987), it was not uniform across the electrode contact, with current densities being higher at the corners of the half-banded contacts. However, Sue et al. again showed that these concentrations of current could be mitigated by recessing the contact into the carrier, though the improvement was more modest than it was for Rubinstein et al.'s model.

4 Discussion

4.1 Computational modelling of stimulation strategies and electrode design

It has become clear that most of the general properties of multipolar stimulation can be understood readily using simple mathematical models of unrolled cochleae. These models can successfully simulate electrical field interaction of electrode contacts, and thereby describe sharpening of the fields due to current focussing techniques quite well (Black and Clark, 1980; Black et al., 1983; O'Leary et al., 1985; Suesserman and Spelman, 1993; Rodenhiser and Spelman, 1995; Spelman et al., 1995; Jolly et al., 1996; Kral et al., 1998; Litvak et al., 2007; Bonham and Litvak, 2008; Goldwyn et al., 2010). When including an estimate of neural excitation through the activation functions, these models can even predict certain features of multipolar stimuli, such as increased localisation of the excitation patterns and the presence of side lobes due to neural excitation near the flanking contacts in tripolar stimulation. Using a more realistic volume conduction model will create a more detailed view of intracochlear potentials and neural excitation; a rotationally symmetric geometry will reveal the possibility of ectopic stimulation at high stimulus amplitudes (Frijns et al., 1995). A spiralling geometry, will additionally show asymmetrical potential distributions through the cochlea (Briaire and Frijns, 2000). However, while realistic volume conduction models are quantitatively more accurate, qualitatively speaking mathematical models are sufficient for a basic understanding of multipolar stimulation strategies. This also strengthens confidence that modelling predictions on multipolar stimulation can be trusted, as they generally agree with each other and make sense from an electrophysical point of view, making it unlikely that such predictions are a result of modelling artefacts.

For matters concerning electrode design, the applicability of simple mathematical models is more limited; while simple models can shed light on the basic consequences of moving the current sources towards the neural elements (i.e., lower thresholds and less spread of excitation), other aspects of electrode design require a realistic three-dimensional volume conduction model of the implanted cochlea. For instance, investigating the effects of changing electrode shape and size in a computational model requires the actual electrode geometry to be represented accurately and not simply reduced to point sources in the scala tympani; this has previously allowed for the investigation of the insulating effects of positioner systems (Frijns et al., 2001) and the probability of facial nerve stimulation by different electrode contact geometries (Frijns et al., 2009a). Furthermore, understanding the effect insertion depth has on neural excitation requires not only a realistic cochlear geometry, but also an accurate modelling of neural trajectories, since these vary considerably over the length of the cochlea, which, in turn was shown to have serious implications for neural recruitment by electrical stimulation (Kalkman et al., 2014).

It should be noted that, while there are many modelling studies that have shown the effect of electrode position in the scala tympani, there have not been many investigations on the shape and size of electrode arrays. Most modelling studies only use one type of electrode array, and the few that use multiple geometries have not made an extensive comparison of different arrays. It is unclear what the reason for this could be; possibly, the electrode

geometry is thought to have little effect on neural excitation, or at least not as much as other factors. Alternatively, the modelling of different electrode geometries could be considered too laborious and time-consuming to be worth the effort. Whatever the case, it is conceivable that there are still some insights to be gained from computational modelling of different electrode array designs.

4.2 Present and future of cochlear implant modelling

Many of the past cochlear implant modelling studies, particularly the early lumped parameter models, have coupled their results with electrophysiological or psychophysical experiments. This was essential, because there is an unavoidable need to validate modelling results by comparing them to data from live subjects. After all, any computational model contains a number of assumptions and simplifications; if these are inappropriately chosen, the model's output will be misleading or outright wrong. In short, a computational model always produces results, but in order to know if one can trust these results, validation is necessary.

The most straightforward way of validation a computational model of an implanted cochlea is by comparing simulated electrical fields to electrophysiological data, since it concerns only directly measurable physical quantities and does not require interpretation of neural signals. While this type of validation is necessary and gives confidence in a model's ability to simulate the electrical properties of the cochlea, electrical field distributions in the cochlea only give limited information about how cochlear implants function. Therefore, to meaningfully investigate the subject of electrical stimulation of the cochlea, one cannot avoid including a neural model.

Most of the models discussed in this review have contained some estimate of neural activity, either by determining the activation function, or by incorporating an electrical cable model of the auditory neurons. However, validation of simulated auditory neural activity is substantially more difficult. The only objective data at one's disposal are eCAPs or electrically evoked auditory brainstem responses (EABRs), and inferior colliculus measurements in animal subjects. Even though eCAPs have been modelled successfully (Briaire and Frijns, 2005; 2006; Whiten, 2007; Smit et al., 2009; Westen et al., 2011; Choi and Wang, 2014), these types of neurophysiological data only offer indirect evidence of model validity, and can usually only verify that the model is producing realistic output in broad strokes. The only other tool available is psychophysical testing, but it has the additional drawback of involving central neural processing, while current cochlear implant models only simulate neural stimulation at the peripheral level. This means that validation will remain the primary challenge that researchers will face when enhancing their computational models in the future.

These future model enhancements will likely include adding more detail to the cochlear geometries. Advances in imaging techniques have made it relatively easy to acquire high resolution three-dimensional anatomical scans, which can be used to create new model geometries. Recent models have already used (micro-)CT data to create more realistically shaped model cochleae with individual anatomical characteristics (Malherbe et al., 2013;

Kalkman et al., 2014; Malherbe et al., 2016), while researchers at the University of Sydney are currently working on a highly detailed model based on scanning thin-sheet laser imaging microscopy (sTSLIM) of the guinea pig cochlea (Wong et al., 2016). In addition to improving the level of detail of the cochlea itself, modelling work from the past years has also seen the inclusion of detailed geometries of the human head (Malherbe et al., 2015; Tran et al., 2015). These enhancements in anatomical detail may lead to new insights regarding electrical field distributions in or around the cochlea and possibly add more realism to simulated neural excitation patterns.

Aside from purely anatomical improvements, several other more fundamental changes to cochlear implant models are possible. First, all of the models thus far have restricted themselves to using isotropic conductivity values in their geometries. This is likely sufficient for most of the cochlear structures, but neural tissue cannot be expected to conduct electrical currents equally well in all directions. Since neural tissue takes up a considerable amount of space in the cochlear modiolus and is obviously the target of electrical stimulation, adding anisotropy to volume conduction models of the cochlea could have significant impact.

Next, the majority of the models presented have employed a quasi-static approximation when calculating electrical field distributions, and have assumed that the electrical fields can be determined by simply multiplying a normalised static field with the time dependent amplitude of the electrode stimulus. This assumption was based on work by Spelman and co-workers, who showed that cochlear potentials in the scala tympani were largely independent of stimulation frequencies of up to 12.5 kHz (Spelman et al., 1982); unpublished data from their group has shown that the assumption of frequency independency is even valid up to 100 kHz (F.A. Spelman, personal communication). However, the electrochemical interface is not completely resistive, and it is possible that a small frequency-dependency of cochlear structures exists. Some investigation has been done into the electrode interface impedance (Lai and Choi, 2007; Sue et al., 2013; Sue et al., 2015), and initial work concerning frequency dependency in the implanted cochlea has been presented (Inguva et al., 2015), but an extensive analysis of the subject has not yet been performed in a full volume conduction model coupled with an active neural model.

The neural models themselves are also still improving, as there is much that is unknown concerning auditory nerve fibre morphology and kinetics. Additionally, the discussed neural models have an ongoing problem of being unable to reasonably predict realistic neural threshold levels, which are invariably higher in the models than they are in clinical reality. It is unclear what the cause of this discrepancy is, since the models do actually simulate electrophysiological experiments on single fibres quite well. To understand this, more input from the field of neurophysiology is necessary.

One obvious addition that can be made to the cochlear implant models is the inclusion of neural stochasticity. While stochasticity has been implemented in models of single nodes or fibres (Bruce et al., 1999a; Bruce et al., 1999b; Rubinstein et al., 1999; Cohen, 2009d; e; Imennov and Rubinstein, 2009; Woo et al., 2010), few of the presented cochlear implant

models have included it, instead relying on activation functions or deterministic electrical cable models of the auditory neurons. The research groups of Hanekom et al. and Frijns et al. recently presented preliminary work on extensions of their models with relatively simple models of stochasticity (Badenhorst et al., 2015; Frijns et al., 2015). Badenhorst et al. investigated the addition of stochasticity to the Hanekom model; the results of this suggested that stochastic fibres will predict more realistic neural thresholds. Frijns et al. used the thresholds calculated by their volume conduction and deterministic neural models as input for a simulation of stochastic variability, which, apart from stochastic thresholds, includes neural adaptation, refractoriness, and neural accommodation; the future goal of this extension is to make predictions on the functioning and effectiveness of speech processing strategies.

Another subject of interest is the exact nature of neural degeneration in the cochlea. Several cochlear implant modelling studies have included neural degeneration in their simulations, but most have modelled it by the complete removal of all peripheral processes from the auditory neurons. Snel-Bongers et al. discussed the possibility of gradually degenerating peripheral processes (Snel-Bongers et al., 2013), in line with findings from the Liberman group (Kujawa and Liberman, 2009; Lin et al., 2011), and only Goldwyn et al. have so far investigated the consequences of hypothetical neural dead regions (Goldwyn et al., 2010). These methods of modelling neural degeneration are somewhat speculative, as the precise mechanisms of neural degeneration in humans are still a subject of research (Kujawa and Liberman, 2009; Lin et al., 2011; Wan and Corfas, 2015).

Tangentially related to neural degeneration is the effect of electrode insertion trauma on cochlear implant stimulation. All of the modelling studies discussed in this review have exclusively used the scala tympani as the location of the stimulating electrodes, even though it is known that many cochlear implant electrode arrays end up perforating cochlear structures such as the basilar membrane and Reissner's membrane, thereby ending up in the scala vestibuli, rather than the scala tympani (Aschendorff et al., 2005; Aschendorff et al., 2007; Skinner et al., 2007; Finley et al., 2008; Holden et al., 2013; Wanna et al., 2014). The unintended position of the electrode and the potential damage to the neural elements caused by this insertion trauma could have noteworthy consequences for cochlear implant stimulation; however, no cochlear implant modelling studies have investigated this subject thus far.

In conclusion, computational modelling of the electrically stimulated cochlea has had a long history. It has been a valuable tool for the study of stimulation techniques and electrode design, enabling types of experimentation that would be difficult or impossible to achieve in clinical or laboratory conditions. There are still many issues left to be investigated and improvements to be made to existing models; the increasing availability of high-resolution imaging techniques and open sourced or commercial modelling software mean that the threshold for developing new models has never been lower, making sure that computational modelling of the electrically stimulated cochlea has a long future ahead. A crucial factor in the further application of models in clinical practice will be the validation of their outcomes and predictions.

References

Aschendorff, A., Kromeier, J., Klenzner, T., Laszig, R. 2007. Quality control after insertion of the nucleus contour and contour advance electrode in adults. Ear Hear 28, 75S-79S.

Aschendorff, A., Kubalek, R., Turowski, B., Zanella, F., Hochmuth, A., Schumacher, M., Klenzner, T., Laszig, R. 2005. Quality control after cochlear implant surgery by means of rotational tomography. Otol. Neurotol 26, 34-37.

Badenhorst, W., Malherbe, T.K., Hanekom, T., Hanekom, J.J. 2015. Development of a Voltage Dependent Current Noise Algorithm for Conductance Based Stochastic Modelling of Auditory Nerve Fibre Populations in Compound Models, Conference on Implantable Auditory Prostheses, Pacific Grove, California, USA.

Black, R.C., Clark, G.M. 1980. Differential electrical excitation of the auditory nerve. J. Acoust. Soc. Am 67, 868-874.

Black, R.C., Clark, G.M., Tong, Y.C., Patrick, J.F. 1983. Current distributions in cochlear stimulation. Ann. N. Y. Acad. Sci 405, 137-145.

Bonham, B.H., Litvak, L.M. 2008. Current focusing and steering: modeling, physiology, and psychophysics. Hear. Res 242, 141-153.

Briaire, J.J., Frijns, J.H.M. 2000. Field patterns in a 3D tapered spiral model of the electrically stimulated cochlea. Hear. Res 148, 18-30.

Briaire, J.J., Frijns, J.H.M. 2005. Unraveling the electrically evoked compound action potential. Hear. Res 205, 143-156.

Briaire, J.J., Frijns, J.H.M. 2006. The consequences of neural degeneration regarding optimal cochlear implant position in scala tympani: a model approach. Hear. Res 214, 17-27.

Bruce, I.C., Irlicht, L.S., White, M.W., O'Leary, S.J., Dynes, S., Javel, E., Clark, G.M. 1999a. A stochastic model of the electrically stimulated auditory nerve: pulse-train response. IEEE Trans. Biomed Eng 46, 630-637.

Bruce, I.C., White, M.W., Irlicht, L.S., O'Leary, S.J., Dynes, S., Javel, E., Clark, G.M. 1999b. A stochastic model of the electrically stimulated auditory nerve: single-pulse response. IEEE Trans. Biomed Eng 46, 617-629.

Carlyon, R.P., Macherey, O., Frijns, J.H.M., Axon, P.R., Kalkman, R.K., Boyle, P., Baguley, D.M., Briggs, J., Deeks, J.M., Briaire, J.J., Barreau, X., Dauman, R. 2010. Pitch comparisons between electrical stimulation of a cochlear implant and acoustic stimuli presented to a normal-hearing contralateral ear. J. Assoc. Res. Otolaryngol 11, 625-640.

Choi, C.T.M., Hsu, C.H. 2009. Conditions for generating virtual channels in cochlear prosthesis systems. Ann. Biomed. Eng 37, 614-624.

Choi, C.T.M., Lai, W.D., Chen, Y.B. 2004. Optimization of cochlear implant electrode array using genetic algorithms and computational neuroscience models. IEEE Transactions on Magnetics 40, 639-642.

Choi, C.T.M., Lai, W.D., Chen, Y.B. 2005. Comparison of the electrical stimulation performance of four cochlear implant electrodes. IEEE Transactions on Magnetics 41, 1920-1923.

Choi, C.T.M., Lai, W.D., Lee, S.S. 2006. A novel approach to compute the impedance matrix of a cochlear implant system incorporating an electrode-tissue interface based on finite element method. IEEE Transactions on Magnetics 42, 1375-1378.

Choi, C.T.M., Wang, S.P. 2014. Modeling ECAP in Cochlear Implants Using the FEM and Equivalent Circuits. IEEE Transactions on Magnetics 50, 7001004.

Clopton, B.M., Spelman, F.A. 1995. Electrode configuration and spread of neural excitation: compartmental models of spiral ganglion cells. Ann. Otol. Rhinol. Laryngol. Suppl 166, 115-118.

Cohen, L.T. 2009a. Practical model description of peripheral neural excitation in cochlear implant recipients: 1. Growth of loudness and ECAP amplitude with current. Hear. Res 247, 87-99.

Cohen, L.T. 2009b. Practical model description of peripheral neural excitation in cochlear implant recipients: 2. Spread of the effective stimulation field (ESF), from ECAP and FEA. Hear. Res 247, 100-111.

Cohen, L.T. 2009c. Practical model description of peripheral neural excitation in cochlear implant recipients: 3. ECAP during bursts and loudness as function of burst duration. Hear. Res 247, 112-121.

Cohen, L.T. 2009d. Practical model description of peripheral neural excitation in cochlear implant recipients: 4. Model development at low pulse rates: General model and application to individuals. Hear. Res 248, 15-30.

Cohen, L.T. 2009e. Practical model description of peripheral neural excitation in cochlear implant recipients: 5. Refractory recovery and facilitation. Hear. Res 248, 1-14.

Colombo, J., Parkins, C.W. 1987. A model of electrical excitation of the mammalian auditory-nerve neuron. Hear. Res 31, 287-311.

Dekker, D.M.T., Briaire, J.J., Frijns, J.H.M. 2014. The impact of internodal segmentation in biophysical nerve fiber models. J. Comput. Neurosci 37, 307-315.

Finley, C.C., Holden, T.A., Holden, L.K., Whiting, B.R., Chole, R.A., Neely, G.J., Hullar, T.E., Skinner, M.W. 2008. Role of electrode placement as a contributor to variability in cochlear implant outcomes. Otol. Neurotol 29, 920-928.

Finley, C.C., Wilson, B.S., White, M.W. 1990. Models of Neural Responsiveness to Electrical Stimulation. In: Miller, J.M., Spelman, F.A., (Eds.), Cochlear Implants: Models of the Electrically Stimulated Ear. Springer New York. pp. 55-96.

Frankenhaeuser, B., Huxley, A.F. 1964. The Action Potential in the Myelinated Nerve Fiber of Xenopus Laevis as Computed on the Basis of Voltage Clamp Data. J. Physiol 171, 302-315.

Frijns, J.H.M., Briaire, J.J., Grote, J.J. 2001. The importance of human cochlear anatomy for the results of modiolus-hugging multichannel cochlear implants. Otol. Neurotol 22, 340-349.

Frijns, J.H.M., de Snoo, S.L., Schoonhoven, R. 1995. Potential distributions and neural excitation patterns in a rotationally symmetric model of the electrically stimulated cochlea. Hear. Res 87, 170-186.

Frijns, J.H.M., de Snoo, S.L., ten Kate, J.H. 1996. Spatial selectivity in a rotationally symmetric model of the electrically stimulated cochlea. Hear. Res 95, 33-48.

Frijns, J.H.M., Dekker, D.M.T., Briaire, J.J. 2011. Neural excitation patterns induced by phased-array stimulation in the implanted human cochlea. Acta Otolaryngol 131, 362-370.

Frijns, J.H.M., Kalkman, R.K., Briaire, J.J. 2009a. Stimulation of the facial nerve by intracochlear electrodes in otosclerosis: a computer modeling study. Otol. Neurotol 30, 1168-1174.

Frijns, J.H.M., Kalkman, R.K., Vanpoucke, F.J., Bongers, J.S., Briaire, J.J. 2009b. Simultaneous and non-simultaneous dual electrode stimulation in cochlear implants: evidence for two neural response modalities. Acta Otolaryngol 129, 433-439.

Frijns, J.H.M., Van Gendt, M.J., Kalkman, R.K., Briaire, J.J. 2015. Modeled Neural Response Patterns from Various Speech Coding Strategies, Conference on Implantable Auditory Prostheses, Pacific Grove, California, USA.

Girzon, G. 1987. Investigation of current flow in the inner ear during electrical stimulation of intracochlear electrodes. M.Sc. thesis, Massachusetts Institute of Technology, MA, USA, Cambridge (MA).

Goldwyn, J.H., Bierer, S.M., Bierer, J.A. 2010. Modeling the electrode-neuron interface of cochlear implants: effects of neural survival, electrode placement, and the partial tripolar configuration. Hear. Res 268, 93-104.

Hanekom, T. 2001. Three-dimensional spiraling finite element model of the electrically stimulated cochlea. Ear Hear 22, 300-315.

Hanekom, T. 2005. Modelling encapsulation tissue around cochlear implant electrodes. Med. Biol. Eng Comput 43, 47-55.

Holden, L.K., Finley, C.C., Firszt, J.B., Holden, T.A., Brenner, C., Potts, L.G., Gotter, B.D., Vanderhoof, S.S., Mispagel, K., Heydebrand, G., Skinner, M.W. 2013. Factors affecting open-set word recognition in adults with cochlear implants. Ear Hear 34, 342-360.

Imennov, N.S., Rubinstein, J.T. 2009. Stochastic population model for electrical stimulation of the auditory nerve. IEEE Trans. Biomed Eng 56, 2493-2501.

Inguva, C., Wong, P., Sue, A., McEwan, A., Carter, P. 2015. Frequency-dependent simulation of volume conduction in a linear model of the implanted cochlea, International IEEE/EMBS Conference on Neural Engineering, 7th ed, Montpellier. pp. 426-429.

Jolly, C.N., Spelman, F.A., Clopton, B.M. 1996. Quadrupolar stimulation for Cochlear prostheses: modeling and experimental data. IEEE Transactions on Biomedical Engineering 43, 857-865.

Kalkman, R.K., Briaire, J.J., Dekker, D.M.T., Frijns, J.H.M. 2014. Place pitch versus electrode location in a realistic computational model of the implanted human cochlea. Hear. Res 315, 10-24.

Kalkman, R.K., Briaire, J.J., Frijns, J.H.M. 2015. Current focussing in cochlear implants: an analysis of neural recruitment in a computational model. Hear. Res 322, 89-98.

Kral, A., Hartmann, R., Mortazavi, D., Klinke, R. 1998. Spatial resolution of cochlear implants: the electrical field and excitation of auditory afferents. Hear. Res 121, 11-28.

Kujawa, S.G., Liberman, M.C. 2009. Adding insult to injury: cochlear nerve degeneration after “temporary” noise-induced hearing loss. J Neurosci 29, 14077-14085.

Lai, W.D., Choi, C.T.M. 2007. Incorporating the electrode-tissue interface to cochlear implant models. IEEE Transactions on Magnetics 43, 1721-1724.

Lin, H.W., Furman, A.C., Kujawa, S.G., Liberman, M.C. 2011. Primary neural degeneration in the Guinea pig cochlea after reversible noise-induced threshold shift. J Assoc. Res. Otolaryngol 12, 605-616.

Litvak, L.M., Spahr, A.J., Emadi, G. 2007. Loudness growth observed under partially tripolar stimulation: model and data from cochlear implant listeners. J. Acoust. Soc. Am 122, 967-981.

Macherey, O., Carlyon, R.P., van, W.A., Deeks, J.M., Wouters, J. 2008. Higher sensitivity of human auditory nerve fibers to positive electrical currents. J Assoc. Res. Otolaryngol 9, 241-251.

Macherey, O., van, W.A., Carlyon, R.P., Dhooge, I., Wouters, J. 2010. Forward-masking patterns produced by symmetric and asymmetric pulse shapes in electric hearing. J Acoust. Soc. Am 127, 326-338.

Malherbe, T.K., Hanekom, T., Hanekom, J.J. 2013. Can subject-specific single-fibre electrically evoked auditory brainstem response data be predicted from a model? Med. Eng Phys 35, 926-936.

Malherbe, T.K., Hanekom, T., Hanekom, J.J. 2015. The effect of the resistive properties of bone on neural excitation and electric fields in cochlear implant models. Hear. Res 327, 126-135.

Malherbe, T.K., Hanekom, T., Hanekom, J.J. 2016. Constructing a three-dimensional electrical model of a living cochlear implant user's cochlea. Int. J. Numer. Method. Biomed. Eng 32.

McNeal, D.R. 1976. Analysis of A Model for Excitation of Myelinated Nerve. IEEE Transactions on Biomedical Engineering 23, 329-337.

Nogueira, W., Würfel, W., Büchner, A. 2014. Development of a Model of the Electrically Stimulated Auditory Nerve. Biomedical Engineering-Biomedizinische Technik 59, S786-S789.

O'Leary, S.J., Black, R.C., Clark, G.M. 1985. Current distributions in the cat cochlea: a modelling and electrophysiological study. Hear. Res 18, 273-281.

Pau, H.W., Grunbaum, A., Ehrt, K., Dahl, R., Just, T., van Rienen, U. 2014. Would an endosteal CI-electrode make sense? Comparison of the auditory nerve excitability from different stimulation sites using ESRT measurements and mathematical models. Eur. Arch. Otorhinolaryngol 271, 1375-1381.

Rattay, F. 1986. Analysis of Models for External Stimulation of Axons. IEEE Transactions on Biomedical Engineering 33, 974-977.

Rattay, F. 1987. Ways to approximate current-distance relations for electrically stimulated fibers. J. Theor. Biol 125, 339-349.

Rattay, F., Leao, R.N., Felix, H. 2001a. A model of the electrically excited human cochlear neuron. II. Influence of the three-dimensional cochlear structure on neural excitability. Hear. Res 153, 64-79.

Rattay, F., Lutter, P., Felix, H. 2001b. A model of the electrically excited human cochlear neuron. I. Contribution of neural substructures to the generation and propagation of spikes. Hear. Res 153, 43-63.

Reilly, J.P., Freeman, V.T., Larkin, W.D. 1985. Sensory Effects of Transient Electrical-Stimulation - Evaluation with A Neuroelectric Model. IEEE Transactions on Biomedical Engineering 32, 1001-1011.

Rodenhiser, K.L., Spelman, F.A. 1995. A method for determining the driving currents for focused stimulation in the cochlea. IEEE Transactions on Biomedical Engineering 42, 337-342.

Rubinstein, J.T., Spelman, F.A., Soma, M., Suesserman, M.F. 1987. Current-Density Profiles of Surface Mounted and Recessed Electrodes for Neural Prostheses. IEEE Transactions on Biomedical Engineering 34, 864-875.

Rubinstein, J.T., Wilson, B.S., Finley, C.C., Abbas, P.J. 1999. Pseudospontaneous activity: stochastic independence of auditory nerve fibers with electrical stimulation. Hear. Res 127, 108-118.

Sapozhnikov, A. 1990. Computer modelling of the implanted cochlea. B.Sc. thesis, University of Melbourne, Australia, Parkville, Victoria, Australia.

Shepherd, R.K., Hatsushika, S., Clark, G.M. 1993. Electrical stimulation of the auditory nerve: the effect of electrode position on neural excitation. Hear. Res 66, 108-120.

Skinner, M.W., Holden, T.A., Whiting, B.R., Voie, A.H., Brunsden, B., Neely, J.G., Saxon, E.A., Hullar, T.E., Finley, C.C. 2007. In vivo estimates of the position of advanced bionics electrode arrays in the human cochlea. Ann. Otol. Rhinol. Laryngol. Suppl 197, 2-24.

Smit, J.E., Hanekom, T., Hanekom, J.J. 2009. Estimation of stimulus attenuation in cochlear implants. J. Neurosci. Methods 180, 363-373.

Snel-Bongers, J., Briaire, J.J., Van der Veen, E.H., Kalkman, R.K., Frijns, J.H.M. 2013. Threshold levels of dual electrode stimulation in cochlear implants. J. Assoc. Res. Otolaryngol 14, 781-790.

Spelman, F.A., Clopton, B.M., Pfingst, B.E. 1982. Tissue impedance and current flow in the implanted ear. Implications for the cochlear prosthesis. Ann. Otol. Rhinol. Laryngol. Suppl 98, 3-8.

Spelman, F.A., Pfingst, B.E., Clopton, B.M., Jolly, C.N., Rodenhiser, K.L. 1995. Effects of electrical current configuration on potential fields in the electrically stimulated cochlea: field models and measurements. Ann. Otol. Rhinol. Laryngol. Suppl 166, 131-136.

Stakhovskaya, O., Sridhar, D., Bonham, B.H., Leake, P.A. 2007. Frequency map for the human cochlear spiral ganglion: implications for cochlear implants. J. Assoc. Res. Otolaryngol 8, 220-233.

Strelioff, D. 1973. A computer simulation of the generation and distribution of cochlear potentials. J. Acoust. Soc. Am 54, 620-629.

Sue, A., Tran, P., Wang, S.P., Li, Q., Carter, P. 2013. Time-Domain Finite Element Models of Electrochemistry in Intracochlear Electrodes, International Conference of the IEEE Engineering in Medicine and Biology Society, 35th Annual ed, Osaka, Japan. pp. 1554-1557.

Sue, A., Wong, P., Tran, P., Li, Q., Carter, P. 2015. Modeling the Effects of Electrode Recessing on Electrochemical Safety in Cochlear Implant Electrodes, International IEEE/EMBS Conference on Neural Engineering, 7th ed, Montpellier, France. pp. 490-493.

Suesserman, M.F. 1992. Noninvasive microelectrode measurement technique for performing quantitative, in vivo measurements of inner ear tissue impedances. PhD thesis, University of Washington, WA, USA, Seattle (WA).

Suesserman, M.F., Spelman, F.A. 1993. Lumped-parameter model for in vivo cochlear stimulation. IEEE Transactions on Biomedical Engineering 40, 237-245.

Tognola, G., Pesatori, A., Norgia, M., Parazzini, M., Di Rienzo, L., Ravazzani, P., Burdo, S., Grandori, F., Svelto, C. 2007. Numerical modeling and experimental measurements of the electric potential generated by cochlear implants in physiological tissues. IEEE Transactions on Instrumentation and Measurement 56, 187-193.

Tran, P., Sue, A., Wong, P., Li, Q., Carter, P. 2015. Development of HEATHER for Cochlear Implant Stimulation Using a New Modeling Workflow. IEEE Transactions on Biomedical Engineering 62, 728-735.

Van Compernolle, D. 1985. Speech processing strategies for a multichannel cochlear prosthesis. PhD thesis, Stanford University, CA, USA, Stanford (CA).

Van den Honert, C., Kelsall, D.C. 2007. Focused intracochlear electric stimulation with phased array channels. J. Acoust. Soc. Am 121, 3703-3716.

Van der Marel, K.S., Briaire, J.J., Wolterbeek, R., Verbist, B.M., Frijns, J.H.M. 2016. Development of insertion models predicting cochlear implant electrode position. Ear Hear 37, 473-82.

Vanpoucke, F.J., Zarowski, A.J., Peeters, S.A. 2004. Identification of the impedance model of an implanted cochlear prosthesis from intracochlear potential measurements. IEEE Transactions on Biomedical Engineering 51, 2174-2183.

Wan, G., Corfas, G. 2015. No longer falling on deaf ears: Mechanisms of degeneration and regeneration of cochlear ribbon synapses. Hear. Res 329, 1-10.

Wanna, G.B., Noble, J.H., Carlson, M.L., Gifford, R.H., Dietrich, M.S., Haynes, D.S., Dawant, B.M., Labadie, R.F. 2014. Impact of electrode design and surgical approach on scalar location and cochlear implant outcomes. Laryngoscope 124 Suppl 6, S1-S7.

Westen, A.A., Dekker, D.M.T., Briaire, J.J., Frijns, J.H.M. 2011. Stimulus level effects on neural excitation and eCAP amplitude. Hear. Res 280, 166-176.

Whiten, D.M. 2007. Electro-anatomical models of the cochlear implant. PhD thesis, Massachusetts Institute of Technology, MA, USA, Cambridge (MA).

Wilson, B.S., Finley, C.C., Lawson, D.T., Wolford, R.D., Eddington, D.K., Rabinowitz, W.M. 1991. Better speech recognition with cochlear implants. Nature 352, 236-238.

Wong, P., George, S., Tran, P., Sue, A., Carter, P., Li, Q. 2016. Development and Validation of a High-Fidelity Finite-Element Model of Monopolar Stimulation in the Implanted Guinea Pig Cochlea. IEEE Trans. Biomed Eng 63, 188-198.

Woo, J., Miller, C.A., Abbas, P.J. 2010. The dependence of auditory nerve rate adaptation on electric stimulus parameters, electrode position, and fiber diameter: a computer model study. J Assoc. Res. Otolaryngol 11, 283-296.

Chapter 3

Place pitch versus electrode location in a realistic computational model of the implanted human cochlea

Randy K. Kalkman
Jeroen J. Briaire
David M.T. Dekker
and Johan H.M. Frijns

Hearing Research 2014 (315), 10–24

Abstract

Place pitch was investigated in a computational model of the implanted human cochlea containing nerve fibres with realistic trajectories that take the variable distance between the organ of Corti and spiral ganglion into account. The model was further updated from previous studies by including fluid compartments in the modiolus and updating the electrical conductivity values of (temporal) bone and the modiolus, based on clinical data. Four different cochlear geometries are used, modelled with both lateral and perimodiolar implants, and their neural excitation patterns were examined for nerve fibres modelled with and without peripheral processes. Additionally, equations were derived from the model geometries that describe Greenwood's frequency map as a function of cochlear angle at the basilar membrane as well as at the spiral ganglion. The main findings are: (I) in the first (basal) turn of the cochlea, cochlear implant induced pitch can be predicted fairly well using the Greenwood function. (II) Beyond the first turn this pitch becomes increasingly unpredictable, greatly dependent on stimulus level, state of the cochlear neurons and the electrode's distance from the modiolus. (III) After the first turn cochlear implant induced pitch decreases as stimulus level increases, but the pitch does not reach values expected from direct spiral ganglion stimulation unless the peripheral processes are missing. (IV) Electrode contacts near the end of the spiral ganglion or deeper elicit very unpredictable pitch, with broad frequency ranges that strongly overlap with those of neighbouring contacts. (V) The characteristic place pitch for stimulation at either the organ of Corti or the spiral ganglion can be described as a function of cochlear angle by the equations presented in this paper.

1 Introduction

Modern cochlear implants (CIs) are multi-channel devices that make use of the cochlea's tonotopical organization by having multiple electrodes stimulate different subpopulations of the auditory nerve fibres in the inner ear. The pitch percept resulting from stimulating such a subpopulation depends on the electrode's location in the cochlea. In practice it is presumed that the frequency alignment of the contacts follows the Greenwood function (Greenwood, 1990), which assigns a characteristic frequency to an auditory nerve fibre based on the position of its peripheral tip along the basilar membrane (BM).

There is evidence that CI patients perform better when the electrically stimulated frequency range corresponds to the acoustic input frequency range, and that patients with bilateral implants or combined electrical and acoustical hearing will benefit from having the frequencies of the two devices or modalities correctly matched to each other (Dorman et al., 1997; Shannon et al., 1998; Fu and Shannon, 1999; Başkent and Shannon, 2004, 2005, 2007; Siciliano et al., 2010; Li and Fu, 2010; Yoon et al., 2011, 2013). As a consequence, it becomes important to correctly estimate the pitch elicited by the CI. With electrical stimulation, neurons will often be stimulated directly in the central axon, rather than at the BM. Therefore, due to non-radial trajectories of auditory nerve fibres in the apex (Ariyasu et al., 1989; Kawano et al., 1996; Stakhovskaya et al., 2007) one can expect that the acoustically derived Greenwood function will not suffice to estimate the correct frequency alignment for electrical stimulation.

There have been several studies of pitch matching performed with CI patients with (contralateral) residual hearing, with varying results. Some pitch matching studies showed no systematic deviations from the Greenwood function (Vermeire et al., 2008; McDermott et al., 2009; Carlyon et al., 2010a), while most studies found pitch matches lower than expected from the Greenwood function (Blamey et al., 1996; Boëx et al., 2006; Baumann and Nobbe, 2006; Reiss et al., 2007; Dorman et al., 2007; Baumann et al., 2011; Schatzer et al., 2013).

Other studies have investigated pitch perception as a function of stimulus level, again with inconsistent results. Shannon et al. (1983) found that in the subject tested for level effects, an increase in stimulation level lead to an increase in perceived pitch. Townshend et al. (1987) tested three patients and reported that for one subject pitch increased with level, while for the other two subjects the pitch decreased. Pulse rate matching experiments done by Pijl (1997) suggested that lower stimulus levels led to higher pitch. Arnoldner presented two pitch scaling studies, the first one (Arnoldner et al., 2006) showed a clear increase in pitch at higher current levels in 10 patients whereas only one patient showed the opposite effect. In the second study (Arnoldner et al., 2008), a pitch increase was found in only 4 patients while for 10 patients pitch decreased with higher stimulus levels. Finally Carlyon et al. (2010b) did a series of experiments to study the effect of pulse rate on pitch perception and concluded that in 16 out of 21 cases, their results were consistent with pitch increasing with signal level, with the remaining 5 cases showing the opposite effect.

The main objective of the present paper is to investigate CI-induced pitch percepts using a computational model of the implanted human cochlea. Although pitch percepts are in reality determined by a combination of place of excitation and temporal cues, this modelling study will focus exclusively on the effects of place pitch, therefore 'pitch' will be used as shorthand for 'place pitch' throughout the paper.

The computational model used in this study is an updated version of the one used in previous studies by Frijns and co-workers, and employs a realistic three-dimensional spiral tapered geometry of the human cochlea, which is based on histological data (Frijns et al., 2000, 2001, 2009a,b, 2011; Briaire and Frijns, 2000a,b, 2005, 2006; Snel-Bongers et al., 2013). In the studies done before 2009, this realistic cochlear geometry contained radially defined auditory nerve fibres; each fibre ran from the BM/organ of Corti (OC) directly to its cell body in the spiral ganglion (SG), located inside Rosenthal's canal. In other words, the fibres did not traverse apically or basally along the cochlear scalae. However, anatomical data show that in reality, auditory fibres in the apical part of the cochlea follow an oblique course; the fibres there do not traverse from the BM to the modiolus directly, but proceed basally along the cochlear scalae before reaching Rosenthal's canal. In fact, Rosenthal's canal ends at around 1.75 cochlear turns, while the OC is usually about one turn longer (Ariyasu et al., 1989; Kawano et al., 1996; Stakhovskaya et al., 2007), meaning that the cell body of an auditory nerve fibre in the apex can be located as much as a full turn more basally into the cochlea than its peripheral tip. The consequence of this is that if electrodes in the apex stimulate neurons near their cell bodies rather than in the peripheral processes (which is likely, since many of today's implants actually target the SG), they will excite a different fibre population than one would expect based on radial nerve fibre trajectories. This could lead to dramatically different pitch percepts than estimations using the Greenwood function would suggest, as the Greenwood function only defines the pitch at the level of the BM. To examine the consequences of the length difference between OC and SG, the existing computational model has been enhanced to incorporate more realistic fibre trajectories that are based on experimental data.

A comparison of electrical field imaging (EFI) recordings (Vanpoucke et al., 2004), obtained intra-operatively in patients and simulated in the computational model, revealed that intra-cochlear potentials in the model were roughly a factor 10 lower than values measured in patients. However, many of the conductivities used in the model were estimated values, particularly the bone conductivity, which was based on measurements from the lateral wall in guinea pig cochleae (Suesserman, 1992) and might have a considerably different conductivity value than the human temporal bone it was intended to model. The conductivity value used for the modiolus is also debatable, as it is a complex structure that has been simplified to a homogeneous object in the model. Furthermore, the modiolus contains neural compartments which are anisotropic in nature, but which have been modelled with isotropic conductivity. Since the conductivities of bone and the modiolus are expected to have the largest impact on the amount of current leaking from the cochlea, the model has been upgraded by including fluid compartments inside the modiolus and by updating the tissue conductivities through use of clinical intra-cochlear recordings.

To assess the influence of anatomical variability, four basic human cochlear geometries were used, with implants modelled in both perimodiolar and lateral wall positions, deeply inserted to also study stimulation in the cochlear apex. The updated model was employed to investigate to what extent the Greenwood function can be used directly to estimate the pitch percept of CI stimulation, especially in the apex of the cochlea. Also, the amount of overlap between the excited neural subpopulations in the model was used to estimate the discriminability of different electrode contacts along the cochlear scalae. Furthermore, geometric data from the model was used to determine OC and SG length at a given cochlear position, in order to describe place pitch as a function of cochlear angle. The results may provide clinical insight into the optimal length and position of electrode arrays, and the functioning of electrode contacts near and beyond the end of the SG.

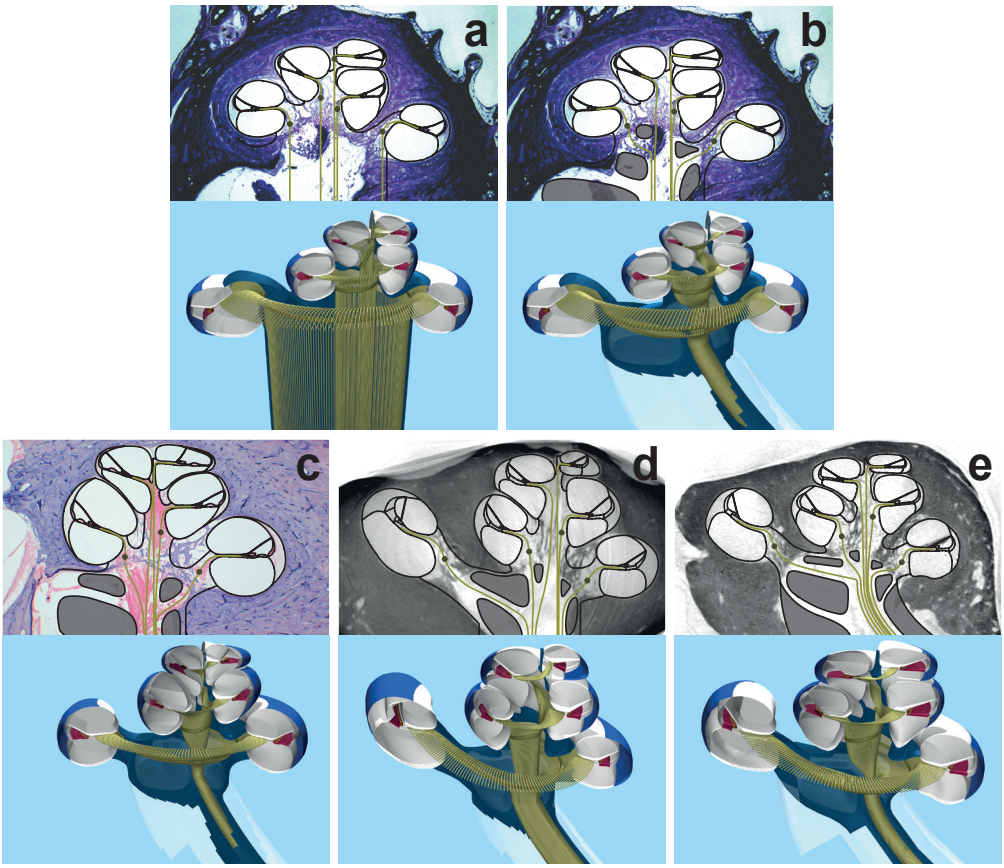

Figure 3.1. *Models of the human cochlea: (a) the original model used in older publications, (b) model HC1, (c) model HC2, (d) model HC3, (e) model HC4. The upper images of each subfigure show the histological midmodiolar cross-sections used to define the meshes, along with the mesh boundaries (black lines) and nerve fibres in that plane, with outlined grey areas representing fluid compartments. The lower parts of the subfigures are ray traced images of the full three-dimensional models.*

2 Materials and methods

The model used in this study is an extension of the previously published computational model of the electrically stimulated cochlea developed at the Leiden University Medical Centre (Briaire and Frijns, 2000a,b, 2005, 2006; Frijns et al., 2000, 2001). The volume conduction part of this model uses a realistic three-dimensional geometry representing a human cochlea implanted with a multi-channel electrode array. Electrical potentials at the Ranvier nodes of the neurons in this geometry are calculated using the Boundary Element Method, and then coupled to an active nerve fibre model to predict neural excitation.

2.1 Geometric changes

For the purpose of this study, the cochlear geometry has been updated in a number of areas, in an effort to more accurately model cochlear anatomy. Firstly the trajectories of the axons of the cochlear nerves have been altered to bundle up together in the modiolus, instead of running parallel to the modiolar axis from the cell bodies downwards (compare figure 3.1a to 3.1b). The diameter of the nerve bundle is roughly 1 mm, comparable to the diameter of a real life cochlear nerve. In addition to bundling up, the trajectory in the modiolus is curved, rather than extended in the direction of the rotational axis of the cochlea. The direction and slope of the curvature was estimated from a number of clinical CT-scans. Furthermore, a fluid sheath has been added around the cochlear nerve bundle, and a spiralling compartment of fluid was made between the nerve fibres inside the modiolus of the model geometry (outlined grey areas in the top images of figure 3.1). These fluid compartments are visible in histological cross-sections of the human cochlea, and could potentially act as a preferential pathway for electrical current during CI stimulation.

The human cochlear geometry from older studies is shown in figure 3.1a, the updated version, based on the same histological image and labelled HC1, is shown in figure 3.1b. In order to take anatomical variability into account in the model, three additional geometries of human cochleae were made. The first of these new geometries, labelled HC2, is shown in figure 3.1c. The histological midmodiolar cross sections used for HC1 and HC2 were provided by F. Linthicum (House Ear Institute). The second and third of the new geometries, named HC3 and HC4, are shown in figure 3.1d and 3.1e. These geometries were based on multiple cross-sections reconstructed from µCT data provided by the University of Antwerp and Advanced Bionics.

2.2 Oblique fibre trajectories

To incorporate realistic nerve fibre trajectories in the cochlea, this study draws on experimental findings made by Stakhovskaya et al. (2007). Their study has shown a relationship between the position of the tip of the peripheral process of a cochlear nerve fibre and the position of its cell body in the SG, which we will refer to as the OC-SG function. This function formed the basis for the oblique fibre trajectories in our model. Figure 3.2

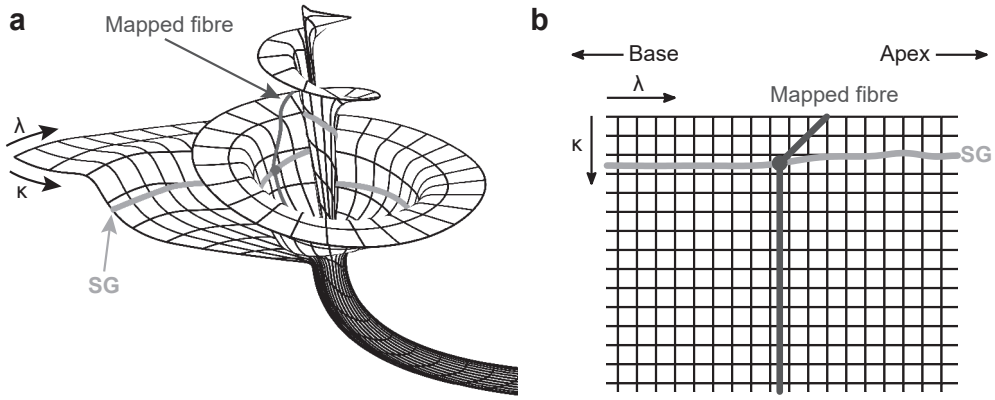

Figure 3.2. *Illustration of how fibres are mapped in the model. Left is the nerve plane, formed by radial fibres in the three-dimensional cochlea model, with the location of the SG indicated by a light grey curve. Right is an unrolled version of the nerve plane, again with the SG as a light grey curve. The dark grey line is an example of a nerve fibre mapped onto the nerve plane. The axes of the nerve plane coordinates κ and λ are indicated in both images.*

illustrates how the function was implemented in the model to generate oblique fibre trajectories. Figure 3.2a shows a curved two-dimensional grid that defined the surface on which nerve fibre trajectories were mapped in the three-dimensional space of HC4; figure 3.2b shows an unrolled, flattened representation of that same grid (black lines). Points on this grid were identified by grid coordinates κ and λ. The vertical gridlines in figure 3.2b (lines along which grid coordinate λ remained constant) defined radial lines in the three-dimensional space of the cochlear geometry, while horizontal gridlines (along which κ remained constant) were formed by connecting equidistant points along those radial lines. As a consequence, these horizontal gridlines formed spiralling curves in three-dimensional space, with the line κ=0 corresponding to the spiral along which the peripheral tips of the nerve fibres were to be located. Vertical gridlines were spaced evenly along the κ=0 spiral, with the same spacing as the horizontal gridlines. The light grey curves shown in figure 3.2a and b represent the position of the SG in HC4 and on the flattened nerve grid. The dark grey lines represent the trajectory of an oblique fibre, which was mapped in the following manner: first, the length of the OC at the peripheral tip of that fibre was determined, and then the OC-SG function was used to calculate the length of the SG of at the location of the fibre's cell body. The corresponding grid coordinates of this cell body were determined, after which the oblique fibre trajectory was defined in the flattened nerve grid as a straight line running from the grid coordinates of the peripheral tip to those of the cell body, followed by a straight line downwards, parallel to the radial lines.

In this manner a set of 320 curved (oblique) nerve fibres was generated for all cochlear geometries, in addition to a set of 320 radial fibres. Since in reality the human cochlea has about 30000 nerve fibres, every nerve in these sets represented roughly 100 actual fibres. The peripheral tips of the modelled fibres were distributed evenly along the length of the BM. As a consequence, the positions of the tips in the radial fibre sets are the same

Geometry	OC length (mm)		SG length (mm)		Ratio total SG/OC
	Modelled	Total	Modelled	Total	
HC1	33.0	35.8	13.9	15.0	0.42
HC2	30.1	32.8	11.5	12.4	0.38
HC3	30.7	33.3	12.6	13.5	0.41
HC4	33.7	36.5	14.2	15.2	0.42

Table 3.1. *Lengths of the OC and SG in the cochlear geometries of this study. The columns labelled 'Modelled' refer to the lengths of the modelled sections of the OC and SG, while the values in the 'Total' columns also include estimated values of the unmodelled sections of the OC and SG (see section 2.2).*

as those in the curved fibre sets. To observe the effects of neural degeneration, a set of degenerated neurons was created from the oblique fibre set by removing the peripheral processes, as done in a previous study (Briaire and Frijns, 2006).

Adapting the OC-SG function from Stakhovskaya et al. (2007) to the model required determining the lengths of the OC and SG in the model geometries. However, there was a limitation with the model in determining the lengths of the OC and SG due to the fact that the model geometries do not include the most basal section of the cochlea, starting at roughly the point of the round window. Assuming a 10.3° angle between the start of the OC and the round window (Cohen et al., 2000), and using data from table I from Bredberg (1968), the length of the missing section of the BM was then estimated at values between 2.6 and 2.8 mm. Since the basal starting point of the SG could not be ascertained, the length of the SG was estimated by assuming that it terminates at 630° from the round window (1.75 cochlear turns), and varying the length of the missing basal section until the OC-SG function yielded cochlear fibre trajectories that were roughly radial in the first cochlear turn and increasingly oblique further into the apex, similar to histological images by C.G. Wright & P.S. Roland (UT Southwestern Medical Centre in Dallas; not presented). Table 3.1 lists the lengths of the modelled section of the OC and SG, as well as their estimated total lengths (the length of the modelled section plus the estimated length of the unmodelled basal section) and the ratio between them. Figure 3.3 shows the implementation of the OC-SG function from Stakhovskaya et al. in all four cochlea models, expressed in cochlear angle.

Since both the Greenwood function and Stakhovskaya's OC-SG function require cochlear position to be described in terms of length along the OC or SG, the model geometries were used to describe length along the OC and SG as a function of cochlear angle, with the goal of describing cochlear place pitch as a function of angle. Percentage length of the OC along the cochlear scalae was determined as a function of cochlear angle for all four cochlear models. The resulting curves were jointly fitted with the following function (using the non-linear least squares method):

$$L_{OC}(\theta) = 100 \cdot (\alpha \cdot \ln(\theta+\beta) - \gamma) \quad (1)$$

Here L_{OC} is the percentage of the total length of the OC from its base to a point given by angle θ. The cochlear angle θ is measured in degrees from the round window. Fitted parameters were α=0.4990, β=177.3 and γ=2.512 (r^2=0.999).

Equation 1 can be applied to the Greenwood function to yield frequency as a function of insertion angle (note that in the Greenwood function OC length is measured from the apex):

$$F_{OC}(\theta) = A\left(10^{a\left(1-\frac{L_{OC}(\theta)}{100}\right)} - k\right) = A(\mu^a(\theta+\beta)^{-av} - k) \tag{2}$$

The function yields frequency in Hz, the constants A, a and k are from Greenwood (1990), with values A=165.4, a=2.1 and k=0.88. The constants μ and v are given by:

$$\begin{aligned} \mu &= 10^{(1+\gamma)} \approx 3251 \\ v &= \alpha \cdot \ln(10) \approx 1.149 \end{aligned} \tag{3}$$

Percentage length of the SG was determined for all geometries as a function of cochlear angle in the same manner as the OC above, but fitted with the following function:

$$L_{SG}(\theta) = \frac{100}{\ln(1+\delta)-\varepsilon} \cdot \left(\ln\left(\frac{\theta}{\theta_t}+\delta\right) - \varepsilon \cdot \frac{\theta}{\theta_t}\right) \tag{4}$$

L_{SG} is the percentage of the total length of the SG at θ, fitted parameters were δ=1.031 and ε=0.4621 (r^2=0.995). The constant θ_t is the termination angle of the SG and was set to 630°, since this was the value used in all of the cochlear models.

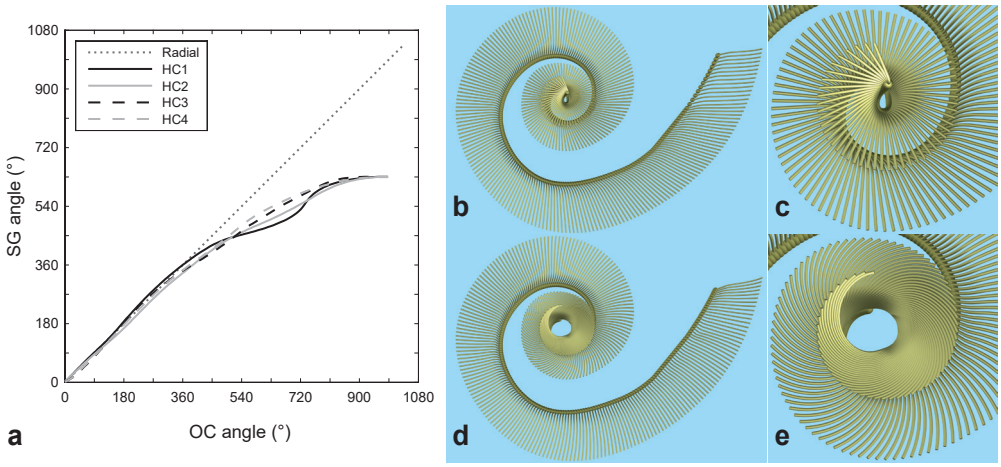

Figure 3.3. *Implementation of the OC-SG function from Stakhovskaya et al. (2007). Figure a shows the angle of the SG in the model geometries plotted against the angle of the corresponding points along the OC. The dotted dark grey line represents this relationship for radially defined fibre sets, while the other lines represent the oblique fibre sets for the four cochlear models. Figure b shows an overview of a radial fibre set as it appears in the three-dimensional model, with figure c providing a close-up of its apical turn. Figure d and e show the overview and close-up of the oblique fibre set in the same cochlear model (HC4).*

Equation 4 can be used to determine an approximate SG-based frequency map as a function of angle. First Stakhovskaya's OC-SG function is used (with symbols renamed for consistency):

$$L_{SG}(L_{OC}) = \frac{100}{1 + \left(A_S \frac{100}{L_{OC}} + B_S \frac{L_{OC}}{100} - A_S - B_S\right)^2} \tag{5}$$

The constants are from Stakhovskaya et al. (2007) and have values A_S=0.22 and B_S=-0.93. Next, this equation is solved for L_{OC}:

$$L_{OC}(\varphi) = 100 \cdot \frac{\varphi - \sqrt{\varphi^2 - 4A_S B_S}}{2B_S} \tag{6}$$

Where

$$\varphi(L_{SG}) = \sqrt{\frac{100}{L_{SG}} - 1} + A_S + B_S \tag{7}$$

This is the inverse of the OC-SG function; it gives the position of the peripheral tip of a cochlear neuron as a function of the location of its cell body along the SG. The position of the cell body is parameterised by φ, given in equation 7 as a function of L_{SG}. Parameter φ can be rewritten as a function of θ by inserting equation 4:

$$\varphi(\theta) = \sqrt{\frac{\ln(1+\delta) - \varepsilon}{\ln\left(\frac{\theta}{\theta_t} + \delta\right) - \varepsilon \frac{\theta}{\theta_t}} - 1} + A_S + B_S \tag{8}$$

As before, the expression of L_{OC} given in equation 6 can be substituted into the Greenwood function, which yields:

$$F_{SG}(\varphi) = A\left(10^{a\left(1 - \frac{L_{OC}(\varphi)}{100}\right)} - k\right) = A\left(10^{a\left(1 - \frac{\varphi - \sqrt{\varphi^2 - 4A_S B_S}}{2B_S}\right)} - k\right) \tag{9}$$

This equation describes the Greenwood frequency (in Hz) of a cell body located at a position described by parameter φ, which in turn can be expressed as a function of SG length (equation 7) or cochlear angle (equation 8).

2.3 Nerve fibre morphology

In our previous modelling studies, the peripheral process of the auditory nerve fibre defined in the nerve fibre model was divided into six segments: five segments of equal length, followed by a segment of half-length (Briaire and Frijns (2005, 2006)). These segments were scaled to account for the variable length of the peripheral processes throughout the cochlea. However, a direct consequence of implementing realistic oblique fibre trajectories

was that the peripheral processes of the modelled nerve fibres in the apex of the cochlea became considerably longer than in previous works. It was discovered that the nerve fibre was unable to propagate an action potential from the peripheral tip through the cell body when the peripheral process was scaled to lengths required for oblique apical fibres (up to ±3 mm). Due to this, some modifications were necessary to the nerve fibre morphology.

First, the segments were made to decrease in length along the peripheral process. Starting from the tip, it now consists of 3 segments of equal length, followed by one segment of 60% length, one segment of 40% length, and one segment of 20% length. This was done analogous to the axon of the auditory nerve fibre, where the internodal distances also decrease as one approaches the cell body.

Secondly, for extremely long peripheral processes the number of segments was increased, in order to limit the length of all segments to a maximum of 400 µm. The added segments were equal in length to the first three segments of the basic model fibre. This maximum segment length was chosen so that without any extra segments the maximum possible length of the peripheral process would be roughly equal to the length of the longest peripheral process used in our previous modelling studies.

Figure 3.4 shows the modified fibre morphology used in this study. All other details concerning the nerve fibre model are the same as in Briaire and Frijns (2005, 2006). Since there is very little physiological data available on the morphology of the peripheral process, the changes to the nerve fibre morphology for this study were made pragmatically, to enable action potential propagation through the cell body for peripheral process lengths up to 3 mm. The changes to the morphology did not affect any of the conclusions drawn in previous work.

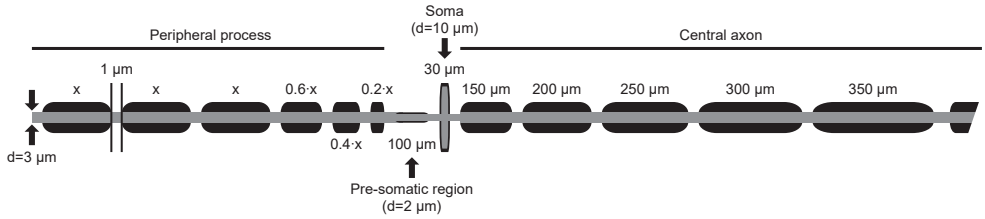

Figure 3.4. *The nerve fibre morphology used in this study. The Ranvier nodes throughout the fibre are 1 µm long and have a diameter of 3 µm. Since the peripheral process varied in length throughout the cochlea, its six segments were scaled in length depending on the fibre's location in the cochlea. The first three segments of the nerve fibre were equal in length (x), while the following three segments successively decreased in length (0.6·x, 0.4·x and 0.2·x, in order). When needed, more segments of length x would be added to the peripheral process to ensure a maximum segment length of 400 µm. All other details concerning the nerve fibre morphology and the nerve fibre computational model are discussed in Briaire and Frijns (2005, 2006).*

2.4 Conductivities of cochlear structures

To improve the intracochlear potentials in the model and make them match clinically recorded values more closely, the conductivity of structures in or surrounding the cochlea had to be changed. A variation of parameters showed that the conductivities for bone and the modiolus had the largest influence on intrascalar potentials; therefore the values of these two structures were optimized using an iterative procedure.

First, for 16 patients implanted with a HiRes90k plus HiFocus1J electrode array, multiplanar reconstructions (MPRs) of both pre- and postoperative CT scans were made (Verbist 2005), which were used to create patient-specific model geometries by scaling models HC1 or HC2 (whichever was most similar to the CT scans) and adapting the shape

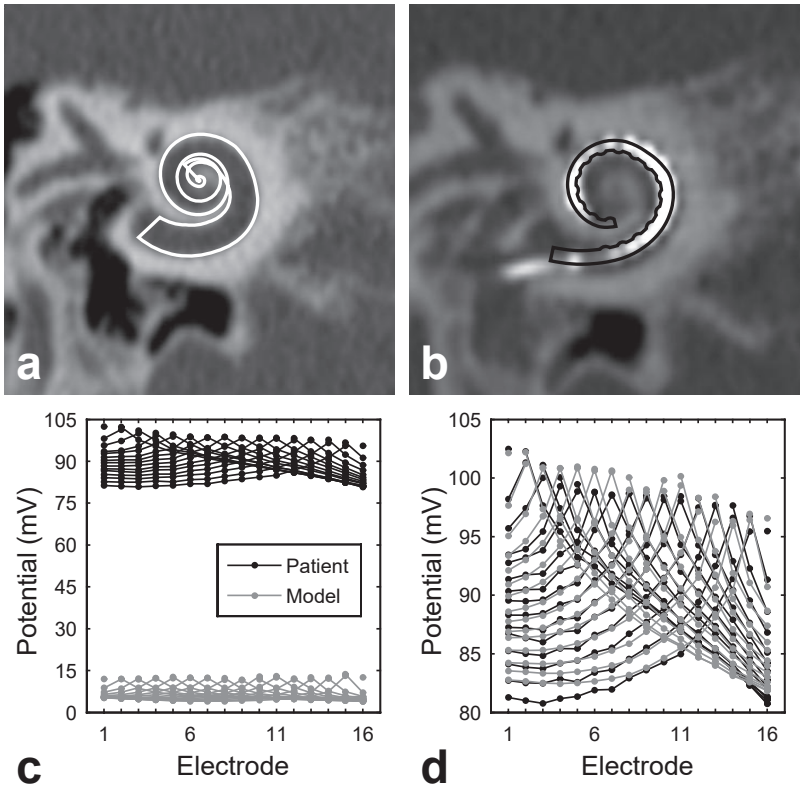

Figure 3.5. *Optimization of the conductivities of temporal bone and the modiolus in patient-specific cochlear models. (a) An MPR slice of a pre-operative CT scan with the outline of the adapted cochlear model overlaid in white. (b) An MPR slice of the post-operative CT scan of the same patient with the outline of the modelled implant overlaid in black. (c) EFI recordings from the patient plotted in black, with simulated EFI recordings from the adapted model plotted in grey. The model EFI used a temporal bone conductivity of 0.156 S/m and a modiolus conductivity of 0.3 S/m, as in Briaire and Frijns (2000a,b, 2005, 2006) and Frijns et al. (2000, 2001). Potentials of stimulating electrode contacts are omitted. (d) Same as c, except the simulated EFI was done for optimized values of temporal bone and modiolus conductivities.*

of the model's cochlear scalae to fit the pre-operative MPR images (figure 3.5a). Electrode arrays were modelled with electrode contacts corresponding to their locations on the post-operative MPR images (figure 3.5b).

EFI recordings (Vanpoucke 2004) of the patients were obtained intra-operatively, and compared to simulated EFI recordings in the adapted models, generated for a range of bone and modiolus conductivities. The conductivities for the newly added fluid compartments described above (see section 2.1) were set to that of perilymph: 1.43 S/m. For each set of conductivities the root mean square (RMS) of the difference between the simulated and clinically recorded EFI was calculated. Since the potentials at the stimulating electrode contacts could not be reliably measured in patients, they were ignored in calculating the RMS, so only the 15x16 off-stim potentials were used. Plotting RMS values versus conductivity and fitting those plots with cubic splines, the conductivity values where the RMS was at a minimum was estimated, and new simulations were run for a range of conductivities around this estimated optimum. This process was iterated, 'zooming in' on the optimal set of conductivities until further iterations would change the estimated optimum conductivities by less than 1%. Figure 3.5c shows a recorded EFI from one patient along with the initial simulated EFI using the conductivity values from previous studies. Figure 3.5d shows the same, but with the optimized simulated EFI.

After optimizations in the 16 patient models, the average conductivity of the temporal bone was 0.014 S/m (standard deviation 0.005 S/m) and the average conductivity of the modiolus was 0.2 S/m (standard deviation 0.1 S/m), both considerably lower than the conductivities used in previous studies (0.156 S/m for bone and 0.3 S/m for the modiolus). The new values were used for all further simulations in this study.

2.5 Electrode configuration

The model electrode array used in this study was based on the design of the HiFocus1J electrode (Advanced Bionics, Valencia, CA). In order to make the arrays span the maximum cochlear range, they were inserted as deeply as the cochlear geometry would allow and when necessary, the modelled arrays were extended by adding more electrode contacts at the basal end. This was done for each cochlear model, both as a medial (modiolus hugging) array and as a lateral wall array. As in most electrode designs, the thickness of

Implant model	HC1			HC2			HC3			HC4		
	B(°)	A(°)	#	B(°)	A(°)	#	B(°)	A(°)	#	B(°)	A(°)	#
Medial normal	15	523	16	29	521	13	13	697	16	20	613	16
Medial thin	44	734	16	21	743	16	20	800	16	27	726	16
Lateral normal	21	497	18	30	500	16	18	701	20	16	630	22
Lateral thin	143	759	16	95	770	16	153	805	16	192	744	16

Table 3.2. *Insertion angles of the most basal ('B') and most apical ('A') electrode contacts of all implant models in this study, and the total number of contacts modelled for each implant ('#').*

the silastic carrier increased from apex to base. However, after the apical 16 electrodes the modelled silastic carrier remained at constant thickness for any additional contacts. In the case of the medial array of HC2, the base implant was too long to fit 16 electrode contacts into the cochlea, therefore 3 contacts were removed from the basal end.

Since the thickness of the model array limited its maximum possible insertion depth in the cochlear geometries, an additional thinner version of the array was created, in order to ascertain the effect of implants inserted beyond 1.75 cochlear turns. Its thickness was scaled down to 80% by shrinking the silastic carrier, but the length of the array and the dimensions of the electrode contacts were left intact. Like the normal array, this thin array was modelled in a medial and lateral position for very deep insertion into the cochlear models; however the number of contacts of the thin array was kept at 16. See table 3.2 for insertion depths and number of contacts for each implant model used in the study.

2.6 Model output

Excitation profiles (XPs) of all electrodes were made for every combination of cochlea, implant configuration and fibre set (radial or oblique). An XP of an electrode contact is a colour coded plot that shows which fibres in the cochlea are excited and in what part the action potential is generated (peripheral process, cell body or axon) for a range of stimulus levels (indicated along the abscissa). The modelled stimulus was a cathodic-first symmetric biphasic current pulse of 37.5 μs phase, in monopolar stimulation mode. The characteristic Greenwood-frequencies of the nerve fibres were plotted along the ordinate. On the basis of a study by Laneau et al. (2004), where it was indicated that place pitch is related to the centroid of the area of excitation, the simulated pitch percept of a given excitation pattern is determined by computing its spatial centre of gravity along the BM and then calculating the pitch at that location according to the Greenwood function.

The expected pitch of an electrode contact was calculated from the Greenwood function by determining the distance along the BM from the base of the cochlea to the electrode's location, and is plotted as a horizontal dashed line in the XPs. Based on findings of Snel-Bongers (2013), threshold excitation level in the model, called I_{th}, was defined as the amount of current necessary to excite a group of fibres that occupies a total of 1 mm along the BM. The current level where the excited fibres occupy 4 mm of the BM, called I_{4mm}, was considered to be the model equivalent of maximum comfortable loudness (Briaire and Frijns, 2006). These current levels were used to define the dynamic range of the contact and are indicated by vertical dashed lines in the XPs.

3 Results

Figure 3.6 shows XPs of electrode contacts in HC1, at roughly 180°, 360°, 540° and 720° from the round window, using radial and oblique fibres with lateral and medial electrode arrays. In radial fibre XPs, threshold excitation occurs at the expected pitch throughout the cochlea. With increasing stimulus levels the excitation area broadens symmetrically to fibres with lower and higher associated pitches. At very high stimulus levels, usually

beyond the dynamic range of the electrodes, secondary regions of excitation occur at fibres originating one turn higher in the cochlea, due to the fact that their central axons pass directly behind those of the main excitation region in the modiolus. This phenomenon is referred to as cross-turn stimulation (Frijns and Briaire, 2001). Disregarding cross-turn stimulation, the symmetric expansion of the region of excitation with radial fibres causes the pitch percept to remain virtually constant in the entire dynamic range of the electrode.

Oblique fibre XPs of both lateral and medial electrode contacts in the first turn are almost identical to the corresponding ones with radial fibres (compare figures 3.6a1–a2 and 3.6e1–e2). Beyond the first turn, however, differences start to emerge. For oblique fibres, the area of excitation expands more asymmetrically than in the radial case, recruiting

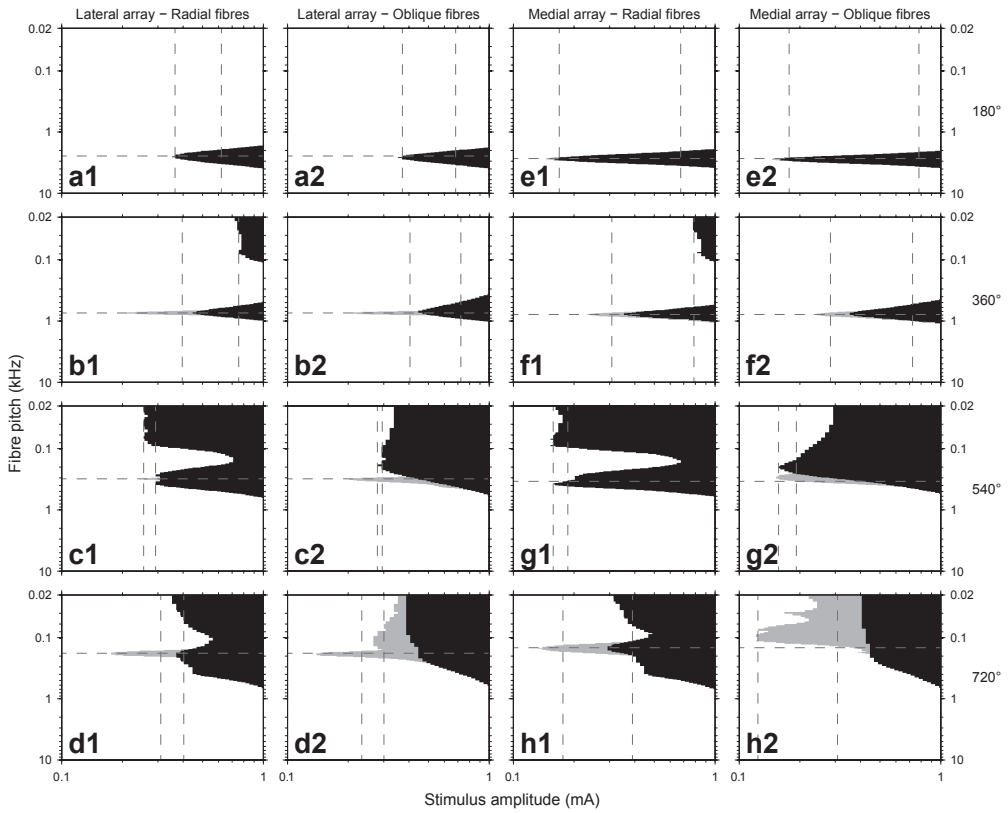

Figure 3.6. *Excitation profiles of several lateral and medial electrode contacts at different insertion depths in HC1. The coloured areas indicate which fibres (ordinate, kHz) are excited at which stimulus current (abscissa, mA). Light grey indicates stimulation in the peripheral process and black indicates stimulation in the central axon. Figures a–d are XPs from lateral contacts at roughly 180°, 360°, 540° and 720°, while figures e–h are from medial contacts at the same insertion depths. XPs from radial fibre sets are labelled number 1 (a1, b1, etc.), and XPs from oblique fibre sets are labelled number 2. Horizontal dashed lines indicate the location of the electrode contacts, and vertical dashed lines indicate the estimated dynamic range of the electrode.*

fibres more rapidly in the apical direction with increasing stimulus level. In the second turn of the cochlea (but before the end of the SG) both lateral and medial contacts can excite a group of fibres in their peripheral processes (light grey areas in the XP) while simultaneously stimulating another group of fibres at their axons (black areas), creating a double peak in the XP near the site of the electrode contact (see figures 3.6c2 and 3.6g2). Another important difference between radial and oblique XPs is the disappearance of cross-turn excitation in the oblique case. In radial fibres, higher stimulus levels result in excitation of the axons from fibres that originate in the apex of the cochlea, which shows in the XPs as a broad peak between 0.02 and 0.1 kHz (figures 3.6b1–d1, 3.6f1–h1). In the oblique fibre set, the axons of the most apical neurons are located as much as a full cochlear turn more basally into the cochlea, which results in the low-frequency peak disappearing from the XPs (figures 3.6b2, 3.6f2) or merging with the main excitation region (figures 3.6c2–d2, 3.6g2–h2). Finally, in the far apex of the cochlea, oblique fibre excitation is much more dependent on peripheral process stimulation than it is in the radial set, due to the absence of nearby cell bodies and axons (compare figures 3.6d1 with 3.6d2 and 3.6h1 with 3.6h2). At I_{4mm}, the excitation regions of contacts around 670° and beyond are very broad and overlap considerably with those of neighbouring contacts, particularly in the oblique case.

In figures 3.7a expected pitch (black line) and elicited pitch at I_{th} (circles) for non-degenerated oblique fibres are plotted as a function of insertion depth for all electrode contacts. While at I_{th} the pitch of lateral electrodes with oblique fibres (solid circles) still roughly correspond to expected values (less than 1.5 semitone difference), pitch at I_{th} of medial electrodes (open circles) beyond the first cochlear turn is shifted downward relative to the expected pitch. Figures 3.8a1–a4 show the difference between pitch excited at I_{th} with oblique fibres and expected pitch, expressed in semitones and plotted as a function

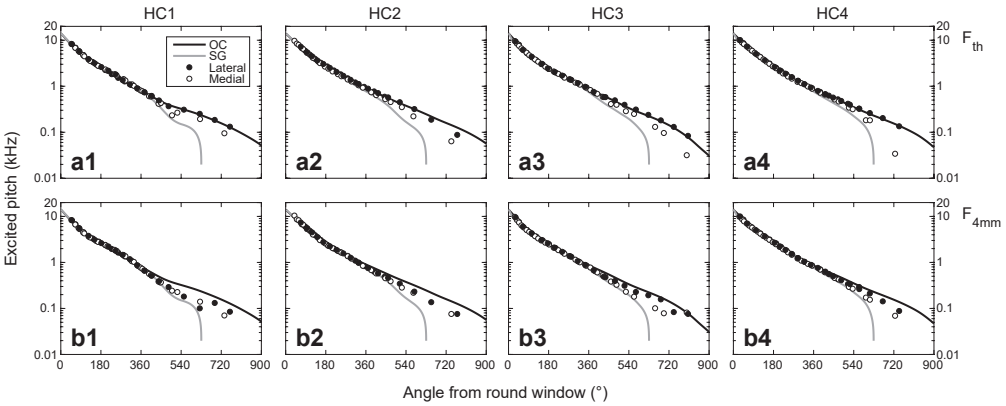

Figure 3.7. *Excited pitch in HC1, HC2, HC3 and HC4 with oblique fibre sets for lateral (filled circles) and medial electrode contacts (open circles) plotted against insertion angles. The solid black lines indicate the Greenwood-frequency along the OC; the solid grey lines indicate the pitch frequency along the SG as a function of cochlear angle. Figures a1–4 show the excited pitch at threshold (F_{th}), figures b1–4 show the model pitch when exciting 4 mm's worth of neurons at the BM (F_{4mm}).*

of insertion depth. The magnitude of the downward shift in pitch at I_{th} of medial electrode contacts (open circles) increases as the contacts are located further into the apex. The maximum pitch shift in the apex differs per cochlear geometry; comparing HC1 and HC4, for example, shows that the pitch shift is 7.5 semitones for a medial contact at 734° in HC1, while the medial contact at 725° in HC4 reaches a pitch shift of nearly 26 semitones (figures 3.8a1 and a4).

Figures 3.7 and 3.8 also show the associated pitch of the SG throughout the cochlea as a function of insertion angle (solid grey line). While the pitch values at I_{th} of medial electrode contacts beyond 360° are lower than their expected values based on stimulation at the OC, they are higher than would be expected from direct SG stimulation. Visual inspection of the excited Ranvier nodes revealed that at I_{th}, medial contacts stimulate the nerve fibres that pass diagonally over the electrode contact. This means they are stimulating fibres which have peripheral tips located apically from the contacts, but have cell bodies located basally, resulting in a pitch percept that lies in-between that of direct OC or SG stimulation.

As stated above, with lateral contacts the pitch at I_{th} deviates less than 1.5 semitones from the expected pitch throughout the cochlea (filled circles in figures 3.8a1–a4). An examination of the locations of the excited Ranvier nodes in the three-dimensional model showed that, at I_{th}, the proximity of the lateral electrode contacts to the BM was causing them to stimulate almost directly at the tip of the peripheral processes, which explains why elicited pitch from a lateral contact differs little from the expected pitch, at least at I_{th}.

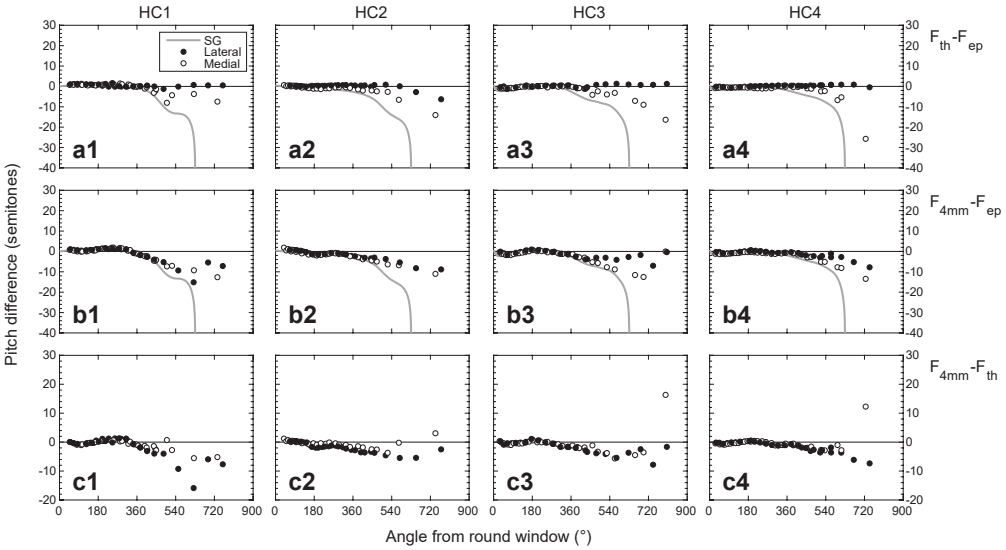

Figure 3.8. *Pitch differences between the Greenwood function and excited pitches in oblique fibre sets are plotted in semitones against cochlear angle of the electrode contacts. Pitch differences between the OC and SG are plotted as solid grey lines. Figures a1–4 show the difference between pitch at threshold in the model (F_{th}) and the Greenwood-frequency at the electrode's position (F_{ep}). Figures b1–4 show the difference between model pitch when exciting 4 mm's worth of neurons at the BM (F_{4mm}) and F_{ep}. Figures c1–4 show the difference between F_{4mm} and F_{th}.*

As shown in figure 3.8a2, the two most apical contacts of the lateral thin array model in HC2 elicited pitches more than one semitone lower than the expected value due to the fact that those contacts were located relatively close to the modiolus, since the shape and dimensions of the scala tympani in the apex of HC2 made true lateral wall insertion for those contacts impossible.

Due to the asymmetrical expansion of the primary excitation region in oblique fibres after the first cochlear turn, the simulated pitch decreases as the stimulus current increases. For medial electrodes this change is gradual, occurring throughout the entire dynamic range, but for lateral electrodes the pitch usually stays relatively constant for the first part of the dynamic range and only shifts later on due to frequent occurrence of the double peak effect illustrated by figure 3.6c2.

Figures 3.7b show pitch elicited at I_{4mm}, figures 3.8b1–b4 show the difference between the pitch at I_{4mm} and pitch predicted by the Greenwood function, while figures 3.8c1–c4 show the difference between pitch at I_{4mm} and at I_{th} for all lateral and medial electrodes in all four model cochleae, plotted against insertion depth. Up until about the beginning of the second turn, I_{4mm} pitch is close to the pitch at I_{th} for both lateral and medial electrodes. In the second turn of the cochlea, the pitch at I_{4mm} is lower than at I_{th}, and the difference between the two generally becomes larger with increasing cochlear depth, up until the start of the apical turn (around 720°). It is worth noting that despite the downward shift in pitch for higher stimulus levels, the excited pitch of a contact beyond the first turn never reaches the value one would expect of direct SG stimulation (solid grey line in figures 3.7 and 3.8).

In the apical turn of the cochlea the pitch difference between I_{4mm} and I_{th} can decrease again, and even swing into positive values (i.e., a pitch at I_{4mm} that is higher than the one at I_{th}), due to a 'clipping effect' at the top of the XPs, corresponding to the apical part of the cochlea. Electrode contacts in the last cochlear turn can in some cases stimulate all of the cochlear nerves apically from it at currents below I_{4mm}, resulting in an excitation region that can only further expand basally into the cochlea (figure 3.6h2). This causes an

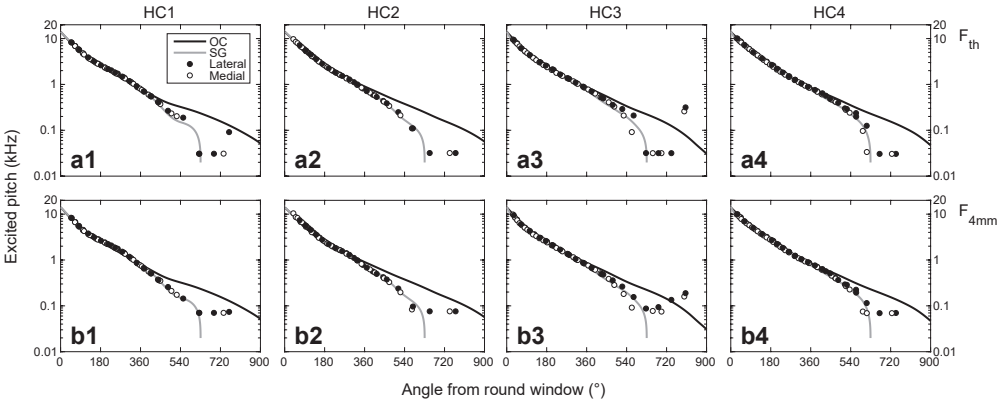

Figure 3.9. *As figure 3.7, but with fibres whose peripheral processes have been removed.*

asymmetrical expansion of the excitation region which will result in a higher pitch percept than would have been the case if there had been more cochlear nerves available for excitation in the apex.

Figures 3.9 and 3.10 show simulated pitches and pitch-differences respectively for neurons with oblique fibre trajectories and degenerated peripheral processes. Up to about 360° they are nearly identical to the pitch excited in non-degenerated neurons due to the fact that not much peripheral process stimulation occurs in the first turn of the cochleae. After the first turn however, different behaviour emerges: first of all, unlike with the non-degenerated neurons, lateral contacts excite roughly the same pitch as medial contacts do throughout the cochlea, both at I_{th} and at I_{4mm}. Secondly, pitch excited in degenerated neurons follows the SG pitch curve closely, as opposed to the non-degenerated case where pitch is always higher than the SG-associated pitch at that angle. Thirdly, until contacts get to around 540°, pitch excited at I_{4mm} differs no more than about 4 semitones from pitch at I_{th}.

With degenerated neurons, pitch elicited by contacts beyond the end of the SG (630°) levels off as one nears the apex of the cochlea itself, at both I_{th} and I_{4mm} (figure 3.9), due to the fact that the most apical contacts all stimulate the same bundle of axons at the end of the SG. The same clipping effect described above often occurs here, frequently causing pitch at I_{4mm} to be higher than at I_{th} (figures 3.10c1–c4). The exceptions to this are the most apical lateral contact of HC1 (figure 3.9a1 and 3.10c1) and the apical most contacts of HC3 (figure 3.9a3 and b3 and 3.10c3, lateral and medial), which elicit higher pitches than their basal neighbours, due to the fact that at I_{th} they stimulate the SG at slightly different locations. Their excited Ranvier nodes are less than 0.5 mm apart, however, since the SG is very dense in this area, such a small difference in excited location can result in a large difference in elicited pitch, which can result in the unpredictable behaviour seen in the apex.

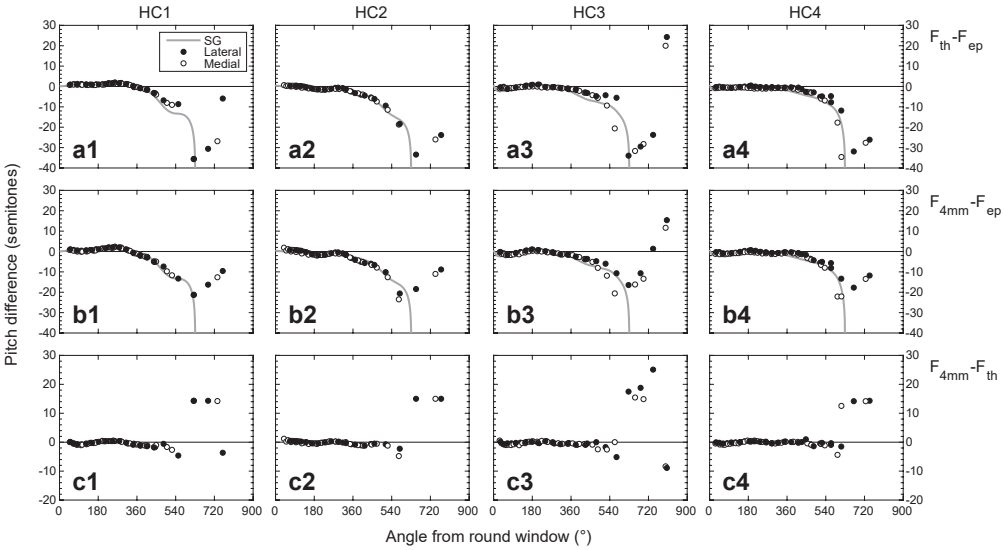

Figure 3.10. *As figure 3.8, but with fibres whose peripheral processes have been removed.*

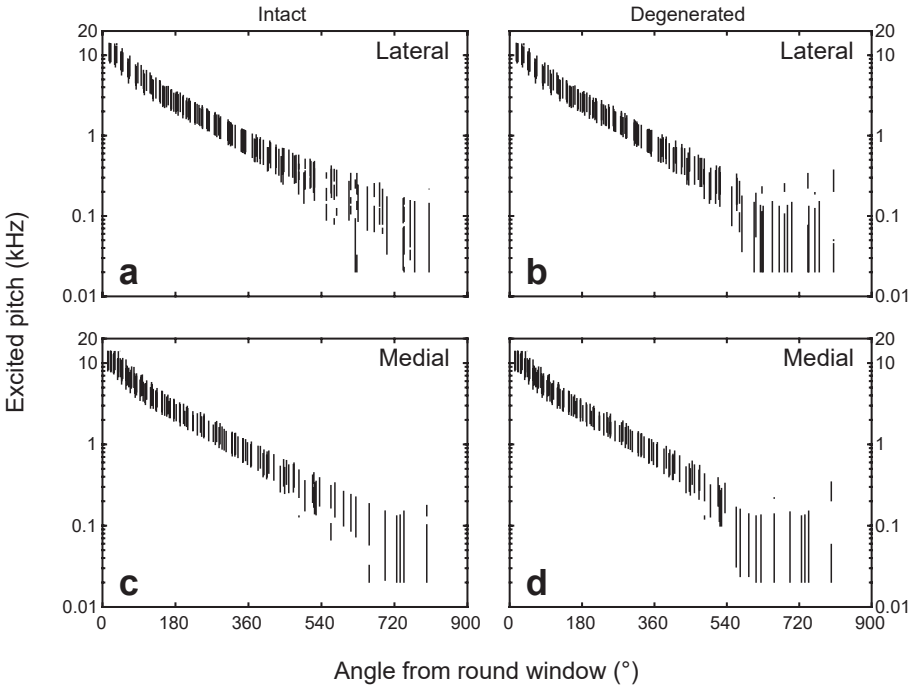

Figure 3.11. *Excited pitch percept ranges around I_{4mm} for all contacts from all models and configurations. Black lines indicate the excited nerve fibres at I_{4mm} according to their Greenwood pitch (ordinate), for contacts at insertion depths given by the abscissa. Figures a and b are plots of lateral contacts, while c and d are of medial contacts. The plots in figures a and c are generated from simulations with intact neurons, while figures b and d are done with degenerated neurons.*

In general, contacts in the apex have more difficulty stimulating small groups of neurons. Excitation regions in the apex can overlap considerably with those of neighbouring contacts; often even exciting identical regions at I_{4mm}, especially when peripheral processes are degenerated. It should also be noted that these contacts have very small dynamic ranges. For degenerated neurons, I_{4mm} pitch around the end of the SG and beyond tends to be higher than pitch at I_{th} (figure 3.10c1–c4), due to the same 'clipping effect' described above.

Figure 3.11 shows excited fibre ranges at I_{4mm} for all contacts from all models and configurations, split up into implant location (3.11a and b for lateral, 3.11c and d for medial electrodes) and neural degeneration (3.11a and c for intact neurons, 3.11b and d for degenerated neurons). In all cases the excited pitch ranges at I_{4mm} for contacts beyond approximately 540° from the round window are much broader than excited pitch ranges before that point, and have considerable overlap. When the neurons are intact, contacts are sometimes able to stimulate a more narrow pitch range by stimulation of the peripheral processes, as is visible in figure 3.11a, between approximately 630° and 720° insertion depth, and in 3.11c, around 610°. When peripheral processes are degenerated

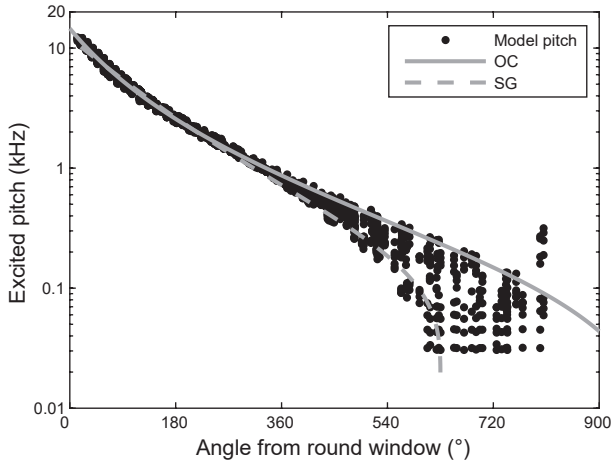

Figure 3.12. *Combined data from the four cochlear models, showing pitch excited in the model, plotted against the insertion angles of the electrode contacts. Black dots indicate average excited pitch percepts from all contacts of all modelled implant locations, from the cochlear models. Pitch values at 1, 2, 3 and 4 mm excitation at the BM are plotted, for both the degenerated and non-degenerated oblique fibre sets. Equation 2 is plotted as a solid grey line, while equation 9 is plotted as a grey dashed line.*

the regions of excitation for all contacts deeper than 540° are nearly identical, regardless of electrode location (figures 3.11b and d).

In clinical practice the amount of information available on the exact size, shape and state of the cochlea and its substructures is limited. Furthermore the implanting surgeon does not have total control over the exact final placement of the electrode array, both in terms of insertion depth as well as distance of the array from the modiolus. In figure 3.12, all of these clinically unknown or uncontrollable factors are combined in a single plot of model pitch versus electrode contact insertion angle. Average excited pitch by contacts from all cochlear models and their modelled implants are plotted for 1, 2, 3 and 4 mm excitation at the BM, for both degenerated and non-degenerated curved fibre sets (black dots). Equation 2 is shown in figure 3.12 as a solid grey line and equation 9 is plotted as a dashed grey line. Figure 3.12 clearly illustrates that in the first cochlear turn the model pitch of an electrode contact does not depend greatly on the contact's distance from the modiolus, the state of the neurons or on the level of stimulation. After the first cochlear turn pitch becomes increasingly unpredictable, for the most part varying between the OC-based frequency-cochlear angle function of equation 2 and the SG-based function of equation 9. The main exception to this is the cluster of points above the OC based function around 800°, which is the result of unpredictable stimulation at the SG of degenerated neurons by contacts in the far apex, as described above for figure 3.9a3 and b3.

4 Discussion

In this study, realistic oblique nerve fibre trajectories were created in an updated version of our three-dimensional volume conduction model, in order to examine the effects these oblique trajectories have on the functioning of medially and laterally inserted arrays, particularly for deep insertions.

4.1 Model enhancements

Despite the differences between the cochlear models, their results with regard to angular insertion depth were very similar, indicating that differences in size and shape of cochlear anatomical structures between individuals does not greatly influence the pitch elicited by an electrode contact at a given cochlear angle. Most of the results are explainable by the (angular) length difference between the SG and the OC, which is comparable for the majority of cochleae (Kawano et al., 1996; Stakhovskaya et al., 2007).

For the model, the helicotrema (and therefore the termination angle of the OC) has been set at 2.75 cochlear turns (990° from the round window) for HC1 and HC2, 2.61 for HC3 (940°) and 2.74 for HC4 (986°). While the number of turns of HC3 and HC4 could be determined from the µCT data that they were based on, the exact termination angle of HC1 and HC2 could not be ascertained from the available histological slices. The number of turns of the cochlea has been reported to vary from less than 2.5 turns to 3 full turns (Kawano et al., 1996; Biedron et al., 2009), and according to Kawano the SG does not always end exactly one turn below the OC, so there is some uncertainty in the verisimilitude of the models regarding the endpoints of the OC and SG. However, while changing the termination angles of the OC and SG would affect the pitch elicited in the apex of the cochlea, the change in the lengths of the OC/SG would be minimal; a difference of 90° in the OC would change its length by about 1 mm, while doing the same to the SG adds or removes about 0.3 mm. Furthermore, the Greenwood function-derived frequencies for fibres in the first 540° of the cochlea are not very sensitive to lengthening or shortening the OC; changing the OC's length by 90° will change the pitch of the fibre at 540° only by about 3 semitones, and fibres located basally from that point are changed less the closer one gets to the round window. However, as the histological slices for HC1 and HC2 show clear cross sections of the cochlear scalae at 900° and no indication of the cochlear scalae at 1080°, the error in the angular length of those models can be expected to be smaller than 90°. In any case, the overall trajectories of the nerve fibres would remain largely unchanged, so while there is an uncertainty of a few semitones in the quantitative results of HC1 and HC2, the qualitative results of this study are not strongly dependent on the accuracy of the termination angles of the OC and SG.

The lengths of the OC of the cochlear models fall within the range of lengths reported by Stakhovskaya et al. (2007), who found values between 31.41 mm and 36.87 mm (mean 33.13 mm). They also found that the ratio between SG length and OC length varied between 0.40 and 0.43 (mean 0.41), in our four cochlea models this ratio was 0.42, 0.38, 0.41 and 0.42 for HC1, HC2, HC3 and HC4 respectively (table 3.1). For HC1, HC3 and HC4 the SG/OC length ratio was therefore in agreement with Stakhovskaya's findings, however the ratio for HC2 falls outside their histological range. One possible explanation of this is the uncertainty in the endpoints of the OC and SG in HC2 described above, but it could also be a result of the fact that HC2 is based on a single histological slice, which meant that the exact shape of the cochlea had to be mathematically interpolated. The details of the basal most half turn are especially uncertain, as the intersection with the basal end of the cochlea is not visible in the histological slice, so its shape and position had to be estimated.

The original value of 0.156 S/m for the conductivity of temporal bone used in our previous modelling studies was based on in vivo guinea pig data from Suesserman (1992). Our patient-specific EFI simulations now indicate that a temporal bone conductivity of 0.014 S/m leads to a more accurate model of intracochlear potentials, a value that is comparable to conductivities measured in bone from the human distal tibia (Faes et al., 1999). Since the conductivity for the fluid in the scala tympani (perilymph) is set at 1.42 S/m, the optimized value for the temporal bone results in a roughly 100:1 fluid to bone conductivity ratio, which is in agreement with other modelling studies which also reported needing a 100:1 fluid to bone ratio to explain clinical intracochlear potentials (Mens et al., 1999; Whiten, 2007).

In computational studies of the cochlea, the modiolus is invariably represented as a homogeneous object (Frijns and Briaire, 2000; Rattay et al., 2001; Hanekom, 2001; Whiten, 2007), though it is actually an aggregate of various structures inside or connected to the cochlear modiolus such as the auditory nerve bundles, the habenula perforata and the osseous spiral lamina. It is therefore a complex structure made of different types of bone, nerve tissue and fluid, which makes it difficult to compare the optimized conductivity value of the aggregate modiolus to measured data. Since most of the fluid compartments are already separately modelled by a fluid spiral in the present model, the modiolus in the model mostly comprises nerve tissue and bone. In that light, it is plausible that the optimized conductivity of the modiolus (0.2 S/m) lies in between that of bone (0.014 S/m) and nerve tissue (0.3 S/m), making the modiolus roughly equivalent to a mix of 35% (temporal) bone and 65% nerve tissue.

4.2 Pitch percepts

The calculation of pitch percepts in the model is based on the assumption that the place pitch of an excitation pattern corresponds to the Greenwood-frequency at its spatial centre of gravity along the BM, as indicated by Laneau et al. (2004). Additionally, although temporal coding is known to play an important part in pitch perception, it is currently not possible to meaningfully interpret simulated temporal effects. Therefore, it is assumed that temporal coding can be ignored when studying place-pitch in the model. While both these assumptions potentially introduce systematic errors in the model results, it should be noted that in the study by Carlyon et al. (2010a) patient-adapted versions of the presented model were in good agreement with psychophysical results. Moreover, in one patient the model was able to correctly predict the occurrence and distance of an electrode slip that happened between the patient's initial CT scan and psychophysical testing. It is expected, therefore, that the results of the present study depict realistic predictions of pitch percepts in CI patients.

Modelling results predict that in the basal end of the cochlea, the pitch of CI-induced percepts corresponds to the Greenwood function. As noted in the introduction, several studies find the same results in patients (Carlyon et al., 2010a; Vermeire et al., 2008; McDermott et al., 2009), though the majority of pitch matching studies find CI-induced pitch to be lower than the Greenwood function suggests (Blamey et al., 1996; Boëx et al.,

2006; Baumann and Nobbe, 2006; Reiss et al., 2007; Dorman et al., 2007; Schatzer et al., 2013). However, Carlyon et al. (2010a) also report that pitch matching experiments are subject to non-sensory biases, and argue that these biases may have influenced the outcomes of earlier studies. Additionally, many of the subjects from the earlier pitch matching studies had been using their implants for more than a year, which may also have affected the results, since there have been reports of CI user's pitch perception changing over time (Reiss et al., 2007, 2008), probably in the direction of the (lower) filter frequencies of the CI speech processor map. It is unclear whether this change over time is due to adaptation, neural degeneration or some other mechanism.

Concerning the level dependency of CI-induced pitch percepts, this study does not show the same variability seen in the patient studies summarized in the introduction. Changes in pitch due to increasing stimulus level are almost always downward in the model, and while the model does show situations where the pitch can increase at higher current levels, the total shift in pitch is generally no more than 1 semitone, unless the contact is inserted very deeply into the cochlea (more than 600° from the round window). The upward shifts in pitch like the ones shown in patient studies (Shannon et al., 1983; Townshend et al., 1987; Arnoldner et al., 2006; Arnoldner et al., 2008; Carlyon et al., 2010b) are apparently not explainable through the model in its current form. It is conceivable that a neural dead region located apically from a stimulating electrode contact could drive the neural excitation area in the basal direction, thereby raising the excited pitch, but it is unlikely that dead regions account for all of the observations made in patient studies. As noted above, it is possible that the used method of determining the place pitch of a simulated excitation pattern is unrealistic. If, for instance, the place pitch corresponded to one of the edges of the excitation region, it would have large consequences to the simulated pitch percepts. However there is no evidence in literature that suggests that this is the case, making it a rather speculative possibility. The most obvious explanation remaining is that the differences in level dependency of pitch between model and patients as well as the differences between the various patient studies themselves can largely be attributed to temporal coding. Carlyon et al. (2010b) offered a conceptual explanation of how temporal code could affect level dependency of pitch perception, but the exact mechanism is unknown at this point.

Brill et al. (2009) performed electrically evoked compound action potential (eCAP) recordings in patients implanted with MED-EL arrays, and reported lower thresholds, higher amplitudes and steeper amplitude growth functions at the apical contacts. Though the exact insertion angles of the electrode contacts were not determined, it is probable that the most apical contacts of the 31 mm array were located beyond the end of the SG, which would be in line with the findings of the present study, since apical contacts in the model have lower thresholds, and are located more closely to the neurons, which would result in higher eCAP amplitudes. Furthermore, the broad excitation regions apical contacts evoke are consistent with steep eCAP amplitude growth curves.

It is known that some CI users with deep insertions are able to discriminate between their most apical contacts (Baumann and Nobbe, 2004), and that they do receive some benefit

from them (Hochmair et al., 2003). However, pitch estimation experiments published by Deman et al. (2004) and Boyd (2011) have shown that for some patients with deep insertions pitch confusion can occur for the most apical contacts of the array. These findings are in line with the results from the present modelling study, which show broad overlapping excitation regions (figure 3.11) and a tendency for average excited pitch to level off beyond 540° insertion depth (figures 3.7b, 3.9b, 3.12).

In a study by Gani et al. (2007) subjects with deeply inserted MED-EL electrode arrays performed better in vowel- and consonant-identification tests when two or three of their most apical electrodes were turned off than when all their contacts were turned on. The contacts that were turned off were located at insertion angles of 540° and deeper, measured from the round window. An earlier study done by Hamzavi and Arnoldner (2006) showed that switching off two of the four most apical contacts of the MED-EL array had no significant effect on speech recognition. It is likely that the contacts that were switched off in these two studies were located in close proximity to the end of Rosenthal's canal and deeper, and therefore that the extremely broad and overlapping excitation regions found in the present study are the reason why the extra contacts were of little use to the subjects.

Overall, the data suggests that stimulation of contacts beyond the end of the SG behaves differently than stimulation of more basally located contacts, as the former produce spectrally broad excitation patterns with relatively small dynamic ranges that are likely to have considerable overlap with the excitation regions of their neighbouring contacts. As such, inserting more than one or two contacts in the final turn of the cochlea might not provide much additional information to the patient.

Equations 1 and 4 describe the lengths of respectively the OC and SG as functions of the cochlear angle. When used in conjunction with the Greenwood function and the OC-SG function they lead to equations 2 and 9, which describe place pitch as a function of cochlear angle, and may be used for estimating cochlear frequencies from patients' CT data. These functions can therefore serve as a guide for matching CI input frequencies for bimodal listeners and bilateral implanted patients. However, the constants in these equations are obtained by curve fitting data from only four cochlear models, two of which are based on single histological cross-sections and are therefore prone to have some inaccuracies in the trajectories of the SG and OC. In addition, as noted above, assumptions have been made regarding the termination angles of the OC and SG and their missing sections in the model, so the angular place pitch functions of the OC and SG presented here (equations 2 and 9) are likely to contain systematic errors, which may result in inaccurate pitch predictions. However, as stated in the beginning of this section, the model's pitch predictions were in good agreement with psychophysics (Carlyon et al., 2010a). In addition, any systematic errors are expected to be equal in both ears of an individual, so when matching input frequencies of bilateral implants, errors in equations 2 and 9 are likely to be of less consequence. The angular place pitch functions are therefore presented for the consideration of clinicians and researchers studying place pitch, with the understanding that future expansion of the number of model cochleae and refinement of the model might introduce some small adaptations.

Finally, it is worthwhile to compare the results of this study (particularly figure 3.12) to the centre frequencies of the filter banks used by the speech processors of devices from the three major CI manufacturers. The Contour Advance array from Cochlear is fitted with a standard filter map using centre frequencies ranging from 251 Hz to 7.438 kHz. The HiFocus1J from Advanced Bionics uses frequencies from 333 Hz to 6.665 kHz, and for MED-EL electrodes the default frequency range is 149 Hz to 7.412 kHz. The upper values of these ranges are all located in the basal end of the cochlea, where the model predicts that CI-induced pitch follows the Greenwood function closely; in the model, for both the Contour Advance as well as the MED-EL electrodes the frequency of the most basal channel corresponds to stimulation at 56° from the round window, while for the HiFocus1J it corresponds to 67°.

The centre frequencies of the most apical channels, however, correspond to angular ranges where modelled pitch shows more variability. From equations 2 and 9, stimulation at the centre frequency of the apical channel of the Contour Advance array (251 Hz) corresponds to a range of 506°–616°. In a study by Escudé et al. (2006), implanting Contour Advance arrays in 6 patients at a depth of 19 mm resulted in a mean insertion angle of 469°, which would elicit a pitch between 334 and 504 Hz in the model. For the HiFocus1J, the apical channel frequency (333 Hz) is stimulated between 469° and 556°. In a radiological analysis of patients implanted at our own clinic, the average angle of the most apical contact of the HiFocus1J was 480° (Van der Marel et al., 2014), which is in the relevant angular range in the model. However, in a study by Skinner et al. (2007), HiFocus1(J) arrays implanted in patients reached an angle of 439° (recalculated from their tables 1&3, by omitting data from the Helix array and HiFocus1 with positioner), so results might depend on the surgeon or surgical technique. Finally, MED-EL's apical channel frequency (149 Hz) is achieved between 561° and 720° in the model. In a recent study, implanting temporal bones with FLEX^{20}, FLEX^{24}, FLEX^{28} and Standard arrays resulted in mean insertion depths of 341°, 477°, 587° and 673°, respectively (Franke-Trieger et al., 2014). The values for the Standard and FLEX^{28} arrays are both in the angular range for the apical channel, while values for the FLEX^{20} and FLEX^{24} arrays are outside that range. It must be noted, however, that the latter two arrays are designed for partial hearing preservation, so in practice they are likely to employ a modified filter map.

Based on these numbers, one can conclude that in the average patient the Contour Advance will stimulate a pitch range that does not match the input frequency range from its speech processor. And while the apical contacts of HiFocus1J, MED-EL Standard and FLEX^{28} arrays are on average in an appropriate angular range, variability in pitch as seen in figure 3.12, as well as variability in surgical results means these electrodes are not guaranteed to elicit pitch percepts that match input frequency. In fact, it is clear that matching the centre frequency of a CI channel's input filter to the actual pitch elicited by the corresponding electrode contact is problematic for all devices; the lower frequencies each implant use to process speech are located in a cochlear region where excited pitch is highly dependent on distance of the array to the modiolus, state of the local neurons and stimulus level.

In summary, the main conclusions of this study are: (I) the simulated pitch of all contacts in the first cochlear turn can be predicted fairly well using the Greenwood function, regardless of stimulation level, distance to the modiolus or degeneration of the peripheral processes. (II) The pitch elicited by contacts beyond the first turn becomes increasingly unpredictable due to the curvature of the nerve fibres. The exact pitch excited at a given insertion depth beyond the first turn depends on stimulation level, the simulating contact's distance from the modiolus and the state of the peripheral processes. (III) For all electrode contacts after the first turn the elicited pitch decreases as stimulus level increases. The pitch does not reach values expected from direct SG stimulation unless the peripheral processes are missing. (IV) Electrode contacts located near the end of Rosenthal's canal or deeper into the cochlea show great variability and unpredictability in elicited pitch, and their neural excitation regions have strong degrees of overlap, making the usefulness of having multiple contacts in this area questionable, especially when there is degeneration of the peripheral processes in the apex. (V) The characteristic place pitch at the OC and SG can be described as functions of cochlear angle by equations 2 and 9 of this paper. These results may provide insight to future CI research and to clinicians attempting to match input frequencies of bilateral implants or bimodal hearing.

Acknowledgements

This study was financially supported by the Heinsius-Houbolt Fund and Advanced Bionics Corporation.

References

Ariyasu, L., Galey, F.R., Hilsinger, R., Jr., Byl, F.M., 1989. Computer-generated three-dimensional reconstruction of the cochlea. Otolaryngol. Head Neck Surg. 100, 87–91.

Arnoldner, C., Kaider, A., Hamzavi, J., 2006. The role of intensity upon pitch perception in cochlear implant recipients. Laryngoscope 116, 1760–1765.

Arnoldner, C., Riss, D., Kaider, A., Mair, A., Wagenblast, J., Baumgartner, W.D., Gstottner, W., Hamzavi, J.S., 2008. The intensity-pitch relation revisited: monopolar versus bipolar cochlear stimulation. Laryngoscope 118, 1630–1636.

Baskent, D., Shannon, R.V., 2004. Frequency-place compression and expansion in cochlear implant listeners. J. Acoust. Soc. Am. 116, 3130–3140.

Baskent, D., Shannon, R.V., 2005. Interactions between cochlear implant electrode insertion depth and frequency-place mapping. J. Acoust. Soc. Am. 117, 1405–1416.

Baskent, D., Shannon, R.V., 2007. Combined effects of frequency compression-expansion and shift on speech recognition. Ear Hear. 28, 277–289.

Baumann, U., Nobbe, A., 2004. Pitch ranking with deeply inserted electrode arrays. Ear Hear. 25, 275–283.

Baumann, U., Nobbe, A., 2006. The cochlear implant electrode-pitch function. Hear. Res. 213, 34–42.

Baumann, U., Rader, T., Helbig, S., Bahmer, A., 2011. Pitch matching psychometrics in electric acoustic stimulation. Ear Hear. 32, 656–662.

Biedron, S., Westhofen, M., Ilgner, J., 2009. On the number of turns in human cochleae. Otol. Neurotol. 30, 414–417.

Blamey, P.J., Dooley, G.J., Parisi, E.S., Clark, G.M., 1996. Pitch comparisons of acoustically and electrically evoked auditory sensations. Hear. Res. 99, 139–150.

Boëx, C., Baud, L., Cosendai, G., Sigrist, A., Kos, M.I., Pelizzone, M., 2006. Acoustic to electric pitch comparisons in cochlear implant subjects with residual hearing. J. Assoc. Res. Otolaryngol. 7, 110–124.

Boyd, P.J., 2011. Potential benefits from deeply inserted cochlear implant electrodes. Ear Hear. 32, 411–427.

Bredberg, G., 1968. Cellular pattern and nerve supply of the human organ of Corti. Acta Otolaryngol. Suppl.

Briaire, J.J., Frijns, J.H.M., 2000a. Field patterns in a 3D tapered spiral model of the electrically stimulated cochlea. Hear. Res. 148, 18–30.

Briaire, J.J., Frijns, J.H.M., 2000b. 3D mesh generation to solve the electrical volume conduction problem in the implanted inner ear. Simulation Practice and Theory 8, 57–73.

Briaire, J.J., Frijns, J.H.M., 2005. Unraveling the electrically evoked compound action potential. Hear. Res. 205, 143–156.

Briaire, J.J., Frijns, J.H.M., 2006. The consequences of neural degeneration regarding optimal cochlear implant position in scala tympani: a model approach. Hear. Res. 214, 17–27.

Brill, S., Muller, J., Hagen, R., Moltner, A., Brockmeier, S.J., Stark, T., Helbig, S., Maurer, J., Zahnert, T., Zierhofer, C., Nopp, P., Anderson, I., Strahl, S., 2009. Site of cochlear stimulation and its effect on electrically evoked compound action potentials using the MED-EL standard electrode array. Biomed. Eng Online. 8, 40.

Carlyon, R.P., Macherey, O., Frijns, J.H.M., Axon, P.R., Kalkman, R.K., Boyle, P., Baguley, D.M., Briggs, J., Deeks, J.M., Briaire, J.J., Barreau, X., Dauman, R., 2010a. Pitch Comparisons between Electrical Stimulation of a Cochlear Implant and Acoustic Stimuli Presented to a Normal-hearing Contralateral Ear. J. Assoc. Res. Otolaryngol. 11, 625–640.

Carlyon, R.P., Lynch, C., Deeks, J.M., 2010b. Effect of stimulus level and place of stimulation on temporal pitch perception by cochlear implant users. Journal of the Acoustical Society of America 127, 2997–3008.

Cohen, L.T., Xu, J., Tycocinski, M., Saunders, E., Raja, D., Cowan, R., 2000. Evaluation of an x-ray analysis method: comparison of electrode position estimates with information from phase contrast x-ray and histology. 5th European Symposium on Paediatric Cochlear Implantation, Antwerp, Belgium, June 4–7, 2000.

Deman, P.R., van, D.B., Offeciers, F.E., Govaerts, P.J., 2004. Pitch estimation of a deeply inserted cochlear implant electrode. Int. J. Audiol. 43, 363–368.

Dorman, M.F., Loizou, P.C., Rainey, D., 1997. Simulating the effect of cochlear-implant electrode insertion depth on speech understanding. J. Acoust. Soc. Am. 102, 2993–2996.

Dorman, M.F., Spahr, T., Gifford, R., Loiselle, L., McKarns, S., Holden, T., Skinner, M., Finley, C., 2007. An electric frequency-to-place map for a cochlear implant patient with hearing in the nonimplanted ear. J. Assoc. Res. Otolaryngol. 8, 234–240.

Escudé, B., James, C., Deguine, O., Cochard, N., Eter, E., Fraysse, B., 2006. The size of the cochlea and predictions of insertion depth angles for cochlear implant electrodes. Audiol. Neurootol. 11 Suppl 1, 27–33.

Faes, T.J., van der Meij, H.A., de Munck, J.C., Heethaar, R.M., 1999. The electric resistivity of human tissues (100 Hz-10 MHz): a meta-analysis of review studies. Physiol Meas. 20, R1–10.

Franke-Trieger, A., Jolly, C., Darbinjan, A., Zahnert, T., Murbe, D., 2014. Insertion depth angles of cochlear implant arrays with varying length: a temporal bone study. Otol. Neurotol. 35, 58–63.

Frijns, J.H.M., Briaire, J.J., Schoonhoven, R., 2000. Integrated use of volume conduction and neural models to simulate the response to cochlear implants. Simulation Practice and Theory 8, 75–97.

Frijns, J.H.M., Briaire, J.J., Grote, J.J., 2001. The importance of human cochlear anatomy for the results of modiolus-hugging multichannel cochlear implants. Otol. Neurotol. 22, 340–349.

Frijns, J.H.M., Kalkman, R.K., Vanpoucke, F.J., Bongers, J.S., Briaire, J.J., 2009a. Simultaneous and non-simultaneous dual electrode stimulation in cochlear implants: evidence for two neural response modalities. Acta Otolaryngol. 129, 433–439.

Frijns, J.H.M., Kalkman, R.K., Briaire, J.J., 2009b. Stimulation of the facial nerve by intracochlear electrodes in otosclerosis: a computer modeling study. Otol. Neurotol. 30, 1168–1174.

Frijns, J.H.M., Dekker, D.M.T., Briaire, J.J., 2011. Neural excitation patterns induced by phased-array stimulation in the implanted human cochlea. Acta Otolaryngol. 131, 362–370.

Fu, Q.J., Shannon, R.V., 1999. Recognition of spectrally degraded and frequency-shifted vowels in acoustic and electric hearing. J. Acoust. Soc. Am. 105, 1889–1900.

Gani, M., Valentini, G., Sigrist, A., Kos, M.I., Boëx, C., 2007. Implications of Deep Electrode Insertion on Cochlear Implant Fitting. J. Assoc. Res. Otolaryngol. 8, 69–83.

Greenwood, D.D., 1990. A cochlear frequency-position function for several species–29 years later. J. Acoust. Soc. Am. 87, 2592–2605.

Hamzavi, J., Arnoldner, C., 2006. Effect of deep insertion of the cochlear implant electrode array on pitch estimation and speech perception. Acta Otolaryngol. 126, 1182–1187.

Hanekom, T., 2001. Three-dimensional spiraling finite element model of the electrically stimulated cochlea. Ear Hear. 22, 300–315.

Hochmair, I., Arnold, W., Nopp, P., Jolly, C., Muller, J., Roland, P., 2003. Deep electrode insertion in cochlear implants: apical morphology, electrodes and speech perception results. Acta Otolaryngol. 123, 612–617.

Kawano, A., Seldon, H.L., Clark, G.M., 1996. Computer-aided three-dimensional reconstruction in human cochlear maps: measurement of the lengths of organ of Corti, outer wall, inner wall, and Rosenthal's canal. Ann. Otol. Rhinol. Laryngol. 105, 701–709.

Laneau, J., Wouters, J., Moonen, M., 2004. Relative contributions of temporal and place pitch cues to fundamental frequency discrimination in cochlear implantees. J. Acoust. Soc. Am. 116, 3606–3619.

Li, T., Fu, Q.J., 2010. Effects of spectral shifting on speech perception in noise. Hear. Res. 270, 81–88.

McDermott, H., Sucher, C., Simpson, A., 2009. Electro-acoustic stimulation. Acoustic and electric pitch comparisons. Audiol. Neurootol. 14 Suppl 1, 2–7.

Mens, L.H., Huiskamp, G., Oostendorp, T., van den Broek, P., 1999. Modelling surface potentials from intracochlear electrical stimulation. Scand. Audiol. 28, 249–255.

Pijl, S., 1997. Pulse rate matching by cochlear implant patients: effects of loudness randomization and electrode position. Ear Hear. 18, 316–325.

Rattay, F., Leao, R.N., Felix, H., 2001. A model of the electrically excited human cochlear neuron. II. Influence of the three-dimensional cochlear structure on neural excitability. Hear. Res. 153, 64–79.

Reiss, L.A., Turner, C.W., Erenberg, S.R., Gantz, B.J., 2007. Changes in pitch with a cochlear implant over time. J. Assoc. Res. Otolaryngol. 8, 241–257.

Reiss, L.A., Gantz, B.J., Turner, C.W., 2008. Cochlear implant speech processor frequency allocations may influence pitch perception. Otol. Neurotol. 29, 160–167.

Schatzer, R., Vermeire, K., Visser, D., Krenmayr, A., Kals, M., Voormolen, M., Van de Heyning, P., Zierhofer, C., 2013. Electric-acoustic pitch comparisons in single-sided-deaf cochlear implant users: Frequency-place functions and rate pitch. Hear. Res. 309C, 26–35.

Shannon, R.V., 1983. Multichannel electrical stimulation of the auditory nerve in man. I. Basic psychophysics. Hear. Res. 11, 157–189.

Shannon, R.V., Zeng, F.G., Wygonski, J., 1998. Speech recognition with altered spectral distribution of envelope cues. J. Acoust. Soc. Am. 104, 2467–2476.

Siciliano, C.M., Faulkner, A., Rosen, S., Mair, K., 2010. Resistance to learning binaurally mismatched frequency-to-place maps: implications for bilateral stimulation with cochlear implants. J. Acoust. Soc. Am. 127, 1645–1660.

Skinner, M.W., Holden, T.A., Whiting, B.R., Voie, A.H., Brunsden, B., Neely, J.G., Saxon, E.A., Hullar, T.E., Finley, C.C., 2007. In vivo estimates of the position of advanced bionics electrode arrays in the human cochlea. Ann. Otol. Rhinol. Laryngol. Suppl 197, 2–24.

Snel-Bongers, J., Briaire, J.J., van der Veen, E.H., Kalkman, R.K., Frijns, J.H., 2013. Threshold levels of dual electrode stimulation in cochlear implants. J. Assoc. Res. Otolaryngol. 14, 781–790.

Stakhovskaya, O., Sridhar, D., Bonham, B.H., Leake, P.A., 2007. Frequency Map for the Human Cochlear Spiral Ganglion: Implications for Cochlear Implants. J. Assoc. Res. Otolaryngol. 8, 220–233.

Suesserman, M.F., 1992. Noninvasive microelectrode measurement technique for performing quantitative, in vivo measurements of inner ear tissue impedances. PhD thesis University of Washington.

Townshend, B., Cotter, N., Van, C.D., White, R.L., 1987. Pitch perception by cochlear implant subjects. J. Acoust. Soc. Am. 82, 106–115.

van der Marel, K.S., Briaire, J.J., Wolterbeek, R., Snel-Bongers, J., Verbist, B.M., Frijns, J.H., 2014. Diversity in cochlear morphology and its influence on cochlear implant electrode position. Ear Hear. 35, e9–e20.

Vanpoucke, F.J., Zarowski, A.J., Peeters, S.A., 2004. Identification of the impedance model of an implanted cochlear prosthesis from intracochlear potential measurements. IEEE Trans. Biomed. Eng 51, 2174–2183.

Verbist, B.M., Frijns, J.H., Geleijns, J., van Buchem, M.A., 2005. Multisection CT as a valuable tool in the postoperative assessment of cochlear implant patients. AJNR Am. J. Neuroradiol. 26, 424–429.

Vermeire, K., Nobbe, A., Schleich, P., Nopp, P., Voormolen, M.H., Van de Heyning, P.H., 2008. Neural tonotopy in cochlear implants: an evaluation in unilateral cochlear implant patients with unilateral deafness and tinnitus. Hear. Res. 245, 98–106.

Whiten, D.M., 2007. Electro-anatomical models of the cochlear implant. PhD thesis Massachusetts Institute of Technology.

Yoon, Y.S., Liu, A., Fu, Q.J., 2011. Binaural benefit for speech recognition with spectral mismatch across ears in simulated electric hearing. J. Acoust. Soc. Am. 130, EL94–100.

Yoon, Y.S., Shin, Y.R., Fu, Q.J., 2013. Binaural benefit with and without a bilateral spectral mismatch in acoustic simulations of cochlear implant processing. Ear Hear. 34, 273–279.

Chapter 4

Stimulation of the Facial Nerve by Intracochlear Electrodes in Otosclerosis: A Computer Modeling Study

Johan H.M. Frijns
Randy K. Kalkman
and Jeroen J. Briaire

Otology & Neurotology 2009 (30), 1168–1174

Abstract

Hypothesis: The increased likelihood of facial nerve stimulation (FNS) with cochlear implantation in advanced cochlear otosclerosis is due to a lowering of the facial nerve excitation threshold with increasing bone demineralization. Background: Facial nerve stimulation can complicate cochlear implant fitting, often necessitating the deactivation of certain electrode contacts.

Methods: High-resolution computed tomographic scans were used to estimate anatomic features of the cochlea and the facial nerve canal. These features were added to a detailed computational model of the implanted human cochlea to examine the consequences of increased conductivity of the bone of the otic capsule. The model took into account the electrode contact type (banded or otherwise) and position (perimodiolar or lateral wall) of the electrode array.

Results: Contrary to the hypothesis, facial nerve thresholds were found to be slightly elevated with increased conductivity of the surrounding bone. However, the threshold and most comfortable loudness levels of the auditory nerve increase more rapidly owing to the reduced current density in the scala tympani as current leaks more easily out of the cochlea. Lateral wall electrodes were predicted to result in an increased likelihood of FNS. A progressively reduced probability of FNS was indicated for the full-band, half-band, and plated electrode arrays, respectively.

Conclusion: The clinical observation of increased FNS in cases of cochlear otosclerosis has been demonstrated in a computational model. Rather than decreased FN threshold, it is the increased levels for cochlear stimulation that is the main factor. Particularly, perimodiolar designs with more shielding against lateral spread of current could reduce the likelihood of FNS.

Introduction

Modern commercially distributed cochlear implants (CIs) have become widely accepted as an effective treatment of severe or profound deafness. The CI produces a sensation of hearing by delivering sequences of electrical current pulses to the cochlear (VIIIth) nerve through electrodes surgically implanted in the scala tympani of the cochlea, the stimulation pulses being modulated by the incoming acoustic signal detected by an externally worn microphone.

Many commercial CIs use silastic electrode arrays that are straight before insertion, and these tend to lie along the outer ("lateral") margins of the scala tympani after insertion. Alternatively, there are several designs of "modiolus-hugging" or "perimodiolar" electrodes (usually having a preformed curved shape), which are designed to lie along the inner ("medial") margin. This results in the stimulating electrodes being located closer to the target neural elements, thus reducing the current amplitudes required and also producing more localized stimulation fields (Balkany et al., 2002; van der Beek et al., 2005; Hughes and Abbas, 2006).

Although the electrical stimulation delivered via the CI is designed to excite the VIIIth nerve, there are situations where stimulation of other nerves has been reported. This is most often in the case with the facial nerve (VIIth; FN) and is more likely to occur when relatively high stimulation currents are required. Facial nerve stimulation (FNS) usually first becomes evident during the programming of the sound processor, where stimulus-locked eye twitches or other facial movements are visible to an observer and may be felt by the patient. Usually, this occurs on a small subset of the available electrodes, and deactivation of such electrodes can still result in a satisfactory programming of the device in most cases (Muckle and Levine, 1994).

Stimulation of the VIIth nerve is presumed to sometimes occur in this way because of its close proximity to the cochlea. In some cases, FNS has been reported from electrodes close to the insertion point (cochleostomy), where the array crosses the facial ridge at the posterior tympanotomy. More often, however, FNS originates from electrodes inserted more deeply into the cochlea, most typically around the top of the first turn, close to the geniculate and labyrinthine segments of the FN (Kelsall et al., 1997).

Previous reports on the incidence of FNS in CI users have suggested widely differing figures, from 3 (Kelsall et al., 1997) to 14.6% (Niparko et al., 1991). One possible explanation for the differences in these estimates may be heterogeneity of the patient groups studied because it seems that FNS is much more commonly observed in certain deafness etiologies, notably those involving anatomic or structural changes to the cochlea. In certain situations, the FN may be closer to some part of the electrode array (as in some cases of malformation) or there might be a reduction in the resistance to current flow reaching the FN, such as fracture or loss of normal bone structure.

One such condition is otosclerosis, which involves demineralization of the otic capsule, as well as a phase of new bone growth (sclerotic phase). The functional consequences, in hearing, are a conductive hearing loss, primarily due to ankylosis of the stapes footplate,

and, less commonly, a sensorineural hearing loss due to new sclerotic bone formation within the lumens of the cochlea (Youssef et al., 1998). “Retrofenestral” or “cochlear” otosclerosis is relatively uncommon but can cause hearing loss sufficiently severe to indicate the use of a CI. Such cases constitute a small but significant proportion of CI recipients, with 6.7% reported by Rotteveel et al. (2004) in a multicenter survey involving a total of 788 adult recipients.

The severe demineralization can cause difficulties with surgical insertion of the electrode array (Ramsden et al., 1997), and the incidence of FNS in CI users has been reported to be much higher in those with cochlear otosclerosis than in the general population; in the study of Rotteveel et al. (2004), 38% of the population with otosclerosis had experienced FNS at some point. It is generally assumed that FNS primarily occurs due to the increased conductivity of the bone insulating the scala tympani from the FN, although the type and position of the electrodes used is also relevant, that is, the laterally positioned and banded electrodes are more likely to produce FNS (Jaekel et al., 2004; Ramsden et al., 2007).

For several years, a detailed computer model of the cochlea has been developed at the Leiden University Medical Center (Frijns et al., 2000; 2001; Briaire and Frijns, 2005), which has been used to gain insight into the working mechanisms of electrical stimulation of the auditory nerve by a CI. On several occasions, the model predictions were in accordance with animal and psychophysical experiments (Frijns et al., 2000; Briaire and Frijns, 2005; Frijns et al., 2009). With this model, it is possible to predict the current flow through the cochlea in far greater detail than is possible from experimental studies. It is also possible to model current flow using different electrode types and positions. In addition, as long as the model can be validated by experimental studies, it can be used to predict the consequences of changes in either the dimensions or the conductivity values of the constituent components, such as might occur in a range of pathologic conditions.

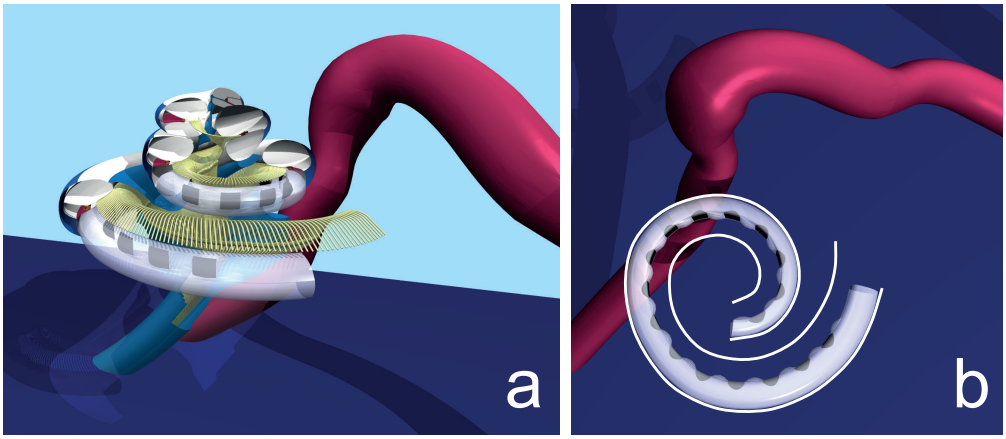

Figure 4.1. *Panel a: partly sliced-open version of the 3-dimensional model of the implanted human cochlea and the modeled segment of the FN. Panel b: the FN segment in relation to the model of the laterally inserted plate contact electrode array. The contours of the basal scala tympani are indicated by white lines.*

For the present study, we extended our computational cochlear model to include the FN in examining the effects of some of the variables relating to the production of FNS by a CI in the otosclerotic ear. A particular goal was to test the assumption that FNS is due primarily, or solely, to an increase in the conductivity of the bone surrounding the cochlea. Further goals were to examine the impact of whether the electrode array was in a lateral or perimodiolar position within the scala. Finally, it was questioned whether the nature of the electrode contact design could be demonstrated to influence the likelihood of FNS, as has been reported from clinical observations (Jaekel et al., 2004; Ramsden et al., 2007).

Materials and methods

This study used the CI model presented in previous publications from the Leiden University Medical Center, which consisted of a volume conduction model and a neural model of the auditory nerve fibers (Briaire and Frijns, 2000; Frijns et al., 2000; Frijns et al., 2001; Briaire and Frijns, 2005; Frijns et al., 2009). The volume conduction model was based on the boundary element method, and its geometry was a realistic representation of the implanted human cochlea, describing the boundaries between different media in the cochlea with quadratically curved triangles. Each medium in the model is considered purely resistive, having its own specific electrical conductivity that is the same in all directions (isotropic), and has no capacitative properties. The neural model was based on the nonlinear generalized Schwarz and Eikhof-Frijns model of primary auditory nerve fibers and used a nerve fiber morphology designed to accurately represent the human auditory nerve (Briaire and Frijns, 2005).

Compared with the previous publications, a number of changes were made to the basic model to more accurately describe the anatomy of the cochlea. Data from Stakhovskaya et al. (2007) have been implemented to generate realistic oblique fiber trajectories instead of the purely radial trajectories used in previous publications. Furthermore, the axons of the nerve fibers have been bundled together in the modiolus rather than extending from their cell bodies in parallel trajectories. The auditory nerve bundle that extends from the cochlea was therefore much narrower than in previous studies, and it followed a more realistic trajectory instead of running parallel to the cochlear rotation axis. A layer of cerebrospinal fluid was added around the nerve trunk, and a cerebrospinal fluid compartment was added inside the modiolus itself. From electrical field imaging (EFI) recordings (Vanpoucke et al., 2004) in patients, a more accurate value of the conductivity of the temporal bone and the modiolus was determined for the model, giving a new bone conductivity value of 0.016 S/m and a modiolus conductivity of 0.2 S/m. With these adapted parameter values, simulated electrical field potentials are in line with actual recordings.

Three different electrode arrays were designed: 1) an equivalent of the Nucleus Straight (Cochlear Ltd., Sydney, Australia) electrode array having a banded annular contact design (with 22 contacts), 2) a version of the Nucleus Straight array model with 22 half-banded electrode contacts (more or less mimicking the Contour array), and 3) an equivalent of the Advanced Bionics HiFocus (Sylmar, CA, USA) electrode array having 16 flat modiolar-facing

plate contacts. The electrode contacts were labeled from 1, for the most basal to 16 of 22 for the most apical contact.

For this study, the dimensions of the FN canal and its orientation relative to the cochlea were ascertained from high-resolution computed tomographic (CT) scans of a patient with otosclerosis (Verbist et al., 2005; 2008) to derive a new model of the FN. The dimensions and shape of the cochlea model were adjusted to match those of the CT scan, giving us a combined cochlea/FN model, which included a segment of the FN as illustrated in Figure 4.1a. The CT scans of the patient with otosclerosis showed a layer of approximately 1-mm thickness around the cochlea where the bone was denser than the surrounding bone. Therefore, such a layer was added to the cochlear model.

The neural response properties of the FN were defined in a similar way to our existing model of the auditory nerve based on the nonlinear generalized Schwarz and Eikhof-Frijns model of primary auditory nerve fibers (Briaire and Frijns, 2000; Frijns et al., 2000; Briaire and Frijns, 2005). The model simulated the response to time-varying potential fields in the cochlea and was applied to both the auditory and the FNs. A bundle of 16 homogenous fibers was positioned along the outer contour of the FN canal. Dimensional characteristics of these fibers were based on data from Schröder et al. (1988), including a 4-μm axonal diameter and 400-μm internodal spacing. Each FN fiber consisted of 88 nodes of Ranvier, resulting in a 34.9-mm section of the FN in closest proximity to the contacts of the electrode array implanted into the scala tympani of the cochlea (Fig. 4.1b).

The primary measures of interest were excitation thresholds of the cochlear nerve and the FN (in mA) and the most comfortable loudness (MCL) levels of the cochlear nerve. As previously, the MCL was defined as the current required to exceed the threshold for a length of 4 mm along the basilar membrane (Frijns et al., 2009). From these measures, it was possible to predict where FNS was likely to occur relative to the auditory dynamic range; that is, whether FNS would reduce the useable dynamic range of an electrode contact or prevent its use completely. Stimulus parameters were symmetrical biphasic current pulses with a phase duration of 37.5 microseconds delivered to each individual electrode contact for the 3 electrode array models. For the purposes of modeling, each electrode array was studied in both lateral and perimodiolar (medial) positions. Note also that to ensure calculations would be made in a comparable manner for each of the electrode array designs, the banded electrode array is modeled as more deeply inserted than would normally be found in clinical practice with the Nucleus Straight array. The main effect of this would be to show the worst-case FNS occurring at different electrode contacts than might be encountered clinically. Because an exact conductivity value of otosclerotic bone is not known, we have performed the above calculations for various bone conductivity values. The lower limit of the conductivity range was 0.016 S/m thought to represent that of a typical healthy otic capsule, whereas for the upper limit, a value of 1.6 S/m was chosen, representing a considerable increase in the ability of electrical current to pass through the demineralized otosclerotic bone (for comparison, perilymph has a conductivity of 1.43 S/m). The dense bone layer around the cochlea was assumed to have a 50% lower electrical conductivity than the normal temporal bone (0.008 S/m).

Results

Figure 4.2 shows the effects of increasing bone conductivity on the excitation thresholds of the FN and cochlear nerve and on the MCL of the cochlear nerve. The situation for full-band, half-band, and plate contacts is shown in the top, middle, and bottom panels, respectively. The 3 panels on the left show results for each electrode array located at the lateral (outer) extent of the scala tympani, whereas the 3 panels on the right show the situation when the electrode array has been placed in a perimodiolar (medial) position. The stimulating electrode illustrated in Figure 4.2 was the one producing the lowest FN threshold by electrode array type: E13 for the lateral full-banded and half-banded arrays, E15 for the medial-banded arrays, and E11 for the plate arrays. In fact, all these contacts were located at an insertion angle of approximately 280 degrees from the round window.

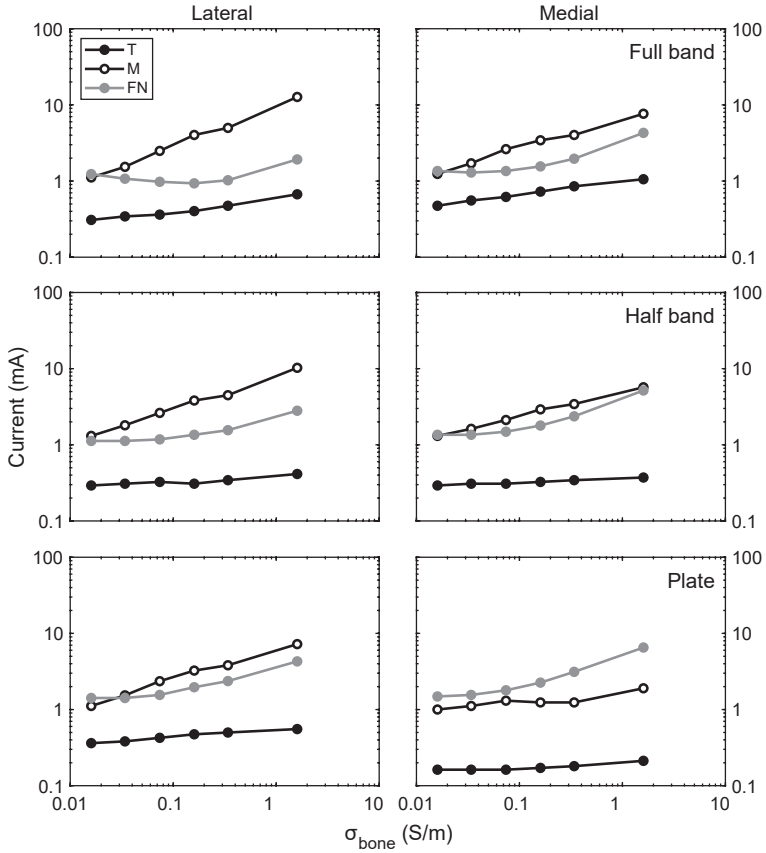

Figure 4.2. *Facial nerve thresholds (filled circles, gray line), cochlear nerve thresholds (filled circles, black line), and cochlear nerve MCLs (open circles, black line) as a function of conductivity of the surrounding bone. Plots are included for a full-banded electrode array (upper panels), a half-banded array (middle panels), and the plate electrode array (lower panels), the latter 2 with contacts facing the modiolus. The panels on the left are for the arrays in the lateral position of the scala tympani, and the panels on the right are for arrays in the medial position. The stimulating electrode contact was the one producing the lowest FN threshold in each case.*

Note that, ideally, the half-band electrode array would take up a perimodiolar position in normal implantation and that the full-band array would normally be in the lateral position.

It is clear that, in all conditions, increased bone conductivity results in slightly increased excitation thresholds of both nerves. However, the MCL of the cochlear nerve, particularly in the lateral positions, increases at a greater rate than the excitation threshold of either nerve. This has 2 effects: 1) the electrical dynamic range of the cochlear nerve appears to be considerably larger at higher bone conductivities and 2) the threshold of FNS occurs at a lower point in the auditory dynamic range at higher bone conductivities.

Figure 4.3 shows the effect of the electrode contact position for the full-band and plate electrode contact designs. Both arrays are modeled in the lateral location. Calculations were made for 3 bone conductivity values: 0.016 (upper panels), 0.16 (middle panels), and 1.6 S/m (lower panels). These conductivities cover a range from normal, moderately

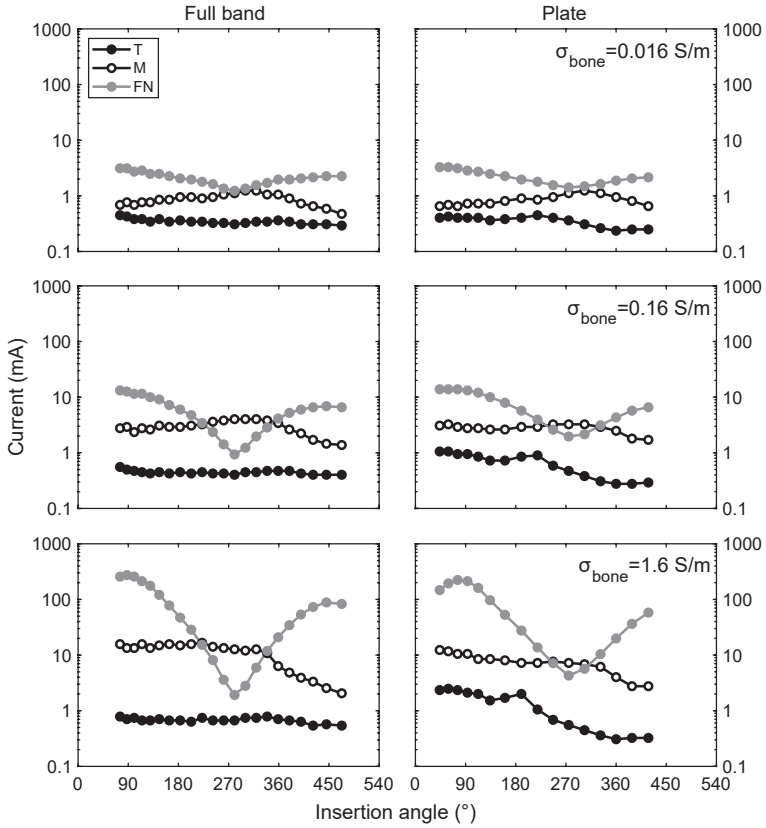

Figure 4.3. *Facial nerve thresholds (filled circles, gray line), cochlear nerve thresholds (filled circles, black line), and cochlear nerve MCLs (open circles, black line) as a function of the angular insertion depth of the stimulating electrode. Left panels are for the full-band array, and right panels are for the plate electrode array. The upper panels are results with normal bone conductivity (0.016 S/m), middle panels are results with a conductivity of 0.16 S/m, and lower panels are results with a conductivity of 1.6 S/m.*

demineralized bone to severely demineralized bone. As explained in Materials and Methods, there are no data regarding the actual conductivity value of the bone in otosclerosis.

Several observations were evident from these plots:

1. Facial nerve threshold has a minimum value at approximately the same angular position in all traces, corresponding to E13 for the full-band contact array and E6 for the plate contact array. These electrodes are in the region of the cochlea closest to the FN.
2. Facial and cochlear nerve excitation thresholds become higher with increasing bone conductivity (as is also evident in Fig. 4.2). However, FN excitation thresholds for the contacts closest to the FN are elevated less, implying an increased risk for FNS.
3. Cochlear nerve MCLs also increase with increasing bone conductivity, but more so than the thresholds, such that the auditory dynamic range also increases with increasing conductivity.
4. There are regions where FN thresholds are lower than auditory MCLs, a trend that is more evident for the electrode array with full-band contacts.
5. For electrodes toward both ends of the array, moving away from the FN location, the FN excitation thresholds are dramatically increased with increasing bone conductivity, such that they become very much higher than the auditory MCLs.

Discussion

The hypothesis that excitation of the FN by a CI is more frequently encountered in cases of cochlear otosclerosis, owing to the increased conductivity of the bone surrounding the cochlea, seems to be supported by our modeling work. However, the mechanism through which this is predicted to occur is not so intuitive. A lowering of the FN excitation threshold with increasing bone conductivity was expected. Unexpectedly, the FN excitation threshold was found to remain relatively constant for conductivities up to approximately 0.3 S/m. The main effect seemed to be an increased current being required to produce MCL with higher bone conductivity. This effect is explained by a higher leakage of stimulation current from the scala tympani as developed and discussed in later paragraphs.

In an earlier study, we examined the field patterns generated by current sources in a 3-dimensional model of the electrically stimulated cochlea (Briaire and Frijns, 2000). From this, it was evident that the highly resistive organ of Corti and the basilar membrane virtually block the current flow out of the scala tympani superiorly. The bone layer between the turns also works to confine the current flow to the scala tympani. On the other hand, the spiral ligament has much higher conductivity and appears to act as a pathway through which current can leak out of the scala tympani. In the normal ear, this is, of course, surrounded by the bone of the otic capsule, which presumably serves to isolate the FN from electrical fields originating in the scala tympani despite their proximity to the top

of the first turn. It was hypothesized that an increased conductivity of the bone could potentially reduce the threshold of the FN to stimulation by such fields.

Counterintuitively, the results of the present study show that increasing bone conductivity tends to increase excitation thresholds for both the cochlear nerve and FN, presumably owing to the reduced current density produced in the scala tympani. For FN thresholds, this effect seems much more pronounced when the stimulating contact is further away from the FN. In addition, MCLs seem to increase more than the auditory nerve thresholds (resulting in an increased electrical dynamic range with higher bone conductivities). Taken together, these factors can result in the presence of a region of the cochlea where the FN excitation threshold is lower than the MCL. This is, of course, exactly what is observed clinically in some patients, where it is not possible to reach the MCL without initiating FNS, such that these electrodes have to be deactivated in a sound processor program. Rotteveel et al. (2004) reported this effect to occur at insertion angles comparable to those predicted by the model.

The effect of raised auditory nerve threshold and MCL in implanted otosclerosis patients has been reported in association with some clinical studies (Quaranta et al., 2005; Sainz et al., 2007), although most studies do not report stimulation levels that differ from patients without otosclerosis. We also checked our own patient data and found that average threshold and MCL levels of our group of patient with otosclerosis (n = 11) were higher than those in a group of 90 patients without otosclerosis (all with a HiFocus electrode), but because of the large variability of stimulation levels in patients, no statistical significance was found. This could mean that it will be difficult to conclusively prove or falsify the model-predicted raised stimulation levels due to otosclerosis in clinical studies.

In the model, certain effects of electrode type and placement were also evident. Although the abovementioned observations were visible in all conditions tested, they were more pronounced in some conditions than in others. In Figure 4.3, the excitation thresholds for the cochlear nerve are predicted to be quite uniform across electrode contact for normal bone density, conforming with the clinical observation where monopolar electrode coupling is used. The absolute value of excitation thresholds is also very much in line with the values encountered clinically. Although this flat profile is maintained with increasing bone conductivity for the full-band design (Fig. 4.3, left panels), the plate electrode design (right panels) is predicted to show more threshold increase for basal contacts than for apical contacts. This may indicate a reduction in efficiency for the plate contacts when more distant from their target neurons and when current leaks more easily through the scala tympani walls.

In Figure 4.2, there is a considerable drop in plate electrode cochlear nerve excitation threshold as the array is moved from a lateral to a medial location. Although this effect is also observed clinically, the model may overestimate it. This effect is much reduced for either the half-band or the full-band design, which shows little threshold change as a result of their move from the lateral to the medial position. The hypothesis explaining this would be that the field generated by the banded array results in a greater leakage of

current through the spiral ligament. There are few indications from the reported literature as to whether this difference is observed clinically.

Considering the influence of the position of the electrode array on FNS, Figure 4.2 shows that this phenomenon is more likely for electrode arrays in the lateral position than when positioned medially; this effect observed for all 3 electrodes modeled. At higher bone conductivities, this seems to be due to an increase in the cochlear nerve MCLs as a result of reduced current density in the scala tympani rather than to a decrease in the FN thresholds. For normal bone conductivity, the effect of an increased distance to the cochlear nerve in the case of laterally placed electrodes appears to be relatively small. These results also seem to match clinical reports.

In conclusion, the results obtained with the computational model have confirmed the clinical observation of increased FNS in cases of advanced cochlear otosclerosis with demineralization of the otic capsule. Rather than a decreased FN threshold, it is the increased levels of cochlear stimulation that is the main factor. On the basis of this finding, it is predicted that an electrode array with an increased bulk of carrier at the lateral side of the stimulating electrode contact would be less likely to produce FNS and hence might convey a clinical benefit.

References

Balkany, T.J., Eshraghi, A.A., Yang, N. 2002. Modiolar proximity of three perimodiolar cochlear implant electrodes. Acta Otolaryngol 122, 363-9.

Briaire, J.J., Frijns, J.H. 2000. Field patterns in a 3D tapered spiral model of the electrically stimulated cochlea. Hear Res 148, 18-30.

Briaire, J.J., Frijns, J.H. 2005. Unraveling the electrically evoked compound action potential. Hear Res 205, 143-56.

Frijns, J.H., Briaire, J.J., Grote, J.J. 2001. The importance of human cochlear anatomy for the results of modiolus-hugging multichannel cochlear implants. Otol Neurotol 22, 340-9.

Frijns, J.H., Kalkman, R.K., Vanpoucke, F.J., Bongers, J.S., Briaire, J.J. 2009. Simultaneous and non-simultaneous dual electrode stimulation in cochlear implants: evidence for two neural response modalities. Acta Otolaryngol 129, 433-9.

Frijns, J.H.M., Briaire, J.J., Schoonhoven, R. 2000. Integrated use of volume conduction and neural models to simulate the response to cochlear implants. Simulat Pract Theory 8, 75-97.

Hughes, M.L., Abbas, P.J. 2006. Electrophysiologic channel interaction, electrode pitch ranking, and behavioral threshold in straight versus perimodiolar cochlear implant electrode arrays. J Acoust Soc Am 119, 1538-47.

Jaekel, K., Aschendorff, A., Klenzner, T., Laszig, R. 2004. Results with the Contour cochlear implant in patients with cochlear otosclerosis. Laryngorhinootologie 83, 457-60.

Kelsall, D.C., Shallop, J.K., Brammeier, T.G., Prenger, E.C. 1997. Facial nerve stimulation after Nucleus 22-channel cochlear implantation. Am J Otol 18, 336-41.

Muckle, R.P., Levine, S.C. 1994. Facial nerve stimulation produced by cochlear implants in patients with cochlear otosclerosis. Am J Otol 15, 394-8.

Niparko, J.K., Oviatt, D.L., Coker, N.J., Sutton, L., Waltzman, S.B., Cohen, N.L. 1991. Facial nerve stimulation with cochlear implantation. VA Cooperative Study Group on Cochlear Implantation. Otolaryngol Head Neck Surg 104, 826-30.

Quaranta, N., Bartoli, R., Lopriore, A., Fernandez-Vega, S., Giagnotti, F., Quaranta, A. 2005. Cochlear implantation in otosclerosis. Otol Neurotol 26, 983-7.

Ramsden, R., Bance, M., Giles, E., Mawman, D. 1997. Cochlear implantation in otosclerosis: a unique positioning and programming problem. J Laryngol Otol 111, 262-5.

Ramsden, R., Rotteveel, L., Proops, D., Saeed, S., van Olphen, A., Mylanus, E. 2007. Cochlear implantation in otosclerotic deafness. Adv Otorhinolaryngol 65, 328-334.

Rotteveel, L.J., Proops, D.W., Ramsden, R.T., Saeed, S.R., van Olphen, A.F., Mylanus, E.A. 2004. Cochlear implantation in 53 patients with otosclerosis: demographics, computed tomographic scanning, surgery, and complications. Otol Neurotol 25, 943-52.

Sainz, M., García-Valdecasas, J., Garófano, M., Ballesteros, J.M. 2007. Otosclerosis: mid-term results of cochlear implantation. Audiol Neurootol 12, 401-6.

Schröder, J.M., Bohl, J., von Bardeleben, U. 1988. Changes of the ratio between myelin thickness and axon diameter in human developing sural, femoral, ulnar, facial, and trochlear nerves. Acta Neuropathol 76, 471-83.

Stakhovskaya, O., Sridhar, D., Bonham, B.H., Leake, P.A. 2007. Frequency map for the human cochlear spiral ganglion: implications for cochlear implants. J Assoc Res Otolaryngol 8, 220-33.

van der Beek, F.B., Boermans, P.P., Verbist, B.M., Briaire, J.J., Frijns, J.H. 2005. Clinical evaluation of the Clarion CII HiFocus 1 with and without positioner. Ear Hear 26, 577-92.

Vanpoucke, F.J., Zarowski, A.J., Peeters, S.A. 2004. Identification of the impedance model of an implanted cochlear prosthesis from intracochlear potential measurements. IEEE Trans Biomed Eng 51, 2174-83.

Verbist, B.M., Frijns, J.H., Geleijns, J., van Buchem, M.A. 2005. Multisection CT as a valuable tool in the postoperative assessment of cochlear implant patients. AJNR Am J Neuroradiol 26, 424-9.

Verbist, B.M., Joemai, R.M., Teeuwisse, W.M., Veldkamp, W.J., Geleijns, J., Frijns, J.H. 2008. Evaluation of 4 multisection CT systems in postoperative imaging of a cochlear implant: a human cadaver and phantom study. AJNR Am J Neuroradiol 29, 1382-8.

Youssef, O., Rosen, A., Chandrasekhar, S., Lee, H.J. 1998. Cochlear otosclerosis: the current understanding. Ann Otol Rhinol Laryngol 107, 1076-9.

Chapter 5

Simultaneous and non-simultaneous dual electrode stimulation in cochlear implants: evidence for two neural response modalities

Johan H.M. Frijns
Randy K. Kalkman
Filiep J. Vanpoucke
Jorien Snel-Bongers
and Jeroen J. Briaire

Acta Oto-Laryngologica 2009 (129), 433–439

Abstract

Conclusion: There are two modalities of dual electrode stimulation: a shifting, continuous excitation, which is the desired effect, and a split excitation with considerable variation in loudness. The first one most likely occurs in the basal turn, with adjacent contacts, stimulated simultaneously rather than sequentially. Objectives: This study examines the effects on place pitch and loudness of simultaneous current steering and sequential stimulation. These can give cochlear implant patients access to more perceptual channels than physical contacts in the electrode array. Materials and methods: For both lateral wall and perimodiolar electrodes, simultaneous current steering as well as sequential stimulation, place pitch and loudness of the percept were predicted with a computational model of the implanted human cochlea. The loudness predictions were validated with psychophysical loudness balancing experiments. Results: Simultaneous stimulation with adjacent electrode contacts in the basal end of the cochlea was generally able to produce a single, gradually shifting intermediate pitch percept. Simultaneous stimulation beyond the first cochlear turn, sequential stimulation and simultaneous stimulation with nonadjacent electrode contacts often produced two regions of excitation. In the case of sequential stimulation the total amount of current to reach most comfortable loudness was raised, both in the model and in the patients.

Introduction

Cochlear implants (CIs) have become a standard rehabilitation method for severely to profoundly hearing impaired children and adults. The main success of CI is in conveying speech information, especially in quiet conditions. Perception of more complex signals, such as music or speech in background noise, still needs improvement. One major limitation with modern implants is in the encoding of pitch, which can be addressed in the temporal and in the spectral domain. In the latter, with monopolar stimulation, the number of pitch percepts is limited to the small number of electrode contacts in the array (12-22 in contemporary CIs). Each of these contacts will induce a place pitch percept corresponding to the centroid (or peak) of excitation, which is induced by this contact. The question arises as to how to induce additional place pitch percepts that lie between the percepts generated by monopolar stimulation of two adjacent electrode contacts.

Dual electrode stimulation has been proposed as a method to accomplish this (Donaldson et al., 2005; Kwon and van den Honert, 2006), either by simultaneous stimulation of the two contacts with biphasic pulse trains of identical polarity (also called current steering) or by sequential stimulation of these contacts in quick succession. The technical advantage of sequential stimulation is that the implant needs only one current source, whereas in simultaneous current steering multiple current sources are needed. While the goal of these two types of dual electrode stimulation is the same, the underlying working principle is not. Current steering tries to make use of the summation of the electrical fields of two stimulating contacts to stimulate the neurons between those two contacts. In sequential stimulation, however, there is no direct electrical field summation. Therefore,

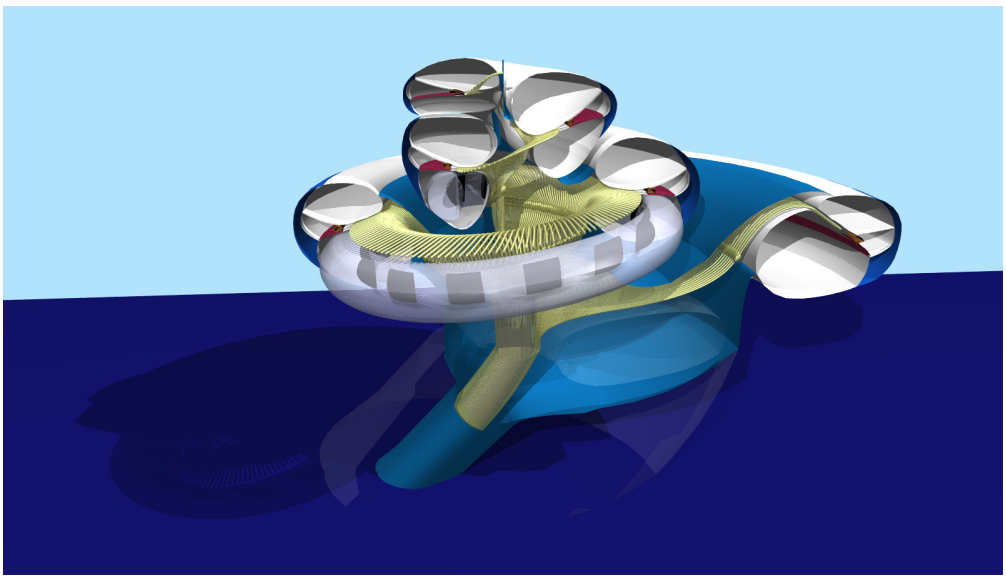

Figure 5.1. *The model of the cochlea used in the simulations. In particular, the trajectories of the primary auditory nerve fibres are more realistic than in previous studies (Frijns et al., 2001; Briaire and Frijns, 2005).*

the interaction between the pulses on both electrode contacts is dependent on capacitive components in the cochlea, especially the neural membranes.

The dual electrode stimulation coefficient α is defined as the fraction of the total current delivered through the more basal contact of the pair. Therefore, α=0 indicates stimulation of the apical contact only and α=1 stimulation of the basal one. Recent trials of large groups of patients have indicated that on average the number of discernible percepts that can be created along the electrode array of a CII/HiRes90K implant ranges between 60 and 80 (Firszt et al., 2007; Koch et al., 2007).

In this study the neural excitation patterns of both simultaneous and sequential dual electrode stimulation were examined. For this purpose detailed computational modelling was combined with a series of psychophysical experiments on loudness corrections with both types of dual electrode stimulation. To our knowledge this is the first report of such experiments in the same subject group. Finally, the modelling study examined the effects of electrode location and stimulus level on the experiments performed.

Material and methods

Computational modelling

A realistic three-dimensional (3D) model of the human cochlea (Figure 5.1) implanted with a geometrically accurate representation of the HiFocus electrode (Advanced Bionics, Sylmar, CA, USA) was used to calculate the electrical fields in the electrically stimulated cochlea. This was coupled to an active nerve fibre model, capable of handling both simultaneous and sequential current pulses to model dual electrode stimulation (Frijns et al., 2001; Briaire and Frijns, 2005). The anatomy of the human cochlear model had been enhanced compared with previous publications with more accurate fibre trajectories, including the difference between the basilar membrane length and the length of the spiral ganglion (Stakhovskaya et al., 2007). Also the conductivities of both nerve fibre tissue and the surrounding bone have been optimized on the basis of electrical field imaging modelling (EFI) recordings in actual patients (Vanpoucke et al., 2004). Details of these improvements are beyond the scope of this paper and will be presented elsewhere.

The outcomes of the model are presented in dual electrode stimulation plots, where the region of neural excitation is grey coded as a function of both location (vertical axis) and α (horizontal axis). The centroid of the neural excitation (indicated by a dashed line) is believed to correspond well to the perceived pitch percept (Laneau et al., 2004). The width of the excitation area indicates the number of fibres that are active, which is assumed to be a measure for the perceived loudness. The current level at which 4 mm along the basilar membrane becomes excited was considered as the most comfortable level (MCL) (Briaire and Frijns, 2006). For all stimulation levels the excitation area was examined while varying α. A smooth transition of a single excitation area from one contact to another was considered an ideal response modality as it resembles the excitation pattern of a series of intermediate physical contacts.

All calculations were performed for arrays located along the medial and the outer wall of the scala tympani, for contacts located at angles of 120°, 240°, 360° and 480° from the round window. Similarly to the psychophysical experiments (see below), equal loudness curves as a function of α were determined from the model data, giving the amount of current, expressed as percentage of the electrical dynamic range (EDR), which is needed to maintain constant loudness at intermediate values of α. When this amount of current deviates from 100% EDR, it will be referred to as 'loudness correction' in this paper.

Psychophysical experiments

Ten adult subjects (mean age 51.4 years, range 36-76 years; mean duration of implant use 10.7 months, range 9-17 months), wearing a HiRes90K device (Advanced Bionics), participated in the study. They were all good performers fitted with a 12 or 16 channel HiRes strategy at a rate of approximately 1400 pps/channel. Their mean phoneme score on open set Dutch monosyllabic (CVC) words in quiet conditions at 65 dB was 86.6%. The study protocol was approved by the Leiden medical ethical committee (P02.106).

Experiments were performed with the research tools BEDCS (Bionic Ear Data Collection System, Advanced Bionics LLC) for the electrical stimulation configuration and PACTS (PsychoACoustic Test Suite) for the psychoacoustic tests. Stimuli were dual electrode contact, 1000 pps biphasic pulse trains (32 μs/phase) with a total duration of 400 ms and 40 ms leading and trailing ramps. The loudness balancing was performed using a two-button screen, one button representing the apical monopolar stimulus at reference loudness, and the other a dual electrode stimulus with variable intensity. The subject indicated which stimulus was the louder one. Intensity was adjusted towards equilibrium by a 2AFC 1-up/1-down staircase procedure. Three contact pairs were tested with either current-steered (simultaneous) pulses or sequential ones (no pauses between pulses): 3-4 (apical), 7-8 (mid) and 12-13 (basal).

First, behavioural threshold (T) and MCL were determined for all individual contacts. The EDR of each contact equals the difference between its MCL and T level, expressed in μA. In this experiment all levels were carefully loudness balanced within and across electrode pairs, as in normal clinical follow-up, in many cases leading to a slight asymmetry in current levels within an electrode pair.

Next, equal loudness curves were determined for the dual electrode stimuli using a 2AFC adaptive staircase procedure. Six intermediate stimulus configurations were created with three steering coefficient values (α=0.25, 0.5 and 0.75) and two stimulation modes (sequential or simultaneous). Stimulus level parameter L was expressed as fraction of the EDR. The stimulus current I1 and I2 for both contacts in the pair was determined as follows by L and α, on the basis of the MCL and T level on the respective contacts:

$$I1 = (1 - \alpha) \cdot (T1 + L \cdot (MCL1 - T1))$$

$$I2 = \alpha \cdot (T2 + L \cdot (MCL2 - T2))$$

Results

Computational model

In Figure 5.2 the current steering plots at four different stimulation levels are presented for an electrode pair at 360° insertion depth (outer wall position) for simultaneous stimulation (top row), sequential stimulation (middle row) and for sequential stimulation with loudness compensation of dual electrode stimulation coefficients with a triangular function peaking at 0.5 (bottom row). At levels close to MCL, the place pitch for simultaneous current steering glides smoothly with α at almost constant loudness (indicated by area width). At lower current levels (Figure 5.2 a1 and a2) one can discern two separate regions of excitation, aligned to the two individual electrode contacts. At α=0 there is only excitation around one contact, with increasing α the excitation area becomes smaller, corresponding to the reduced current on that electrode contact. At a certain level (α=0.3 in Figure 5.2

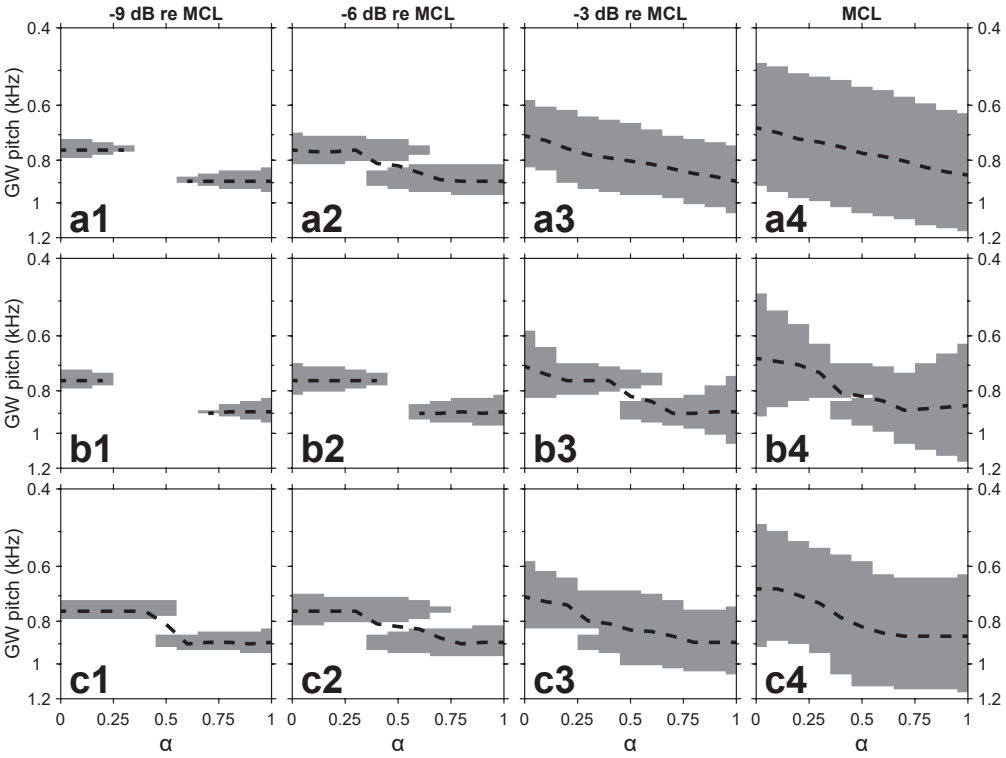

Figure 5.2. *Current steering plots for contacts around 360° in a HiFocus 1 electrode (outer wall position). The ordinate axis denotes the associated place pitch of the fibres according to the Greenwood map (Greenwood, 1990). The excitation area is shaded grey and its centre is indicated by a dashed line. Panes from left to right show results for stimulation levels from near threshold (-9 dB re MCL) to MCL. (a) Simultaneous current steering, (b) sequential mode, (c) sequential mode with loudness compensation.*

a2), the current on the other electrode reaches threshold and causes excitation, also centred around that contact. The first excitation area disappears when the current on the first contact drops below threshold with increasing α. Consequently, the centre of excitation jumps from one electrode contact region to the other. At the lowest levels towards threshold there is not even continuous stimulation for all α values.

In sequential stimulation mode this double peak behaviour is exaggerated when no loudness compensation is applied (Figure 5.2b). Also, the width of the region of excitation depends more on α. Figure 5.3a, b shows the equal loudness plots in % EDR for the model simulations as a function of α. For simultaneous stimulation these curves are almost flat, while the sequential stimulation requires much more current to maintain a constant loudness for α=0.5. Figure 5.2c shows the excitation plots for sequential stimulation with loudness compensation of α by a triangular function, determined at MCL. With this loudness correction a more gradual transition of place pitch is obtained, also at lower levels. For sequential dual electrode stimulation medial contacts require less loudness correction (150%-200% EDR, Figure 5.3b) than lateral ones (200%-320% EDR, Figure 5.3a). However, the model still predicts that loudness will vary with α at stimuli below MCL.

The differentiation between the response modalities with single and dual area excitation is present in various degrees for different electrode locations. At almost all configurations the dual area excitation is present at the very low levels. Perimodiolar contacts and contacts beyond the first cochlear turn demonstrate dual area excitation up to higher current levels. However, for simultaneous stimulation on lateral wall contacts in the base of the cochlea the regions of stimulation fuse at levels just above threshold. In addition, for simultaneous dual electrode stimulation the model indicates a slightly increased loudness for α=0.5 on medially placed electrodes, but a constant loudness for outer wall electrodes (Figure 5.3a, b).

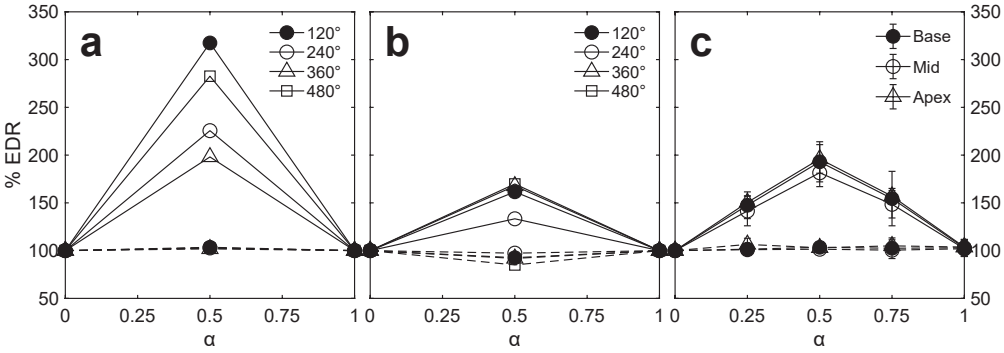

Figure 5.3. *The total stimulus level needed to keep loudness at MCL as a function of steering coefficient α. Dashed lines, simultaneous stimulation; full lines, sequential stimulation. (a) Model data for lateral electrodes, (b) model data for medial electrodes, (c) group average. In the patient data apical contacts were in the range of 358°-420° from the round window, middle contacts were at 251°-302° and basal contacts were at 149°-187°.*

Psychophysical loudness balancing

Figure 5.3c shows the equal loudness curves expressed as percentage EDR, averaged for all subjects. For simultaneous stimulation these curves are almost flat, implying an almost constant loudness percept as α is varied. The standard deviation is 6.7% or 0.56 dB. For sequential stimulation, there is a substantial and systematic loudness reduction if the total current is constant as α is varied. Some subjects even reported that the stimulus became inaudible around α=0.5. The decrease had to be compensated by increasing the total current level. The equal loudness compensation is approximately triangular, peaking at α=0.5 with a doubling of the EDR for all electrode pairs. The standard deviation around this equal loudness model is 16.4% or 1.32 dB.

Discussion

In the model two response modalities to dual electrode stimulation were identified: one with a single region of neural excitation that shifts gradually for different values of the steering parameter α, and the other with two separate regions of excitation located around the stimulating contacts. Dual area excitation occurred in situations where the excitation regions of the individual contacts of the pair did not overlap and there was not enough electrode interaction to excite the intermediate region of neurons. As a consequence, sequential stimulation was inherently more prone to this modality, since there was only interaction at a neural level and no direct electric field interaction. In contrast, with simultaneous stimulation, electric field summation can cause excitation of neurons that would not be excited by either of the two stimulating contact individually, possibly fusing the two excitation regions together. The current steered potential field can approximate the field generated by an intermediate real electrode quite well but it has its limitations. For instance, at locations where the two individual potential fields of the two current steering contacts are equal to each other, the total potential will remain invariant, independent of α. This is due to the fact that at those locations, changing the value of α will increase the contributed potential from one contact, but it will also decrease the potential from the other contact by an equal value, thus leaving the total potential constant. In a highly spatially selective condition, the potential at the neurons closest to the stimulating contacts may be considerably larger than the potential at the neurons near an invariant point. In such a case, it is likely that the neurons at that invariant point will not be excited at lower stimulus levels, causing dual region excitation. This can only be compensated by a stimulation level correction factor.

This is illustrated by the results described in the final paragraph of the subsection ‘Computational model’, which suggest that spatial selectivity is the underlying factor deciding between the response modalities with a single or dual response area. While a high spatial selectivity has been considered a desirable condition for classical, sequential single electrode stimulation (such as continuous interleaved sampling, CIS), it precludes fusion of the response areas to a single region, as desired with dual electrode stimulation. This interpretation is in line with the results shown for stimulus levels just above threshold in Figure 5.2 a1, b1 and c1. The limited spread of excitation inherent to

such low stimulus levels results in two separate regions of excitation, which become fused at higher levels, both in sequential and simultaneous stimulation modes. This can be illustrated by comparison of Figure 5.2 b4 and 5.2 c4. These show that at high stimulation levels loudness correction at α=0.5 managed to widen the individual excitation regions with sequential stimulation sufficiently to cause an overlap, which is not present at lower stimulus levels due to the lack of electrode interaction.

The model predicts that the centroid of this added excitation region will shift along the basilar membrane in a non-linear fashion with respect to α. This can be seen in Figure 5.2 c4, where this centroid shifts much more rapidly around α=0.5 than near α=0 and α=1. However, it may be possible to compensate for this non-linearity by choosing suitable non-linear functions for currents I1(α) and I2(α). Psychophysical experiments, as described by McDermott and McKay (McDermott and McKay, 1994) could be used for this purpose. The change in stimulus level (in clinical units rather than microamperes) over α used in their sequential dual electrode experiments could roughly be described as hyperbolic functions; I2 would increase sharply at α=0, but quickly level off, while I1 decreased slowly and dropped rapidly near α=1. With these functions, they found a more linear shift in pitch, comparable to that found in the present study with the model for simultaneous current steering near MCL (Figure 5.2 a3 and a4).

For sequential dual electrode stimulation the magnitude of the loudness correction McDermott and McKay found in their psychophysical experiment (McDermott and McKay, 1994) is comparable to that found in the present study (Figure 5.3c). Also the virtually flat loudness matching curves for simultaneous dual electrode stimulation closely resemble the findings reported previously by Donaldson et al. (2005). Therefore, our findings confirm those of previous studies: sequential stimulation requires a loudness correction of roughly two times the EDR, while simultaneous current steering requires almost no correction for loudness at all. This is in line with the concept that in sequential dual electrode stimulation it compensates for the attenuation of the electrical field (proportional to α).

Generally speaking, the model predictions (Figure 5.3a, b) were in good agreement with the psychophysical data, once again showing that, contrary to simultaneous stimulation, a loudness correction is needed for sequential stimulation. However, the average correction factor needed for sequential stimulation on lateral electrodes (the electrode location expected to correspond to those of most patients) predicted by the model was approximately 50% of EDR higher than in the patient group. Moreover, contrary to the patients, the correction factor in the model depends strongly on electrode location, but it must be realized that the model study does not take into account known variations in, for example, cochlear size and morphology, electrode position and neural survival.

The model predicts that simultaneous current steering at high current levels with adjacent contacts produced a fused excitation region with a centroid that moves gradually with α (Figure 5.2 a4). In line with this, hardly any loudness correction was needed at α=0.5 in both the model and psychophysical experiments. It is important to note, however, that at low stimulation levels both simultaneous and sequential stimulation were predicted to produce two distinct excitation areas. These model findings are supported by Bonham

and Litvak's inferior colliculus recordings for current steering in the guinea pig (Bonham and Litvak, 2008). Their Figure 5.3 shows identical patterns: at low current levels there was separation of excitation, at the medium levels stimulation around the contacts with a sudden jump from one contact to the other and at high levels a smooth transition.

From the findings of this study it can be inferred that the amount of loudness correction needed is a potential measure of the effectiveness of the dual electrode stimulation in a particular case. For example, the model predicts for the HiFocus electrode that, without loudness correction, sequential dual electrode stimulation and current steering with non-adjacent electrode contacts (so-called spanning) commonly lead to separation of the excitation areas up to the MCL (data not shown here). If the separation of these two regions becomes too large, loudness balancing is not sufficient to produce a single excitation area. The model predicts that this situation easily occurs with electrode spanning.

All investigations on the generation of intermediate pitches have used medium to high current levels (Donaldson et al., 2005; Kwon and van den Honert, 2006; Firszt et al., 2007; Koch et al., 2007). On the basis of the findings in these studies loudness balancing was discarded in clinical approaches to simultaneous stimulation, for instance in the HiRes120 strategy of Advanced Bionics. However, even when no correction is needed at MCL (which is in line with our psychophysical results for simultaneous current steering), this would not mean that dual electrode stimulation is working

correctly at low levels. From the sequential case, where correction at MCL was applied and separation at low levels was maintained, it can even be deduced that different corrections are needed for various levels to produce accurate steering at all levels.

Acknowledgements

This research was financially supported by the Heinsius-Houbolt Fund.

Declaration of interest: The authors report no conflicts of interest. The authors alone are responsible for the content and writing of the paper.

References

Bonham, B.H., Litvak, L.M. 2008. Current focusing and steering: modeling, physiology, and psychophysics. Hear Res 242, 141-53.

Briaire, J.J., Frijns, J.H. 2005. Unraveling the electrically evoked compound action potential. Hear Res 205, 143-56.

Briaire, J.J., Frijns, J.H. 2006. The consequences of neural degeneration regarding optimal cochlear implant position in scala tympani: a model approach. Hear Res 214, 17-27.

Donaldson, G.S., Kreft, H.A., Litvak, L. 2005. Place-pitch discrimination of single- versus dual-electrode stimuli by cochlear implant users (L). J Acoust Soc Am 118, 623-6.

Firszt, J.B., Koch, D.B., Downing, M., Litvak, L. 2007. Current steering creates additional pitch percepts in adult cochlear implant recipients. Otol Neurotol 28, 629-36.

Frijns, J.H., Briaire, J.J., Grote, J.J. 2001. The importance of human cochlear anatomy for the results of modiolus-hugging multichannel cochlear implants. Otol Neurotol 22, 340-9.

Greenwood, D.D. 1990. A cochlear frequency-position function for several species--29 years later. J Acoust Soc Am 87, 2592-605.

Koch, D.B., Downing, M., Osberger, M.J., Litvak, L. 2007. Using current steering to increase spectral resolution in CII and HiRes 90K users. Ear Hear 28, 38S-41S.

Kwon, B.J., van den Honert, C. 2006. Dual-electrode pitch discrimination with sequential interleaved stimulation by cochlear implant users. J Acoust Soc Am 120, EL1-6.

Laneau, J., Wouters, J., Moonen, M. 2004. Relative contributions of temporal and place pitch cues to fundamental frequency discrimination in cochlear implantees. J Acoust Soc Am 116, 3606-19.

McDermott, H.J., McKay, C.M. 1994. Pitch ranking with nonsimultaneous dual-electrode electrical stimulation of the cochlea. J Acoust Soc Am 96, 155-62.

Stakhovskaya, O., Sridhar, D., Bonham, B.H., Leake, P.A. 2007. Frequency map for the human cochlear spiral ganglion: implications for cochlear implants. J Assoc Res Otolaryngol 8, 220-33.

Vanpoucke, F.J., Zarowski, A.J., Peeters, S.A. 2004. Identification of the impedance model of an implanted cochlear prosthesis from intracochlear potential measurements. IEEE Trans Biomed Eng 51, 2174-83.

Chapter 6

Current focussing in cochlear implants: An analysis of neural recruitment in a computational model

Randy K. Kalkman
Jeroen J. Briaire
and Johan H.M. Frijns

Hearing Research 2015 (322), 89–98

Abstract

Several multipolar current focussing strategies are examined in a computational model of the implanted human cochlea. The model includes a realistic spatial distribution of cell bodies of the auditory neurons throughout Rosenthal's canal. Simulations are performed of monopolar, (partial) tripolar and phased array stimulation. Excitation patterns, estimated thresholds, electrical dynamic range, excitation density and neural recruitment curves are determined and compared. The main findings are: (I) Current focussing requires electrical field interaction to induce spatially restricted excitation patterns. For perimodiolar electrodes the distance to the neurons is too small to have sufficient electrical field interaction, which results in neural excitation near non-centre contacts. (II) Current focussing only produces spatially restricted excitation patterns when there is little or no excitation occurring in the peripheral processes, either because of geometrical factors or due to neural degeneration. (III) The model predicts that neural recruitment with electrical stimulation is a three-dimensional process; regions of excitation not only expand in apical and basal directions, but also by penetrating deeper into the spiral ganglion. (IV) At equal loudness certain differences between the spatial excitation patterns of various multipoles cannot be simulated in a model containing linearly aligned neurons of identical morphology. Introducing a form of variability in the neurons, such as the spatial distribution of cell bodies in the spiral ganglion used in this study, is therefore essential in the modelling of spread of excitation.

1 Introduction

Modern cochlear implants (CIs) have multiple electrode contacts along the scala tympani, each potentially capable of electrically stimulating a different sub-population of the surviving auditory neurons in the cochlea. These contacts are usually stimulated in so-called monopolar mode, in which current is injected through a contact in the scala tympani, and returned to a far-field electrode contact. As a result, electrical potential field patterns caused by monopolar stimulation are broad in nature; potentials drop off relatively slowly as one moves away from the stimulating contact. Since electrical potential fields from different sources add up, potential fields induced by different monopoles in the cochlea can greatly influence one another when the contacts are stimulated simultaneously or in rapid succession. This phenomenon, commonly referred to as electrical field interaction, is considered deleterious for speech perception with cochlear implants (Shannon, 1983; White et al., 1984; Wilson et al., 1991; Stickney et al., 2006). On the other hand, these interactions can also be used to reduce the spreading of current, in so-called multipole configurations. In this study the mechanisms underlying current focussing using multipoles will be investigated.

The main goal of current focussing is to increase spatial selectivity, thereby improving spectral resolution and speech intelligibility (Henry et al., 2005; Litvak et al. 2007b; Srinivasan et al. 2013). Multipolar stimulation also allows for reduced far field potentials, which could possibly be used to minimise interactions and allow parallel stimulation of implant channels without negative impact on speech perception. Several different multipolar configurations have been proposed to achieve these goals: bipolar stimulation, (partial) tripoles and phased array stimulation. These have been shown to produce smaller spread of excitation than monopolar stimulation, but at the expense of an increase in the amount of current required to achieve a given loudness (Miller et al. 2003; Snyder et al., 2004; Bierer and Faulkner, 2010; Zhu et al. 2012; Landsberger et al., 2012; Long et al. 2014).

Another method for reducing spread of excitation is to move the electrode array closer to the modiolus, which lowers the threshold of excitation and decreases the dispersion of the injected current towards the neurons. This raises the question of whether it is possible to combine perimodiolar placement of the electrode array with current focussing to improve CI performance. On the other hand, in a perimodiolar position the electrode contacts are very close to the neurons. Consequently, the neurons are in the direct electrical field of the contacts while the benefits of the multipolar stimulation depend on interaction in the far field.

Previous modelling studies that investigated multipolar stimulation in the implanted cochlea have used linearly aligned neurons, with cell bodies of consecutive nerve fibres arranged along a straight line or spiralling curve (Briaire and Frijns, 2000a; Rattay et al., 2001; Hanekom, 2001, 2005; Whiten, 2007; Litvak et al., 2007a; Bonham and Litvak, 2008; Goldwyn et al., 2010; Frijns et al., 2011a; Snel-Bongers et al., 2013; Wu and Luo, 2013). The consequence of modelling the neurons in this manner is that excited neural

regions can only expand apically or basally along the cochlea and do not allow for the computation of excitation densities at a specific location.

In reality, the cell bodies in the spiral ganglion (SG) are not aligned in a purely linear fashion, but are distributed throughout a spiralling tunnel in the modiolus called Rosenthal's canal. As a consequence, neural recruitment is not only possible in apical and basal directions, but also by penetrating deeper into the SG. It is therefore conceivable that different stimulation paradigms produce different three-dimensional excitation patterns, even at an equal number of excited neurons.

Another point of interest is the nature of neural degeneration in the human cochlea. A study by Linthicum and Fayad showed that, contrary to most animal models, loss of hair cells and the peripheral processes of cochlear neurons does not necessarily lead to loss of spiral ganglion cells in humans (Linthicum and Fayad, 2009). Since the state of the cochlear neurons currently cannot be determined in living subjects, this makes it unclear to which extent the peripheral processes are present in the cochleae of CI users. This is a potentially important issue, as previous modelling studies have shown that the presence or absence of peripheral processes can have consequences for neural excitation in the cochlea (Rattay et al. 2001; Hanekom, 2001, 2005; Briaire and Frijns, 2006; Whiten, 2007; Snel-Bongers et al., 2013; Kalkman et al., 2014).

The current study will present an updated version of the computational model of the implanted human cochlea developed at Leiden University Medical Centre (Frijns et al., 2000, 2001, 2009a,b, 2011a; Briaire and Frijns, 2000a,b, 2005, 2006; Snel-Bongers et al., 2013; Kalkman et al. 2014). The trajectories of the neurons in the model have been modified to include a more realistic spatial distribution of cell bodies throughout Rosenthal's canal, and have been modelled both with and without peripheral processes. The excitation patterns of monopoles, (partial) tripoles and phased array stimulation will be examined and compared for lateral and medial electrode arrays.

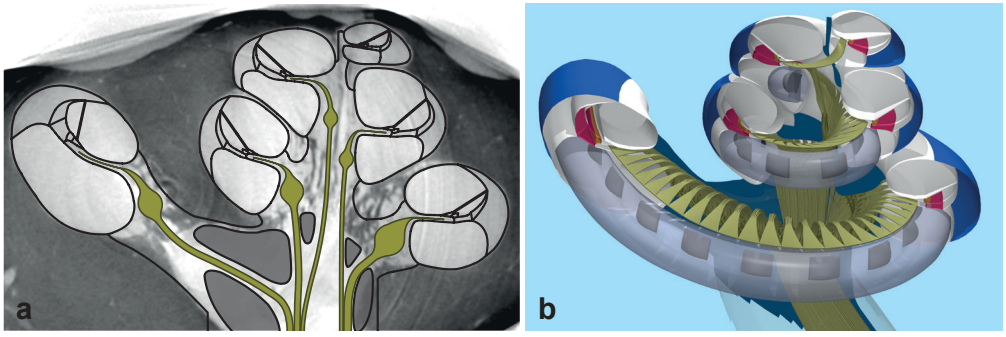

Figure 6.1. *Visual representations of one of the model's cochlear geometries. Figure a shows a mid-modiolar cross-section from μCT imaging data of a human temporal bone, provided by Advanced Bionics and the University of Antwerp. The lines overlaid on the μCT reconstruction represent the boundaries of the modelled cochlear geometry and the modelled neurons. Figure b is a ray traced image of the three dimensional model cochlea, cut open to reveal the neurons and a laterally inserted electrode array.*

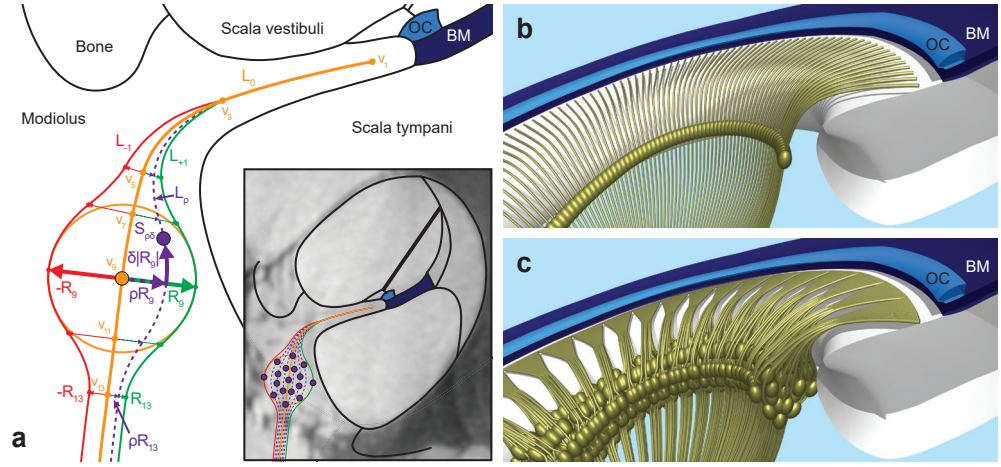

Figure 6.2. *Illustration of the implementation of spatially distributed cell bodies. Figure a shows a mid-modiolar cross-section of one of the model geometries at 360° from the round window (black lines). Coloured curves indicate neural trajectories; purple circles in the insert indicate modelled cell body locations. Figure b is a ray traced image of a section of the geometry corresponding to figure a containing the nerve fibres with SG cells aligned along a spiralling curve, as they were modelled in previous studies. Figure c shows the same section with the updated nerve fibres with spatially distributed cell bodies.*

2 Materials and Methods

The computational model of the electrically stimulated human cochlea used in this study consists of a volume conduction model, which uses the Boundary Element Method to calculate the potential distribution in a three-dimensional geometry representing an implanted human cochlea (Figure 6.1), and an active generalised Schwarz-Eikhof-Frijns (GSEF) nerve fibre model (Frijns et al., 1995), that simulates neural responses in the cochlear geometry. Four different cochlear geometries are included, each modelled with both lateral wall and medial (perimodiolar) electrode arrays, which are model equivalents of the HiFocus1J electrode array. For this study, the model needed to be modified to include spatial distribution of the cell bodies of the auditory nerve fibres and the number of nerve fibres has been increased from 320 to 3200 to retain sufficient resolution along the cochlear duct. These changes are explained in section 2.1; the morphology of the neurons and all other details of the model are described in Kalkman et al. (2014) and for brevity will not be repeated here.

2.1 Spatial distribution of cell bodies

Figure 6.2 illustrates the way the cell body distribution was implemented. The nerve fibre trajectory used in the previous model studies served as a starting point (figure 6.2b); this trajectory is indicated by the orange line in figure 6.2a, and is referred to as the base nerve line L_0. The neuron is defined by 21 vertices. Vertex v_9 corresponds to the position of the cell bodies in our previous modelling studies and is located at the centre of the SG, as is

visible in the histological image on which the model geometry is based (insert in Figure 6.2a).

For the present study, alternative nerve lines were defined and the locations of the cell bodies were varied in a circle around v_9 with radius R_9, which encompassed the SG on the histological image. These nerve lines are shown in the insert of figure 6.2a as green, red and purple curves, the positions of the cell bodies are shown as purple circles. For each cochlear geometry a set of 3200 auditory neurons was modelled, with the neural trajectories and cell bodies distributed in a pseudo-random fashion. In addition, the neurons were grouped in 80 bundles of 40 fibres each, similar to how auditory neurons are known to be bundled in human cochlear anatomy (Bredberg, 1968). The implementation of the spatial distribution of cell bodies and nerve fibre bundles is described in more detail in the appendix.

Figure 6.2c shows a three-dimensional view of the resulting cochlear geometry, illustrating the modelled nerve fibres, the scala tympani, organ of Corti (OC) and basilar membrane (BM). For comparison, figure 6.2b shows the same cochlear position with nerve fibres as they were modelled in Kalkman et al. (2014). Finally, as in previous studies, a set of degenerated neurons was generated for each geometry, which was achieved by removing the peripheral processes from the nerve fibre sets described above (Briaire and Frijns, 2006; Snel-Bongers et al. 2013; Kalkman et al. 2014).

2.2 Stimulation paradigms

Four different stimulation paradigms were used in this study: monopole (MP), tripole (TP), partial tripole (pTP) and phased array (PA). In MP stimulation current is injected on only one intracochlear electrode contact, whereas in the other paradigms multiple intracochlear electrodes are active. For TP one contact (referred to as the centre contact) is stimulated, while at the same time the two adjacent contacts (called flanking contacts) are stimulated with opposite polarity, at half the amplitude of the centre contact. The combined current on the flanking contacts is therefore equal to the current on the centre contact, but opposite in polarity. The pTP paradigm is a modification of TP stimulation, where the stimulus amplitude on the flanking contacts is multiplied by a factor σ. This means that for σ=1, pTP is identical to the TP paradigm and for σ=0, it is identical to MP stimulation. In this study we will use the pTP paradigm exclusively with σ=0.75, which means that the amplitude on both flanking contacts is -0.375 times the amplitude on the centre contact.

The fourth paradigm, PA, is based on a study by Van den Honert and Kelsall (2007) and is designed to stimulate all contacts of the electrode array in such a way that the electrical potential on all non-centre contacts is reduced to zero. This is achieved by determining an impedance matrix from electrical potential recordings of the implant electrodes, and using that impedance matrix to calculate current vectors (Van den Honert and Kelsall, 2007). It should be noted that due to technical limitations, it is clinically impossible to determine the diagonal elements of the impedance matrix (which represent normalized electrical

potentials on stimulating contacts); as a consequence their values have to be estimated in clinical situations. However, in the computational model these diagonal elements could be determined from the simulated surface potentials of the electrode contacts; therefore, PA current vectors in the model were determined using these simulated values of the diagonal elements of the impedance matrices, as in Frijns et al. (2011a).

Simulations were done with biphasic, cathodic first pulses with 37.5 μs per phase. The pulse amplitude on the centre contact is referred to as the stimulus amplitude, which means that for non-MP stimulation the stimulus amplitude did not equal the total amount of current injected. For pTP and TP stimulation the total injected current was 1.75 and 2 times the stimulus amplitude respectively, while for PA the total injected current was dependent on the current vector that has been calculated for a given geometry and channel. However, the sum of absolute values of the PA current vectors was found to be relatively consistent for different set-ups; for lateral contacts the mean total current was 1.97 times the stimulus amplitude (stdev 0.01), and for medial contacts it was 1.94 (stdev 0.01).

With the exception of TP stimulation, the net current injected into the cochlea (the sum of signed amplitudes on all intracochlear electrode contacts) generally did not equal zero. To avoid an electrical potential offset, the net current returned to an extracochlear current source/sink located in the far field.

2.3 Model output

In this study, the main output of the model was in the form of excitation profiles (XPs, like Figure 6.3a). These XPs indicate which neurons are excited when stimulating a given channel of a specific set-up (geometry, implant location, stimulation paradigm and centre contact) for a range of stimulus amplitudes. An XP is plotted as a two-dimensional colour coded plot, where the grey scale at (x,y) indicates the initial site of excitation at stimulus amplitude x along the abscissa for the nerve fibre at position y along the ordinate; black corresponds to stimulation in the axon, grey represents peripheral process excitation, while white means no excitation. Nerve fibre position was defined by the location of the tip of the peripheral process along the BM. As in previous studies, loudness in the model was defined by the total length along the BM occupied by excited neurons. Threshold was defined as I_{th}, the stimulus amplitude needed to excite a number of fibres that correspond to a length of 1 mm along the BM (roughly 100 neurons), referred to as an excitation width of 1 mm in the paper (Snel-Bongers et al., 2013). The model analogue of Maximum Comfortable Loudness was defined as I_{4mm}, the amplitude needed for an excitation width of 4 mm (roughly 400 nerve fibres), as in Briaire and Frijns (2006). The difference between I_{th} and I_{4mm} was considered to be the electrical dynamic range of a model implant channel.

The data from the XPs were used to determine excitation density (ED) plots, which indicate the percentage of neurons that are excited at a given stimulus amplitude, as a function of distance along the BM. The percentage of neurons excited (i.e., excitation density) at a point λ along the BM was determined by calculating a moving average over the neurons

that have their peripheral tips located in a 1 mm segment of the BM, centred on λ. ED was calculated in this way at the tip of every modelled nerve fibre, resulting in a curve of 3200 data points, which was then smoothed with a first order low-pass Butterworth filter. These ED curves provide a way to easily visualize differences in excitation patterns; a continuous, spatially restricted excitation region will result in a high and narrow peak in the ED curve, whereas exciting the same number of neurons in a spatially broad and discontinuous pattern will produce a wide and shallow ED peak.

3 Results

Figure 6.3 shows the effect of the distribution of the spiral ganglion cells on the computed excitation patterns for monopolar stimulation of a lateral electrode contact at 250° from the round window. Figure 6.3a is an XP generated in a set of 320 nerve fibres from Kalkman et al. (2014), with cell bodies arranged in a spiralling curve, while figure 6.3b shows the corresponding XP generated from the updated nerve fibre set with the spatial distribution of the 3200 cell bodies introduced in this study. The vertical dashed lines indicate the stimulus amplitudes necessary to reach 1 mm (blue), 2.5 mm (green) and 4 mm (red) excitation width. Figures 6.3c1–c3 show excitation patterns of the XP in figure 6.3a, at the indicated stimulus amplitudes. Figures 6.3d1–d3 show the same for the XP in figure 6.3b. In figures 6.3c and 6.3d, excited fibres are marked according to the colour of the corresponding stimulus amplitude.

As can be seen in figures 6.3a and 6.3c, for the old modelled nerve fibre trajectories there is only one single continuous region of neural excitation between stimulus amplitudes of about 0.4 to 2 mA. This region expands as the amplitude increases, without skipping any fibres. Introducing a spatial distribution of cell bodies causes a great deal of variability in the excitation thresholds of individual nerve fibres, especially near the stimulating contact. As a consequence, there is no longer a continuous region of excitation, but one with many gaps of one or more fibres (figures 6.3d). These discontinuous regions of excitation result in a 'noisy' XP (figure 6.3b). In spite of this difference, the stimulus amplitudes necessary to achieve the loudness levels marked by the dashed lines in figure 6.3a are roughly the same as in figure 6.3b, indicating that the spread of cell bodies has little systematic effect on neural recruitment with monopolar stimulation.

Figures 6.3e show ED plots of the excitation patterns pictured in figures 6.3c and 6.3d. The dotted lines are ED plots resulting from the excitation regions of the old neural trajectories (figures 6.3c), while the solid lines correspond to the excitation regions of the updated nerve fibre trajectories that incorporate spatial distribution of cell bodies (figures 6.3d). At 1 mm excitation width, the ED plot for the old neural trajectories is a triangular curve that reaches 100% density at the centre of excitation, due to the fact that the moving average is calculated over a 1 mm segment and the neural excitation pattern forms a continuous region (dotted curve figure 6.3e1; note that, unlike all other ED plots presented, the dotted curves have not been smoothed with a low-pass filter). At higher levels the excited region expands in apical and basal directions while remaining continuous, causing the ED curves to broaden into trapezoid shaped curves (dotted lines in figures 6.3e2 and e3). For the

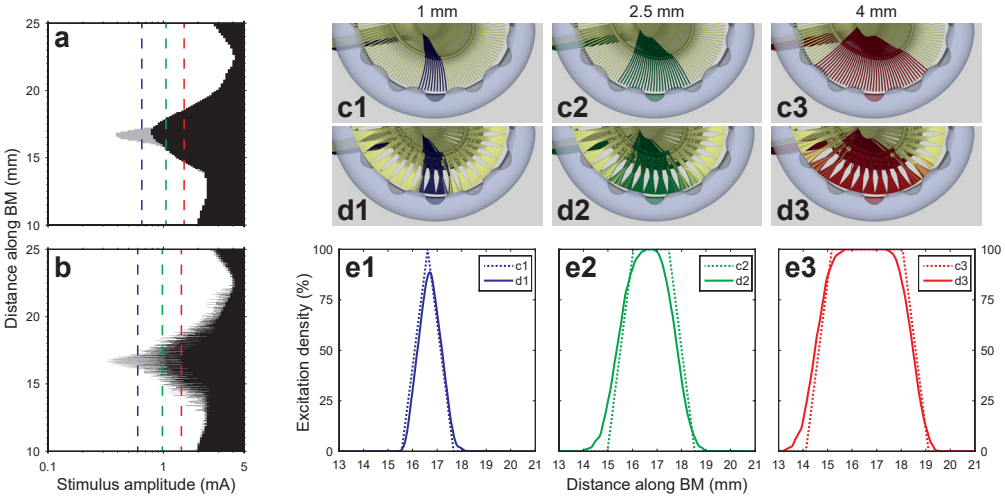

Figure 6.3. *Figures a and b show example XPs of monopolar stimulation in the model, one with the aligned nerve fibres distribution (a) and one with the updated nerve fibres with spatially distributed cell bodies (b). The abscissa indicates stimulus level and the ordinate indicates position of the tips of the nerve fibres along the BM, expressed in millimetre from the basal end of the cochlea. Black areas indicate stimulation in the axon, grey areas represent stimulation in the peripheral process and white means no excitation. Blue, green and red dashed vertical lines designate stimulus amplitudes necessary to achieve 1, 2.5 and 4 mm excitation widths respectively. Figures c and d show excitation patterns at these stimulus levels in a segment of the modelled neurons, with stimulated neurons coloured according to the relevant excitation width. Figures c1–c3 illustrate excitation patterns from the XP of figure a (aligned cell bodies), while figures d1–d3 depict patterns from the XP in figure b (spatially distributed cell bodies). Figures e show the corresponding excitation density curves; the dotted curves represent the excitation patterns shown in figures c, and the solid curves represent the patterns shown in figures d.*

new neural trajectories the excitation patterns are always continuous at the centre, but discontinuous at the edges (figures 6.3d). This means that the excited neurons span a larger area of the cochlea, resulting in ED curves that are broader but more shallow than their equivalents from the old neural trajectories (solid curves figure 6.3e1–e3).

3.1 Excitation profiles

In figure 6.4, XPs of the stimulation paradigms described in section 2.2 are shown for several electrode locations in one of the model geometries (XPs for the other three geometries are similar and are not shown here). Figures 6.4a1–a4 represent stimulation of a lateral wall array with the centre contact closest to 100° insertion depth, figures 6.4b1–b4 are for the same array, but with the centre contact closest to 250° from the round window. Figures 6.4c1–c4 and 6.4d1–d4 are XPs of medial arrays, with centre contacts at the same insertion angles as in the corresponding lateral array. The columns in figure 6.4 designate MP (a1–d1), pTP (a2–d2), TP (a3–d3) and PA stimulation (a4–d4), respectively. The vertical dashed lines in the XPs indicate I_{th} and I_{4mm} amplitudes.

In the basal half turn of the cochlea, MP stimulation on lateral contacts mostly excites the central axons of the modelled neurons (black area between dashed lines in figure 6.4a1), while more deeply inserted lateral contacts are more likely to excite the peripheral process at low amplitudes (grey area in figure 6.4b1).In contrast, MP stimulation using medial arrays will produce only a small amount of stimulation at the peripheral processes (grey areas in figure 6.4c1 and d1), irrespective of the angular position of the contact. Medial electrodes have lower MP thresholds than lateral contacts at the same insertion angles, while I_{4mm} is roughly the same for the two array positions (compare dashed lines of figure 6.4c1 and d1 to 6.4a1 and b1). As a consequence the dynamic range is larger for medial contacts. In contrast, it is clear from Figure 6.4, that for all multipolar configurations the electrical dynamic range (between I_{th} and I_{4mm}) as a whole shifts to lower amplitudes when going from a lateral to a medial electrode position.

In most pTP configurations so-called 'side lobes' are visible in the XP, with the exception of the XP for lateral pTP stimulation at 100° (Figure 6.4a2), These side lobes are secondary regions of excitation on either side of the main excitation area, which are caused by the flanking contacts if the stimulus amplitude exceeds local thresholds (figures 6.4b2–d2). In addition, the pTP paradigm is more likely to generate action potentials in the peripheral

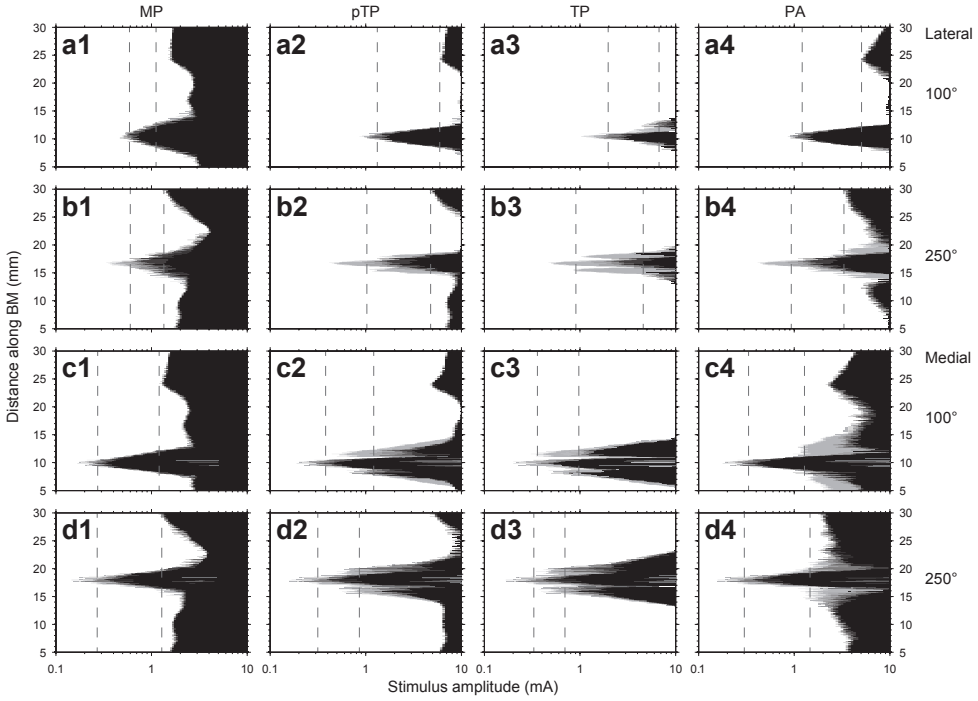

Figure 6.4. *XPs of all four stimulation paradigms studied in one of the model geometries. Axes and meaning of colour codes are identical to figures 6.3a and b. Vertical dashed lines indicate stimulus amplitudes necessary to achieve 1 and 4 mm excitation widths. Rows a and b correspond to lateral contacts at 100° and 250° insertion depth respectively, rows c and d correspond to medial contacts at the same angles. Column 1 corresponds to MP stimulation, column 2 to pTP, column 3 to TP and column 4 to PA stimulation.*

processes than MP stimulation (compare grey areas between figures 6.4a1–d1 and a2–d2), which underlies the appearance of side lobes in lateral stimulation at 250° (figure 6.4b2). Relative to MP stimulation, pTP requires larger stimulus amplitudes to reach threshold in all cases, although for medial contacts the difference in I_{th} is less than for lateral contacts. Averaged for all geometries, I_{th} for the lateral contacts is 5.6 dB higher for pTP than it is for MP, while for the medial it is 1.8 dB. For lateral contacts, I_{4mm} is also larger for pTP than it is for MP, leading to a larger dynamic range. For the medial arrays the values of I_{4mm} do not yield a consistent pattern across the modelled cochlear geometries.

For medial electrode positions, the excitation patterns for TP are similar to the ones for pTP. Lateral contacts, however show clear differences between these stimulation paradigms: TP induces more pronounced side lobes, which come into play at lower stimulus amplitudes. Again, these side lobes are predominantly caused by stimulation of the peripheral processes. In a number of situations side lobes are even present at or near threshold (e.g., figure 6.4b3 and c3). Generally speaking, TP thresholds are comparable to the ones of the pTP paradigm.

PA stimulation produces XPs similar to those of pTP, but largely without side lobes (figure 6.4a4–d4). However, at high amplitudes excitation of peripheral processes can occur near non-centre contacts (b4–d4).

It is worth noting that the spatial centre of excitation along the BM at a specific excitation width does not vary greatly between different stimulation paradigms, except when asymmetric side lobes are involved. At I_{th}, the average difference between the centre of excitation of the current focussing paradigms and that of MP stimulation is equivalent to a pitch shift of about 0.17 semitones. At I_{4mm}, side lobes in TP stimulation can cause the centre of excitation to shift to an equivalent of up to 2 semitones relative to MP stimulation.

3.2 Excitation density

Figure 6.5 shows ED plots for the same cochlear geometry and electrode configurations as the XPs in figure 6.4 to study the three-dimensional neural recruitment properties of the different multipoles. Blue curves represent MP stimulation, green pTP, red TP, while orange curves correspond to PA; for easier comparison all curves are aligned with respect to their maxima. Figure 6.5a1 shows ED curves at I_{th} of the lateral array with centre contacts at 100° (corresponding to the excited neurons at the left dashed vertical lines in the XPs of figure 6.4a1–a4). While pTP, TP and PA curves are very similar to each other, the ED curve of MP stimulation is broader and shallower, whereas the other paradigms are able to excite a more spatially selective group of nerve fibres.

ED curves at I_{th} of the lateral array at 250° are shown in figure 6.5b1. Here, pTP and PA curves are virtually identical to each other and very similar to their equivalents in figure 6.5a1. The MP curve however is sharper here than it is at 100°, meaning that MP excitation patterns are more spatially selective at this cochlear angle. In fact, it is almost as selective as the pTP and PA paradigms. From the XPs in figure 6.4a1 and b1 it can be seen that the reason for this increased selectivity is a greater amount of peripheral

process stimulation at threshold. However, the biggest difference between the ED curves of figure 6.5a1 and b1 is in the curve for TP stimulation, which is the shallowest at 250° and is asymmetric due to a shoulder at the basal side of the curve, caused by a side lobe visible in figure 6.4b3.

As peripheral process stimulation is responsible for the main differences between figure 6.5a1 and b1, a second set of ED curves were determined, based on XPs calculated from neurons with degenerated peripheral processes; these degenerated ED curves for the lateral array are plotted in figure 6.5a2 and b2. At 100°, removing the peripheral processes has little effect on the ED curves, though the curves are slightly shallower for all four paradigms (compare figure 6.5a2 to a1). However, at 250° the ED curves become much broader and shallower when no peripheral processes are present, and the differences between pTP, TP and PA become more pronounced (compare figure 6.5b2 to b1).

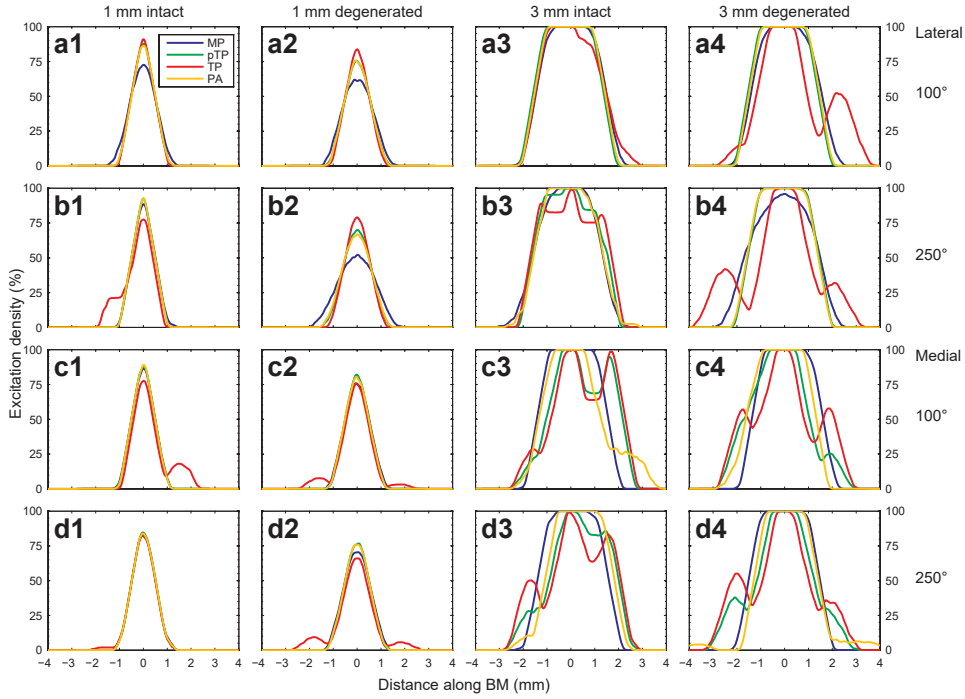

Figure 6.5. *ED plots of the XPs in figure 6.4. The abscissa represents position along the BM, centred on the peak of the ED curves, the ordinate represents the percentage of excited neurons in a 1 mm segment at a given position of the BM. Rows a and b correspond to lateral contacts at 100° and 250° insertion depth respectively, rows c and d correspond to medial contacts at the same angles.; column 1 consists of ED curves at 1 mm excitation width from simulations with intact neurons, column 2 is the same but from simulations with neurons that had degenerated peripheral processes. Columns 3 and 4 consist of ED plots at 3 mm excitation width, with intact and degenerated neurons respectively. Blue curves represent MP stimulation, green represents pTP, red TP and orange corresponds to PA stimulation.*

Figures 6.5c1, c2, d1 and d2 show ED curves for the medial arrays at the same cochlear angles and neural conditions as the lateral array curves of figures 6.5a1, a2, b1 and b2 respectively. For the medial array, MP, pTP and PA curves are mostly identical to each other, though loss of peripheral processes does make the ED curves slightly broader as it does in the lateral array case. The tendency of TP to induce side lobes for medial array, as described in section 3.1, is also reflected in the corresponding ED curves.

Figure 6.5a3–d3 and 6.5a4–d4 present the ED curve plots described above, but at 3 mm excitation width, rather than I_{th}. At this level, side lobes occur more frequently for all multipolar paradigms and they are more prominent than at threshold. Unlike in the threshold curves, side lobes also occur for the medial array with pTP and to a lesser extent PA stimulation (figure 6.5c3–d3 and 6.5c4–d4). However, where there are no side lobes, pTP and PA produce very similar ED curves; these curves are generally narrower than those of MP stimulation, as is most clearly visible in figure b4.

3.3 Neural recruitment

Finally, neural excitation widths are plotted against stimulus amplitude in figure 6.6 as so-called neural recruitment curves. Since the results for the different cochlear geometries were only marginally different, the stimulus amplitudes have been averaged for each excitation width over all four model geometries. In almost all cases, MP stimulation requires lower amplitudes to achieve a given excitation width. The exceptions are pTP and

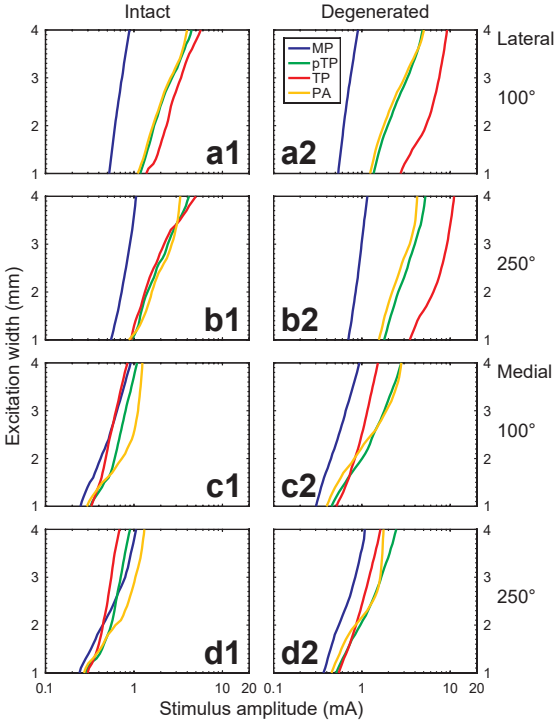

Figure 6.6. *Neural recruitment curves of the four studies stimulation paradigms, averaged across all four model geometries. The ordinate indicates excitation width in millimetre and the abscissa is the average stimulus amplitude necessary to reach a certain excitation width across all four geometries. The curves have the same colour coding as in figure 6.5. Rows a and b correspond to lateral contacts at 100° and 250° insertion depth respectively, rows c and d correspond to medial contacts at the same angles. The left column consists of neural recruitment curves of simulations with intact neurons; the right column consists of curves from simulations with degenerated peripheral processes.*

TP stimulation on the medial array with intact neurons (figure 6.6c1 and d1), which have considerable contributions of side lobes. In those cases I_{4mm} and the dynamic range turned out to be less than that of MP stimulation. It should be noted, however, that in terms of total injected current (i.e., the sum of absolute current amplitudes on all active contacts) the MP paradigm always requires less current than any of the other three paradigms used in the study.

Irrespective of the neural degeneration status, with lateral arrays neural recruitment curves for PA and pTP are essentially the same, as are the slopes of the curves for TP stimulation. However, stimulus levels are generally highest for TP if the peripheral processes are either absent or XPs indicate limited stimulation peripheral to the cell body.

For medial electrodes the order of the neural recruitment curves is much more variable for the different electrode configurations. The electrical dynamic ranges differ less compared to the lateral arrays, but the slopes are largely influenced by the presence of side lobes and they show clear variations over the dynamic range.

4 Discussion and Conclusions

In this study several current focussing paradigms were investigated in a computational model of the human cochlea, consisting of a three-dimensional volume conduction model and an active nerve fibre model. In contrast to previous modelling studies, where the cell bodies of the auditory neurons were arranged along a spiral, the present study incorporated a realistic spatial distribution of the auditory neurons' cell bodies throughout Rosenthal's canal. Cell body positions were distributed in pseudo-random patterns; repeating model simulations with nerve fibre sets generated with a different pseudo-random seed number only had a marginal effect on the presented data, indicating that the results were robust to different cell body distributions.

Results from the present study show that current focussing can stimulate a more spatially restricted group of neurons than monopolar stimulation, by achieving deeper penetration into the SG. This is particularly the case in situations where the peripheral processes are either not present or only excited to a limited degree, which is especially the case for lateral electrode positions. This spatial restriction is consistent with subjective reports from patients at our clinic that current focused stimuli sound 'clearer', or more 'thin', which could indicate that they are stimulating a more narrow spectral range.

The model predicts that for perimodiolar electrodes current focussing does not achieve increased spatial selectivity to the same degree as it does for lateral electrodes, and that it certainly does not provide an additive benefit to combine medial electrode placement with multipolar strategies. The close proximity of the medial electrodes places the auditory neurons in the electrical near field; however this field typically has not been shaped by the multipolar configuration. Therefore, at this distance the field essentially has monopolar characteristics. Consequently, the presence of side lobes in the XPs can be seen as direct neural excitation by the compensating currents, resulting in a broader region of excitation along the cochlear duct. It should be possible to clinically investigate these model findings

by determining the distances of electrodes to the cochlear modiolus from CT data, and correlating them to objectively or psychophysically obtained spread of excitation measurements. If the model prediction is accurate, then current focused stimulation at a greater distance from the modiolus will more frequently result in sharpened spread of excitation curves.

Side lobes can also occur from stimulation of lateral contacts, particularly when peripheral process stimulation is prevalent. In such cases one could argue that the peripheral processes are located in the electrical near field, despite the relatively large distance of the electrode contacts to the SG. Comparing the different current focussing paradigms, TP stimulation is most likely to produce side lobes due to the fact that the compensating current on the flanking contacts is higher than the current on individual non-centre contacts in pTP or PA stimulation. For the same reason, pTP is more likely to create side lobes than PA stimulation, though in other aspects pTP and PA behave similarly.

For pTP and TP stimulation, the results of the present study are consistent with two psychophysical studies done by Bierer and Faulkner (2010) and Landsberger et al. (2012), which both performed forward masking experiments and concluded that for some but not all patients, (p)TP stimulation has a smaller spread of excitation than MP stimulation at equal loudness. A modelling study by Goldwyn et al. (2010) suggested that differences between individuals may be caused by neural dead regions, but the present study offers the explanation that the state of the peripheral processes can also explain their results. Looking at the thresholds of TP stimulation in figure 6.6, one can observe that degeneration of the nerve fibres is sufficient to induce a threshold shift in the TP configuration relative to MP stimulation. This demonstrates that (partial) loss of peripheral processes is sufficient to explain the observed variability in TP thresholds, and that a completely dead neural region is not the only explanation.

Psychophysical data shows that current focussing paradigms require more current to achieve loudness equal to MP stimulation, which is consistent with the findings of the present study (Bierer and Faulkner, 2010; Bierer et al. 2011; Landsberger et al., 2012; Long et al., 2014). Figure 6.7 shows preliminary data from psychophysical experiments performed in our own clinic, presented at CIAP2011 (Frijns et al., 2011b). Loudness growth curves were determined in 8 post-lingually deaf users of the HiRes90k implant with HiFocus1J electrode array (average duration of deafness 20 years, range 11–38 years). In each experiment, electrode contact 8 served as centre contact of the stimulus. Radiological analysis with a method described by Van der Marel et al. (2014) revealed that the arrays were in lateral position, with the centre contacts at an average distance of 1.2 mm from the modiolar wall (range 1.1–1.5 mm), at an average insertion angle of 257° from the round window (range 230–281°). Subjective loudness was determined on an 8-point scale, with a method adapted from Potts et al. (2007); figure 6.7 shows the average stimulus amplitudes for each loudness level, for the same four stimulation paradigms used in the present study. The average loudness growth curves of MP, pTP and TP stimulation in figure 6.7 are most similar to the neural recruitment curves in figures 6a1, a2 and b2. These model figures correspond to situations where excitation of the

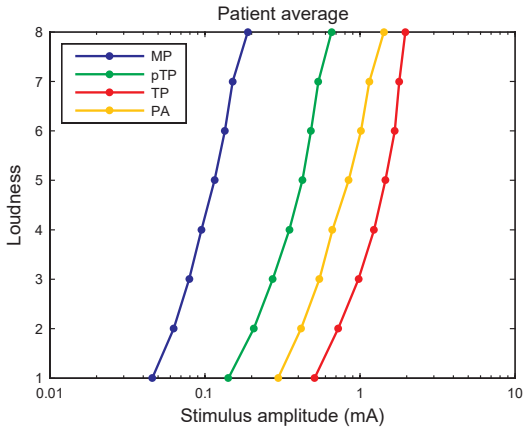

Figure 6.7. *Average loudness growth data of 8 patients from data presented in Frijns et al. (2011b). The ordinate indicates subjective loudness level on an 8 point scale (1 is threshold, 8 is maximum comfortable loudness), the abscissa indicates the average stimulus amplitude needed in mA. The four curves correspond to the same stimulation paradigms used in the present study: MP (blue), pTP (green), TP (red) and PA (orange).*

peripheral processes is limited (figure 6.6a1) or are entirely missing (figure 6.6a2 and b2). This suggests that in the experimental situation, excitation of the peripheral processes stimulation does not play a major role.

However, for PA stimulation, the model data is not in agreement with the psychophysical loudness growth curves shown in figure 6.7. In the model plots of figure 6.6, neural recruitment of PA stimulation is mostly similar to that of pTP, whereas in the psychophysical data the PA loudness growth curve lies in between those of pTP and TP stimulation. This disagreement may be due to the fact that the PA current vectors were determined differently for the psychophysical experiments. As noted in section 2.2, the PA current vectors in the model were calculated using simulated values of the diagonal elements of the impedance matrices. In clinical practice it is necessary to estimate the diagonal elements of the impedance matrix, as they cannot be determined directly (Van den Honert and Kelsall, 2007). In our psychophysical experiments these diagonal elements were interpolated by fitting exponential decays through the non-diagonal elements; the resulting current vectors used an average total current of 2.2 times the stimulus amplitude (stdev 0.2), which is considerably more than in the model simulations. This could indicate that the diagonal impedance matrix elements were underestimated in our psychophysical experiments, leading to an overcompensation of current and therefore higher stimulus amplitudes needed to achieve loudness levels. Regardless of whether or not this is the case, it can generally be said that the method for estimating the diagonal elements influences the calculations of the PA vectors, which in turn affects the potential fields generated during stimulation. Since different methods of estimating the diagonals are possible, each capable of producing different outcomes, the present study only used ‘ideal’ impedance matrices with diagonals determined from simulated potentials at the stimulating contacts.

From a modelling perspective, the results make it clear that certain aspects of implant induced neural excitation patterns can only be simulated with a realistic spatial distribution of cell bodies in the SG. In previous modelling studies, excitation patterns from different stimulation paradigms at a given position in the cochlea were frequently indistinguishable if the number of excited fibres was the same, due to the linear arrangement of the

neurons. The three-dimensional distribution of cell bodies in the present model allows the calculation of excitation densities along the cochlea. As expected, this turned out to be particularly relevant when comparing neural recruitment for different multipolar configurations. This is most clearly illustrated in figure 6.5b2 and b4, where differences in spread of excitation are apparent, despite the equal number of recruited fibres in all curves in each plot. The focused currents tend to penetrate deeply into the SG and easily recruit all nerve fibres in the central region, while monopoles show less dense recruitment patterns in a broader region of the SG.

The results also underline the importance of positioning the SG itself in a histologically accurate place. Studies by Rattay et al. and Hanekom have placed the SG in considerably different locations compared to the present study: Rattay's cell bodies are located farther along the central axon, while Hanekom's SG is located next to the osseous spiral lamina (Rattay et al., 2001; Hanekom, 2001, 2005). This results in peripheral processes that are respectively far longer or shorter than can be realistically expected, which will have consequences for the amount of peripheral process stimulation predicted by the models.

In conclusion, the main findings of this study are: (I) Current focussing requires electrical field interaction to focus the current. For medial electrode arrays the distance to the neurons is too small, which causes excitation of the neurons by non-centre contacts, resulting in side lobes. (II) The model predicts that current focussing only produces more restricted excitation patterns when there is little or no excitation occurring in the peripheral processes, either because of geometrical factors or due to neural degeneration. (III) The model predicts that neural recruitment with electrical stimulation is a three-dimensional process; regions of excitation not only expand in apical and basal directions, but also by penetrating deeper into the SG. (IV) Consequently, at equal loudness certain differences between the spatial excitation patterns of various multipoles cannot be simulated in a model containing linearly aligned neurons of identical morphology. Introducing a form of variability in the neurons, such as the spatial distribution of cell bodies in the SG used in this study, is therefore essential in the modelling of spread of excitation.

Acknowledgements

This study was financially supported by the Heinsius-Houbolt Fund and Advanced Bionics Corporation.

Appendix

In the presented model the trajectories of the neurons have been modified to include a more realistic spatial distribution of cell bodies throughout Rosenthal's canal. In this appendix the implementation of the spatial distribution of cell bodies and nerve fibre bundles is described in detail.

Figure 6.2a shows a mid-modiolar cross section of one of the model geometries at roughly 360° from the round window. Black lines indicate boundaries between modelled cochlear structures; the orange curve represents the base nerve line, L_0. This nerve line is defined as 10 quadratically interpolated line segments, subtended by 21 vertices, labelled v_1 through v_{21} (only odd numbered vertices up to v_{13} are shown). Vertex v_3 corresponds to the point where the neural peripheral process exits the modiolus and enters the osseous spiral lamina, while v_9 corresponds to the centre of the SG as it is seen in the histological image used to define the model geometry. L_0 represents a radial nerve fibre trajectory and by combining the base nerve lines from mid-modiolar cross-sections throughout the cochlear geometry a nerve plane is formed on which auditory neuron trajectories can be mapped, as described in Kalkman et al. (2014).

In order to vary the position of the nerve line in a given cross-section, at each vertex v_n a vector orthogonal to L_0 was defined, called R_n. These vectors point to a new set of vertices v_n+R_n, which define a shifted nerve line L_1, shown as a green curve. The vertices of L_0 can also be shifted in the opposite direction by $-R_n$, leading to nerve line L_{-1} (red curve). The vector length of R_9, which we will refer to as $|R_9|$, is set in such a way that a circle around v_9 with radius $|R_9|$ encompasses Rosenthal's canal as it was visible on the histological mid-modiolar cross-section that the cochlear geometry was based on. Lengths of R_1, R_2 and R_3 are set to zero, meaning that between vertices v_1 and v_3 the nerve lines L_0, L_1 and L_{-1} overlap. Furthermore, $|R_{13}|$ through $|R_{21}|$ are set to $|R_9|/4$, while the vector lengths at the remaining vertices are chosen so that L_1 and L_{-1} form smooth curves that define the boundaries of the nerve trajectories in the mid-modiolar cross-section. With these vertices and their orthogonal vectors, it is possible to generate additional nerve lines by introducing a parameter ρ which shifts vertices v_n by $\rho \cdot R_n$, where $-1 \leq \rho \leq 1$. The vertices shifted in this manner form a new nerve line L_ρ, the purple dashed curve in figure 6.2a is an example of such a nerve line.

As stated above, vertex v_9 on L_0 corresponds to the centre of the SG, and in Kalkman et al. (2014) this vertex invariably corresponded to the position of modelled cell bodies at the cochlear angle of that particular mid-modiolar cross-section. Varying the nerve lines as described above allowed for a variation of the neural trajectories and the location of the SG, however since we can only shift v_9 in one dimension with parameter ρ (i.e., orthogonal to L_0), it was necessary introduce another parameter, called δ, to move the location of the SG along nerve line L_ρ by a distance of $\delta \cdot |R_9|$ from the shifted v_9, with $-1 \leq \delta \leq 1$. The resulting SG location is $S_{\rho\delta}$, an example of which is shown as a black outlined purple circle in figure 6.2a. When forming a nerve plane from nerve lines L_ρ, SG locations $S_{\rho\delta}$ define a curve that describes all possible cell body positions on that nerve plane, which we will call its SG curve.

By using parameters ρ and δ to vary the nerve lines in mid-modiolar cross-sections throughout the cochlea, 17 nerve planes were defined for each cochlear geometry: the first of these was formed by nerve lines L_0 with SG locations S_{00}, which is identical to the nerve planes and SG curves used in Kalkman et al. (2014), and will be referred to as the base nerve plane. The remaining 16 nerve planes, called variant nerve planes, were formed by nerve lines with parameters $\rho_k=(1/4)\cdot(3+(-1)^k)\cdot\cos(k\cdot\pi/8)$ and $\delta_k=(1/4)\cdot(3+(-1)^k)\cdot\sin(k\cdot\pi/8)$, where $k\in\{0...15\}$. In mid-modiolar cross-sections this corresponded approximately to an even circular distribution of cell bodies around S_{00} (vertex v_9) with radii alternating between $|R_9|$ and $|R_9|/2$. The insert of figure 6.2a shows the distribution of SG locations as purple circles, as well as their nerve lines.

Realistic nerve fibre trajectories that take the length difference between the OC and SG into account were mapped onto the nerve planes in the manner described in Kalkman et al. (2014), with some modifications for the current study. For a given nerve fibre originating at a certain point along the length of the OC, the OC-SG position function from Stakhovskaya et al. (2007) was used to calculate the distance along the SG where that fibre's cell body was located, which defined the trajectory of the peripheral process from the OC to its entry into Rosenthal's canal. Determining the distance along the SG was done exclusively on the main nerve plane, since S_{00} represents the centre of the SG, where Stakhovskaya et al. did their measurements. Therefore, when mapping a nerve fibre on a variant nerve plane, the cell body position was first calculated along the SG curve on the main nerve plane, after which the cochlear angle of that point was determined and the cell body position on the variant plane was set along its SG curve at the same cochlear angle.

For each model geometry a set of 3200 nerve fibres was generated, the peripheral tips of which were spaced evenly along the OC. For each of these fibres, one of the 17 nerve planes was chosen onto which that fibre would be mapped. To ensure a uniform distribution of cell body positions without repeating patterns, the nerve planes were selected by following pseudo-random permutations of the 17 available nerve planes. In other words: in the first 17 fibres of the cochlea, each of the available nerve planes was chosen exactly once, in pseudo-random order. The same was done for every subsequent set of 17 consecutive nerve fibres, with the order in which the nerve planes were selected changing each time.

Finally, the nerve fibre trajectories were modified so that their peripheral processes exit the modiolus in bundles, rather than entering the osseous spiral lamina individually. The neurons were divided into 80 bundles of 40 consecutive fibres each; the spacing between the fibres at the transition from the modiolus into the osseous spiral lamina (v_3 in figure 6.2a) was set to 1/5 times the fibre spacing at the peripheral tips. Shortly before the cell body, the fibres spread out so that the cell bodies occupy the SG without gaps, at positions determined by Stakhovskaya's OC-SG position function (as described above). After the cell bodies, the axons of the fibres regroup into bundles again.

References

Bierer, J.A., Faulkner, K.F., 2010. Identifying cochlear implant channels with poor electrode-neuron interface: partial tripolar, single-channel thresholds and psychophysical tuning curves. Ear Hear. 31, 247–258.

Bierer, J.A., Faulkner, K.F., Tremblay, K.L., 2011. Identifying cochlear implant channels with poor electrode-neuron interfaces: electrically evoked auditory brain stem responses measured with the partial tripolar configuration. Ear Hear. 32, 436–444.

Bonham, B.H., Litvak, L.M., 2008. Current focusing and steering: modeling, physiology, and psychophysics. Hear. Res. 242, 141–153.

Bredberg, G., 1968. Cellular pattern and nerve supply of the human organ of Corti. Acta Otolaryngol. (Suppl. 236), 1+. Briaire, J.J., Frijns, J.H.M., 2000a. Field patterns in a 3D tapered spiral model of the electrically stimulated cochlea. Hear. Res. 148, 18–30.

Briaire, J.J., Frijns, J.H.M., 2000b. 3D mesh generation to solve the electrical volume conduction problem in the implanted inner ear. Simulation Practice and Theory 8, 57–73.

Briaire, J.J., Frijns, J.H.M., 2005. Unraveling the electrically evoked compound action potential. Hear. Res. 205, 143–156.

Briaire, J.J., Frijns, J.H.M., 2006. The consequences of neural degeneration regarding optimal cochlear implant position in scala tympani: a model approach. Hear. Res. 214, 17–27.

Frijns, J.H.M., de Snoo, S.L., Schoonhoven, R., 1995. Potential distributions and neural excitation patterns in a rotationally symmetric model of the electrically stimulated cochlea. Hear. Res. 87, 170–186.

Frijns, J.H.M., Briaire, J.J., Schoonhoven, R., 2000. Integrated use of volume conduction and neural models to simulate the response to cochlear implants. Simulation Practice and Theory 8, 75–97.

Frijns, J.H.M., Briaire, J.J., Grote, J.J., 2001. The importance of human cochlear anatomy for the results of modiolus-hugging multichannel cochlear implants. Otol. Neurotol. 22, 340–349.

Frijns, J.H.M., Kalkman, R.K., Vanpoucke, F.J., Bongers, J.S., Briaire, J.J., 2009a. Simultaneous and non-simultaneous dual electrode stimulation in cochlear implants: evidence for two neural response modalities. Acta Otolaryngol. 129, 433–439.

Frijns, J.H.M., Kalkman, R.K., Briaire, J.J., 2009b. Stimulation of the facial nerve by intracochlear electrodes in otosclerosis: a computer modeling study. Otol. Neurotol. 30, 1168–1174.

Frijns, J.H.M., Dekker, D.M.T., Briaire, J.J., 2011a. Neural excitation patterns induced by phased-array stimulation in the implanted human cochlea. Acta Otolaryngol. 131, 362–370.

Frijns, J.H.M., Kalkman, R.K., Dekker, D.M.T., Vellinga, D., Vanpoucke, F.J., Briaire, J.J., 2011b. Neural excitation patterns of a variety of multipolar electrode configurations. Conference on Implantable Auditory Prostheses, Pacific Grove, California, USA, July 25–29, 2011.

Goldwyn, J.H., Bierer, S.M., Bierer, J.A., 2010. Modeling the electrode-neuron interface of cochlear implants: effects of neural survival, electrode placement, and the partial tripolar configuration. Hear. Res. 268, 93–104.

Hanekom, T., 2001. Three-dimensional spiraling finite element model of the electrically stimulated cochlea. Ear Hear. 22, 300–315.

Hanekom, T., 2005. Modelling encapsulation tissue around cochlear implant electrodes. Med. Biol. Eng Comput. 43, 47–55.

Henry, B.A., Turner, C.W., Behrens, A., 2005. Spectral peak resolution and speech recognition in quiet: normal hearing, hearing impaired, and cochlear implant listeners. J. Acoust. Soc. Am. 118, 1111–1121.

Kalkman, R.K., Briaire, J.J., Dekker, D.M., Frijns, J.H., 2014. Place pitch versus electrode location in a realistic computational model of the implanted human cochlea. Hear. Res. 315, 10–24.

Landsberger, D.M., Padilla, M., Srinivasan, A.G., 2012. Reducing current spread using current focusing in cochlear implant users. Hear. Res. 284, 16–24.

Linthicum, F.H., Jr., Fayad, J.N., 2009. Spiral ganglion cell loss is unrelated to segmental cochlear sensory system degeneration in humans. Otol. Neurotol. 30, 418–422.

Litvak, L.M., Spahr, A.J., Emadi, G., 2007a. Loudness growth observed under partially tripolar stimulation: model and data from cochlear implant listeners. J. Acoust. Soc. Am. 122, 967–981.

Litvak, L.M., Spahr, A.J., Saoji, A.A., Fridman, G.Y., 2007b. Relationship between perception of spectral ripple and speech recognition in cochlear implant and vocoder listeners. J. Acoust. Soc. Am. 122, 982–991.

Long, C.J., Holden, T.A., McClelland, G.H., Parkinson, W.S., Shelton, C., Kelsall, D.C., Smith, Z.M., 2014. Examining the electro-neural interface of cochlear implant users using psychophysics, CT scans, and speech understanding. J. Assoc. Res. Otolaryngol. 15, 293–304.

Miller, C.A., Abbas, P.J., Nourski, K.V., Hu, N., Robinson, B.K., 2003. Electrode configuration influences action potential initiation site and ensemble stochastic response properties. Hear. Res. 175, 200–214.

Potts, L.G., Skinner, M.W., Gotter, B.D., Strube, M.J., Brenner, C.A., 2007. Relation between neural response telemetry thresholds, T- and C-levels, and loudness judgments in 12 adult nucleus 24 cochlear implant recipients. Ear Hear. 28, 495–511.

Rattay, F., Leao, R.N., Felix, H., 2001. A model of the electrically excited human cochlear neuron. II. Influence of the three-dimensional cochlear structure on neural excitability. Hear. Res. 153, 64–79.

Shannon, R.V., 1983. Multichannel electrical stimulation of the auditory nerve in man. II. Channel interaction. Hear. Res. 12, 1–16.

Snel-Bongers, J., Briaire, J.J., van der Veen, E.H., Kalkman, R.K., Frijns, J.H., 2013. Threshold levels of dual electrode stimulation in cochlear implants. J. Assoc. Res. Otolaryngol. 14, 781–790.

Snyder, R.L., Bierer, J.A., Middlebrooks, J.C., 2004. Topographic spread of inferior colliculus activation in response to acoustic and intracochlear electric stimulation. J. Assoc. Res. Otolaryngol. 5, 305–322.

Srinivasan, A.G., Padilla, M., Shannon, R.V., Landsberger, D.M., 2013. Improving speech perception in noise with current focusing in cochlear implant users. Hear. Res. 299, 29–36.

Stakhovskaya, O., Sridhar, D., Bonham, B.H., Leake, P.A., 2007. Frequency map for the human cochlear spiral ganglion: implications for cochlear implants. J. Assoc. Res. Otolaryngol. 8, 220–233.

Stickney, G.S., Loizou, P.C., Mishra, L.N., Assmann, P.F., Shannon, R.V., Opie, J.M., 2006. Effects of electrode design and configuration on channel interactions. Hear. Res. 211, 33–45.

Van den Honert, C., Kelsall, D.C., 2007. Focused intracochlear electric stimulation with phased array channels. J. Acoust. Soc. Am. 121, 3703–3716.

Van der Marel, K.S., Briaire, J.J., Wolterbeek, R., Snel-Bongers, J., Verbist, B.M., Frijns, J.H., 2014. Diversity in cochlear morphology and its influence on cochlear implant electrode position. Ear Hear. 35, e9–20.

White, M.W., Merzenich, M.M., Gardi, J.N., 1984. Multichannel cochlear implants. Channel interactions and processor design. Arch. Otolaryngol. 110, 493–501.

Whiten, D.M., 2007. Electro-anatomical models of the cochlear implant. PhD thesis Massachusetts Institute of Technology.

Wilson, B.S., Finley, C.C., Lawson, D.T., Wolford, R.D., Eddington, D.K., Rabinowitz, W.M., 1991. Better speech recognition with cochlear implants. Nature 352, 236–238.

Wu, C.C., Luo, X., 2013. Current steering with partial tripolar stimulation mode in cochlear implants. J. Assoc. Res. Otolaryngol. 14, 213–231.

Zhu, Z., Tang, Q., Zeng, F.G., Guan, T., Ye, D., 2012. Cochlear-implant spatial selectivity with monopolar, bipolar and tripolar stimulation. Hear. Res. 283, 45–58.

Chapter 7

The relation between polarity sensitivity and neural degeneration in a computational model of cochlear implant stimulation

Randy K. Kalkman
Jeroen J. Briaire
David M.T. Dekker
and Johan H.M. Frijns

Hearing Research 2022 (415), 108413

Abstract

The main aim of this computational modelling study was to test the validity of the hypothesis that sensitivity to the polarity of cochlear implant stimulation can be interpreted as a measure of neural health. For this purpose, the effects of stimulus polarity on neural excitation patterns were investigated in a volume conduction model of the implanted human cochlea, which was coupled with a deterministic active nerve fibre model based on characteristics of human auditory neurons. The nerve fibres were modelled in three stages of neural degeneration: intact, with shortened peripheral terminal nodes and with complete loss of the peripheral processes. The model simulated neural responses to monophasic, biphasic, triphasic and pseudomonophasic pulses of both polarities. Polarity sensitivity was quantified as the so-called polarity effect (PE), which is defined as the dB difference between cathodic and anodic thresholds.

Results showed that anodic pulses mostly excited the auditory neurons in their central axons, while cathodic stimuli generally excited neurons in their peripheral processes or near their cell bodies. As a consequence, cathodic thresholds were more affected by neural degeneration than anodic thresholds. Neural degeneration did not have a consistent effect on the modelled PE values, though there were notable effects of electrode contact insertion angle and distance from the modiolus. Furthermore, determining PE values using charge-balanced multiphasic pulses as approximations of monophasic stimuli produced different results than those obtained with true monophasic pulses, at a degree that depended on the specific pulse shape; in general, pulses with lower secondary phase amplitudes showed polarity sensitivities closer to those obtained with true monophasic pulses.

The main conclusion of this study is that polarity sensitivity is not a reliable indicator of neural health; neural degeneration affects simulated polarity sensitivity, but its effect is not consistently related to the degree of degeneration. Polarity sensitivity is not simply a product of the state of the neurons, but also depends on spatial factors.

1. Introduction

In most clinical stimulation strategies, cochlear implants (CIs) use symmetric biphasic pulses to electrically excite the auditory neurons located in the cochlea (Loizou, 2006). These symmetric biphasic pulses consist of a rectangular cathodic and anodic phase of equal duration and amplitude, which is the simplest way to construct a charge balanced electrical pulse that can be used safely, without causing harmful electrochemical reactions in the cochlea (Brummer et al., 1983; Donaldson and Donaldson, 1986). However, nerve fibres in general are not equally responsive to anodic and cathodic stimuli, since the ions involved in the transmission of neural signals all have positive charge and are therefore not indifferent to the polarity of an external electric field (Frankenhaeuser and Huxley, 1964; Colombo and Parkins, 1987). Indeed, psychophysical and electrophysiological studies in humans and animals have confirmed that there are differences in thresholds and dynamic range between the two polarities (Miller et al., 1999; Macherey et al., 2006; van Wieringen et al., 2008; Macherey et al., 2010; Undurraga et al., 2010; Carlyon et al., 2013; Undurraga et al., 2013; Macherey and Cazals, 2016; Carlyon et al., 2017); however, this sensitivity to stimulus polarity is not yet fully understood. Recently, several studies have hypothesized that polarity sensitivity can be interpreted as an indicator of neural health (Mesnildrey, 2017; Carlyon et al., 2018; Hughes et al., 2018; Goehring et al., 2019; Jahn and Arenberg, 2019a; Mesnildrey et al., 2020). If this is the case, then polarity sensitivity experiments would be a valuable tool for assessing the state of the auditory neurons in individual CI subjects. The aim of the present study is therefore to shed more light on this subject by investigating the effects of CI stimulus polarity and neural degeneration in a computational model of the human cochlea.

Objective measures and psychophysical experiments have either suggested or demonstrated that at high stimulus amplitudes, human subjects are more sensitive to anodic pulses than to cathodic ones (Macherey et al., 2006; Macherey et al., 2008; van Wieringen et al., 2008; Macherey et al., 2010; Undurraga et al., 2010; Carlyon et al., 2013; Undurraga et al., 2013; Carlyon et al., 2017; Hughes et al., 2018). Conversely, animal experiments have shown that, at high amplitude, animals such as cats and guinea pigs are more sensitive to cathodic pulses rather than anodic ones (Miller et al., 1999; Macherey and Cazals, 2016), implying that polarity sensitivity is affected by species specific cochlear anatomy, neurophysiology, etiology/duration of deafness or some combination of these. Additionally, computational modelling studies have suggested that different parts of the auditory neurons respond to different polarities; specifically, that cathodic pulses tend to stimulate the peripheral processes of the neurons and that anodic pulses are more likely to stimulate the central axons (Rattay, 1999; Rattay et al., 2001a; Rattay et al., 2001b; Potrusil et al., 2020). Furthermore, computational modelling studies have also shown that the degree of peripheral process stimulation can vary depending on both the location of the stimulating contact along the cochlear duct as well as its distance from the modiolus (Frijns et al., 1995; 1996; 2001; Hanekom, 2001; Briaire and Frijns, 2006; Smit et al., 2010; Kalkman et al., 2015; Potrusil et al., 2020), raising the question of how much the positions of the electrode contacts affect their polarity sensitivity.

Recent studies have investigated polarity sensitivity in human CI subjects at perceptual threshold and have found inconsistent results. Although anodic thresholds were usually lower than cathodic thresholds, there was a great amount of variability, both between subjects and within each subject (Mesnildrey, 2017; Carlyon et al., 2018; Goehring et al., 2019; Jahn and Arenberg, 2019a; Mesnildrey et al., 2020). The insights provided by computational modelling has prompted the researchers of these experiments to hypothesise that their inconsistent results could partially be explained by differences in neural health (i.e. the state of the surviving auditory neurons), specifically that greater sensitivity to cathodic stimuli indicates the presence of healthy peripheral processes. The underlying reasoning is that degeneration of the peripheral processes will affect the cathodic thresholds considerably, while their absence should not make much difference for the anodic thresholds, since those are more dependent on the central axons. This kind of retrograde degeneration, the gradual disappearance of peripheral processes, has indeed been observed in human auditory neurons after hearing loss (Kujawa and Liberman, 2009; Lin et al., 2011; Wu et al., 2019), indirectly adding to the plausibility of the hypothesis.

Despite this, the evidence supporting the neural health hypothesis is inconclusive, as there are still unknown factors that could play a role. A potentially complicating factor is the fact that all experiments in humans must be performed with charged balanced multiphasic pulses; many of the cited studies use either pseudomonophasic pulses or triphasic pulses as charge-balanced approximations of monophasic pulses, since true monophasic stimuli are not safe for clinical use. This raises the additional question whether the use of these pulses has distorted the results or not, particularly for triphasic pulses, since their ‘undesired’ phases still have considerable amplitudes. Computational modelling can provide valuable insight in these matters, as they allow researchers to manipulate factors and variables that are unchangeable or unknown in human CI subjects and make it possible to simulate clinically unsafe stimuli such as monophasic pulses.

The main goal of the present study was to test the validity of the hypothesis that polarity sensitivity can be interpreted as an indicator of neural health in CI stimulation. For this purpose, the study used a computational model of the implanted human cochlea, which was developed over the years at the Leiden University Medical Centre (Frijns et al., 1995; Frijns et al., 1996; Briaire and Frijns, 2000a; Briaire and Frijns, 2000b; Frijns et al., 2000; Frijns et al., 2001; Briaire and Frijns, 2005; 2006; Frijns et al., 2009a; Frijns et al., 2009b; Frijns et al., 2011; Westen et al., 2011; Snel-Bongers et al., 2013; Kalkman et al., 2014; Kalkman et al., 2015), updating its neural model with a human-based kinetics scheme and an accompanying auditory nerve fibre morphology, represented as an electrical double cable (Dekker et al., 2014). This model was used to simulate neural responses to monophasic, biphasic, triphasic and pseudomonophasic pulses in five cochlear geometries implanted with lateral, mid-scalar and medial electrode arrays, under three different states of neural health (i.e. healthy intact nerve fibres, neurons with minor degeneration at the peripheral tip and fibres that were completely missing their peripheral processes).

2. Methods

The present study used an updated version of a previously published model of the implanted human cochlea, which consisted of a volume-conduction model for simulating electrical field distributions and a deterministic active nerve fibre model for simulating the resulting neural responses (Kalkman et al., 2014; 2015).

2.1. Model geometry

The volume-conduction model is based on the Boundary Element Method (BEM) and is used to calculate quasi-static electrical potential fields in a three-dimensional geometrical representation of a human cochlea implanted with an electrode array. The model contains five human cochlear geometries, labelled CM1 through CM5, the first two of which were derived from histological cross-sections while CM3, CM4 and CM5 were based on µCT reconstructions. CM1 through CM4 are the same cochlear geometries used previously in Kalkman et al. (2015); CM5 is a not previously published geometry and is depicted in figure 7.1.

Electrode arrays were modelled in a lateral, mid-scalar and medial (peri-modiolar) position in each of the five cochlear geometries, leading to a total of 15 model geometries. The modelled array dimensions were based on the HiFocus1J electrode (Advanced Bionics, Valencia, CA, USA) and have rectangular plate contacts with a longitudinal length of 0.5 mm, a transversal length of 0.4 mm, and an electrode spacing of 1.1 mm (centre to centre). The arrays were inserted as deeply as possible without touching the walls of the scala tympani and the number of modelled electrode contacts for each individual array was chosen so that the electrodes span the maximum possible cochlear range in all

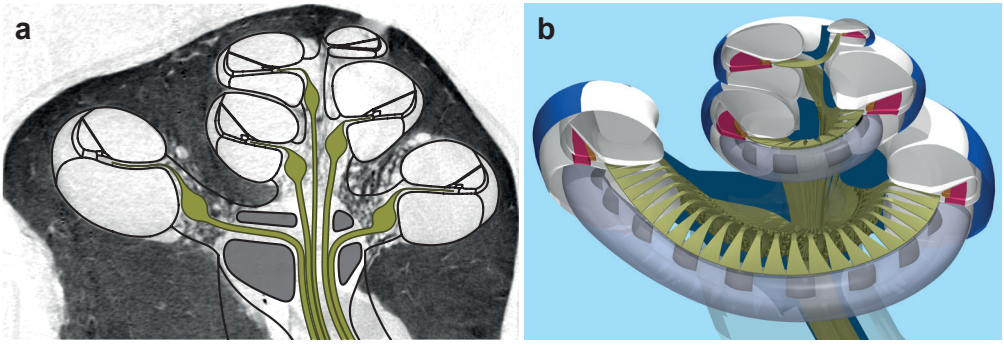

Figure 7.1. *Illustration of one of the cochlear geometries used in this study (CM5). Panel a shows a mid-modiolar plane through a human cochlea, reconstructed from µCT imaging of a human temporal bone, obtained from Advanced Bionics and the University of Antwerp. Black lines in panel a indicate boundaries between cochlear structures used to define the compartments of the model geometry; the green lines indicate the outlines of the neural trajectories. Panel b shows a ray-traced image of a cut-through of the final three-dimensional geometry, implanted with an electrode array in lateral position. Modelled intact neural trajectories are shown in yellow.*

modelled cochleae. Table 7.1 shows the active angular ranges and number of contacts for each geometry used in this study.

The auditory nerve fibre trajectories in each cochlear geometry are modelled in the manner described in our previous studies (Kalkman et al., 2014; 2015). The model geometries all contain 3200 neurons, the peripheral tips of which are evenly distributed along the basilar membrane (BM) while the cell bodies are spatially distributed in Rosenthal's canal in pseudo-random fashion without breaking their tonotopic organisation (i.e. from base to apex the fibres retain the same order in Rosenthal's canal as they have along the BM). The modelled neurons are grouped into 80 bundles of 40 nerve fibres; these nerve bundles condense when they enter the Habenula Perforata, expand around the spiral ganglion, and condense again when they exit Rosenthal's canal. The trajectory of the central line of each nerve bundle is determined by applying data from a histological study by Stakhovskaya et al. (2007), which found a relationship between the positions of the auditory neurons' peripheral tips along the organ of Corti and the positions of their cell bodies along the spiral ganglion.

2.2. Neural model

The auditory nerve fibre model from our previous studies, which was largely based on animal data, was found to insufficiently behave like human (auditory) neurons in experimental studies, particularly in terms of predicting action potential shape, latencies and conduction velocity (Briaire and Frijns, 2005; Bachmaier et al., 2019). To remedy some of these shortcomings, a new auditory nerve fibre model was used which incorporated some human anatomical features and properties that were absent in the previous model. First, the new neural model described nerve fibres as an electrical double cable, rather than a single cable, in order to include peri-axonal current between the axon and the first layer of myelin (Berthold, 1978; Berthold and Rydmark, 1983). In addition, the previously used generalised Schwarz-Eikhof-Frijns (gSEF) kinetics, which were derived from rat and cat experiments, were replaced with the so-called Schwarz-Reid-Bostock (SRB) neural kinetics scheme (Schwarz et al., 1995), which was based on human data. This neural model was previously published using a homogenous nerve fibre morphology (Dekker et

Cochlear model	Lateral			Mid-scalar			Medial		
	Basal	Apical	#	Basal	Apical	#	Basal	Apical	#
CM1	21°	497°	18	14°	488°	17	15°	523°	16
CM2	30°	500°	16	18°	501°	15	29°	521°	13
CM3	18°	701°	20	12°	673°	18	13°	697°	16
CM4	16°	630°	22	20°	625°	19	20°	613°	16
CM5	18°	517°	20	18°	537°	18	18°	574°	16

Table 7.1. *Insertion angles of the most basal and apical electrode contacts of all model geometries used in the study (angles are measured in degrees from the round window), as well as the number of electrode contacts of each array geometry ('#').*

al., 2014); for this study the morphology was adapted to match the human auditory neuron (illustrated in figure 7.2), incorporating anatomical details from histological observations (Spoendlin and Schrott, 1989).

As shown in figure 7.2a, the modelled nerve fibres consisted of a thinly myelinated cell body flanked by two 1 µm long Ranvier nodes, connecting it to a peripheral process and a central axon. The central axon consisted of 22 myelinated segments separated by Ranvier nodes; the lengths of these segments increased from 150 µm to 350 µm in steps of 50 µm, in central direction starting from the cell body. The peripheral process of the base fibre illustrated in figure 7.2 consisted of 6 myelinated segments of equal length, likewise separated by Ranvier nodes, with a 10 µm long unmyelinated terminal at the tip. Since the peripheral processes vary in length throughout the cochlea, the lengths of the myelinated peripheral segments were adjusted accordingly. However, an upper limit was placed on the peripheral segment lengths as it was found that longer segments would block the propagation of action potentials. Therefore, in extremely long peripheral processes (particularly those in the apex) segments were added to ensure that their lengths would not exceed 280 µm, equivalent to the length limitation that was necessary for the previous version of the neural model (Kalkman et al., 2014). As a result, the lengths of the peripheral segments in the cochlear geometries ranged from 131 µm to 280 µm, with the number of segments ranging from 6 to 11.

In order to simulate the effects of neural degeneration, the neurons were modelled in three conditions: completely intact (as described above and depicted as the top fibre in figure 7.2a), with shortened peripheral terminals and with complete loss of the peripheral processes. For the short terminal condition the 10 µm unmyelinated nodes at the tips of the peripheral processes of all modelled neurons were shortened to 1 µm (middle fibre in figure 7.2a), in the same manner as in a previous study (Snel-Bongers et al., 2013), where it was shown that this seemingly minor change in neural morphology can have a noteworthy impact on neural activation. This condition was based on animal studies that showed that the initial stage of auditory neural degeneration is loss of the peripheral terminal (Kujawa and Liberman, 2009; Lin et al., 2011). For the third neural condition, the entire peripheral process was removed from all modelled neurons, leaving only a 1 µm long Ranvier node on the peripheral side of the cell body (bottom fibre in figure 7.2a). This condition represents a state of severe neural degeneration where it is nevertheless still possible to excite the auditory nerve fibres electrically.

2.3. Stimulus configuration

With the implanted cochlear geometries and the model neurons defined, the volume-conduction model was used to calculate the electrical potentials at each Ranvier node and myelinated internode (see figure 7.2b) resulting from injecting a monopolar 1 µA current at one of the modelled electrode contacts. Since the volume-conduction model was purely resistive, the potentials could simply be multiplied by an electrode stimulus pulse to obtain time-dependent nerve fibre potentials, which could then be used as external field

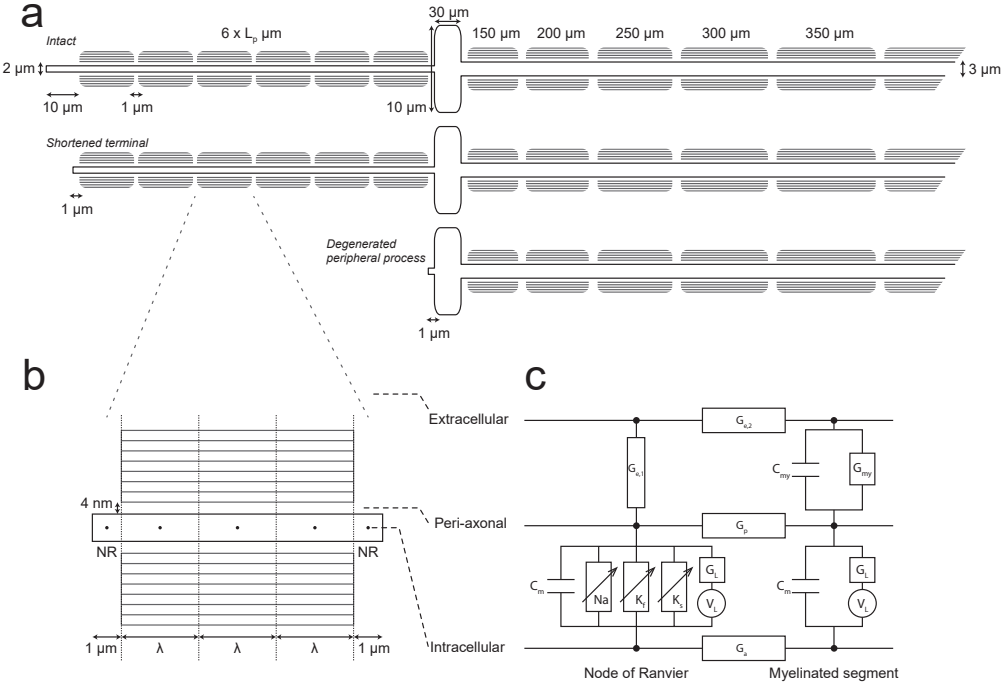

Figure 7.2. *Schematic representation of the model's intact auditory nerve fibre morphology (not to scale). The top fibre depicted in subfigure a illustrates how the base intact model fibre is built out of myelinated segments; the peripheral process consists of six myelinated segments (left side) and has an axon diameter of 2 µm. The peripheral segments are all the same length (L_p), which varies throughout the cochlea, ranging from 131 µm to 280 µm. It is followed by a cell body of 30 µm length and 10 µm diameter, flanked by two nodes of Ranvier. The central axon (right side) consists of 23 segments and has an axon diameter of 3 µm. The first myelinated segment after the cell body is 150 µm long and each segment after that if 50 µm longer than the previous, up to a maximum of 350 µm. All nodes of Ranvier are 1 µm long, except the terminal node of the peripheral process (left end of the figure), which is 10 µm long for an intact neuron. The middle fibre in subfigure a represents a partially degenerated neuron, in which the peripheral terminal node has been reduced to a length of 1µm; the bottom fibre shows a more severe state of degeneration where the entire peripheral process has been removed. Subfigure b gives a more detailed illustration of a myelinated segment flanked by nodes of Ranvier (NR), showing how the segment is split into three subsegments of equal length (λ). The myelin sheath on each segment consists of a number of layers: 20 for the peripheral process, 1 for the cell body and 70 for the central axon. Furthermore, there is a peri-axonal layer located between the axon and the myelin sheath, which is 4 nm wide. Subfigure c shows the modelled electrical diagram of a node of Ranvier (left part) and the first myelinated subsegment. The following symbols are used: C_m for membrane capacitance; P_{Na} for voltage dependent sodium permeability; g_{Kf} and g_{Ks} for voltage dependent conductance for the fast and slow potassium currents; G_L for membrane leak conductance; V_L for leakage equilibrium potential; G_a, G_p, G_{e1} and $G_{e,2}$ for axonal, peri-axonal and extracellular conductance; C_{my} for myelin capacitance; G_{my} for myelin conductance.*

for the neural simulations. To study the effects of stimulus polarity on neural excitation, simulations were run with four types of pulse shape: monophasic, biphasic, triphasic and pseudomonophasic pulses, as illustrated in figure 7.3. The monophasic pulses were simulated to isolate polarity effects without the complication of opposite polarity phases interacting with each other; these were compared to biphasic pulses (the standard pulse shape in clinical settings), as well as triphasic and pseudomonophasic pulses (clinically safe pulse shapes that are frequently used as approximations of monophasic pulses in clinical experiments (van Wieringen et al., 2005; Macherey et al., 2006; Macherey et al., 2008; van Wieringen et al., 2008; Macherey et al., 2010; Carlyon et al., 2013; Macherey and Cazals, 2016; Carlyon et al., 2017; Mesnildrey, 2017; Carlyon et al., 2018; Goehring et al., 2019; Jahn and Arenberg, 2019a; b; Mesnildrey et al., 2020)).

The simulated monophasic pulses consisted of a single 40 µs rectangular pulse with either anodic polarity (MA; figure 7.3a1) or cathodic polarity (MC; figure 7.3a2). The biphasic pulses used in this study consisted of two phases of 40 µs duration with no interphase gap; the two phases were rectangular pulses with equal amplitude but opposite polarity. Biphasic pulses lead with either the anodic phase (BA; figure 7.3b1) or with the cathodic phase (BC; figure 7.3b2). Triphasic pulses consisted of a central 40 µs phase flanked by two opposite polarity phases with the same duration but half amplitude and no interphase gaps. These triphasic pulses were named by the polarity of their central phase, which was expected to be its dominant phase due to its higher amplitude; figure 7.3c1 shows the triphasic anodic pulse (TA) used in this study, while figure 7.3c2 shows the triphasic cathodic pulse (TC). Pseudomonophasic pulses were essentially modified biphasic pulses;

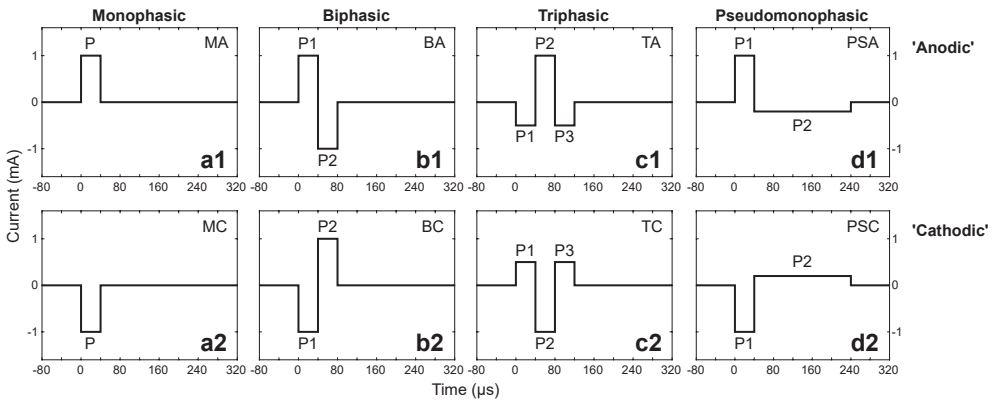

Figure 7.3. *Illustration of the different pulse shape definitions: monophasic (a1&a2), symmetric biphasic (b1&b2), triphasic (c1&c2) and pseudomonophasic pulses (d1&d2). The top row of panels (a1–d1) represent the pulses where the anodic phase is expected to be dominant (or simply the first phase, in the case of biphasic pulses), while the bottom row (a2–d2) represents their cathodic counterparts. The main pulse duration for all pulses in the study is 40 µs, for pseudomonophasic pulses this is the duration of the first phase (the duration of the second phase is variable, but it is 200 µs long in the example in panels d1&d2). See the methods section for further details.*

the amplitude of the second phase of a biphasic pulse was reduced with an arbitrary ratio R_{ps}, while the duration of the second phase was increased with the same ratio to maintain charge balance (i.e. with the first phase set at 40 μs, the second phase was R_{ps}·40 μs long). For a sufficiently large value of R_{ps}, this pulse was expected to behave like a monophasic pulse, with the benefit of being charge balanced and therefore usable in clinical practice. An example of a pseudomonophasic anodic pulse (PSA) with R_{ps}=5 is shown in figure 7.3d1, and the corresponding pseudomonophasic cathodic pulse (PSC) is shown in figure 7.3d2. Three different values of R_{ps} were used for the simulations: R_{ps}=2 (with the resulting pseudomonophasic pulses referred to as PSA2 and PSC2), R_{ps}=4 (PSA4 and PSC4), and R_{ps}=8 (PSA8 and PSC8).

2.4. Model output

Using the pulse definitions above as monopolar stimuli on each electrode contact in all 15 geometries, simulated neural responses were calculated for all modelled nerve fibres under the three described conditions of neural degeneration. For each simulation it was recorded whether an action potential propagated to the central end of the given nerve fibre, and if so, at which node the action potential originated. Stimulus amplitudes (i.e. the amplitude of the main phase of each pulse type) ranged from 0.05 mA to 5 mA in steps of 0.404 dB; once the calculations for this amplitude range were completed, additional iterative simulations were done to determine the threshold of excitation of each individual fibre more precisely, to within 0.1% of its precise value. Of these additional iterations only the lowest above-threshold value for the stimulus amplitude and the corresponding node of excitation were recorded.

For each individual electrode contact and stimulus pulse, simulation results were compiled into so-called excitation profiles, which were represented as two-dimensional colour maps that indicate which model neurons were excited at a given stimulus amplitude, with different colours indicating in which part of the fibre the excitation took place: peripheral process, cell body or central axon (excitation in one of the two Ranvier nodes on either side of the cell body was considered to be excitation at the cell body (Frijns et al., 1995; Frijns et al., 1996; Briaire and Frijns, 2000a)).

As in our previous studies, simulated loudness levels were quantified by the amount of space the excited neurons occupied along the BM. Each modelled nerve fibre was considered to occupy a certain amount of length along the BM at their peripheral tips (for this purpose, degenerated nerve fibres were treated as if they were still intact) and thus the simulated loudness level of a given stimulus was determined by summing the lengths along the BM for all excited neurons. Based on comparisons of our model to psychophysical data, perceptual threshold was considered to be equivalent to 1 mm excitation along the BM in the model (Snel-Bongers et al., 2013), while maximum comfortable loudness (MCL) was considered to be comparable to an excitation width of 4 mm; the stimulus amplitude needed to reach perceptual threshold and MCL in the model will therefore be referred to as I_{1mm} and I_{4mm}, respectively.

In order to quantify polarity sensitivity, several studies have defined the so-called polarity effect (PE) as the difference between the perceptual thresholds of cathodic and anodic stimuli (Mesnildrey, 2017; Carlyon et al., 2018; Goehring et al., 2019; Jahn and Arenberg, 2019a; Mesnildrey et al., 2020), using the following equation:

$$PE = 20 \cdot {}^{10}\log\left(\frac{I_{cathodic}}{I_{anodic}}\right)$$

Here, PE is expressed in dB, $I_{cathodic}$ is the current amplitude at threshold for the cathodic stimulus, and I_{anodic} is the current amplitude at threshold for the anodic stimulus.

3. Results

3.1. Excitation patterns

Figure 7.4 shows excitation profiles for monophasic pulses on a lateral electrode contact at 210° from the round window in cochlear geometry CM5, for four different conditions. Figure 7.4a is an excitation profile of MA stimulation in a cochlea with intact neurons, while figure 7.4b shows the profile for MC stimulation on the same contact. Figure 7.4c also shows excitation patterns for an MC pulse, but for the case where all modelled neurons have shortened terminal nodes. The bottom figure 7.4d shows the same again but with a complete loss of peripheral processes. The plots in figure 7.4 are typical examples that illustrate how stimulus polarity and neural degeneration determined the location of excitation along the auditory nerve fibres. In general, MA pulses excited neurons almost exclusively along the central axon, which can be seen in figure 7.4a, where all excitation is coded blue. This was the case regardless of array type, electrode contact or degree of neural degeneration (data not shown), though these factors did affect the I_{1mm} and I_{4mm} levels. It should be noted, however, that neural degeneration had only a minor impact on simulated perceptual loudness levels for MA stimulation.

By contrast, in simulations with MC pulses, neurons near the stimulating electrode contact were rarely excited along the central axon. For intact and short terminal neurons, excitation occurred mostly along the peripheral processes (green area in figure 7.4b and c), while a complete loss of peripheral processes moved the place of excitation to the cell bodies (red areas in figure 7.4d). When MC pulses excited neurons at the central axon, they generally did so at high stimulus levels (above I_{4mm}) at sites deep in the modiolus, in neurons associated with higher/lower cochlear turns (blue areas in figures 7.4 b–d). This kind of unintended excitation was reported in previous studies, where it was referred to as cross-turn stimulation (Frijns et al., 1995; Briaire and Frijns, 2000a; Frijns et al., 2001; Kalkman et al., 2014). Notably, the threshold for cross-turn stimulation is considerably lower for MC stimulation than it is for MA stimuli (compare blue areas in the top right corners of figures 7.4b–d to the same area in figure 7.4a).

Additionally, the dependency on the peripheral processes also meant that I_{1mm} and I_{4mm} levels of MC stimuli were much more affected by neural degeneration than those of MA pulses. One notable observation from the excitation profiles is that, for lateral contacts,

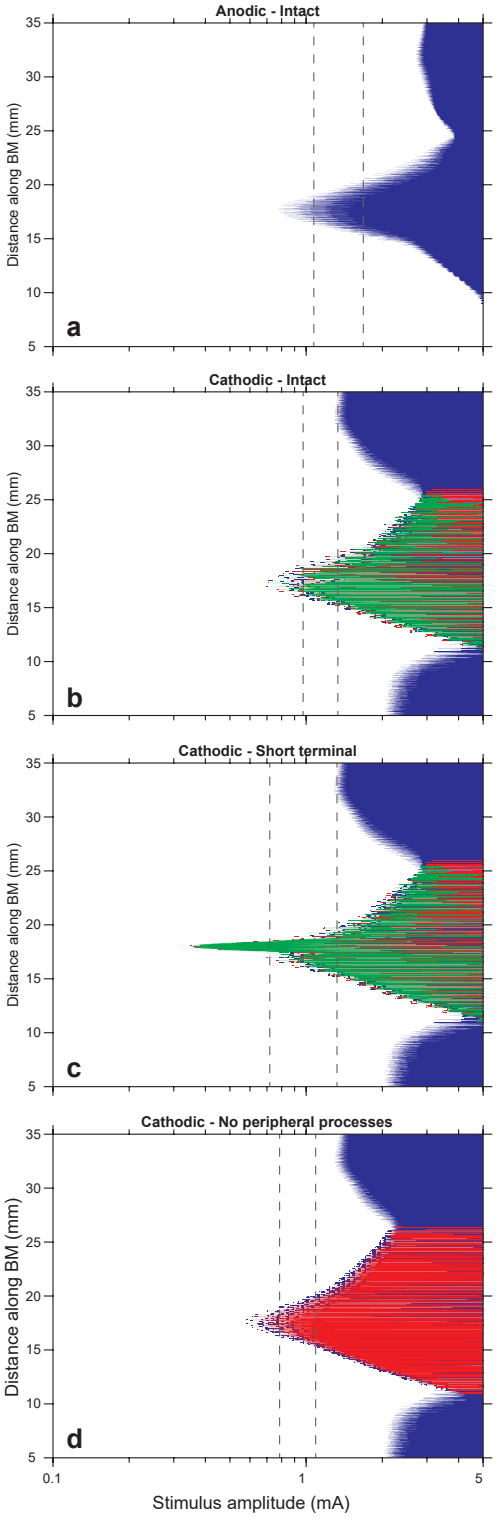

Figure 7.4. *Neural excitation patterns of monophasic stimuli on a lateral electrode contact at an insertion angle of 210° in cochlear geometry CM5, for three different conditions. Each panel shows an excitation profile, a colour-coded map of neural excitation patterns of a given stimulus in a specific model configuration; the abscissa of the indicates stimulus amplitude in mA, while the ordinate indicates positions of the modelled neurons along the basilar membrane, measured in mm starting from the base of the cochlea. Coloured areas indicate excitation in the peripheral process (green), excitation near the cell body (red), excitation in the central axon (blue), or no excitation (white); vertical dashed lines indicate the simulated dynamic range of the stimulus (I_{1mm} and I_{4mm}, left and right dashed lines in each panel, respectively); the non-white areas between the dashed lines therefore represent the most relevant region(s) of excitation. Panel a shows the excitation profile of MA stimulation when all neurons are modelled as intact, panel b shows the same for MC stimulation, panel c shows MC excitation patterns when all neurons have shortened peripheral terminal nodes and panel d shows MC excitation patterns when all neurons have their peripheral processes removed.*

the I_{1mm} threshold was generally lower for short terminal neurons than it was for intact neurons, due to the presence of a spatially restricted area of excitation at the peripheral tips of the neurons closest to the stimulating contact (visible as a sharp peak left of the dashed lines at 18 mm along the BM in figure 7.4c). This region of excitation was much more present in short terminal neurons and lead to a lower I_{1mm} than was found for intact neurons (compare figure 7.4b to 7.4c).

3.2. Simulated loudness levels and PE values in different cochlear geometries

The top row of panels in figure 7.5 shows I_{1mm} levels and resulting PE values of MA and MC pulses, stimulated on all lateral array contacts in each cochlear geometry, modelled with intact neurons. Figure 7.5a1 shows I_{1mm} for MA pulses along the ordinate, figure 7.5b1 shows the same for MC pulses, and the corresponding PE values are plotted in figure 7.5c1. The abscissa in each plot indicates the insertion angle of the electrode contacts in the consensus cochlear coordinate system (Verbist et al., 2010), which is measured in degrees from the round window. The data points connected by dotted lines correspond to thresholds from individual lateral electrode contacts of the five cochlear geometries, the black open circles connected by solid lines are average values across all five cochlear

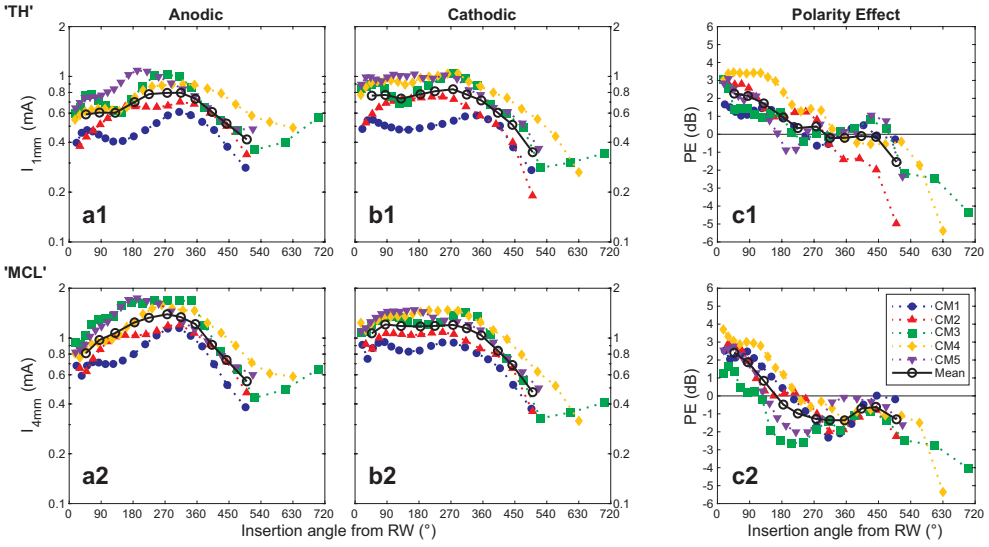

Figure 7.5. *Simulated perceptual thresholds and PE values of lateral electrode arrays in five individual cochlear geometries with intact neurons, as well as their average trends. Panel a1 shows simulated perceptual thresholds (I_{1mm}) for monophasic anodic pulses on the ordinate (in mA), while the abscissa indicates electrode insertion angle measured in degrees from the round window. The coloured data points connected by dotted lines correspond to the five cochlear geometries used in this study; the black circles connected by solid lines show the model average. Panel b1 shows the same for monophasic cathodic pulses and panel c1 shows the resulting PE values in dB. Panels a2–c2 repeat the same plots using simulated MCL (I_{4mm}) instead of perceptual thresholds.*

geometries. The bottom row of figure 7.5 (panels a2–c2) repeats the same plots, but using I_{4mm} levels, rather than I_{1mm} levels (the PE values in panel c2 are therefore calculated at simulated MCL, rather than threshold).

Simulated thresholds, MCLs and PE values of individual geometries generally followed the same trend as the model average, with some individual variations (compare dotted curves to the solid black curves in figure 7.5). The model average PE in panel c1 showed a nearly monotonically decreasing curve, going from 2.3 dB at the basal end of the cochlea (which means that MA thresholds were 2.3 dB lower than MC thresholds), to -1.5 dB at 495° (which means MC thresholds were 1.5 dB lower than MA thresholds), while the curves for the individual geometries showed erratic variations to the average trend (figure 7.5c). Most notably, although the average PE curve only crosses the 0 dB line once, individual PE curves can cross it multiple times (blue circles, green squares and purple triangles for CM1, CM3 and CM5 respectively in figure 7.5c), which indicates that the favoured polarity of these geometries changed several times along the lengths of their arrays. PE values calculated using I_{4mm} levels were similar to those calculated at I_{1mm}, though PE values were shifted downwards by about 1 dB between roughly 90° and 360° insertion angle.

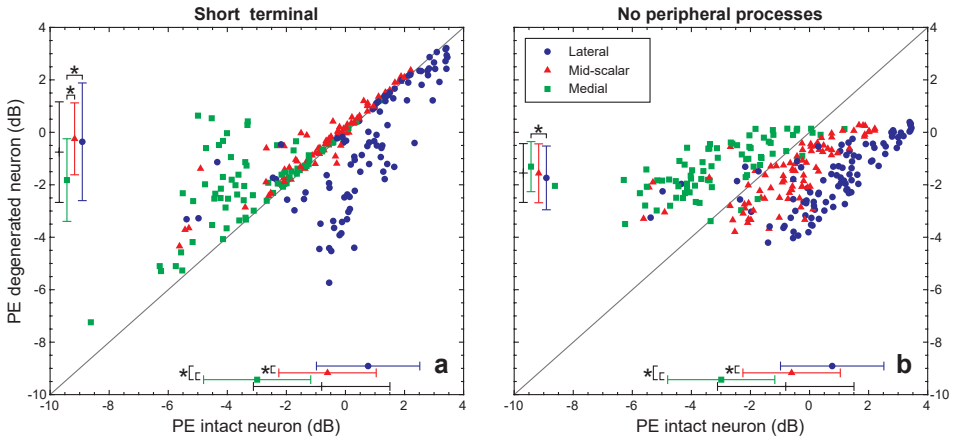

Figure 7.6. *The effect of neural degeneration on simulated PE values of monophasic stimulation, for all contacts in all model geometries (cochleae and array types). The abscissa in both panels indicates PE values obtained from simulations with intact neurons, while the ordinate indicates PE values from degenerated neurons (short terminals in panel a, complete loss of peripheral processes in panel b). Each point in the plots represents an individual electrode contact from one of the model geometries, the data has been split up by array type (blue circles for lateral arrays, red triangles for mid-scalar arrays and green squares for medial arrays). Error bars along the axes indicate the means and standard deviations of the PE values, with the black error bars representing the total data set and the other bars corresponding to the data sets indicates by their colours and symbols. Black asterisks next to the error bars indicate statistical significance between the data sets.*

3.3. Comparing degenerated neurons to healthy neurons

The effects of neural degeneration on polarity sensitivity are demonstrated in figure 7.6. PE values were determined using monophasic stimuli on all electrode contacts of each electrode array and cochlear geometry, for all three neural conditions and were plotted against each other. In figure 7.6a, PE values of individual contacts stimulating short terminal neurons are plotted along the ordinate, while the abscissa indicates the corresponding PE values for the intact neurons. Figure 7.6b shows the same plot, but with PE values of neurons with completely degenerated peripheral processes along the ordinate. In both plots the data points are split up by array type (blue circles for lateral contacts, red triangles for mid-scalar contacts and green squares for medial contacts) and the grey diagonal lines indicate the line where the PE values for the degenerated neurons were equal to those of intact neurons. The error bars along the axes indicate the means and standard deviations of the PE values for the corresponding neural condition, split up by array type (the black error bar represents all three array types combined). Asterisks next to the error bars denote statistically significant differences between data sets ($p<0.05$).

In both plots of figure 7.6 it is apparent that the modelled changes in neural condition did not have a consistent effect on PE values, as the data is spread out on both sides of the diagonal, which means that neural degeneration increased the PE for some contacts (data points above the diagonals) but decreased it for others (data points below the diagonals). However, there was a clear effect of array type, reflected by the way the data points for each type of array are clustered together in figure 7.6. This clustering was mainly due to the fact that PE values for intact neurons were strongly affected by electrode array type (compare the error bars along the abscissae), while mean PE values for degenerated neurons were less affected (compare the error bars along the ordinates). For lateral contacts, neural degeneration tended to shift the PE downward (blue circles in figures 7.6a and b), as opposed to PE values of medial electrodes, which were more likely to be shifted upwards (green squares). For mid-scalar electrode contacts, shortening the terminal node of the modelled neurons had a relatively minor impact on the PE, as the corresponding data points are mostly located close to the diagonal, but on average slightly shifted upwards (red triangles in figure 7.6a), whereas completely removing the peripheral processes mostly shifted PE values downwards (red triangles in figure 7.6b). Paired t-tests revealed that these changes in the PE values between neural conditions were all statistically significant for each individual array type; when the data for all three array types were merged, paired t-tests still showed significant differences between the neurons without peripheral processes and the other two neural conditions, but not between the intact and short terminal neurons.

3.4. Comparing multiphasic pulses to monophasic pulses

Next, the effect of pulse shape on the calculated PE values at I_{1mm} was examined; the results are plotted in figure 7.7. The figure shows PE values obtained with simulated perceptual thresholds of multiphasic pulses on the ordinate, plotted against the corresponding PE values of monophasic pulses on the abscissa. Data from five different cathodic/anodic

multiphasic pulse pairs are plotted: three implementations of pseudomonophasic pulses, namely PSC8/PSA8 (Pseudomonophasic 8; blue circles), PSC4/PSA4 (Pseudomonophasic 4; red upward pointing triangles), PSC2/PSA2 (Pseudomonophasic 2; green squares), biphasic pulses BC/BA (yellow diamonds) and triphasic pulses TC/TA (purple downward pointing triangles). Each data point represents an individual electrode contact in one of the 15 geometries, under one of the three neural conditions, and the grey diagonal represents the line where the PE values of the multiphasic pulses were equal to the PE values obtained with monophasic pulses.

PE values obtained with pseudomonophasic 8 pulses were very similar to those found with true monophasic pulses, as indicated by the fact that their data points (blue circles) follow the grey diagonal closely in figure 7.7. Inspection of simulated threshold levels show that, on average, I_{1mm} of PSC8 and PSA8 pulses were slightly shifted up from their monophasic counterparts by about 0.4 dB and 0.3 dB respectively, resulting in PE values that were on average 0.1 dB higher than monophasic PE values. At the other extreme end, PE values of biphasic pulses deviated from the diagonal substantially, with the data points arranged almost horizontally in figure 7.7 (yellow diamonds), indicating that there was a much smaller difference between I_{1mm} values of BC and BA pulses than there was between those of MC and MA pulses. The average PE value obtained with biphasic pulses was -0.7 dB, showing that the model tended to be slightly more sensitive to BC pulses than to BA pulses. Since a pseudomonophasic pulse with R_{ps}=1 is identical to a biphasic pulse, the plots for pseudomonophasic 4 and pseudomonophasic 2 pulses in figure 7.7 can be seen as a stepwise transition from pseudomonophasic 8 pulses to biphasic pulses, with the data points going from arranged close to the diagonal to being arranged along a decreasing slope.

With triphasic pulses, PE values were consistently higher than those obtained with monophasic pulses, as evidenced by the fact that the data points for triphasic pulses are all located above the diagonal in figure 7.7 (purple downward pointing triangles). This shift was on average 1.2 dB and was mostly due to an increase in cathodic thresholds; I_{1mm} levels for TC pulses were on average 2.2 dB higher than those of MC pulses, while I_{1mm} levels of TA pulses were only 1 dB higher than those of MA pulses.

3.5. Normalised simulated loudness levels and PE values

To remove the variance between subjects, recent studies have normalised their data by subtracting average values for each subject (Mesnildrey, 2017; Carlyon et al., 2018; Mesnildrey et al., 2020). The same was done for the modelling results of this study in figure 7.8, where normalised PE values of triphasic pulses are plotted against their normalised average thresholds (panels a1–c1), analogous to the manner the psychophysical data was plotted in Carlyon et al. (2018). For this figure, every combination of cochlear geometry, array type and neural condition was treated as a 'virtual subject'; the data points in the plot correspond to individual electrode contacts of these subjects. The data was normalised by calculating the average values across the entire array and subtracting them from the values of each individual electrode contact for each virtual subject. The ordinates show

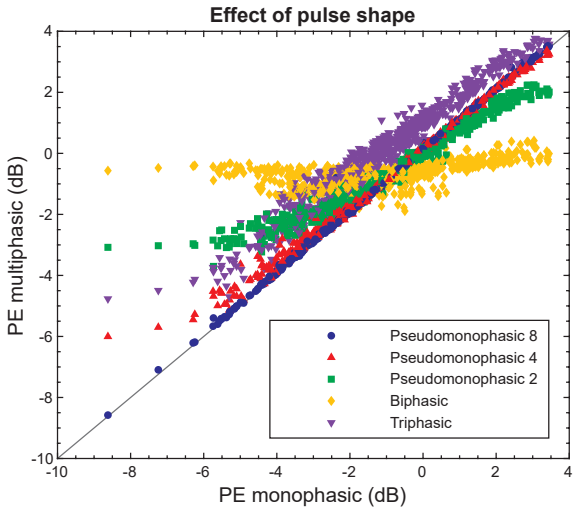

Figure 7.7. *Effect of pulse shape on simulated polarity sensitivity of each electrode contact in all model geometries (cochleae and array types) and all three neural conditions. The abscissa indicates PE values obtained with monophasic pulses, while the ordinate indicates the corresponding PE values derived from simulations with multiphasic pulses, namely pseudomonophasic pulses with R_{ps} equal to 8, 4 and 2 (blue circles, red upward pointing triangles and green squares, respectively), symmetric biphasic pulses (yellow diamonds) and triphasic pulses (purple downward pointing triangles). The grey diagonal represents the line where simulations with monophasic pulses result in PE values that are identical to their multiphasic equivalents.*

normalised PE values, while the abscissae indicate the average of the I_{1mm} levels of TA and TC pulses, with I_{1mm} expressed in dB relative to 1 mA. In each panel of figure 7.8 the data is split by array type: blue circles for lateral arrays, red triangles for mid-scalar arrays and green squares for medial arrays. The three panels illustrate the effects of different neural conditions; the data for intact neurons is plotted in panels a1 and a2, the results of the short peripheral terminals are shown in panels b1 and b2, and panels c1 and c2 corresponds to complete loss of peripheral processes. The black line in each panel shows a linear regression fit of the plotted data points.

Figure 7.8 shows significant positive correlations between PE and average threshold level for intact neurons and short terminal neurons (panels a1 and b1), as was apparent from the linear regression lines (panel a1: r^2=0.26, p<<0.001, panel b1: r^2=0.09, p<<0.001). When there is a complete loss of peripheral processes, the correlation was negative but non-significant (panel c1: r^2=0.01, p=0.09). Splitting the data by array type revealed no significant differences between their regression slopes, but there was an effect of insertion angle. To illustrate this, the normalised PE values have been replotted in panels a2–c2, but here the abscissa indicates the insertion angles of the electrode contacts, rather than normalised average I_{1mm} levels. For each neural condition there was a negative correlation between normalised PE value and insertion angle, as indicated by the linear regression lines (panel a2: r^2=0.62, panel b2: r^2=0.32, panel c2: r^2=0.50; p<<0.001 for all three regression lines).

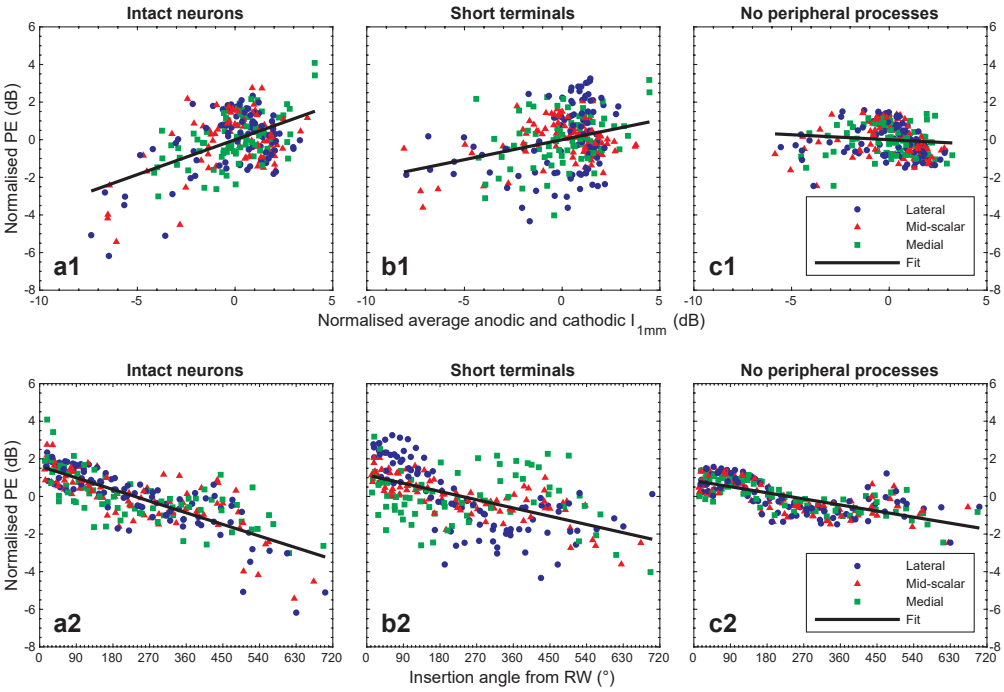

Figure 7.8. *Normalised PE values for all contacts in all model geometries, plotted separately for each neural condition; panels a1 and a2 show data from simulations with intact neurons, panels b1 and b2 show data from short terminal neurons and panels c1 and c2 contain results from neurons with missing peripheral processes. The top row of panels (a1–c1) shows the relationship between normalised PE values and normalised average thresholds, plotted analogously to the psychophysical data in Carlyon et al. (2018). Simulated perceptual thresholds are obtained with anodic and cathodic triphasic pulses; the average values of these two are normalised and plotted on the abscissa, while the resulting PE values are also normalised and plotted on the ordinate. The data are normalised for each combination of cochlear geometry, array type and neural condition, by calculating the average value across the entire array and subtracting the result from that of each individual electrode contact. In each panel, blue circles represent lateral electrode contacts, red triangles represent mid-scalar contacts and green squares correspond to medial contacts; linear regression fits are plotted as black lines (panel a1: r^2=0.26, p<<0.001, panel b1: r^2=0.09, p<<0.001, panel c1: r^2=0.01, p=0.09). The bottom row of panels (a2–c2) shows the same data as in the top row, but now plotted against electrode insertion angle (measured in degrees from the round window) along the abscissa. Data in each panel is again split by array type and black lines are the linear regression fits (panel a2: r^2=0.62, panel b2: r^2=0.32, panel c2: r^2=0.50; p<<0.001 for each regression line).*

To expand on this analysis a multivariate regression was performed with the normalised PE values as response variables and with the predictor variables consisting of the normalised average I_{1mm} threshold levels of TA and TC pulses, the insertion angles, the interaction between those two variables, and an intercept term (i.e. PE ~ 1 + Angle + Mean_I_{1mm} + Angle:Mean_I_{1mm}, in Wilkinson-Rogers notation (Wilkinson and Rogers, 1973), as it is generally implemented in software packages such as MATLAB and R). Performing this multivariate regression separately for each neural condition reiterated that normalised PE was significantly negatively correlated with insertion angle ($p<<0.001$ for each neural condition). However, in contrast to the results of the simple linear regressions of figure 7.8, correlations with normalised average threshold levels were weak and non-significant for intact and short terminal neurons ($p=0.6$ and $p=0.4$, respectively), while there was a significant negative correlation for neurons without peripheral processes ($p<<0.001$). Significant but weak positive correlations were found between normalised PE and the interaction between normalised average threshold and insertion angle, but only for intact fibres and neurons without peripheral processes ($p=0.03$ and $p<<0.001$, respectively); for short terminal neurons the correlation was negative but not significant ($p=0.1$). The r^2 values of the multivariate regression fits were 0.64 for the intact neurons, 0.32 for the short terminal neurons and 0.69 for the neurons without peripheral processes.

4. Discussion

This computational modelling study was performed to test the hypothesis that polarity sensitivity of CI stimulation can be seen as an indicator of neural health. Neural responses to anodic and cathodic stimuli were simulated in a realistic model of a human cochlea implanted with an electrode array, which consisted of a volume conduction model and an active nerve fibre model. The latter was updated to better simulate the human auditory neurons by employing a new morphology and using the Schwarz-Reid-Bostock neural kinetics scheme (Schwarz et al., 1995), both of which were based on human data. Modelled stimuli consisted of monophasic, biphasic, triphasic and pseudomonophasic pulses, which were applied to lateral, mid-scalar and medial electrode contacts in five different representations of human cochlea. Neural responses were simulated for three different conditions of neural health: intact, with shortened peripheral terminal nodes and with missing peripheral processes.

The modelling of neural health was based on observations of gradual retrograde degeneration in histological studies (Kujawa and Liberman, 2009; Lin et al., 2011; Wu et al., 2019). To limit the scope of this study, only uniform degeneration (or lack thereof) was modelled and no attempt was made to implement more lifelike neural conditions, where the extent and type of degeneration varies along the cochlear duct. Furthermore, truly realistic representations of neural degeneration would not only be limited to a shortening of the peripheral processes and would include different types of degeneration or neural dysfunction that were not accounted for in this study. For instance, there are reports of demyelination of auditory neurons after hearing loss in animal studies (Tagoe et al., 2014; Wan and Corfas, 2017). A recent modelling study looked at the effects of

such axonal myelin loss and concluded that it caused changes in the polarity sensitivity of the auditory neurons (Resnick et al., 2018), which is pertinent to the present study. As another example, certain (genetic) diseases or cochlear trauma may affect the density or functioning of sodium channels in the auditory neurons (Fryatt et al., 2011; Heffner et al., 2019; Meisler et al., 2021). As a preliminary investigation, we attempted to gauge the effect of sodium channel degeneration/dysfunction by repeating a subset of our simulations with the voltage dependent sodium permeability parameter P_{Na} reduced by 50%. We found that this raised PE values for neurons with (mostly) intact peripheral processes, but that for neurons without peripheral processes the PE values were largely unaffected (data not shown); in other words, the polarity sensitivity changes due to reducing P_{Na} interacted with the effects of degeneration of the peripheral processes. This illustrates how complex it would be to rigorously model neural health, since the different types of neural degeneration/dysfunction discussed here are not mutually exclusive and any combination could have some interaction effect. So, while they were relevant to the present study, alternative types of neural degeneration were ignored here in favour of simplicity. The way neural health was represented in this study should therefore not be seen as comprehensive or lifelike, but rather as an exploration of specific extreme cases to gain insight into how polarity sensitivity can change.

4.1. Polarity dependency of the site of excitation

Model results showed that anodic pulses predominantly excited the auditory neurons in their central axons, while cathodic stimuli tended to excite them in their peripheral processes or near their cell bodies. This was in line with previous modelling work in literature (Rattay, 1999; Rattay et al., 2001a; Rattay et al., 2001b; Potrusil et al., 2020); as in those studies, the polarity-dependent site of excitation was determined by the way the model geometries shaped the electrical potential fields and by the trajectories of the modelled neurons in them. Site of excitation was therefore not an innate property of the modelled neurons, but mainly a result of spatial factors, including electrode position (i.e. both the distance from the modiolus as well as the cochlear insertion angle of the stimulating contact). Despite this, changes in lateral to medial electrode positioning did not meaningfully affect the 'targeted areas' of the two polarities, though they did affect anodic and cathodic thresholds, as well as the resulting PE.

The tendency of the two polarities to excite the auditory neurons in different locations also meant that, in general, thresholds of cathodic stimuli were more affected by neural degeneration than anodic thresholds were. As a result, changes in PE values due to neural degeneration were mostly the result of changes in cathodic thresholds. However, the effects of degeneration were inconsistent at perceptual threshold and sometimes counter intuitive. For example, simulations showed that shortening the terminal node on the peripheral processes of the auditory neurons or removing the peripheral processes altogether often lowered simulated thresholds, rather than raising them as one would expect. The explanation for this is that the terminal node and the peripheral process itself both have a capacitance that must be overcome in order to generate an action potential

at the terminal node or near the cell body, respectively. Shortening the terminal node or removing the peripheral process reduces that capacitance, which makes it easier to excite the peripheral end of the neuron (or the remainder thereof). However, this effect and its magnitude depended not only on stimulus polarity, but also on the stimulating contact's distance from the modiolus and its insertion angle.

4.2. Using multiphasic approximations of monophasic pulses

When comparing the model's results to clinical data, one should keep in mind that the model predicts that multiphasic pulses designed to approximate monophasic pulses will not generally behave exactly as true monophasic pulses. The resulting difference in obtained PE values will depend on the multiphasic pulse used; pseudomonophasic pulses with long, shallow second phases will act similarly to monophasic pulses (in figure 7.7, the simulated PE values using PSA8 and PSC8 pulses were on average only about 0.1 dB higher than those determined with MA and MC pulses), but the range of measured PE values will become increasingly narrow as the second phase becomes shorter and its amplitude higher. For triphasic pulses, PE values are consistently shifted upwards relative to monophasic pulses, by about 1.2 dB on average (figure 7.7). This is important since most recent studies have used triphasic pulses in their polarity sensitivity experiments and even a 1.2 dB shift can have a considerable effect on the number of electrode contacts that have positive or negative PE values.

At perceptual threshold (I_{1mm}), the model's average polarity sensitivity to monophasic stimuli is mostly in agreement with psychophysical data. The absolute values of model thresholds are much higher than thresholds of actual CI subjects, but this is a known problem of the type of model used in this study (Kalkman et al., 2016). Despite this, the average range of simulated PE values is similar to those found in human test subjects (Mesnildrey, 2017; Goehring et al., 2019; Jahn and Arenberg, 2019a; Mesnildrey et al., 2020), though the model leans more towards negative PE values, whereas the literature reports mostly positive PE values. However, model results are brought more in line with the psychophysical data if one considers that these studies all used triphasic pulses. For individual geometries, model simulations showed erratic changes in PE values along the electrode array (figure 7.5), comparable to psychophysical data (Mesnildrey, 2017; Carlyon et al., 2018; Goehring et al., 2019; Jahn and Arenberg, 2019a; Mesnildrey et al., 2020). Notably though, these kinds of erratic patterns are present in simulations with completely intact neurons and idealised electrode array positioning, so they arise mostly from inhomogeneities in cochlear anatomy and neural trajectories.

4.3. Polarity sensitivity at high stimulus levels

Unfortunately, simulated PE values at MCL (I_{4mm}) are much less consistent with data from literature. While findings in human subjects are inconsistent, most studies report that their human test subjects were more sensitive to high amplitude anodic stimuli than cathodic ones (Macherey et al., 2006; Macherey et al., 2008; van Wieringen et al.,

2008; Macherey et al., 2010; Undurraga et al., 2010; Carlyon et al., 2013; Undurraga et al., 2013; Carlyon et al., 2017; Hughes et al., 2018). However, the model more often shows the reverse, which cannot entirely be explained by the use of monophasic versus multiphasic stimuli, so there may be some shortcoming of either the model itself or the interpretation of its output. Both the volume conduction model and the neural model are based on well-known laws of physics, but there remains some uncertainty in the precise details and electrochemical properties of the cochlea and the auditory neurons, despite the available data in literature.

However, there is one important unknown involved in interpreting the model's data, namely the question of how loudness is coded; in both the present study as well as past ones, loudness in the model has been assumed to be linearly proportional to the number of excited neurons. This has previously led to model results that were comparable to psychophysical data, particularly when simulating loudness growth curves of multipolar current focussing strategies (Kalkman et al., 2015). Nevertheless, this is a very simplistic way to model loudness, since it ignores temporal information such as spike rate and spike timing. Furthermore, in this study only single pulse stimuli have been simulated, while experiments with real life test subjects are usually performed with pulse trains, which means that for a more thorough comparison, stochastic neural effects should also be included in the model. If there were large enough differences in stochasticity between

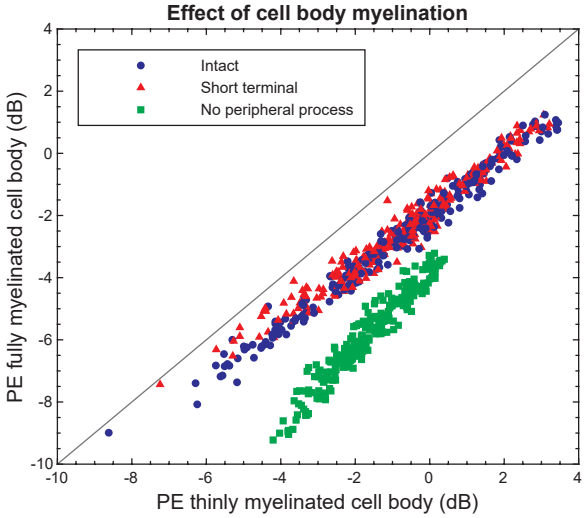

Figure 7.9. *Effect of cell body myelination on simulated polarity sensitivity of each electrode contact in all model geometries (cochleae and array types), under the three conditions of neural degeneration. The ordinate indicates PE values obtained with fully myelinated neurons, while the abscissa indicates PE values simulated using the default thinly myelinated model neurons; PE values are calculated using* I_{1mm} *as simulated perceptual threshold. Each data point represents one contact in one of the fifteen model geometries; blue circles are values obtained with intact neurons, red triangles with short terminal neurons and green squares with neurons without peripheral processes. The grey diagonal line shows where PE values of fully myelinated and thinly myelinated cell bodies would be equal to each other.*

different parts of the neurons or polarity dependent effects, then that may explain the discrepancy in high stimulus amplitude polarity sensitivity between model and clinical data. Van Gendt et al. have made steps to expand the computational model to include stochasticity and enable pulse train simulations in a practical manner (van Gendt et al., 2016; 2017; 2019), but its application lies outside the scope of the present study.

To further expand on interpreting loudness in the model, the present study found no occurrences of the kind of non-monotonic loudness growth that has been reported in psychophysical studies with quadriphasic and triphasic pulses (Macherey et al., 2017; Mesnildrey, 2017). The authors of these studies speculated that their findings may have been the result of a 'cathodal block' that was observed in physiological experiments (Ranck, 1975) and simulated in a previous modelling study (Frijns et al., 1996). A cathodal block occurs when a stimulus depolarises one node, but (nearly) simultaneously hyperpolarises another node that is located more centrally along the nerve fibre, thereby preventing the action potential from propagating. Although cathodal blocks were also observed in the present study (data not shown), they mainly happened just below the threshold levels of individual nerve fibres. In other words, the presence of a cathodal block effectively raised the thresholds of some model neurons, and once stimulus amplitude was high enough to overcome the block, the action potential would propagate along the rest of the fibre. There were rare cases of cathodal blocks occurring at higher current levels, but only for isolated fibres and within small ranges of amplitudes, which meant that they did not meaningfully affect the simulated loudness growth curves. The model is therefore currently unable to confirm the cathodal block hypothesis posed by Macherey et al. and Mesnildrey as an explanation for their findings. This could indicate that the model is not behaving realistically enough yet, but it is also possible that the explanation for non-monotonic loudness growth must be found elsewhere, for example in temporal effects such as spike timing.

4.4. Differences in polarity sensitivity between animals and humans

As mentioned in the introduction, experiments in humans have revealed different polarity sensitivity than animal experiments. Although properly investigating these differences in our model would require repeating the simulations of this study in an equivalent animal model, some preliminary insight could be gained from the present study by running additional simulations with modified neural morphologies. Since the most notable difference between the auditory neurons of humans and experimental animals is the degree of myelination of the cell bodies, the number of myelin layers around the modified neurons' cell bodies was increased from 1 to 100 (Dekker et al., 2014). In all other aspects these neurons were identical to the neurons used in the rest of this study, including being modelled in three stages of neural degeneration. The results of these simulations are compared to those of the default (human-like) model neurons in figure 7.9, which shows PE values from the modified neurons plotted along the ordinate, against the corresponding PE values from the default model neurons along the abscissa.

Adding myelin around the cell bodies of the model neurons universally decreased the PE of all model geometries, electrode contacts and neural conditions, which is apparent

from the fact that all data points in figure 7.9 are located below the diagonal. The degree to which the PE decreased was dependent on the presence of the peripheral processes; PE values from neurons without peripheral processes were lowered considerably more than those from intact neurons and neurons with shortened terminal nodes. Examining the I_{1mm} levels of the anodic and cathodic monophasic pulses individually revealed that adding myelin around the cell bodies increased the threshold levels of anodic pulses and decreased those of cathodic pulses; both effects therefore contributed to the decrease in PE values.

These results suggest that differences in the degree of myelination around the cell bodies of the auditory neurons are an important factor underlying the differences in polarity sensitivity between humans and animals. Similar observations were made recently by Potrusil et al. (Potrusil et al., 2020), though they did not observe a change in anodic thresholds. Additionally, they only varied the amount of cell body myelination of neurons without peripheral processes, while results of the present study indicate that this effect occurs with healthy neurons and neurons with shortened peripheral terminal nodes as well, though the changes in PE values were more severe when peripheral processes were missing entirely.

It should be reiterated that these are inconclusive findings, as there are significant differences between animals and humans that have not been accounted for (chiefly cochlear anatomy, precise neural morphology and neural kinetics), so they should be the subject of future research (cf. Frijns et al., 2001).

4.5. The neural health hypothesis

The results of this study cast doubt on the neural health hypothesis, which is exemplified by the fact that neural degeneration in the model had counter-intuitive and often inconsistent effects. The electrode array's distance from the modiolus greatly affected the direction in which the simulated PE changed when comparing different states of neural health (though not at higher stimulus levels). Furthermore, in the most extreme case of neural degeneration included in this study, the model average PE values were universally negative, which meant that cathodic thresholds were lower than those of anodic pulses. This is the opposite of what would be expected based on the neural health hypothesis, which assumes that loss of peripheral processes would make anodic stimulation more favourable and thus lead to positive PE values. The important observation here is that, for the average lateral and mid-scalar electrode arrays, severe neural degeneration tended to decrease PE rather than increase it, while for the average medial array neural degeneration did increase PE at threshold, but never to positive values. Although again, using triphasic stimuli instead of true monophasic pulses produced higher PE values (on average 1.2 dB) than the model averages shown in the error bars along the axes in figure 7.6. This was a large enough shift to lead to positive PE values in a number of cases, particularly in the most basal half turn of the cochlea, so it provides at least a partial explanation for why model PE values tended to be lower than those found in psychophysical studies.

As stated above, erratic changes in PE values along electrode arrays could be seen in simulations involving completely intact neurons, meaning that similar patterns found in psychophysical studies may not necessarily arise from localised neural degeneration, also known as dead regions. Similarly, results from a psychophysical study by Carlyon et al. (2018) were replicated while simulating healthy neurons (figure 7.8a1). Carlyon et al. found a significant positive correlation between normalised PE values and normalised average threshold of anodic and cathodic stimuli, which, at first glance, seemed consistent with the idea that absence of the peripheral processes would increase the cathodic thresholds but not the anodic ones, which would increase their combined average as well as their resulting PE value. However, the present study complicates that interpretation, as it shows that this correlation can also arise from cochleae with completely healthy neurons. Moreover, figure 7.8b1 and c1 show that in the model the correlation disappears when neural degeneration becomes more severe.

Plotting the same data from our model against insertion angle, rather than normalised average thresholds, revealed that the normalised PE was negatively correlated with the insertion angle of the stimulating contact, regardless of array type or neural degeneration (figure 7.8a2–c2). The same could also be seen for non-normalised model average PE values, in which both the thresholds and the PE trended downwards for more deeply inserted electrode contacts. Subsequent multivariate regression analysis of the normalised PE values reinforced the observation that normalised PE mainly correlates with electrode contact insertion angle. The effect of normalised average thresholds (the mean of the I_{1mm} levels of TA and TC pulses) on normalised PE values is less clear; it likely interacts with the insertion angle and only showed a negative significant correlation when all peripheral processes were removed.

Though Carlyon et al. reported a significant decrease in anodic and cathodic thresholds from base to apex, they did not find a significant decrease in PE values for more deeply inserted contacts. It should be noted, however, that they only looked at electrode numbers and not cochlear insertion angles; there is considerable variability in the cochlear insertion angles of a given contact number between users of the same device due to anatomical differences and surgical techniques (van der Marel et al., 2014; 2016), so it is unclear if a correlation would have emerged if insertion angle had been taken into account. Other studies have not explicitly reported on the relationship between PE and electrode contact insertion angle, though gauging from their plotted data, there does not seem to be a universal downwards trend (Mesnildrey, 2017; Goehring et al., 2019; Jahn and Arenberg, 2019a; Mesnildrey et al., 2020). However, in real-life subjects neither neural degeneration nor electrode array position would be as uniform or idealised as represented in the model; this means that the downwards trend in PE values from base to apex could be obscured in cases where the type and degree of neural degeneration varies along the cochlea, or where the array's distance from the modiolus is inconsistent, as it would make the change in PE value along the array even more erratic.

Regarding lateral to medial positioning of the electrode array, several studies also included estimations of the electrode-to-modiolus distance (EMD) based on CT scans (Mesnildrey,

2017; Jahn and Arenberg, 2019a; Mesnildrey et al., 2020) and found significant correlations between perceptual thresholds and (normalised) EMD, which is consistent with the findings of this study. Mesnildrey (2017) found a significant correlation between normalised EMD and PE, but this finding was not replicated in the other studies. However, Mesnildrey et al. (2020) did conclude that EMD and PE were both contributing factors to variance in measured thresholds. This is also consistent with the results of this study, though to reiterate, the model implies that electrode contact insertion angle is also an important factor. Due to the scala tympani becoming narrower towards the apex, the EMD will generally decrease with increasing insertion angle, so ideally, they should both be accounted for. A more thorough analysis of clinically obtained PE measurements, EMD's and their relation to electrode insertion angles might be able to confirm the model's findings, but currently these predictions cannot be directly compared to literature.

Finally, although the model results imply that the state of the neurons cannot reliably be deduced from measuring the PE on a single contact, especially when important spatial factors such as electrode insertion depth and distance from the modiolus are unknown, it must be noted that there were statistical differences between the modelled neural conditions when looking at the combined data from all electrode contacts across all model geometries. In figures 7.6 and 7.8 there are notable differences between averages and ranges/standard deviations of (normalised) PE values between different neural conditions, so it may be possible to observe similar statistical differences between groups of CI subjects with comparable states of neural health.

4.6. Conclusions

The main conclusion of this study is that polarity sensitivity was not a reliable measure of neural health. While neural degeneration did affect simulated polarity sensitivity, its effect was not consistent; polarity sensitivity was not simply a product of the state of the neurons, but also depended on spatial factors (particularly array type and electrode contact insertion angle). Moreover, these spatial factors are at best poorly quantifiable in imaging methods available today, so in light of this study's findings, it seems difficult or impossible to determine with certainty what the underlying reasons for clinically measured polarity sensitivity data are. However, the results do suggest that there may be statistical differences between groups of subjects/electrodes with similar types and degrees of neural damage, but estimating neural health from the polarity sensitivity of an individual electrode contact seems unfeasible.

Additionally, the other notable findings of this study are:

(I) In agreement with previous studies, anodic pulses mostly excited auditory neurons in their central axons, while cathodic stimuli generally excited neurons in their peripheral processes or near their cell bodies.

(II) As a consequence, cathodic thresholds were generally more affected by neural degeneration than anodic thresholds were.

(III) Measuring polarity sensitivity using charge-balanced multiphasic pulses as approximations of monophasic stimuli produced different results than those obtained with true monophasic pulses. The degree to which this occurred depended on the specific pulse shape, but in general the lower the amplitudes of the charge balancing phases were, the closer the polarity sensitivity was to that of true monophasic pulses.

(IV) Differences in polarity sensitivity between humans and animal can be explained by differences in the amount of myelin around the cell bodies of the auditory neurons. Increasing the number of myelin wraps around the cell bodies of human neurons increased sensitivity to cathodic pulses while decreasing anodic sensitivity.

Acknowledgements

This study was financially supported by the Heinsius-Houbolt Fund.

References

Bachmaier, R., Encke, J., Obando-Leiton, M., Hemmert, W., Bai, S. 2019. Comparison of Multi-Compartment Cable Models of Human Auditory Nerve Fibers. Front Neurosci 13, 1173.

Berthold, C.H. 1978. Morphology of normal peripheral axons. In: Waxman, S.G., (Ed.), Physiology and pathobiology of axons, New York. pp. 3-63.

Berthold, C.H., Rydmark, M. 1983. Electrophysiology and morphology of myelinated nerve fibers. VI. Anatomy of the paranode-node-paranode region in the cat. Experientia 39, 964-76.

Briaire, J.J., Frijns, J.H. 2000a. Field patterns in a 3D tapered spiral model of the electrically stimulated cochlea. Hear Res 148, 18-30.

Briaire, J.J., Frijns, J.H. 2005. Unraveling the electrically evoked compound action potential. Hear Res 205, 143-56.

Briaire, J.J., Frijns, J.H. 2006. The consequences of neural degeneration regarding optimal cochlear implant position in scala tympani: a model approach. Hear Res 214, 17-27.

Briaire, J.J., Frijns, J.H.M. 2000b. 3D mesh generation to solve the electrical volume conduction problem in the implanted inner ear. Simulat Pract Theory 8, 57-73.

Brummer, S.B., Robblee, L.S., Hambrecht, F.T. 1983. Criteria for selecting electrodes for electrical stimulation: theoretical and practical considerations. Ann N Y Acad Sci 405, 159-71.

Carlyon, R.P., Cosentino, S., Deeks, J.M., Parkinson, W., Arenberg, J.G. 2018. Effect of Stimulus Polarity on Detection Thresholds in Cochlear Implant Users: Relationships with Average Threshold, Gap Detection, and Rate Discrimination. J Assoc Res Otolaryngol 19, 559-567.

Carlyon, R.P., Deeks, J.M., Macherey, O. 2013. Polarity effects on place pitch and loudness for three cochlear-implant designs and at different cochlear sites. J Acoust Soc Am 134, 503-9.

Carlyon, R.P., Deeks, J.M., Undurraga, J., Macherey, O., van Wieringen, A. 2017. Spatial Selectivity in Cochlear Implants: Effects of Asymmetric Waveforms and Development of a Single-Point Measure. J Assoc Res Otolaryngol 18, 711-727.

Colombo, J., Parkins, C.W. 1987. A model of electrical excitation of the mammalian auditory-nerve neuron. Hear Res 31, 287-311.

Dekker, D.M., Briaire, J.J., Frijns, J.H. 2014. The impact of internodal segmentation in biophysical nerve fiber models. J Comput Neurosci 37, 307-15.

Donaldson, N.D., Donaldson, P.E. 1986. When are actively balanced biphasic ('Lilly') stimulating pulses necessary in a neurological prosthesis? I. Historical background; Pt resting potential; Q studies. Med Biol Eng Comput 24, 41-9.

Frankenhaeuser, B., Huxley, A.F. 1964. The Action Potential in the Myelinated Nerve Fiber of Xenopus Laevis as Computed on the Basis of Voltage Clamp Data. J Physiol 171, 302-15.

Frijns, J.H., Briaire, J.J., Grote, J.J. 2001. The importance of human cochlear anatomy for the results of modiolus-hugging multichannel cochlear implants. Otol Neurotol 22, 340-9.

Frijns, J.H., de Snoo, S.L., Schoonhoven, R. 1995. Potential distributions and neural excitation patterns in a rotationally symmetric model of the electrically stimulated cochlea. Hear Res 87, 170-86.

Frijns, J.H., de Snoo, S.L., Schoonhoven, R. 2000. Improving the accuracy of the boundary element method by the use of second-order interpolation functions. IEEE Trans Biomed Eng 47, 1336-46.

Frijns, J.H., de Snoo, S.L., ten Kate, J.H. 1996. Spatial selectivity in a rotationally symmetric model of the electrically stimulated cochlea. Hear Res 95, 33-48.

Frijns, J.H., Dekker, D.M., Briaire, J.J. 2011. Neural excitation patterns induced by phased-array stimulation in the implanted human cochlea. Acta Otolaryngol 131, 362-70.

Frijns, J.H., Kalkman, R.K., Briaire, J.J. 2009a. Stimulation of the facial nerve by intracochlear electrodes in otosclerosis: a computer modeling study. Otol Neurotol 30, 1168-74.

Frijns, J.H., Kalkman, R.K., Vanpoucke, F.J., Bongers, J.S., Briaire, J.J. 2009b. Simultaneous and non-simultaneous dual electrode stimulation in cochlear implants: evidence for two neural response modalities. Acta Otolaryngol 129, 433-9.

Fryatt, A.G., Mulheran, M., Egerton, J., Gunthorpe, M.J., Grubb, B.D. 2011. Ototrauma induces sodium channel plasticity in auditory afferent neurons. Mol Cell Neurosci 48, 51-61.

Goehring, T., Archer-Boyd, A., Deeks, J.M., Arenberg, J.G., Carlyon, R.P. 2019. A Site-Selection Strategy Based on Polarity Sensitivity for Cochlear Implants: Effects on Spectro-Temporal Resolution and Speech Perception. J Assoc Res Otolaryngol 20, 431-448.

Hanekom, T. 2001. Three-dimensional spiraling finite element model of the electrically stimulated cochlea. Ear Hear 22, 300-15.

Heffner, R.S., Koay, G., Heffner, H.E. 2019. Normal audiogram but poor sensitivity to brief sounds in mice with compromised voltage-gated sodium channels (Scn8a(medJ)). Hear Res 374, 1-4.

Hughes, M.L., Choi, S., Glickman, E. 2018. What can stimulus polarity and interphase gap tell us about auditory nerve function in cochlear-implant recipients? Hear Res 359, 50-63.

Jahn, K.N., Arenberg, J.G. 2019a. Evaluating Psychophysical Polarity Sensitivity as an Indirect Estimate of Neural Status in Cochlear Implant Listeners. J Assoc Res Otolaryngol 20, 415-430.

Jahn, K.N., Arenberg, J.G. 2019b. Polarity Sensitivity in Pediatric and Adult Cochlear Implant Listeners. Trends Hear 23, 2331216519862987.

Kalkman, R.K., Briaire, J.J., Dekker, D.M.T., Frijns, J.H.M. 2014. Place pitch versus electrode location in a realistic computational model of the implanted human cochlea. Hear. Res 315, 10-24.

Kalkman, R.K., Briaire, J.J., Frijns, J.H. 2015. Current focussing in cochlear implants: an analysis of neural recruitment in a computational model. Hear. Res 322, 89-98.

Kalkman, R.K., Briaire, J.J., Frijns, J.H. 2016. Stimulation strategies and electrode design in computational models of the electrically stimulated cochlea: An overview of existing literature. Network 27, 107-134.

Kujawa, S.G., Liberman, M.C. 2009. Adding insult to injury: cochlear nerve degeneration after "temporary" noise-induced hearing loss. J Neurosci 29, 14077-85.

Lin, H.W., Furman, A.C., Kujawa, S.G., Liberman, M.C. 2011. Primary neural degeneration in the Guinea pig cochlea after reversible noise-induced threshold shift. J Assoc Res Otolaryngol 12, 605-16.

Loizou, P.C. 2006. Speech processing in vocoder-centric cochlear implants. Adv Otorhinolaryngol 64, 109-143.

Macherey, O., Carlyon, R.P., Chatron, J., Roman, S. 2017. Effect of Pulse Polarity on Thresholds and on Non-monotonic Loudness Growth in Cochlear Implant Users. J Assoc Res Otolaryngol 18, 513-527.

Macherey, O., Carlyon, R.P., van Wieringen, A., Deeks, J.M., Wouters, J. 2008. Higher sensitivity of human auditory nerve fibers to positive electrical currents. J Assoc Res Otolaryngol 9, 241-51.

Macherey, O., Cazals, Y. 2016. Effects of Pulse Shape and Polarity on Sensitivity to Cochlear Implant Stimulation: A Chronic Study in Guinea Pigs. Adv Exp Med Biol 894, 133-142.

Macherey, O., van Wieringen, A., Carlyon, R.P., Deeks, J.M., Wouters, J. 2006. Asymmetric pulses in cochlear implants: effects of pulse shape, polarity, and rate. J Assoc Res Otolaryngol 7, 253-66.

Macherey, O., van Wieringen, A., Carlyon, R.P., Dhooge, I., Wouters, J. 2010. Forward-masking patterns produced by symmetric and asymmetric pulse shapes in electric hearing. J Acoust Soc Am 127, 326-38.

Meisler, M.H., Hill, S.F., Yu, W. 2021. Sodium channelopathies in neurodevelopmental disorders. Nat Rev Neurosci 22, 152-166.

Mesnildrey, Q. 2017. Towards a Better Understanding of the Cochlear Implant - Auditory Nerve Interface: from intracochlear electrical recordings to psychophysics, Aix-Marseille Universite.

Mesnildrey, Q., Venail, F., Carlyon, R.P., Macherey, O. 2020. Polarity Sensitivity as a Potential Correlate of Neural Degeneration in Cochlear Implant Users. J Assoc Res Otolaryngol 21, 89-104.

Miller, C.A., Abbas, P.J., Robinson, B.K., Rubinstein, J.T., Matsuoka, A.J. 1999. Electrically evoked single-fiber action potentials from cat: responses to monopolar, monophasic stimulation. Hear Res 130, 197-218.

Potrusil, T., Heshmat, A., Sajedi, S., Wenger, C., Chacko, L.J., Glueckert, R., Schrott-Fischer, A., Rattay, F. 2020. Finite element analysis and three-dimensional reconstruction of tonotopically aligned human auditory fiber pathways: A computational environment for modeling electrical stimulation by a cochlear implant based on micro-CT. Hear Res 393, 108001.

Ranck, J.B., Jr. 1975. Which elements are excited in electrical stimulation of mammalian central nervous system: a review. Brain Res 98, 417-40.

Rattay, F. 1999. The basic mechanism for the electrical stimulation of the nervous system. Neuroscience 89, 335-46.

Rattay, F., Leao, R.N., Felix, H. 2001a. A model of the electrically excited human cochlear neuron. II. Influence of the three-dimensional cochlear structure on neural excitability. Hear Res 153, 64-79.

Rattay, F., Lutter, P., Felix, H. 2001b. A model of the electrically excited human cochlear neuron. I. Contribution of neural substructures to the generation and propagation of spikes. Hear Res 153, 43-63.

Resnick, J.M., O'Brien, G.E., Rubinstein, J.T. 2018. Simulated auditory nerve axon demyelination alters sensitivity and response timing to extracellular stimulation. Hear Res 361, 121-137.

Schwarz, J.R., Reid, G., Bostock, H. 1995. Action potentials and membrane currents in the human node of Ranvier. Pflugers. Arch 430, 283-292.

Smit, J.E., Hanekom, T., van Wieringen, A., Wouters, J., Hanekom, J.J. 2010. Threshold predictions of different pulse shapes using a human auditory nerve fibre model containing persistent sodium and slow potassium currents. Hear Res 269, 12-22.

Snel-Bongers, J., Briaire, J.J., van der Veen, E.H., Kalkman, R.K., Frijns, J.H. 2013. Threshold levels of dual electrode stimulation in cochlear implants. J Assoc Res Otolaryngol 14, 781-90.

Spoendlin, H., Schrott, A. 1989. Analysis of the human auditory nerve. Hear Res 43, 25-38.

Stakhovskaya, O., Sridhar, D., Bonham, B.H., Leake, P.A. 2007. Frequency map for the human cochlear spiral ganglion: implications for cochlear implants. J. Assoc. Res. Otolaryngol 8, 220-233.

Tagoe, T., Barker, M., Jones, A., Allcock, N., Hamann, M. 2014. Auditory nerve perinodal dysmyelination in noise-induced hearing loss. J Neurosci 34, 2684-8.

Undurraga, J.A., Carlyon, R.P., Wouters, J., van Wieringen, A. 2013. The polarity sensitivity of the electrically stimulated human auditory nerve measured at the level of the brainstem. J Assoc Res Otolaryngol 14, 359-77.

Undurraga, J.A., van Wieringen, A., Carlyon, R.P., Macherey, O., Wouters, J. 2010. Polarity effects on neural responses of the electrically stimulated auditory nerve at different cochlear sites. Hear Res 269, 146-61.

van der Marel, K.S., Briaire, J.J., Wolterbeek, R., Snel-Bongers, J., Verbist, B.M., Frijns, J.H. 2014. Diversity in cochlear morphology and its influence on cochlear implant electrode position. Ear Hear 35, e9-20.

van der Marel, K.S., Briaire, J.J., Wolterbeek, R., Verbist, B.M., Frijns, J.H. 2016. Development of Insertion Models Predicting Cochlear Implant Electrode Position. Ear Hear 37, 473-82.

van Gendt, M.J., Briaire, J.J., Frijns, J.H.M. 2019. Effect of neural adaptation and degeneration on pulse-train ECAPs: A model study. Hear Res 377, 167-178.

van Gendt, M.J., Briaire, J.J., Kalkman, R.K., Frijns, J.H.M. 2016. A fast, stochastic, and adaptive model of auditory nerve responses to cochlear implant stimulation. Hear Res 341, 130-143.

van Gendt, M.J., Briaire, J.J., Kalkman, R.K., Frijns, J.H.M. 2017. Modeled auditory nerve responses to amplitude modulated cochlear implant stimulation. Hear Res 351, 19-33.

van Wieringen, A., Carlyon, R.P., Laneau, J., Wouters, J. 2005. Effects of waveform shape on human sensitivity to electrical stimulation of the inner ear. Hear Res 200, 73-86.

van Wieringen, A., Macherey, O., Carlyon, R.P., Deeks, J.M., Wouters, J. 2008. Alternative pulse shapes in electrical hearing. Hear Res 242, 154-63.

Verbist, B.M., Skinner, M.W., Cohen, L.T., Leake, P.A., James, C., Boex, C., Holden, T.A., Finley, C.C., Roland, P.S., Roland, J.T., Jr., Haller, M., Patrick, J.F., Jolly, C.N., Faltys, M.A., Briaire, J.J., Frijns, J.H. 2010. Consensus panel on a cochlear coordinate system applicable in histologic, physiologic, and radiologic studies of the human cochlea. Otol Neurotol 31, 722-30.

Wan, G.Q., Corfas, G. 2017. Transient auditory nerve demyelination as a new mechanism for hidden hearing loss. Nat Commun 8.

Westen, A.A., Dekker, D.M., Briaire, J.J., Frijns, J.H. 2011. Stimulus level effects on neural excitation and eCAP amplitude. Hear Res 280, 166-76.

Wilkinson, G.N., Rogers, C.E. 1973. Symbolic Description of Factorial Models for Analysis of Variance. Roy Stat Soc C-App 22, 392-399.

Wu, P.Z., Liberman, L.D., Bennett, K., de Gruttola, V., O'Malley, J.T., Liberman, M.C. 2019. Primary Neural Degeneration in the Human Cochlea: Evidence for Hidden Hearing Loss in the Aging Ear. Neuroscience 407, 8-20.

Chapter 8

General discussion

This thesis presents a historical review of computational cochlear implant models (chapter 2) and five studies on cochlear implant functioning (chapters 3 through 7), which used a computational model originally developed by Johan H.M. Frijns (Frijns, 1995) and Jeroen J. Briaire (Briaire, 2008). The model was expanded and updated for each study, which covered a wide variety of aspects and applications of cochlear implant stimulation. The general goal of these studies was to make the model more realistic in ways that could be validated and would lead to clinically relevant insights and predictions.

Place pitch estimation

In chapter 3, nerve fibre trajectories in the model were updated from purely radial to realistically oblique ones. In addition, the conductivity value for temporal bone was adjusted based on available intrascalar potential recording from human CI subjects. The updated model was used to predict place pitch percepts in CI users and to derive clinically useful tonotopic maps that predicted place pitch as a function of cochlear angle. Results showed that pitch percepts from electrode contacts in the basal turn of the cochlea followed the Greenwood function (Greenwood, 1990), but that for contacts located more deeply in the cochlea they occurred in ranges loosely bounded by tonotopic maps that were based on stimulation at either the organ of Corti (OC) or spiral ganglion (SG). The range of pitch percepts was especially large in the apex of the cochlea (deeper than 540° from the round window).

The updated trajectory of the modelled nerve fibres relied heavily on the data from Stakhovskaya et al. (Stakhovskaya et al., 2007). Recently, Helpard et al. published an imaging study of human cochleae which used a combination of synchrotron radiation phase-contrast imaging and computed tomography (Helpard et al., 2021). In their data they were able to trace the trajectories of cochlear nerves and apply the Greenwood function to derive relationships between tonotopic frequencies and cochlear angle for the OC as well as the SG, equivalently to Stakhovskaya's study. The OC-based relationship between cochlear angle and tonotopic frequency that they present is similar to the one from Stakhovskaya et al. and the one derived in chapter 3 of this thesis, but the SG-based angular tonotopic maps are noticeably different from each other when compared directly (figure 8.1). This can be illustrated by looking at the termination angles of the SG that each function implies: in Stakhovskaya's function the SG frequency-position function reaches 20 Hz (the lower frequency limit of human hearing according to the Greenwood function) around 740° from the round window, whereas the function from Helpard et al. reaches that value around 900°, which is a considerable angular difference. Furthermore, in the Leiden CI model the terminal angle of the SG is set at 630°, a far lower value than either of these functions.

It should be noted here that the SG terminal angle in the Leiden CI model was not derived from the histological slices or radiological images that the model geometries were based on, but was set manually to a fixed value that was consistent with the available literature at the time. Since this value now lies below the range demonstrated by Stakhovskaya et al. and Helpard et al., this suggests that the SG is too short in the model. However, there

are some mitigating points to make: first, there appears to be a discrepancy between the terminal angles implied by the place pitch functions and the angular lengths of the SG reported in their corresponding publications. Stakhovskaya et al. reported terminal angles between 630° and 720° in their specimens, while Helpard et al. stated a mean angular length of 720° for the SG. In other words, these place pitch functions do not accurately represent the average terminal angles of the SG from their respective data sets, since these angles were much lower in the analysed specimens than in the resulting place pitch functions; presumably this is an artefact of the fitting methods used by their authors.

Next, fibre trajectories in the model were based on Stakhovskaya et al.'s relationship between points along the lengths of the OC and the SG, rather than the angular data they reported, so the focus was on ensuring that our modelled lengths of both the SG and OC as well as their ratios were in line with Stakhovskaya et al.'s findings. However, as also mentioned in the discussion section of chapter 3, changing the terminal angle of the SG does relatively little to change its total length. This is related to the more important issue at play here, which is that the terminal angle of the SG is inherently ill-defined due to the fact that the apical end of the SG is located in an area of the modiolus where the rotational axis of the cochlear coordinate system is placed. There is no strict objective definition for this axis, meaning that its position and orientation are arbitrary, to a certain degree, which affects measurements derived from the coordinate system, such as the vertical slope profile of the cochlea (Demarcy et al., 2017). Since the rotational axis passes right by or even straight through the apical end of the SG, moving or tilting the axis even

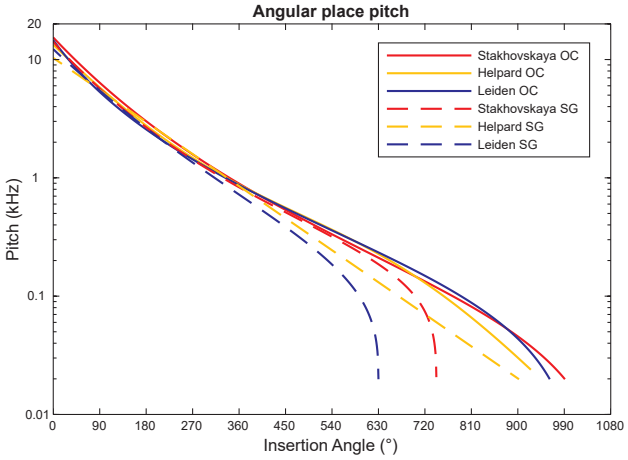

Figure 8.1. *Angular place pitch functions derived by Stakhovskaya et al. (2007), Helpard et al. (2021) and the Leiden model (equations 2 and 9 from chapter 3). The abscissa indicates position along the OC or SG, given by the cochlear angle as measured in degrees from the round window (Verbist et al., 2010); the characteristic place pitch at that cochlear angle is plotted along the ordinate, in kHz. The OC-based place pitch functions are plotted as solid lines, while the dashed lines represent the SG-based ones. Curves from Stakhovskaya et al. are plotted in red, those from Helpard et al. are plotted in yellow and the blue curves indicate the place pitch functions from the Leiden model. Note: the OC-based function from Helpard et al. has a parameter for the number of cochlear turns; this has been set to 2.57 turns (≈925°), which was the mean OC angular length they reported.*

slightly could conceivably change the terminal angle of the SG by as much as 180° in either direction. In this light, describing the SG-based tonotopic frequency at the apical end of the cochlea as a function of cochlear angle becomes questionable and potentially misleading, as different choices surrounding the placement of the rotational coordinate axis could have drastically changed the SG-based tonotopic frequency associated with a given apical cochlear angle, which in turn would have resulted in a very different angular tonotopic map in the cochlear apex. Therefore, the SG-based angular tonotopic maps suggest a clear and precise relationship between place pitch and cochlear angle that does not exist in any practical/objective sense for the apical end of the SG. Nonetheless, the frequency-position data from Helpard et al. has provided a new pair of tonotopic maps of the human cochlea for researchers to take into consideration (though of course they are ultimately still founded on the Greenwood map), with the caveat that in the apex of the cochlea, any SG-based angular tonotopic map should be looked at with a critical eye.

On the psychophysical front, there have been multiple studies that investigated place pitch perception in cochlear implant listeners since the study presented in chapter 3 was published. Recently published studies of pitch-matching experiments show inconsistent outcomes, often with pitch estimates that do not fall in the ranges expected from organ of Corti and spiral ganglion based place pitch functions (Plant et al., 2014; Vermeire et al., 2015; Peters et al., 2016; Adel et al., 2019; Marozeau et al., 2020). These diverging results can be explained by the fact that acoustically and electrically evoked sound percepts are fundamentally different and therefore difficult to compare to one another. In addition, changing the place of excitation does not only raise or lower pitch, but can also change other aspects of the perceived sound, such as its loudness and character (e.g., beeping or noisy sound), which complicates pitch-matching experiments (Adel et al., 2019; Marozeau et al., 2020). Furthermore, it is known that CI subjects adapt to mismatched frequency allocations over time, meaning that the pitch they perceive from a CI stimulus no longer corresponds to initial/expected place pitch relationships (Reiss et al., 2015; Svirsky et al., 2015).

These inconsistent results make it difficult to determine whether the model's predictions on pitch perception are accurate or not. However, it should be reiterated that in a study published by Carlyon et al., model results were generally in good agreement with psychophysical testing and were not only able identify that an electrode migration had occurred in one subject, but also accurately predicted the distance of that migration (Carlyon et al., 2010). It is likely that the wide range of results in psychophysics are due to the difficult nature of performing pitch-matching experiments with CI users and are not necessarily indicative of some inherently unpredictable or not yet understood mechanism of pitch perception. Nevertheless, if researchers want to make strides in pitch-matching CI speech coding programs to acoustic hearing, then more clarity is needed from psychophysical data. Tempering expectations on this subject somewhat, there is evidence that suggests that even though initial speech perception can be improved by minimizing the mismatch between tonotopic frequencies and the filter frequencies of CI subjects' speech coding programs, there may not actually be any significant long-term benefit of doing so (Mertens et al., 2022).

Facial nerve stimulation

Chapter 4 concerns a study of the effects of otosclerosis on facial nerve stimulation, which was accomplished by adding a representation of the facial nerve to the model and simulating the advancement of otosclerosis by varying the conductivity of the temporal bone surrounding the cochlea. The main conclusion was that otosclerosis increased the likelihood of facial nerve stimulation, mainly by raising auditory maximum comfortable loudness level (MCL) relative to the threshold of stimulation for the facial nerve. The study also corroborated the clinical impression that peri-modiolar electrode arrays with modiolus-facing contacts less easily cause facial nerve stimulation than arrays positioned along the lateral wall, or electrode arrays with banded contacts.

Clinical reports have confirmed that otosclerosis increases the risk of facial nerve stimulation below auditory MCL (Claussen and Gantz, 2022), so there is continued clinical interest both in investigating the effects of otosclerosis as well as facial nerve stimulation in general. Recently, the Hanekom-group at the University of Pretoria used their model to perform a similar study of facial nerve stimulation to the one presented in chapter 4 (Badenhorst et al., 2021). They added facial nerves to patient-specific cochlear geometries and varied the conductivity/resistivity of the bone surrounding the cochlea, as well as modelled ossification of the cochlear ducts and degeneration of the peripheral processes of the auditory nerve fibres. When modelling limited ossification, their results were comparable to the ones from the Leiden model. However, they also found that increased ossification in combination with lowered overall bone resistivity had an aggravating effect on thresholds and made facial nerve stimulation more likely. In a separate study, they investigated the possibility of reducing facial nerve stimulation by using the most apical contact of the CI's electrode array as the reference electrode (van der Westhuizen et al., 2022). In their model they found that using the apical reference electrode raised thresholds for facial nerve stimulation and lowered auditory thresholds; these results were then corroborated by psychophysical thresholds and EMG recordings of two test subjects, which not only validated the model's results, but also revealed another option for mitigating facial nerve stimulation.

Since the publication of the facial nerve/otosclerosis study of chapter 4, collaboration with the University of Würzburg has led to new insights into the mechanisms of facial nerve stimulation. Electrophysiological experiments by Bahmer et al. showed that facial nerve stimulation can be reduced by stimulating with cathodic-leading triphasic pulses, rather than symmetric biphasic pulses or anodic-first triphasic pulses (Bahmer and Baumann, 2016; Bahmer et al., 2017). Following this, an updated version of the model presented in chapter 4 of this thesis was used to simulate stimulation using monophasic, biphasic and triphasic pulses, which revealed that the modelled facial nerve was strongly sensitive to stimulus polarity, with cathodic pulses having a much lower threshold for facial nerve stimulation than anodic pulses (Herrmann et al., 2019). The consequence of this was that a cathodic-first triphasic pulse would become less effective at stimulating the facial nerve relative to an equivalent biphasic or anodic-first triphasic pulse, due the fact that the cathodic phase was split into two weaker phases, separated by a stronger anodic phase,

thereby raising the threshold for facial nerve stimulation.

All of this makes it clear that the issue of facial nerve stimulation remains of clinical interest and that computational models have a continued role to play in understanding the phenomenon and finding effective ways to deal with it.

Dual electrode stimulation

The focus of chapter 5 was to examine the effectiveness and underlying mechanisms of dual electrode stimulation in the model. The model showed that dual electrode stimulation can either produce a gradually shifting region of excitation or they create two more distinct (though possibly overlapping) regions of excitation that alternate in size and lead to a non-linearly shifting centre of excitation. Simultaneous dual electrode stimulation at higher stimulus levels in the basal turn tended to produce a gradually shifting percept, while sequential stimulation, contacts beyond the basal turn or lower stimulus levels were much more likely to produce a non-linearly shifting percept. Results also showed that sequential dual electrode stimulation and stimulation at lower stimulus levels generally demanded additional current to correct for drops in loudness, while loudness stayed relatively constant for simultaneous dual electrode stimulation at higher levels.

Not long after this study was published, the model was used to supplement the findings of psychophysical experiments done at Leiden University Medical Centre for the PhD thesis of Dr Snel-Bongers (Snel-Bongers, 2013). In one of their psychophysical studies, Snel-Bongers et al. performed loudness balancing experiments using current steered stimuli (i.e., simultaneous dual electrode stimuli) at perceptual threshold, for different values of the steering parameter α (Snel-Bongers et al., 2013). They discovered that in some subjects, the amount of current needed to maintain equal loudness decreased around α=0.5, thereby creating a dip in the corresponding plots of stimulus current versus α. The model was able to reproduce a similar dip by assuming that perceptual threshold corresponded to stimulation of a small group of neurons, rather than a single nerve fibre, as well as modelling these neurons with peripheral processes that had shortened unmyelinated terminal nodes. This result also formed the basis for the 1 mm excitation width criterium for simulated perceptual threshold used in chapters 3, 6 and 7 of this thesis.

Subsequent studies from other groups have reaffirmed that simultaneous or sequential dual electrode stimulation can indeed invoke intermediate pitch percepts in CI listeners (Landsberger and Galvin, 2011; Goehring et al., 2014a; b; Padilla et al., 2017). Despite this, it has since been shown that the Fidelity120 speech coding strategy, which uses current steered pulses, does not demonstrably improve speech understanding (Donaldson et al., 2011; Buchner et al., 2012; Langner et al., 2017). However, stimulating with two electrode contacts simultaneously does reduce power consumption compared to conventional monopolar stimulation (Langner et al., 2017), which is clinically quite useful. Expanding on this, Nogueira et al. used their computational cochlear implant model to simulate modified current steered pulses with additional positive or negative current on the contacts flanking

the current steered pair (Nogueira et al., 2017). Model results showed that same polarity current on the flanking contacts lowered power consumption, which was confirmed in subsequent psychophysical experiments.

On a related note, an alternative method for shifting the region of excitation/pitch percept has been proposed in the form of so-called phantom electrode stimulation (Saoji and Litvak, 2010). Like in current steering, phantom electrodes manipulate the electric field by stimulating two contacts simultaneously, but the main difference is that the phantom electrode contacts are stimulated with opposite polarity, rather than same polarity. The other technical difference is that the current is not 'shunted' back and forth between the contacts, but rather the amplitude of one contact (considered the main contact) is set at a given level, while a fraction of that current (given by parameter σ) is presented in opposite polarity on a compensating contact; as such, phantom electrode stimulation can also be described as partial bipolar stimulation. The idea behind this form of stimulation is that the opposite polarity stimulus from the compensating contact counteracts one side of the electrical field generated by the main contact, causing that field to become more asymmetric and having its 'centre' shift away from the electrode pair. In principle this should allow a CI to stimulate neural populations that are slightly out of reach with monopolar stimulation, if the phantom electrode pair is chosen at the very end of the electrode array.

Studies have demonstrated that phantom stimulation is indeed capable of shifting pitch percepts away from the stimulating contacts (Saoji and Litvak, 2010; Macherey et al., 2011; Macherey and Carlyon, 2012; Saoji et al., 2013; Klawitter et al., 2018; Saoji et al., 2018; de Jong et al., 2020; Lamping et al., 2020). Psychophysical experiments by Snel-Bongers et al. also confirmed this pitch shift and compared their results to simulations from the Leiden CI model (Snel-Bongers, 2013). The experiments and model results showed that, at high stimulus levels, the pitch shift increased for greater values of σ, but that in some cases there was a point where the pitch would shift back again. A closer look at the model simulations indicated that this was the result of a second region of excitation appearing near the compensating contact when the current amplitude on that contact reached a critical point. In addition, the model predicted that the maximum achievable pitch shift would become much smaller at lower stimulus levels, to the point where it was non-existent at simulated perceptual threshold. Furthermore, both model and psychophysics showed that shifting the pitch with phantom stimulation comes at the cost of increased power consumption. These results suggest that while the possibility of extending the range of the electrode array is appealing, there are some downsides to consider in clinical practice. However, some experimental speech processing strategies using phantom stimulation have been tested and although they did not show benefits to speech understanding, subjects could subjectively discriminate between phantom and non-phantom speech processing strategies and in some cases preferring the one with phantom stimulation (Carlyon et al., 2014; Munjal et al., 2015; Nogueira et al., 2015).

Current focussing

Chapter 6 describes how the model's neural trajectories were updated to include a more realistic spatial distribution of cell bodies, for the purpose of gaining better insight into the excitation patterns of current focussing stimuli. The modelling results demonstrate how current focussing strategies can spatially 'sculpt' the region of neural excitation to some extent, which allows them to stimulate more deeply into the spiral ganglion than monopolar stimuli, at the same loudness (i.e., an equal number of excited neurons in the model). In principle this should result in less spread of excitation, more easily discriminable channels and, presumably, better speech understanding when using current focussing strategies. Although more studies with different methodologies have emerged that showed that current focussed stimuli had a reduced spread of excitation (George et al., 2015; Luo and Wu, 2016; Padilla and Landsberger, 2016), there were mixed reports on the benefits to speech intelligibility (Srinivasan et al., 2013; Bierer and Litvak, 2016; Arenberg et al., 2018; Luo et al., 2021).

An experimental stimulation strategy called dynamic current focussing (DCF) was tested at the Leiden University Medical Centre, which essentially used partial tripolar stimuli at fixed amplitude while controlling the loudness level by changing the current compensation factor σ, with lower values of σ resulting in less compensating current and louder stimulus perception (de Jong et al., 2019a). Spectral ripple tests showed significant improvement of spectral resolution with the DCF strategy compared to the test subjects' clinical maps, while speech intelligibility remained the same, despite the fact that the subjects only had a few hours experience with the DCF strategy. However, a subsequent take-home trial was not able to reveal conclusive evidence that DCF stimulation significantly improved speech intelligibility (de Jong et al., 2019b). A comparable stimulation strategy was also investigated by Arenberg et al, who found that dynamic focussing improved vowel identification (Arenberg et al., 2018).

Other studies have tried combining current focussing techniques with current steering. Unpublished data from the Leiden CI model demonstrated that the two principles could be successfully combined, allowing for gradually shifting regions of excitation steering focussed channels, at least for lateral wall electrodes (Kalkman et al., 2011). Landsberger and Srinivasan performed virtual channel discrimination tests with so-called 'quadrupolar virtual channels', which were essentially current steered electrode pairs flanked by two compensating electrodes stimulating at fixed opposite polarity amplitudes equal to half the combined current on the centre pair, multiplied by σ (Landsberger and Srinivasan, 2009); their results showed that their subjects were significantly better at discriminating the focussed virtual channels than the conventional non-focussed ones. In a subsequent study, pitch ranking tests of these quadrupolar virtual channels and 'virtual tripoles' (current steering with two 'interlaced' partial tripoles with flanks spaced two contacts from their corresponding centres) demonstrated that steering the quadrupolar channels could lead to a non-monotonically shifting pitch, which was not the case for current steered monopoles or virtual tripoles (Padilla et al., 2017). Meanwhile, the previously mentioned study by Nogueira et al. did not find improved virtual channel discrimination for their

implementation of focussed current steering (which was different from the quadrupolar virtual channels from Landsberger and Srinivasan in that the compensating current was also steered) and discovered that the pitch range of their focussed virtual channels were diminished by the compensating current, though the total number of discriminable percepts stayed the same (Nogueira et al., 2017). Recently, Luo et al. tested speech coding strategies that used partial tripolar stimuli with steered compensating current and found that they improved sentence recognition in noise (Luo et al., 2021).

These studies show promising results that support further clinically investigating current focusing techniques, but also illustrate uncertainties and potential problems. The most important question is whether or not it gives enough benefits to speech understanding to justify its cost, since current focussing inherently demands an increase in power consumption compared to monopolar stimulation (Vellinga et al., 2017a; chapter 6). However, it must be said that CI users are able to subjectively hear a difference between strategies and may sometimes prefer current focussed stimulation (Bierer and Litvak, 2016; de Jong et al., 2019a; de Jong et al., 2019b), so there may be value to current focussing strategies outside of measurable improvements to speech intelligibility.

A different possible use for current focussing might not so much lie in a reduced spread of excitation for individual channels, but rather in a decrease in channel interaction. Aided by the Leiden CI model, Vellinga et al. examined several options of using multipolar stimulation to compensate for electrical channel interaction in an attempt to simultaneously stimulate two channels at once, without incurring significant negative effects to speech understanding (Vellinga et al., 2017b). The idea behind this was that parallel stimulation could either be used to improve temporal resolution by allowing for effectively doubled stimulation rates per channel, or, conversely, make it possible to double the pulse duration without increasing each channel's pulse rate, thereby lowering power consumption. The study showed that partial tripolar stimuli, as well as a novel strategy derived from phased array stimulation, were able to reduce electrical interaction. These were promising results, but further studies are needed to see if speech intelligibility can be maintained with this kind of parallel stimulation.

Polarity sensitivity

In chapter 7 the model was used to test the so-called neural health hypothesis regarding the polarity sensitivity of CI stimuli. This study also included an updated auditory nerve fibre morphology, modelled as an electrical double cable and using a human-derived neural kinetics scheme; these fibres were modelled in three stages of neural health in order to examine the effect of neural degeneration on polarity sensitivity. The resulting model simulations showed that although neural degeneration did affect polarity sensitivity, the effects were not consistent, sometimes counter intuitive and also depended on spatial factors such as electrode position.

Several research groups have recently directed their attention at the possibility of interpreting various objective measures derived from eCAP recordings (such as polarity

sensitivity and the so-called interphase gap effect) as an indicator of cochlear neural health (Brochier et al., 2021a; Brochier et al., 2021b; Heshmat et al., 2021; Langner et al., 2021; Zhou et al., 2021; Garadat et al., 2022; Hughes, 2022). Brochier et al. suggested that different measures may reflect different aspects of neural health, specifically that polarity sensitivity is most affected by the health of the peripheral processes and that the interphase gap (IPG) effect is related to the degree of central axon myelinization (Brochier et al., 2021a). However, the results of the modelling study chapter 7 imply that polarity sensitivity cannot be simply interpreted as an indicator of the presence or health of the peripheral processes. Furthermore, preliminary results from the Leiden CI model showed that although the IPG effect is affected by the degree of neural degeneration, the changes in the IPG effect are small and inconsistent, in addition to being dependent on lateral to medial electrode positioning (Kalkman et al., 2021).

The Leiden model has so far not revealed any straightforward relationships between eCAP measures and neural health, though it should be noted that there are several types of neural degeneration that have not been included in the model yet, such as demyelination, reduction of axon diameter and degeneration/dysfunction of ion channels. A more comprehensive look at neural degeneration is needed to obtain better insight, but for the time being researchers should be cautious in using eCAP-derived measures as a diagnostic tool for gauging neural health. While these measures are undoubtedly affected by changes in neural functioning, the model has thus far shown that these effects may be inconsistent or counter-intuitive and that spatial factors such as electrode-modiolus distance and insertion depth are important elements that should be taken into account.

State of the model and its future perspectives

Although the Leiden CI model consists of two equally important parts, namely a volume-conduction model and an active nerve fibre model, the main focus of the work of this thesis was on aspects of the volume-conduction half of the model. Since its earliest version, the volume-conduction model has been based on the Boundary Element Method (BEM), and as such, improvements to it have mainly concerned changes to the model geometries and the conductivity values of their component structures. Geometries in the BEM are defined in terms of the boundaries between different conductive media and these boundaries are described by discrete surface elements, unlike in the commonly used Finite Element Method (FEM), where those same media would be discretised using volume elements. The advantage of this is that adding new objects to the model geometry is trivial and does not require a remeshing of the existing geometry, provided none of the new surface elements are required to connect to any of the old ones and none of them intersect with each other. This is quite useful when changing the positioning of the electrode array, swapping out the array for a different design, or adding new structures near the cochlea, such as the facial nerve described in chapter 4. Unfortunately, when a new addition to the geometry is intentionally required to touch or intersect existing structures (e.g., having an electrode array puncture the basilar membrane), it becomes much more difficult to assure that the new mesh is viable, as new vertices would have to be created, surface elements would

need to be split up, connected properly and both sides of each element would need to have the correct electrical medium assigned to them.

This is made more difficult by the Leiden model's use of quadratically curved triangles as surface elements, as opposed to using more straight-forward flat triangles. While these quadratically curved triangles improve the BEM's accuracy compared to flat triangles (Frijns et al., 2000), generating a suitable mesh with them can be challenging, since incorrect placement of vertices can make the curved triangles unexpectedly intersect with each other or even fold in on themselves, causing serious numerical errors in the model's output. Furthermore, it is much more difficult to determine if and where two quadratically curved triangles are intersecting than it is for two flat triangles, which makes it even more impractical to merge two geometries with intersecting structures. To alleviate this issue, it may prove wise to abandon quadratically curved triangles in favour of flat triangles in the future. While this would mean a loss in numerical accuracy, the practical benefits to making new geometries may be worth it. Furthermore, the decision to use curved triangles was made at a time when the available hardware for running the model was modest and it was essential to achieve more accurate results while using the same amount of system memory (which is the main limiting factor for the BEM). With the more powerful computational hardware available today, it might be feasible to compensate for the decrease in accuracy by simply increasing the number of flat triangles.

One other noteworthy limitation of using the BEM for the volume conduction model is that it has problems in accurately computing the electrical potential on boundaries with high conductivity differences. For the Leiden model specifically, this is an issue for the platinum contacts of the electrode array, which are several orders more conductive than the silicone and perilymph they share boundaries with. If a realistic value for the electrical conductivity of platinum is used in the volume-conduction model, it introduces/magnifies numerical errors in the resulting solution which causes the potentials at the stimulating electrode contacts to approach 0 V, which is obviously not physically correct. Theoretically this issue can be avoided by making the surface elements of the electrode contact boundaries small and dense enough, but this would increase the number of vertices in the geometry far beyond what currently available hardware can process. Instead, the conductivity value was set to 100 S/m (which is about 4 or 5 orders of magnitude lower than would be realistic, but still 2 orders higher than perilymph) and the surface elements of the electrode contacts were made as small as necessary to minimise numerical errors. Since the electrode contacts are physically a small part of the total geometry, this low conductivity value for platinum does not significantly affect the potential fields in the cochlea, but it does mean that there is a slight potential gradient across the contacts, which the electrodes realistically should not have. However, apart from this small gradient (the lowest potential on each contact's surface is about 2% lower than its highest), the potentials on the electrode contacts do have appropriate values, since they are primarily determined by the other structures in the geometry. In other words, despite having to compromise on the conductivity value for the platinum contacts, the model does produce sufficiently realistic potentials.

Looking at the present version of the model as a whole, while it is capable of realistically simulating many aspects of CI functioning, it is notably unable to predict realistic values for the stimulus amplitudes needed to reach perceptual threshold (T-level) and MCL (M-level). Previously published data showed that CI-patients at the Leiden University Medical Centre had average T-levels around 50 CU (clinical units), which for 40 μs/phase pulses results in amplitudes of 97 μA, while average M-levels were roughly 200 CU, corresponding to 389 μA amplitudes (van der Beek et al., 2015). Data from the polarity sensitivity study of chapter 7 shows that the model's average T- and M-levels for lateral electrode contacts are respectively about 7 and 3 times higher than the values reported by van der Beek et al., which is a considerable deviation from clinical reality.

This problem is not unique to the Leiden model, however, as other similar models have also been unable to accurately predict stimulus levels (see chapter 2). It is therefore clear that there is some gap in knowledge, incorrect assumption or oversimplification in the models that is responsible for this issue. Since the Leiden model consists of two independent parts (i.e., the volume conduction model and the auditory nerve fibre model), either half of the model could contain some inaccuracy that is causing simulated neural thresholds to be much larger than they ought to be.

There is good reason to suspect that the volume conduction model is at least partly responsible for this issue; aside from high neural thresholds, the model generally also predicts relatively low spread of excitation (Biesheuvel et al., 2022), which cannot exclusively be attributed to possible flaws in the neural model. The main aspect of the volume conduction model that is most likely in need of improvement is the modiolus of the cochlear geometries, which should either have its level of detail increased, have its electrical conductivity values updated, or both. The modiolus is currently modelled as a fairly homogenous structure, without a distinct volume to specifically represent neural tissue. This has consequences for the flow of electrical current, as in reality the modiolus contains dense bundles of relatively conductive nerve fibres surrounded by less conductive porous bone. Separately modelling the neural tissue and giving it its own conductivity value while lowering the conductivity of the surrounding bone should direct more current along the nerve fibres, which would likely make it easier to excite them and could also increase spread of excitation. Furthermore, the neural tissue should ideally be given anisotropic conductivities (i.e., different conductivity values along different directions), since electrical conductivity along the length of a bundle of nerve fibres can be expected to be greater than the conductivity orthogonal to it due to the fact that the axons are largely wrapped in electrically insulating myelin. However, implementing anisotropic conductivities in the BEM is considerably more difficult than it is in the FEM, so it may be necessary to switch to a FEM-based volume conduction model in the future.

For the neural model there are no obvious components that can be identified as the possible cause of the overestimated threshold levels. This is not to say that the neural model cannot be improved; on the contrary, there are many parameters and aspects of the neural model that are either simplified for practical reasons, founded on incomplete/imperfect data or based on conjecture due to the lack of suitable experimental data. For

example, disregarding neural degeneration, the model uses one basic neural morphology for all auditory neurons, which only differs from one fibre to the other in the number of peripheral process segments and their scale factors, which are adjusted to set the lengths of the peripheral processes to fit their respective trajectories in the cochlear geometry. This is a simplification, as in reality there is variability in nerve fibre morphology throughout the cochlea, for example in axon diameter (Spoendlin and Schrott, 1989). Furthermore, there is currently no definitive data on the typical number and lengths of myelinated segments of the auditory neurons, which means that these parameters had to be estimated; as a consequence, each model of the auditory nerve fibre has resulted in different choices being made for its neuronal segmentation (Bachmaier et al., 2019). In addition, information on diameter dependent properties of human auditory nerve fibres (e.g., the action potential conduction velocity and absolute refractory period) is relatively scarce, so the neural model would benefit from additional experimental data.

Arguably the most obvious feature of neural behaviour that is missing from all versions of the neural model used throughout this thesis is stochasticity. In the neural modelling presented here, the auditory nerve fibres behave purely deterministically, meaning they will always give identical responses when given identical inputs. In other words, for a given stimulus, the threshold of neural excitation in the deterministic model is absolute; below this threshold the neuron will never fire, while at or above it, the neuron is guaranteed to fire (unless the stimulus amplitude is absurdly and unrealistically high, in which case the model neuron tends to stop firing again). In real life, however, neurons behave stochastically and therefore will only have a probability of firing as a response to a stimulus (though this probability depends on the stimulus and its intensity).

While the absence of stochastic behaviour was not a problem in the studies presented in this thesis, it did effectively limit the model to simulating single pulse responses, since simulating responses to pulse trains or more complex stimuli (e.g., the output of speech processing algorithms) would not be as meaningful without stochastic behaviour and, not unimportantly, would also be very computationally demanding. The PhD work of Dr van Gendt has sought to remedy these issues by building an additional stochastic layer on top of the deterministic model (van Gendt, 2021). Essentially, the expanded model used the deterministic thresholds of the individual model nerve fibres as the base levels for their firing probability curves in a computationally efficient phenomenological model of neural behaviour, which included various (stochastic) properties that are either too time consuming to simulate in the deterministic model or simply not present in it. Using this hybrid approach, it was possible to simulate responses to longer, more complex stimuli (van Gendt et al., 2016; 2017; van Gendt et al., 2019; van Gendt et al., 2020b).

The stochastic expansion of the model will be the basis of future research that will attempt to simulate and hopefully optimize speech coding strategies. Since the deterministic model is used as its foundation, it will remain important to make continued updates to it. However, it is difficult to say what part of the deterministic neural model is most in need of improving; unless some significant new experimental data or insights become available, changes to the neural model in the near future will likely be iterative, rather than substantial.

Aside from improvements to the model itself, there is also still progress to be made in the interpretation of its results. After all, even if the model's output was flawlessly realistic (which is not the case), there would still be uncertainty in precisely how the brain processes the signals coming from the auditory neurons. One of the most fundamental examples of this is the question of how exactly loudness is coded, an issue that is very relevant to this thesis. Thus far, loudness in the model is assumed to simply be directly proportional to the number of nerve fibres excited by a single pulse; although this approach is able to realistically simulate loudness growth curves (chapter 6) and predict loudness balancing experiments (Snel-Bongers et al., 2013), this is nevertheless a simplistic approach. In psychophysics, loudness experiments are typically performed with pulse trains, rather than single pulses, which means that temporal factors such as pulse rate and temporal integration play important roles (McKay, 2020). The expanded model from van Gendt et al. can be used to make more realistic predictions of simulated loudness, which could then be more meaningfully compared to psychophysical data.

In addition to expanding the model with stochasticity, van Gendt et al. also connected the volume-conduction model to a model of inner and outer hair cell activation, in order to simulate intracochlear electrocochleography (ECochG) recordings performed by a cochlear implant electrode array (van Gendt et al., 2020a). Despite the fact that the model was not originally designed for this purpose, it was able to produce realistic results that compared well to recordings from human subjects, especially when partial hair cell degeneration was taken into account. This illustrates the versatility of physics-based computational modelling and shows that, with adjustments, the Leiden CI-model can be applied beyond its original purpose.

Perspectives for the near future also include using machine learning to develop a surrogate of the deterministic nerve fibre model, in conjunction with the Leiden Institute of Advanced Computer Science. The basic principle of this is to train a surrogate model to predict the output of the nerve fibre model in order to create an 'artificial' substitute that can generate simulated neural responses to arbitrary stimuli much faster and more efficiently than can be achieved by running a full simulation with the neural model. Of course, this will not make the nerve fibre model completely redundant, since the surrogate will likely only be reliable for input that is relatively similar to the data it has been trained with, so the neural model will still be needed to verify the surrogate's output from time to time and to retrain it when needed. Furthermore, the surrogate would only be valid for the present version of the nerve fibre model, which means that any changes to it would involve creating a new surrogate. However, once it is sufficiently validated, the surrogate model promises to be a useful tool for rapidly exploring and developing new stimulation strategies.

Another potential direction is the development of personalised models for individual CI subjects. The Leiden model has already been used to create personalised cochlear geometries for some patients, for the purpose of estimating the characteristic place pitch elicited by their electrode contacts (Frijns et al., 2007; Carlyon et al., 2010) and optimising the model's conductivity values based on the subjects' clinically obtained intrascalar potential recordings (chapter 3). However, these personalised models were manually

created by adjusting one of the existing cochlear geometries to match a subject's CT images, which was a time-consuming process and unfeasible to perform for every patient at our clinic. More importantly, at that time the model was not yet advanced enough to produce data that could be used to verifiably improve a specific user's speech coding strategy. However, with recent and future improvements to the model and advances in radiological image processing it will be interesting to revisit the possibility of making personalised models for clinical practice. Several other groups have also been working on implementing personalised CI models (Malherbe et al., 2013; 2015; 2016; Nogueira et al., 2016; Badenhorst et al., 2017; Cakir et al., 2017; Liu et al., 2020; Badenhorst et al., 2021), but they have not managed to become a part of standard clinical practice yet.

To conclude, the studies presented in this thesis have brought the Leiden CI model closer to clinical reality, though more work can be done to bridge the gap between them completely. Since the Leiden model is built on physical principles it is essential to continue to validate and refine it with the help of data from animal studies and clinical experiments and not haphazardly adjusting arbitrary parameters to make the model output seem more realistic. However, it is important not to add more realistic detail simply for its own sake, since adding more 'life-like' characteristics to biophysical models tends to make their output more chaotic and more difficult to interpret and error-check. At the same time, improving the model will allow it to continue to shed new light on experimental findings that are not yet fully understood, assist in understanding the differences between animal and human data and hopefully lead to better insights for clinical practice.

References

Adel, Y., Nagel, S., Weissgerber, T., Baumann, U., Macherey, O. 2019. Pitch Matching in Cochlear Implant Users With Single-Sided Deafness: Effects of Electrode Position and Acoustic Stimulus Type. Front Neurosci 13, 1119.

Arenberg, J.G., Parkinson, W.S., Litvak, L., Chen, C., Kreft, H.A., Oxenham, A.J. 2018. A Dynamically Focusing Cochlear Implant Strategy Can Improve Vowel Identification in Noise. Ear Hear 39, 1136-1145.

Bachmaier, R., Encke, J., Obando-Leiton, M., Hemmert, W., Bai, S. 2019. Comparison of Multi-Compartment Cable Models of Human Auditory Nerve Fibers. Front Neurosci 13, 1173.

Badenhorst, W., Hanekom, T., Gross, L., Hanekom, J.J. 2021. Facial nerve stimulation in a post-meningitic cochlear implant user: using computational modelling as a tool to probe mechanisms and progression of complications on a case-by-case basis. Cochlear Implants Int 22, 68-79.

Badenhorst, W., Hanekom, T., Hanekom, J.J. 2017. Analysis of a purely conductance-based stochastic nerve fibre model as applied to compound models of populations of human auditory nerve fibres used in cochlear implant simulations. Biol Cybern 111, 439-458.

Bahmer, A., Adel, Y., Baumann, U. 2017. Preventing Facial Nerve Stimulation by Triphasic Pulse Stimulation in Cochlear Implant Users: Intraoperative Recordings. Otol Neurotol 38, e438-e444.

Bahmer, A., Baumann, U. 2016. The Underlying Mechanism of Preventing Facial Nerve Stimulation by Triphasic Pulse Stimulation in Cochlear Implant Users Assessed With Objective Measure. Otol Neurotol 37, 1231-7.

Bierer, J.A., Litvak, L. 2016. Reducing Channel Interaction Through Cochlear Implant Programming May Improve Speech Perception: Current Focusing and Channel Deactivation. Trends Hear 20.

Biesheuvel, J.D., Briaire, J.J., Kalkman, R.K., Frijns, J.H.M. 2022. The effect of stimulus level on excitation patterns of individual electrode contacts in cochlear implants. Hear Res 420, 108490.

Briaire, J.J. 2008. Cochlear implants: from model to patients.

Brochier, T., Guerit, F., Deeks, J.M., Garcia, C., Bance, M., Carlyon, R.P. 2021a. Evaluating and Comparing Behavioural and Electrophysiological Estimates of Neural Health in Cochlear Implant Users. J Assoc Res Otolaryngol 22, 67-80.

Brochier, T., McKay, C.M., Carlyon, R.P. 2021b. Interpreting the Effect of Stimulus Parameters on the Electrically Evoked Compound Action Potential and on Neural Health Estimates. J Assoc Res Otolaryngol 22, 81-94.

Buchner, A., Lenarz, T., Boermans, P.P., Frijns, J.H., Mancini, P., Filipo, R., Fielden, C., Cooper, H., Eklof, M., Freijd, A., Lombaard, S., Meerton, L., Pickerill, M., Vanat, Z., Wesarg, T., Aschendorff, A., Kienast, B., Boyle, P., Arnold, L., Meyer, B., Sterkers, O., Muller-Deile, J., Ambrosch, P., Helbig, S., Frachet, B., Gallego, S., Truy, E., Jeffs, E., Morant, A., Marco, J. 2012. Benefits of the HiRes 120 coding strategy combined with the Harmony processor in an adult European multicentre study. Acta Otolaryngol 132, 179-87.

Cakir, A., Dwyer, R.T., Noble, J.H. 2017. Evaluation of a high-resolution patient-specific model of the electrically stimulated cochlea. J Med Imaging (Bellingham) 4, 025003.

Carlyon, R.P., Macherey, O., Frijns, J.H., Axon, P.R., Kalkman, R.K., Boyle, P., Baguley, D.M., Briggs, J., Deeks, J.M., Briaire, J.J., Barreau, X., Dauman, R. 2010. Pitch comparisons between electrical stimulation of a cochlear implant and acoustic stimuli presented to a normal-hearing contralateral ear. J Assoc Res Otolaryngol 11, 625-40.

Carlyon, R.P., Monstrey, J., Deeks, J.M., Macherey, O. 2014. Evaluation of a cochlear-implant processing strategy incorporating phantom stimulation and asymmetric pulses. Int J Audiol 53, 871-9.

Claussen, A.D., Gantz, B.J. 2022. Cochlear Implantation in Advanced Otosclerosis: Pitfalls and Successes. Curr Otorhinol Rep 10, 49-57.

de Jong, M.A.M., Briaire, J.J., Biesheuvel, J.D., Snel-Bongers, J., Bohringer, S., Timp, G., Frijns, J.H.M. 2020. Effectiveness of Phantom Stimulation in Shifting the Pitch Percept in Cochlear Implant Users. Ear Hear 41, 1258-1269.

de Jong, M.A.M., Briaire, J.J., Frijns, J.H.M. 2019a. Dynamic Current Focusing: A Novel Approach to Loudness Coding in Cochlear Implants. Ear Hear 40, 34-44.

de Jong, M.A.M., Briaire, J.J., van der Woude, S.F.S., Frijns, J.H.M. 2019b. Dynamic current focusing for loudness encoding in cochlear implants: a take-home trial. Int J Audiol 58, 553-564.

Demarcy, T., Vandersteen, C., Guevara, N., Raffaelli, C., Gnansia, D., Ayache, N., Delingette, H. 2017. Automated analysis of human cochlea shape variability from segmented µCT images. Comput Med Imaging Graph 59, 1-12.

Donaldson, G.S., Dawson, P.K., Borden, L.Z. 2011. Within-subjects comparison of the HiRes and Fidelity120 speech processing strategies: speech perception and its relation to place-pitch sensitivity. Ear Hear 32, 238-50.

Frijns, J.H., de Snoo, S.L., Schoonhoven, R. 2000. Improving the accuracy of the boundary element method by the use of second-order interpolation functions. IEEE Trans Biomed Eng 47, 1336-46.

Frijns, J.H.M. 1995. Cochlear implants : a modelling approach, [S.l. : s.n.].

Frijns, J.H.M., Kalkman, R.K., Dekker, D.M.T., Verbist, B.M., Briaire, J.J. 2007. Model-based individualized frequency maps: A first clinical application, Conference on Implantable Auditory Prostheses, Granlibakken Conference Center, Lake Tahoe, California.

Garadat, S.N., Colesa, D.J., Swiderski, D.L., Raphael, Y., Pfingst, B.E. 2022. Estimating health of the implanted cochlea using psychophysical strength-duration functions and electrode configuration. Hear Res 414, 108404.

George, S.S., Wise, A.K., Fallon, J.B., Shepherd, R.K. 2015. Evaluation of focused multipolar stimulation for cochlear implants in long-term deafened cats. J Neural Eng 12, 036003.

Goehring, J.L., Neff, D.L., Baudhuin, J.L., Hughes, M.L. 2014a. Pitch ranking, electrode discrimination, and physiological spread-of-excitation using Cochlear's dual-electrode mode. J Acoust Soc Am 136, 715-27.

Goehring, J.L., Neff, D.L., Baudhuin, J.L., Hughes, M.L. 2014b. Pitch ranking, electrode discrimination, and physiological spread of excitation using current steering in cochlear implants. J Acoust Soc Am 136, 3159.

Greenwood, D.D. 1990. A cochlear frequency-position function for several species--29 years later. J Acoust Soc Am 87, 2592-605.

Helpard, L., Li, H., Rohani, S.A., Zhu, N., Rask-Andersen, H., Agrawal, S., Ladak, H.M. 2021. An Approach for Individualized Cochlear Frequency Mapping Determined From 3D Synchrotron Radiation Phase-Contrast Imaging. IEEE Trans Biomed Eng 68, 3602-3611.

Herrmann, D.P., Kalkman, R.K., Frijns, J.H.M., Bahmer, A. 2019. Investigating the Reduction of Facial Nerve Stimulation in Cochlear Implants by Triphasic Pulses, Jahrestagung der Deutschen Gesellschaft für Audiologie, Heidelberg, Germany.

Heshmat, A., Sajedi, S., Schrott-Fischer, A., Rattay, F. 2021. Polarity Sensitivity of Human Auditory Nerve Fibers Based on Pulse Shape, Cochlear Implant Stimulation Strategy and Array. Front Neurosci 15, 751599.

Hughes, M.L. 2022. Characterizing Polarity Sensitivity in Cochlear Implant Recipients: Demographic Effects and Potential Implications for Estimating Neural Health. J Assoc Res Otolaryngol 23, 301-318.

Kalkman, R.K., Briaire, J.J., Frijns, J.H.M. 2021. Examining the interphase gap offset effect and its relation to neural health in a computational model, Conference on Implantable Auditory Prostheses, Virtual Conference.

Kalkman, R.K., Dekker, D.M.T., Briaire, J.J., Frijns, J.H.M. 2011. The potential benefits of combining intracochlear current focusing techniques with dual electrode stimulation: a computational study, Conference on Implantable Auditory Prostheses, Asilomar Conference Grounds, Pacific Grove, California.

Klawitter, S., Landsberger, D.M., Buchner, A., Nogueira, W. 2018. Perceptual changes with monopolar and phantom electrode stimulation. Hear Res 359, 64-75.

Lamping, W., Deeks, J.M., Marozeau, J., Carlyon, R.P. 2020. The Effect of Phantom Stimulation and Pseudomonophasic Pulse Shapes on Pitch Perception by Cochlear Implant Listeners. J Assoc Res Otolaryngol 21, 511-526.

Landsberger, D., Galvin, J.J., 3rd. 2011. Discrimination between sequential and simultaneous virtual channels with electrical hearing. J Acoust Soc Am 130, 1559-66.

Landsberger, D.M., Srinivasan, A.G. 2009. Virtual channel discrimination is improved by current focusing in cochlear implant recipients. Hear Res 254, 34-41.

Langner, F., Arenberg, J.G., Buchner, A., Nogueira, W. 2021. Assessing the relationship between neural health measures and speech performance with simultaneous electric stimulation in cochlear implant listeners. PLoS One 16, e0261295.

Langner, F., Saoji, A.A., Buchner, A., Nogueira, W. 2017. Adding simultaneous stimulating channels to reduce power consumption in cochlear implants. Hear Res 345, 96-107.

Liu, Z., Cakir, A., Noble, J.H. 2020. Auditory Nerve Fiber Health Estimation Using Patient Specific Cochlear Implant Stimulation Models. Simul Synth Med Imaging 12417, 184-194.

Luo, X., Wu, C.C. 2016. Symmetric Electrode Spanning Narrows the Excitation Patterns of Partial Tripolar Stimuli in Cochlear Implants. J Assoc Res Otolaryngol 17, 609-619.

Luo, X., Wu, C.C., Pulling, K. 2021. Combining current focusing and steering in a cochlear implant processing strategy. Int J Audiol 60, 232-237.

Macherey, O., Carlyon, R.P. 2012. Place-pitch manipulations with cochlear implants. J Acoust Soc Am 131, 2225-36.

Macherey, O., Deeks, J.M., Carlyon, R.P. 2011. Extending the limits of place and temporal pitch perception in cochlear implant users. J Assoc Res Otolaryngol 12, 233-51.

Malherbe, T.K., Hanekom, T., Hanekom, J.J. 2013. Can subject-specific single-fibre electrically evoked auditory brainstem response data be predicted from a model? Med Eng Phys 35, 926-36.

Malherbe, T.K., Hanekom, T., Hanekom, J.J. 2015. The effect of the resistive properties of bone on neural excitation and electric fields in cochlear implant models. Hear Res 327, 126-35.

Malherbe, T.K., Hanekom, T., Hanekom, J.J. 2016. Constructing a three-dimensional electrical model of a living cochlear implant user's cochlea. Int J Numer Method Biomed Eng 32.

Marozeau, J., Gnansia, D., Ardoint, M., Poncet-Wallet, C., Lazard, D.S. 2020. The sound sensation of a pure tone in cochlear implant recipients with single-sided deafness. PLoS One 15, e0235504.

McKay, C.M. 2020. Applications of Phenomenological Loudness Models to Cochlear Implants. Front Psychol 11, 611517.

Mertens, G., Van de Heyning, P., Vanderveken, O., Topsakal, V., Van Rompaey, V. 2022. The smaller the frequency-to-place mismatch the better the hearing outcomes in cochlear implant recipients? Eur Arch Otorhinolaryngol 279, 1875-1883.

Munjal, T., Roy, A.T., Carver, C., Jiradejvong, P., Limb, C.J. 2015. Use of the Phantom Electrode strategy to improve bass frequency perception for music listening in cochlear implant users. Cochlear Implants Int 16 Suppl 3, S121-8.

Nogueira, W., Litvak, L.M., Landsberger, D.M., Buchner, A. 2017. Loudness and pitch perception using Dynamically Compensated Virtual Channels. Hear Res 344, 223-234.

Nogueira, W., Litvak, L.M., Saoji, A.A., Buchner, A. 2015. Design and evaluation of a cochlear implant strategy based on a "Phantom" channel. PLoS One 10, e0120148.

Nogueira, W., Schurzig, D., Buchner, A., Penninger, R.T., Wurfel, W. 2016. Validation of a Cochlear Implant Patient-Specific Model of the Voltage Distribution in a Clinical Setting. Front Bioeng Biotechnol 4, 84.

Padilla, M., Landsberger, D.M. 2016. Reduction in spread of excitation from current focusing at multiple cochlear locations in cochlear implant users. Hear Res 333, 98-107.

Padilla, M., Stupak, N., Landsberger, D.M. 2017. Pitch ranking with different virtual channel configurations in electrical hearing. Hear Res 348, 54-62.

Peters, J.P.M., Bennink, E., Grolman, W., van Zanten, G.A. 2016. Electro-acoustic pitch matching experiments in patients with single-sided deafness and a cochlear implant: Is there a need for adjustment of the default frequency allocation tables? Hear Res 342, 124-133.

Plant, K.L., McDermott, H.J., van Hoesel, R.J., Dawson, P.W., Cowan, R.S. 2014. Factors influencing electrical place pitch perception in bimodal listeners. J Acoust Soc Am 136, 1199.

Reiss, L.A., Ito, R.A., Eggleston, J.L., Liao, S., Becker, J.J., Lakin, C.E., Warren, F.M., McMenomey, S.O. 2015. Pitch adaptation patterns in bimodal cochlear implant users: over time and after experience. Ear Hear 36, e23-34.

Saoji, A.A., Koka, K., Litvak, L.M., Finley, C.C. 2018. Pure-Tone Masking Patterns for Monopolar and Phantom Electrical Stimulation in Cochlear Implants. Ear Hear 39, 124-130.

Saoji, A.A., Landsberger, D.M., Padilla, M., Litvak, L.M. 2013. Masking patterns for monopolar and phantom electrode stimulation in cochlear implants. Hear Res 298, 109-16.

Saoji, A.A., Litvak, L.M. 2010. Use of "phantom electrode" technique to extend the range of pitches available through a cochlear implant. Ear Hear 31, 693-701.

Snel-Bongers, J. 2013. Dual electrode stimulation in cochlear implants : from concept to clinical application.

Snel-Bongers, J., Briaire, J.J., van der Veen, E.H., Kalkman, R.K., Frijns, J.H. 2013. Threshold levels of dual electrode stimulation in cochlear implants. J Assoc Res Otolaryngol 14, 781-90.

Spoendlin, H., Schrott, A. 1989. Analysis of the human auditory nerve. Hear Res 43, 25-38.

Srinivasan, A.G., Padilla, M., Shannon, R.V., Landsberger, D.M. 2013. Improving speech perception in noise with current focusing in cochlear implant users. Hear Res 299, 29-36.

Stakhovskaya, O., Sridhar, D., Bonham, B.H., Leake, P.A. 2007. Frequency map for the human cochlear spiral ganglion: implications for cochlear implants. J Assoc Res Otolaryngol 8, 220-33.

Svirsky, M.A., Fitzgerald, M.B., Sagi, E., Glassman, E.K. 2015. Bilateral cochlear implants with large asymmetries in electrode insertion depth: implications for the study of auditory plasticity. Acta Otolaryngol 135, 354-63.

van der Beek, F.B., Briaire, J.J., Frijns, J.H. 2015. Population-based prediction of fitting levels for individual cochlear implant recipients. Audiol Neurootol 20, 1-16.

van der Westhuizen, J., Hanekom, T., Hanekom, J.J. 2022. Apical Reference Stimulation: A Possible Solution to Facial Nerve Stimulation. Ear Hear 43, 1189-1197.

van Gendt, M.J. 2021. Cochlear implants: Modeling electrophysiological responses.

van Gendt, M.J., Briaire, J.J., Frijns, J.H.M. 2019. Effect of neural adaptation and degeneration on pulse-train ECAPs: A model study. Hear Res 377, 167-178.

van Gendt, M.J., Briaire, J.J., Kalkman, R.K., Frijns, J.H.M. 2016. A fast, stochastic, and adaptive model of auditory nerve responses to cochlear implant stimulation. Hear Res 341, 130-143.

van Gendt, M.J., Briaire, J.J., Kalkman, R.K., Frijns, J.H.M. 2017. Modeled auditory nerve responses to amplitude modulated cochlear implant stimulation. Hear Res 351, 19-33.

van Gendt, M.J., Koka, K., Kalkman, R.K., Stronks, H.C., Briaire, J.J., Litvak, L., Frijns, J.H.M. 2020a. Simulating intracochlear electrocochleography with a combined model of acoustic hearing and electric current spread in the cochlea. J Acoust Soc Am 147, 2049.

van Gendt, M.J., Siebrecht, M., Briaire, J.J., Bohte, S.M., Frijns, J.H.M. 2020b. Short and long-term adaptation in the auditory nerve stimulated with high-rate electrical pulse trains are better described by a power law. Hear Res 398, 108090.

Vellinga, D., Briaire, J.J., van Meenen, D.M.P., Frijns, J.H.M. 2017a. Comparison of Multipole Stimulus Configurations With Respect to Loudness and Spread of Excitation. Ear Hear 38, 487-496.

Vellinga, D., Bruijn, S., Briaire, J.J., Kalkman, R.K., Frijns, J.H. 2017b. Reducing interaction in simultaneous paired stimulation with CI. PLoS One 12, e0171071.

Verbist, B.M., Skinner, M.W., Cohen, L.T., Leake, P.A., James, C., Boex, C., Holden, T.A., Finley, C.C., Roland, P.S., Roland, J.T., Jr., Haller, M., Patrick, J.F., Jolly, C.N., Faltys, M.A., Briaire, J.J., Frijns, J.H. 2010. Consensus panel on a cochlear coordinate system applicable in histologic, physiologic, and radiologic studies of the human cochlea. Otol Neurotol 31, 722-30.

Vermeire, K., Landsberger, D.M., Van de Heyning, P.H., Voormolen, M., Kleine Punte, A., Schatzer, R., Zierhofer, C. 2015. Frequency-place map for electrical stimulation in cochlear implants: Change over time. Hear Res 326, 8-14.

Zhou, N., Zhu, Z., Dong, L., Galvin, J., 3rd. 2021. Sensitivity to Pulse Phase Duration as a Marker of Neural Health Across Cochlear Implant Recipients and Electrodes. J Assoc Res Otolaryngol 22, 177-192.

Chapter 9

Nederlandse samenvatting

Cochleaire implantaten (CI) zijn medische apparaten die inmiddels decennialang gebruikt worden om het gehoor te herstellen bij mensen met bepaalde vormen van ernstig gehoorverlies. Het basisprincipe waarop cochleaire implantaten werken is dat ze geluidswaarneming opwekken door het direct stimuleren van de gehoorzenuw met behulp van elektrische pulsen. Momenteel zijn cochleaire implantaten de meest succesvolle prothese voor het herstellen van gehoor bij mensen die, om wat voor reden dan ook, geen (versterkt) akoestisch geluid meer kunnen verstaan, maar die nog wel functionele gehoorzenuwen bezitten.

Er zijn verschillende CI-fabrikanten, die elk meerdere CI-types op de markt hebben gebracht, maar het basisontwerp van het cochleaire implantaat is eigenlijk altijd hetzelfde; er is een extern deel, met microfoon, spraakprocessor en zend/ontvangstspoel en er is een daadwerkelijk geïmplanteerd deel, bestaande uit een hoofdbehuizing met elektrode. De elektrode is in essentie een dun siliconen slangetje dat in de cochlea ingebracht wordt; langs de lengte van deze siliconen drager bevinden zich meerdere elektrodecontacten die los van elkaar elektrische signalen kunnen sturen naar de gehoorzenuwen die zich in de cochlea (het slakkenhuis) bevinden. Vanwege de spreiding van de elektrodecontacten zullen deze verschillende subpopulaties van de gehoorzenuwen aansturen en omdat de gehoorzenuwen tonotopisch georganiseerd zijn (dat wil zeggen: ze liggen naar toonhoogte gerangschikt in de cochlea, met de hoge tonen in de basis van de cochlea en de lage tonen in de top), zal elk contact een andere toonhoogtewaarneming opwekken.

In de dagelijkse praktijk worden cochleaire implantaten vrijwel altijd monopolair aangestuurd (er is op elk moment maar één elektrodecontact tegelijk actief), met zogeheten symmetrisch bifasische elektrische pulsen (pulsen met een positieve en een negatieve stroomfase die even sterk en even lang zijn). Dit is voldoende om de meeste CI-gebruikers goede spraakherkenning te geven, maar de kwaliteit van het 'geluid' laat te wensen over en CI's zijn berucht om het feit dat ze zeer slecht in staat zijn om toonhoogte (bijvoorbeeld van muziek) goed over te brengen. Verder kan het voorkomen dat het implantaat onbedoeld de verkeerde zenuwen stimuleert, zoals de aangezichtszenuw (nervus facialis), wat leidt tot het ongewenst samentrekken van de aangezichtsspieren. Ondanks het succes van cochleaire implantaten is er dus nog steeds een noodzaak voor meer onderzoek, zodat hun functioneren beter begrepen en hopelijk verbeterd kan worden.

Er liggen echter diverse beperkingen op het uitvoeren van dit onderzoek: de menselijke cochlea is klein (ongeveer 1 cm in doorsnede) en volledig omringd door bot, dus directe interactie met de cochlea en een geïmplanteerde elektrode is ethisch gezien vrijwel onmogelijk. Menselijk onderzoek is dus beperkt tot het uitvoeren van psychofysische experimenten en het gebruik van de meetmogelijkheden van het implantaat zelf. Dierexperimenteel onderzoek maakt meer mogelijk, maar heeft het probleem dat er veel anatomische en (neuro)fysiologische verschillen zijn tussen mens en dier.

Echter, de achterliggende natuurkundige principes rond elektrische stimulatie van (gehoor) zenuwen kunnen goed begrepen worden in termen van klassiek elektromagnetisme. Het binnenoor is te complex om analytisch te beschrijven, maar het is een ideale

kandidaat voor computermodellering; de stroomverdeling in de geïmplanteerde cochlea kan gesimuleerd worden in een zogeheten volumegeleidingsmodel door het numeriek oplossen van de betreffende Maxwellvergelijkingen in een driedimensionale benadering van het binnenoor. De reacties van de gehoorzenuwen op de berekende elektrische velden kunnen vervolgens gesimuleerd worden in een actief zenuwmodel door de zenuwvezels te modelleren als elektrische netwerken.

Dit proefschrift beschrijft de ontwikkeling en toepassing van een dergelijk computermodel zodat er meer inzicht verkregen kon worden in de werking van CI-stimulatie en virtuele experimenten uitgevoerd konden worden die in het echt niet uitvoerbaar zouden zijn. Het gebruikte model is eerder ontwikkeld in het Leids Universitair Medisch Centrum door mijn promotor, prof. dr. ir. Johan H.M. Frijns en mijn copromotor, dr. ir. Jeroen J. Briaire; als zodanig vormt dit proefschrift een voortzetting van hun promotieonderzoek.

De drie algemene doelen van het onderzoek in dit proefschrift waren:

(I) Het verbeteren van het Leidse CI-computermodel zodat er een beter begrip van door CI opgewekt gehoor verkregen kan worden.

(II) Waar mogelijk, het valideren van het computermodel met data uit elektrofysiologische of psychofysische experimenten.

(III) Het model gebruiken om voorspellingen te doen die mogelijk in de toekomst het functioneren of het ontwerp CI's kunnen verbeteren.

Hoofdstuk 2 vormt een overzicht van de geschiedenis van computermodelonderzoek naar cochleaire implantaten, met de nadruk op biofysische modellen waarmee aspecten van multipolaire stimulatie en elektrode-ontwerp zijn onderzocht. We zien hierin een stapsgewijze evolutie van relatief eenvoudige wiskundige modellen naar complexe driedimensionale volumegeleidingsmodellen die worden gecombineerd met actieve zenuwmodellen. De voorlopers en ontwikkeling van het Leidse CI-model maken hier ook deel van uit, samen met het soortgelijke modelwerk dat parallel door andere onderzoeksgroepen is uitgevoerd.

Het eerste onderzoek in dit proefschrift wordt beschreven in **hoofdstuk 3** en gaat over het voorspellen van toonhoogtewaarneming als gevolg van elektrische stimulatie van de gehoorzenuw, met behulp van het Leidse CI-model. Toonhoogtewaarneming met een CI is voor een belangrijk deel afhankelijk van de plaatsen van de stimulerende elektrodecontacten binnen de cochlea. Om het verband tussen toonhoogte en elektrodelocatie te onderzoeken in het CI-model hebben de zenuwvezels in de driedimensionale cochleamodellen in **hoofdstuk 3** een meer natuurgetrouw gekromd verloop gekregen dat is gebaseerd op gepubliceerde histologische gegevens. Daarnaast is de natuurlijke menselijke tonotopie die beschreven wordt door de zogeheten Greenwood-functie gebruikt om elke modelvezel een karakteristieke geluidsfrequentie toe te wijzen. Gesimuleerde excitatiepatronen in een viertal slakkenhuizen, geïmplanteerd met elektrodes in verschillende posities, toonden aan dat de te verwachten opgewekte toonhoogte van elektrodecontacten in de eerste winding

van de cochlea vrij dicht de Greenwood-functie volgde. Maar voor contacten die zich dieper in de cochlea bevinden werd de toonhoogte steeds grilliger en onvoorspelbaarder, wat afhing van stimulusniveau, toestand van de zenuwvezels en afstand tot de binnenwand van de cochlea. In de laatste winding was de toonhoogte bijzonder onvoorspelbaar en stimuleerden contacten bredere en grotendeels met elkaar overlappende groepen vezels.

In de klinische praktijk kan het voorkomen dat bij CI-stimulatie de nervus facialis (aangezichtszenuw) onbedoeld ook meegestimuleerd wordt, wat leidt tot ongewenste samentrekkingen van gezichtspieren bij de patiënt. Het is bekend dat CI-gebruikers met otosclerose, een aandoening waarbij het bot om de cochlea heen gedemineraliseerd wordt, een verhoogd risico hebben op facialisstimulatie. Om de relatie tussen otosclerose en facialisstimulatie te onderzoeken is in **hoofdstuk 4** een model van de facialis-zenuw afgeleid uit radiologische beelden en daarna toegevoegd aan het Leidse CI-model. In dit uitgebreide model werden gehoordrempels en drempels voor facialisstimulatie gesimuleerd voor verschillende elektrodeposities en -ontwerpen, waarbij de vordering van otosclerose nagebootst werd door het verhogen van de elektrische geleidbaarheid van het bot om de cochlea. In tegenstelling tot wat op voorhand verwacht werd, lieten de resultaten zien dat otosclerose niet zozeer de drempel voor facialisstimulatie verlaagde, maar dat vooral de gehoordrempels omhooggingen doordat er meer stroom uit de cochlea kon lekken. Verder bleek dat de positie en het ontwerp van de elektrode van invloed was op de mate van facialisstimulatie; elektrodes die langs de buitenwand van de cochlea waren geplaatst waren meer geneigd tot het stimuleren van de facialis dan elektrodes langs de binnenwand en elektrodes met ringvormige contacten hadden meer kans op facialisstimulatie dan elektrodes met half-ringvormige contacten, die op hun beurt weer meer kans hadden dan elektrodes met vlakke plaatjes als contacten. Dit alles impliceerde dat facialisstimulatie verminderd kan worden door elektrodes langs de binnenwand van de cochlea te plaatsen, met voldoende isolator aan de buitenzijde van de elektrode om de contacten elektrisch te isoleren.

In de meeste klinische toepassingen wordt elk elektrodecontact apart gestimuleerd en gezien als een onafhankelijk ‘kanaal’ met diens eigen toonhoogte-percept, welke afhankelijk is van de plaats van het elektrodecontact in de cochlea. Het is echter in principe mogelijk om een paar elektrodecontacten in samenwerking te stimuleren (gelijktijdig of kort na elkaar, met dezelfde stroomrichting) zodat ze een nieuw percept opwekken dat in toonhoogte ligt tussen die van de individuele contacten. Deze mogelijkheid is in **hoofdstuk 5** onderzocht in het Leidse CI-model door zenuwexcitatie te simuleren met paarsgewijze stimulatie van elektrodecontacten. Hierbij werd steeds stapsgewijs de stimulusamplitude opgevoerd in het ene contact terwijl dat van het andere in dezelfde mate afnam; de simulaties werden uitgevoerd met zowel simultane paarsgewijze stimulatie (ook wel *current steering* genoemd) als niet-simultane stimulatie.

Het model liet zien dat het op deze manier stimuleren van twee contacten inderdaad in staat is tussenliggende percepten op te wekken, en dat het verloop van het achterliggende excitatiepatroon op twee manieren (modaliteiten) plaatsvond: ofwel als één groep geëxciteerde zenuwvezels die geleidelijk verschoof wanneer de stimulusamplitudes van

de contacten aangepast worden, ofwel als twee aparte groepen vezels die respectievelijk groter en kleiner werden en een meer een abrupte verschuiving van het percept impliceerden. Bij de eerste modaliteit, die vooral optrad bij het stimuleren van aanliggende elektrodecontacten in de basale winding van de cochlea, bleef de luidheid (het aantal geëxciteerde zenuwvezels) relatief constant. Bij de tweede modaliteit zakte de luidheid in wanneer de stimulus verdeeld was over de twee contacten; dit werd ook bevestigd door psychofysische experimenten met CI-gebruikers. Deze modaliteit vond vooral plaats bij stimulatie van meer apicaal gelegen contacten, bij niet-simultaan gestimuleerde contacten en bij niet-aanliggende contactparen.

De monopolaire stimuli die over het algemeen in klinische praktijk gebruikt worden staan bekend om het feit dat ze vrij brede, sterk overlappende groepen zenuwvezels exciteren vanwege de brede spreiding van de elektrische stroom die met monopolaire stimulatie gepaard gaat; door deze brede excitatie kan het voor de CI-gebruiker lastig zijn om contacten van elkaar te onderscheiden. Maar het is technisch mogelijk om het elektrische veld 'aan te scherpen' door middel van zogeheten *'current focussing'*-strategieën, waarbij naast het 'hoofdcontact' gelijktijdig andere contacten worden meegestimuleerd, met tegengestelde polariteit (omgekeerde stroomrichting). Het idee hiervan is dat contacten aan weerszijden van het 'hoofdcontact' het elektrische veld aan de randen geheel of gedeeltelijk opheffen, waardoor het excitatiegebied ruimtelijk beperkt wordt, wat hopelijk leidt tot makkelijker van elkaar te onderscheiden kanalen en beter spraakverstaan.

Om de ruimtelijke effecten van *current focussing* technieken te kunnen simuleren, zijn in **hoofdstuk 6** de zenuwvezels in het Leidse CI-model voorzien van een realistische ruimtelijke spreiding van de cellichamen in het spirale ganglion binnen de cochleaire modiolus. Vervolgens zijn er simulaties gedaan met monopolaire stimuli en verschillende *current focussing*-strategieën, te weten (partiële) tripolen en zogeheten *'phased array'*-stimulatie. Uit de modelresultaten was duidelijk dat *current focussing* alleen effectief was als er voldoende elektrische interactie tussen de relevante elektrodecontacten was en dat perimodiolaire contacten (elektrodes die langs de binnenwand van de cochlea geplaatst zijn) dit niet hadden vanwege de relatief korte afstand van de elektrode naar de zenuwen. Verder slaagde *current focussing* er alleen in om het excitatiegebied ruimtelijk te beperken als er weinig of geen sprake was van excitatie in de perifere uitlopers van de gehoorzenuwvezels. Daarnaast was in het model te zien dat zenuwrekrutering van elektrische stimulatie in drie dimensies plaats vond, dus niet alleen richting apex of basis van de cochlea, maar ook in de diepte binnen het spirale ganglion. Dit betekende dus dat bij gelijke luidheid verschillen tussen excitatiepatronen van multipoolstimulatie niet weerspiegeld werden als de gehoorzenuwvezels beschreven werden als lineair gerangschikte identieke neuronen, maar dat een vorm van variabiliteit zoals de ruimtelijke spreiding van cellichamen nodig was om de spreiding van excitatie te modelleren.

Bij CI-stimulatie is de mate van zenuwexcitatie afhankelijk van de polariteit (stroomrichting) van het aangeboden signaal; het verschil in excitatiedrempel tussen kathodale pulsen (negatieve stroom) en anodale pulsen (positieve stroom) wordt de polariteitsgevoeligheid van de elektrische stimulatie genoemd. Het is bekend uit klinische

en elektrofysiologische experimenten dat deze polariteitsgevoeligheid verschilt tussen mens en dier, tussen mensen onderling en ook tussen de afzonderlijke elektrodecontacten van een proefpersoon. Eerdere computermodelonderzoeken lieten zien dat de twee stimuluspolariteiten de neiging hebben de gehoorzenuwen op verschillende plaatsen te exciteren; kathodale pulsen in de perifere uitlopers van de gehoorzenuwen en anodale pulsen in het centrale axon. Mede hierdoor is de hypothese ontstaan dat verschillen in polariteitsgevoeligheid veroorzaakt worden door de gezondheid van de zenuwvezels in de buurt van het stimulerende contact, waarbij een grotere gevoeligheid voor kathodale pulsen zou duiden op de aanwezigheid van de perifere uitlopers (en dus intacte vezels) en omgekeerd dat een grotere gevoeligheid voor anodale pulsen juist zou aangeven dat de perifere uitlopers afgestorven zijn.

Deze hypothese is in **hoofdstuk 7** onderzocht in het Leidse CI-model. Hiervoor is het zenuwmodel verbeterd door gebruik te maken van een zenuwkinetiek die op menselijke data gebaseerd was en door een vernieuwde zenuwmorfologie in te voeren waarbij de vezels gemodelleerd werden als elektrische dubbelkabels. De vezels werden gemodelleerd in drie fases van neurale degeneratie: gezonde (intacte) vezels, vezels met een beginnende vorm van degeneratie aan het perifere uiteinde en vezels waarbij de perifere uitlopers geheel afgestorven waren. Hiermee werden de zenuwreacties op kathodale en anodale pulsen gesimuleerd, op verschillende elektrodeposities.

Wat het model liet zien is dat, hoewel de polariteitsgevoeligheid afhankelijk was van de toestand van de zenuwvezels en de drempels van kathodale pulsen meer werd beïnvloed door de toestand van de perifere uitlopers, het effect van neurale degeneratie op polariteitsgevoeligheid niet consequent en soms zelfs tegen-intuïtief was. Verder waren er effecten te zien van elektrode-insertiediepte en afstand tot de cochleaire modiolus; over het algemeen waren meer apicaal gelegen elektrodecontacten gevoeliger voor kathodale pulsen.

Een bijkomstige conclusie van het onderzoek was dat het verschil in polariteitsgevoeligheid tussen mensen en dieren verklaard kon worden door verschillen in de hoeveelheid myeline om de cellichamen. De voornaamste conclusie was echter dat de polariteitsgevoeligheid geen betrouwbare indicator was van neurale gezondheid en dat polariteitsgevoeligheid niet alleen afhangt van de toestand van de zenuwvezels, maar ook van ruimtelijke factoren.

Het proefschrift sluit af met een algemene discussie in **hoofdstuk 8**, over het onderzoek dat in de voorgaande hoofdstukken beschreven is, waarbij recentere onderzoeken besproken worden. Verder wordt er gereflecteerd op de huidige stand en toekomst van het Leidse CI-model.

De onderzoeken die in dit proefschrift gepresenteerd zijn hebben het Leidse CI-model dichter bij de klinische realiteit gebracht, maar er kan nog meer gedaan worden om de kloof verder te overbruggen. Aangezien het Leidse CI-model gebaseerd is op natuurkundige principes, is het van essentieel belang het te blijven valideren en verfijnen met behulp van data uit dierexperimenteel en klinisch onderzoek en om niet lukraak willekeurige parameters te gaan aanpassen om de modelresultaten realistischer te doen lijken.

Maar het is belangrijk te realiseren dat het toevoegen van meer detail aan het model geen doel op zichzelf is, aangezien de toevoeging van ‘levensechte’ eigenschappen aan biofysische modellen de neiging heeft hun uitkomsten variabeler te maken en moeilijker te interpreteren of te controleren op fouten. Tegelijkertijd zal het verbeteren van het model ervoor zorgen dat het door kan gaan met het werpen van nieuw licht op experimentele bevindingen die nog niet volledig begrepen worden, kan helpen in het begrijpen van de verschillen tussen gegevens van dieren en mensen en hopelijk leiden tot betere inzichten voor de klinische praktijk.

Appendix

List of abbreviations

3D	Three-dimensional
BA	Biphasic anodic-first
BC	Biphasic cathodic-first
BEM	Boundary element method
BM	Basilar membrane
CI(s)	Cochlear implant(s)
CIS	Continuously interleaved sampling
CM#	Label for individual human cochlear geometries in the Leiden CI-model
CT	Computed tomography/tomographic
CVC	Consonant-Vowel-Consonant (syllable pattern)
eCAP(s)	Electrically evoked compound action potential(s)
ED	Excitation density
EDR	Electrical dynamic range
EFI	Electrical field imaging
FDM	Finite difference method
FEM	Finite element method
FN	Facial nerve
FNS	Facial nerve stimulation
gSEF	Generalised Schwarz-Eikhof-Frijns
HC#	Label for individual human cochlear geometries in the Leiden CI-model
MA	Monophasic anodic
MC	Monophasic cathodic
MCL	Maximum comfortable loudness level
MP	Monopole/monopolar
MPR	Multiplanar reconstruction
I_{1mm}	Simulated perceptual threshold level in the Leiden CI-model
I_{4mm}	Simulated maximum comfortable loudness level in the Leiden CI-model
IPG	Interphase gap
I_{th}	Simulated perceptual threshold level in the Leiden CI-model
OC	Organ of Corti
PA	Phased array
PE	Polarity effect
PSA	Pseudomonophasic anodic-first
PSA#	Same as PSA; # refers to the ratio between phase durations/amplitudes
PSC	Pseudomonophasic cathodic-first
PSC#	Same as PSC; # refers to the ratio between phase durations/amplitudes
pTP	Partial tripole/tripolar
SEF	Schwarz-Eikhof-Frijns
SG	Spiral ganglion
SRB	Schwarz-Reid-Bostock
TA	Triphasic with anodic middle phase
TC	Triphasic with cathodic middle phase
TH	Threshold
TP	Tripole/tripolar
XP	Excitation profile

List of publications

Frijns, J.H.M., **Kalkman, R.K.**, Vanpoucke, F.J., Snel-Bongers, J., Briaire, J.J.
Simultaneous and non-simultaneous dual electrode stimulation in cochlear implants: evidence for two neural response modalities
Acta Otolaryngol. 2009; 129(4):433–9

Frijns, J.H.M., **Kalkman, R.K.**, Briaire, J.J.
Stimulation of the Facial Nerve by Intracochlear Electrodes in Otosclerosis: A Computer Modeling Study
Otol Neurotol. 2009; 30(8):1168–74

Carlyon, R.P., Macherey, O., Frijns, J.H.M., Axon, P.R., **Kalkman, R.K.**, Boyle, P., Baguley, D.M., Briggs, J., Deeks, J.M., Briaire, J.J., Barreau, X., Dauman, R.
Pitch comparisons between electrical stimulation of a cochlear implant and acoustic stimuli presented to a normal-hearing contralateral ear
J Assoc Res Otolaryngol. 2010; 11(4):625–40

Snel-Bongers, J., Briaire, J.J., Van der Veen, E.H., **Kalkman, R.K.**, Frijns, J.H.M.
Threshold levels of dual electrode stimulation in cochlear implants
J Assoc Res Otolaryngol. 2013; 14(5):781–90

Kalkman, R.K., Briaire, J.J., Dekker, D.M.T., Frijns, J.H.M.
Place pitch versus electrode location in a realistic computational model of the implanted human cochlea
Hear Res. 2014; 315:10–24

Kalkman, R.K., Briaire, J.J., Frijns, J.H.M.
Current focussing in cochlear implants: An analysis of neural recruitment in a computational model
Hear Res. 2015; 322:89–98

Kalkman, R.K., Briaire, J.J., Frijns, J.H.M.
Stimulation strategies and electrode design in computational models of the electrically stimulated cochlea: An overview of existing literature
Network. 2016; 27(2–3):107–134

Van Gendt, M.J., Briaire, J.J., **Kalkman, R.K.**, Frijns, J.H.M.
A fast, stochastic, and adaptive model of auditory nerve responses to cochlear implant stimulation
Hear Res. 2016; 341:130–143

Vellinga, D., Bruijn, S., Briaire, J.J., **Kalkman, R.K.**, Frijns, J.H.M.
Reducing interaction in simultaneous paired stimulation with CI
PLoS One. 2017; 12(2):e0171071

Van Gendt, M.J., Briaire, J.J., **Kalkman, R.K.**, Frijns, J.H.M.
Modeled auditory nerve responses to amplitude modulated cochlear implant stimulation
Hear Res. 2017;351:19–33

Van der Jagt, M.A., **Kalkman, R.K.**, Briaire, J.J., Verbist, B.M., Frijns, J.H.M.
Variations in cochlear duct shape revealed on clinical CT images with an automatic tracing method
Sci Rep. 2017; 7(1):17566

Van Gendt, M.J., Koka, K., **Kalkman, R.K.**, Stronks, H.C., Briaire, J.J., Litvak, L., Frijns, J.H.M.
Simulating intracochlear electrocochleography with a combined model of acoustic hearing and electric current spread in the cochlea
J Acoust Soc Am. 2020; 147(3):2049

Kalkman, R.K., Briaire, J.J., Dekker, D.M.T., Frijns, J.H.M.
The relation between polarity sensitivity and neural degeneration in a computational model of cochlear implant stimulation
Hear Res. 2022; 415:108413

Biesheuvel, J.D., Briaire, J.J., **Kalkman, R.K.**, Frijns, J.H.M.
The effect of stimulus level on excitation patterns of individual electrode contacts in cochlear implants
Hear Res. 2022; 420:108490

About the Author

Randy Kalkman was born in Vlaardingen, The Netherlands, on May 30th, 1978. He finished his secondary education (VWO) in 1996 at De Ring van Putten in Spijkenisse and started studying physics at Leiden University in the same year. In 2003 he received his master's degree after performing his thesis work at the Quantum Optics group of the faculty of physics and at the ENT-department of the Leiden University Medical Centre. Since 2003 he has worked at the Leiden University Medical Centre's ENT-department, initially as a research software developer and since 2006 as a full time researcher. In addition to working on the Leiden CI-model he has collaborated with and provided support for the (PhD) work of Berit Verbist, Jorien Snel-Bongers, Feddo van der Beek, Kim van der Marel, Monique de Jong, Annerie van der Jagt, Margriet van Gendt, Yu Dong, Dick Biesheuvel and others, leading to several co-authored papers (see the list of publications). He also provides (neural) telemetry support for the cochlear implant surgeries performed at Leiden University Medical Centre.

A